

**Production of Light and Intermediate  
Mass Residual Nuclides  
by Proton Induced Reactions at  
Medium Energies**

Der Fakultät für Mathematik und Physik  
der Gottfried Wilhelm Leibniz Universität Hannover

zur Erlangung des Grades

Doktorin der Naturwissenschaften

Dr. rer. nat

genehmigte Dissertation

von

Dipl. Ing. Mihaela Tutuc

geboren am 25. Mai 1981 in Bukarest, Rumänien

Referent: Prof. Dr. Rolf Michel  
Korreferent: PD Dr. Ingo Leya  
Tag der Promotion: 10. November 2009



How are we to be happy without curiosity,  
without questions, doubt and arguments?  
Without joy in thinking?

Pascal Mercier



To Daniel



---

## Abstract

Cross sections for the production of residual nuclides are a key issue for medium energy applications. Due to the large range of relevant target elements and the amount of product nuclides it will not be possible to measure all the cross sections needed. One will have to widely rely on models and codes to calculate the required data. The demand for reliable theoretical predictions of production cross sections is by no means satisfied by the models and codes which are available today. In this context it is essential that reliable and comprehensive databases do exist which can serve as benchmarks for code development and validation.

In this work a systematic survey was done for the production of intermediate mass fragments by proton induced reactions. It covers all previous available and new data for the production of residual nuclides with masses between 3 and 30, over an energy range extending from thresholds up to 2.6 GeV with targets spreading over the entire chart of nuclides. The experimental data are exemplarily compared with calculations using the TALYS and INCL4+ABLA codes.

This study was performed as a contribution to the NUDATRA work package 5.4 “High Energy Experiments for Radioactivity, Chemical Modifications and Damage Assessment” for the EUROpean Research Programme for the TRANSmutation of High Level Nuclear Waste in an Accelerator Driven System (EUROTRANS).

We have extended the range of this survey and a number of older experiments were evaluated and the results are now available. Cross sections for energies up to 2.6 GeV were obtained also for residual nuclides with masses higher than 30 by combined experiments using accelerators at LNS/Saclay ( $E=200-2600\text{MeV}$ ) and at TSL/Uppsala ( $E=70-180\text{MeV}$ ). Cross sections were determined by target activation experiments and offline  $\gamma$ -spectrometry of radionuclides at the Center for Radiation Protection and Radioecology, ZSR, Leibniz Universität Hannover.

The capabilities of some available codes to predict cross sections for the production of residual nuclides in thin and thick target experiments are tested and a comparison between experiment and theory is made.

**Keywords:** cross sections, residual nuclides, protons, medium energy



---

## Kurzzusammenfassung

Wirkungsquerschnitte für die Erzeugung von Restkern-Nukliden sind von sehr großer Bedeutung für Anwendungen in Bereich der mittleren Energien. Durch die Vielzahl relevanter Target-Elemente und Produkt-Nuklide ist die experimentelle Ermittlung aller notwendigen Wirkungsquerschnitte nicht möglich, sodass man auf die Berechnung der benötigten Daten mithilfe von Modellen und Rechencodes angewiesen ist. Allerdings kann die große Nachfrage nach zuverlässigen theoretischen Vorhersagen von Erzeugungswirkungsquerschnitten nicht annähernd durch die bereits verfügbaren Modelle und Codes gedeckt werden. In diesem Zusammenhang sind zuverlässige und umfassende Datensätze, die als Vergleichsbasis für die weitere Entwicklung und Validierung von Programmpaketen dienen, unerlässlich.

Diese Arbeit gibt einen systematischen Überblick über die Erzeugung mittelschwerer Restkerne durch protoneninduzierte Reaktionen. Dabei werden im berücksichtigten Energiebereich bis 2,6 GeV alle bereits verfügbaren und neuen Daten für die Produktion von Restkernen mit  $3 \leq A \leq 30$  und mit über die gesamte Nuklidkarten verteilten Target-Nukliden abgedeckt. Die Experimentellen Daten werden exemplarisch mit Berechnungen anhand der Programme TALYS und INCL4+ABLA verglichen.

Diese Untersuchung ist ein Beitrag für das NUDATRA arbeitspaket 5.4 “High Energy Experiments for Radioactivity, Chemical Modifications and Damage Assessment” des “EUROpean Research Programme for the TRANSmutation of High Level Nuclear Waste in an Accelerator Driven System” (EUROTRANS).

Anschließend konnten mittels der Auswertung früherer Messungen über die bereits genannten Untersuchungen hinausgehende Erkenntnisse gewonnen werden. So wurden durch Aktivierungsexperimente an den Beschleunigern LNS/Saclay ( $E=200-2600\text{MeV}$ ) sowie TSL/Uppsala ( $E=70-180\text{MeV}$ ) Wirkungsquerschnitte für Energien bis zu 2,6 GeV zusätzlich auch für Restkerne mit  $A \geq 30$  ermittelt. Die Messung der Wirkungsquerschnitte erfolgte durch Offline-Gammaspektrometrie am Zentrum für Strahlenschutz und Radioökologie (ZSR) der Leibniz Universität Hannover.

Die Leistungsfähigkeit einiger verfügbarer Programmpakete im Hinblick auf die Berechnung von Wirkungsquerschnitten für die Erzeugung von Restkern-Nukliden in dünnen und dicken Targets wird anhand des Vergleichs von experimentellen und theoretischen Daten analysiert.

**Schlagnworte:** Wirkungsquerschnitte, Restkern-Nukliden, Protonen, mittlere Energien





---

# Contents

<b>Abstract</b>	<b>i</b>
<b>Kurzzusammenfassung</b>	<b>iii</b>
<b>1 Introduction</b>	<b>1</b>
<b>2 Aim of this work</b>	<b>5</b>
<b>3 Theoretical Background</b>	<b>7</b>
3.1 Nuclear Reactions . . . . .	7
3.1.1 Q-Value for a reaction . . . . .	8
3.1.2 Threshold energy for a nuclear reaction . . . . .	9
3.1.3 Nuclear reaction cross-section . . . . .	10
3.1.4 Regimes of nuclear reactions . . . . .	10
3.2 Experimental Approach . . . . .	15
3.2.1 Classical kinematics . . . . .	15
3.2.2 Inverse kinematics . . . . .	16
3.3 Determination of Cross-Sections for the Production of Residual Nuclides	17
3.3.1 General case . . . . .	17
3.3.2 Independent and cumulative cross-sections . . . . .	19
3.3.3 Corrections for radioactive progenitors . . . . .	20
3.3.4 Corrections for $\gamma$ -interferences . . . . .	20
<b>4 Experiments at TSL and LNS</b>	<b>23</b>
4.1 Overview . . . . .	23
4.2 Targets and Irradiations . . . . .	23
4.3 Measurements and evaluation of experimental data . . . . .	26
4.3.1 $\gamma$ Spectrometry . . . . .	26
4.3.2 Analysis of spectra . . . . .	28
4.3.3 Contribution of uncertainties . . . . .	33
4.4 Flux monitoring . . . . .	36
4.5 Experimental results . . . . .	36
4.5.1 Results from UPPS0H . . . . .	37
4.5.2 Results from SACL0L . . . . .	41
4.5.3 Results from UPPS0S . . . . .	48
4.5.4 Comparison with TALYS . . . . .	52

<b>5</b>	<b>NUDATRA Project</b>	<b>57</b>
5.1	Overview . . . . .	57
5.2	Target and Product Nuclide Coverage . . . . .	58
5.3	Experimental Data . . . . .	61
5.3.1	$^3\text{He}$ and $^4\text{He}$ . . . . .	61
5.3.2	$^7\text{Be}$ and $^{10}\text{Be}$ . . . . .	65
5.3.3	$^{21}\text{Ne}$ , $^{22}\text{Na}$ , and $^{24}\text{Na}$ . . . . .	68
5.4	Empirical systematic . . . . .	85
5.5	Comparison between experiment and theory . . . . .	105
5.5.1	Modeling of residual nuclide production at medium energies . .	105
5.5.2	TALYS . . . . .	112
5.5.3	INCL4+ABLA . . . . .	123
<b>6</b>	<b>Conclusions</b>	<b>129</b>
<b>7</b>	<b>Acknowledgements</b>	<b>131</b>
	<b>References</b>	<b>133</b>
	<b>List of Tables</b>	<b>147</b>
	<b>List of Figures</b>	<b>149</b>
<b>A</b>	<b>Studied reactions for NUDATRA project</b>	<b>157</b>
<b>B</b>	<b>Product-target overview for NUDATRA data</b>	<b>161</b>
<b>C</b>	<b>Excitation functions for the NUDATRA experimental data</b>	<b>163</b>
<b>D</b>	<b>Product-target combinations covered for Talys calculations</b>	<b>193</b>
<b>E</b>	<b>Comparison with Talys for NUDATRA data</b>	<b>195</b>
<b>F</b>	<b>Experimental data for SACLOL, UPPS0H and UPPS0S</b>	<b>201</b>
<b>G</b>	<b>Comparison with Talys for SACLOL, UPPS0H and UPPS0S data</b>	<b>209</b>
<b>H</b>	<b>Curriculum Vitae</b>	<b>215</b>
<b>I</b>	<b>Publications</b>	<b>217</b>

---

# 1 Introduction

The atomic nucleus is a fascinating object to study. The properties of nuclei are important for such diverse phenomena as energy generation in stars and the design of microelectronic devices. Although nuclei have been studied for over a century there are still open questions. For example, properties of nuclei far from the valley of stability, the formation of super-heavy elements and nuclear reactions which result in nuclei with high excitation energy. No complete theoretical description exists of these reactions but many models have been created, e.g. [Ni95, Gu83, Bo95a, Ai91], which are able to explain some features of the reactions, such as direct reactions, pre-equilibrium emission, evaporation and multifragmentation. The models often rely on assumptions which may not be justified in the whole energy range from a few MeV to several GeV and no firm energy limits exist where these assumptions are valid. Even within the same energy interval physically different models exist, e.g. [Ni95, Gu83]. In order to experimentally distinguish between the models, more high quality data are needed.

The reactions cross section gives the probability that a particle will undergo a nonelastic process when passing through a nuclear medium. Therefore reaction cross section data are of importance, not only from a theoretical point of view, but also for applications in such diverse fields as medicine, biology, astrophysics and accelerator-driven transmutation of nuclear waste.

Protons have been used for treatment of cancer and other medical conditions for more than 50 years. The treatment utilizes the effect of the Bragg peak, where the main part of the delivered dose is distributed in a well defined and relatively small region, minimizing the dose to normal tissue surrounding the target. Although the proton energy is deposited mainly through electromagnetic interactions with atomic electrons, large improvements of the therapeutic methods may be achieved with better information about the nuclear reactions that also occur in the human body during treatment, primarily with C, O and Ca. The use of radioactive isotopes for medical diagnosis and treatment is a growing industry, where a variety of isotopes spread over the periodic table are used. While many of the isotopes are produced in nuclear reactors through neutron capture and fission, others are preferably produced with accelerated proton beams in the intermediate energy range, or with novel techniques where an intense neutron source is created with a proton beam interacting with light or heavy targets.

The interaction of high energy cosmic radiation with biological matter is of concern, not only for astronauts, but also for passengers in commercial airplanes. The

projectile-target combinations of interest are similar to those for medical therapy, as well as the natural elements of air (N, O, Ar) and potential shielding materials in manned spacecrafts (H, C, Al).

Digital electronic devices may suffer random re-programming or permanent damage, so-called Single Event Effects (SEE) and Single Event Upsets (SEU), when a single ionizing particle from cosmic radiation (mainly protons) deposits free charge within the device. This effect is relatively small at sea level due to the natural shielding from the atmosphere, but the problem increases with altitude and is therefore of concern for airplane and satellite electronics. An obvious target for the study is  $^{28}\text{Si}$ , the basic material for most of nowadays electronic devices, but other nuclides used in electronic components are also of interest.

Cross sections for the production of residual nuclides by proton induced reactions are basic nuclear quantities for an accurate modelling of the interaction of solar cosmic protons with matter, e.g. meteorites, planetary surfaces and the upper earth atmosphere. By these interactions a large variety of stable and radioactive nuclides - the so-called cosmogenic nuclides - are produced and can be measured either by their decay or as positive isotope anomalies in the target materials. The study of cosmogenic nuclides is relevant for geo- and cosmochemical processes and allows the description of the cosmic ray exposure history of lunar samples, meteorites and cosmic dust.

Several projects involving large scale accelerator driven systems (ADS) are under development for subcritical nuclear energy production as well as for the reduction of long-lived radioactive waste through nuclear transmutation. The basic idea for such systems is to use high-intensity proton accelerators for the production of an intense neutron flux through spallation processes. The neutrons, with energies from the thermal region up to 1 GeV, will then drive the subcritical nuclear reactor. While these projects obviously require large amounts of nuclear data for intermediate energy neutrons, the accelerator driven neutron source also requires better information of proton induced reactions for the neutron production target (Pb, Bi, W, U), as well as for surrounding structural materials (Al, Fe, Ni, Zr). An overview of the above described applications of reaction cross-sections is given in Table 1.

The various applications described in this chapter reveal an extensive need of nuclear data for a vast number of nuclei, reaction type, and over a large energy range. The OECD Nuclear Energy Agency (NEA) has issued a report on an evaluation of intermediate energy data [Ko98]. In the report it was emphasized that if all the measurements important for various applications would be performed it would keep the existing experimental facilities busy for about a millenium. Therefore one will have

---

## **Nuclear Physics**

- Systematic of nuclear reactions
- Pre-equilibrium and intra-nuclear cascade model
- Pre-equilibrium decay, spallation and fragmentation
- Fission at medium energies

## **Astrophysics**

- Abundance of heavy CR particles
- p-process nucleosynthesis
- T-Tauri and WR stars

## **Cosmophysics and -chemistry**

- Cosmic ray exposure history of extraterrestrial matter
- Terrestrial ages of meteorites
- Variations of cosmic radiation with space and time

## **Particle Accelerator Technology**

- Activation of detectors
- Radiation protection
- Online mass separation
- Radioactivity in beampipes

## **Medicine**

- Radionuclide production
- Radiation therapy

## **Space and Aeronautical Technology**

- Radiation protection
- Material damage

Table 1.1: Examples for applications of nuclear data.

to rely widely on models and codes to calculate the required data. The demand for reliable theoretical predictions of production cross sections is by no means satisfied by the models and codes which are available today. In this context it is essential that reliable and comprehensive databases do exist which can serve as benchmarks for code development and validation.



---

## 2 Aim of this work

One of the goals of this work is to complete the cross-sections database for proton induced reactions by the evaluation of previous  $\gamma$ -spectrometric measurements and by the measurement of long-lived radioactive progenitors in targets of earlier experiments performed using accelerators at LNS(Laboratoire National Saturne)/Saclay (E=200-2600MeV) and at TSL(Svedberg Laboratory Uppsala)/Uppsala(E=70-180MeV).

As a contribution to the NUDATRA work package 5.4 "High Energy Experiments for Radioactivity, Chemical Modifications and Damage Assessment" for the EUROpean Research Programme for the TRANSmutation of High Level Nuclear Waste in an Accelerator Driven System (EUROTRANS) a systematic survey shall be performed, in the second part of this thesis, for the production of intermediate mass fragments by proton induced reactions. This study will cover all previous available and new data for the production of residual nuclides with masses between 3 and 30, over an energy range extending from thresholds up to 2.6 GeV with targets spreading over the entire chart of nuclides. This will contribute to testing the recently developed codes TALYS and INCL4 and to do empirical systematics to see whether residual nuclides production and light particle production can be attributed to the same production mode.





## 3 Theoretical Background

### 3.1 Nuclear Reactions

Radioactive decays of nuclides allow obtaining informations about them. This informations are however limited to a small number of nuclides - the naturally radioactive ones - and only to some of their properties. We have to emphasize that the number of naturally radioactive nuclides is small and is limited, with a few exceptions, to the nuclides from the three main radioactive series; the number of radioactive nuclides artificially produced, in nuclear reactions, is considerably bigger. This is the reason why the information gained from radioactive decays is for the artificial radionuclides produced in nuclear reactions.

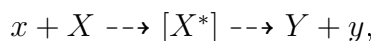
Nowadays, it is well known that nuclear reactions are the main “source” for informations about the properties of nuclei: dimensions, charge and mass distribution, kinetic, electric and magnetic moments for the ground states and for the excited states, probabilities of transition etc.

These informations are the basis for our knowledge about the fundamental laws of matter since substantial parts of the universe is concentrated in the atomic nuclei.

Nuclear reactions are described by specifying the type of the incident radiation, the nuclear target, the products of the reaction, the probability that the reaction will take place, called “cross section”, and the distributions in energy and angle of the reaction products.

A nuclear reaction can be defined as the change in the identity or characteristic of an atomic nucleus, induced by bombarding it with an energetic particle. The bombarding particle may be an alpha particle, a gamma ray photon, a neutron, a proton or a heavy ion. A typical nuclear reaction involves two reacting particles - and produces new particles - a residual product nucleus and one or more lighter ejected particle. In the first observed nuclear reaction (1919), Ernest Rutherford bombarded nitrogen with alpha particles and identified the ejected lighter particles as hydrogen nuclei or protons ( ${}^1\text{H}$  or  $p$ ) and the product nuclei as a rare oxygen isotope. In the first nuclear reaction produced by artificially accelerated particles (1932), the English physicists J.D. Cockcroft and E.T.S. Walton bombarded lithium with accelerated protons and thereby produced two helium nuclei, or alpha particles.

A nuclear reaction can be written:



where  $x$  is the projectile,  $X$  is the target nucleus,  $X^*$  is the excited composite nucleus,  $Y$  is the product nucleus, and  $y$  is the ejectile.

For a nuclear reaction to occur the incident particle must interact with the nucleus. And in this situation the energy must be high enough to overcome the Coulombs barrier between the interacting partners. Observation has proved that if the energy is lower than the height of the Coulomb barrier, the nucleons will bounce each other. The height of the barrier depends on the atomic numbers of target and projectile nuclei, i.e.,

$$E_c = \frac{1}{4\pi\epsilon_0} \frac{Z_1 \cdot e \cdot Z_2 \cdot e}{r} \quad (3.1)$$

or

$$E_c = k \frac{Z_1 \cdot e \cdot Z_2 \cdot e}{r} \quad (3.2)$$

$r$  represents the distance between the two nuclides. This holds down to a distance  $r_1$  where the nuclear forces becomes operative. For  $r_1$  we have the relation

$$r_1 = r_0(A_1^{1/3} + A_2^{1/3}) \quad (3.3)$$

with

$$r_0 = 1.4 \times 10^{-13} \text{ cm} \quad (3.4)$$

### 3.1.1 Q-Value for a reaction

In a nuclear reaction, from conservation of energy, the total energy including the rest-mass energy must be the same before and after the reaction i.e.

$$\left(\sum_i [E_i + m_i c^2]\right)_{before} = \left(\sum_i [E_i + m_i c^2]\right)_{after} \quad (3.5)$$

where  $E_i$  and  $m_i$  are the kinetic energy and rest mass of particle respectively. Any change in the total kinetic energy before and after the reaction must be accompanied by an equivalent change in the total rest mass. The  $Q$ -value of a reaction is defined as the change in kinetic energy or rest mass in a reaction i.e.

$$Q = (\text{kinetic energy})_{after} - (\text{kinetic energy})_{before} \quad (3.6)$$

or

$$Q = (\text{rest mass})_{after} c^2 - (\text{rest mass})_{before} c^2. \quad (3.7)$$

If the kinetic energy of the products is greater than that of the reactants, the reaction is exothermic and  $Q$  is positive. If energy is required to induce a reaction, the reaction is endothermic and  $Q$  is negative. In such endothermic reactions a minimum kinetic energy of reactants is required for the reaction to proceed.

In a binary nuclear reaction  $a + X \rightarrow Y + b$ , the  $Q$ -value is given by

$$Q = (E_Y + E_b) - (E_a + E_X) = [(m_a + m_X) - (m_Y + m_b)] c^2 \quad (3.8)$$

In most binary reactions, the number of protons is conserved and the same number of electron masses can be added to both sides of the above reactions. Neglecting the differences in electron binding energies, the  $Q$ -value can be expressed in terms of atomic masses i.e.

$$Q = (E_Y + E_b) - (E_a + E_X) = [(M_a + M_X) - (M_Y + M_b)] c^2. \quad (3.9)$$

In radioactive decay reactions a parent nuclide decays to a daughter with the emission of a particle, i.e.  $P \rightarrow D + d$ . The  $Q$ -value is given by  $Q = (E_D + E_d)$  since the parent nuclide is at rest, hence

$$Q = (E_D + E_d) = [m_P - m_D - m_d] c^2 > 0. \quad (3.10)$$

It should be noted that in some types of radioactive decay, such as beta decay and electron capture, the number of protons is not conserved. In such cases the evaluation of the  $Q$ -value using atomic masses may be inaccurate.

### 3.1.2 Threshold energy for a nuclear reaction

The actual amount of energy required in the laboratory frame to bring about a nuclear reaction is slightly greater than the  $Q$ -value. This is due to the fact that not only energy but also momentum must be conserved in any nuclear reaction. From conservation of momentum, a fraction  $m_a/(m_a + M_X)$  of the kinetic energy of the incident particle  $a$  must be retained by the products. This implies that only a fraction  $M_X/(m_a + M_X)$  of the incident particle mass is available for the reaction. It follows that the threshold energy is higher than the  $Q$ -value and is given by

$$E_{th} = \frac{Q(m_a + M_X)}{M_X} \quad (3.11)$$

### 3.1.3 Nuclear reaction cross-section

In a nuclear reaction a fraction of particles is absorbed and another one is scattered. The macroscopic cross section  $\Sigma$  is defined as:

$$\Sigma = N\sigma,$$

where  $N$  is the number of target nuclei per unit volume and  $\sigma$  is the cross section.

The mechanism involved during the interaction of a particle with nuclei has different values of cross sections:

$$\text{scattering: } \sigma_s = \sigma_e + \sigma_{in}$$

$$\text{absorbtion: } \sigma_a = \sigma_\gamma + \sigma_f$$

If we combine all these cross section values we get the macroscopic cross section in the form

$$\Sigma_{tot} = \Sigma_s + \Sigma_a \tag{3.12}$$

the resulting  $\Sigma_{tot}$  is the probability per unit path length that any type of reaction will occur [Ha87].

Let us assume that a beam of an area  $A$  interacts with the foil. We say that part of the particle beam reacts with the target. Suppose that the foil has  $N(\text{atoms}/\text{cm}^2)$ , then the area  $A$  covered by the nuclei is  $N(\text{atoms}/\text{cm}^2) \times A(\text{cm}^2) \times$  the effective area, which is subtended by one atom ( $\text{cm}^2/\text{atom}$ ). So we can say to this effective area as a cross section of the nuclear reaction  $\sigma$

$$\sigma = \frac{\text{number of reactions per unit time}}{\text{number of target nuclei}(N) \times \text{projectile flux density } (\Phi)} \tag{3.13}$$

Typical nuclear diameter is of the order of  $10^{-12}$  cm. We might therefore expect the cross section for the nuclear reaction to be the order of  $\pi r^2$ , or  $10^{-24}$   $\text{cm}^{-2}$ . It has been found convenient to use the separate name for this area. The name adopted is barn and is equivalent to  $10^{-24}\text{cm}^{-2}$ .

### 3.1.4 Regimes of nuclear reactions

An outline of the general theory and modeling of nuclear reactions can be given in many ways.

- A common classification is in term of time scales: short reaction times are associated with direct reactions and long reaction times with compound nucleus processes. At intermediate time scales, pre-equilibrium processes occur.

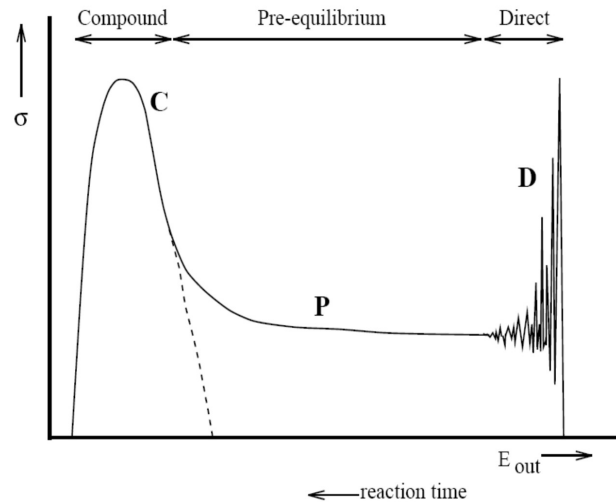


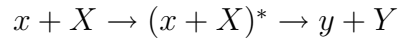
Figure 3.1: Schematic drawing of an outgoing particle spectrum. The energy regions to which direct (D), pre-equilibrium (P) and compound (C) mechanisms contribute are indicated. The dashed curve distinguishes the compound contribution from the rest in the transitional energy region, [Ko07].

- An alternative, more or less equivalent, classification can be given with the number of intranuclear collisions, which is one for direct reactions, a few for pre-equilibrium reactions and many for compound reactions, respectively. As a consequence, the coupling between the incident and outgoing channels decreases with the number of collisions and the statistical nature of the nuclear reaction theories increases with the number of collisions.
- Another way to classify nuclear reactions can be made in terms of energy of the incident particle.

1. At low energy there are two main competing reactions: direct reactions and compound reactions.

When the energy of a projectile is higher than the Coulomb barrier it interacts with the nucleons in the target nucleus. The projectile can either be absorbed and form a new nucleus, more probable at lower energies, or interact with individual nucleons and then leave the nucleus. When the incoming proton interacts only with one or a few nucleons in the target it is called a direct reaction. Direct reactions occur preferably in peripheral collisions since the nuclear density is lower at the surface. The transfer of energy and momentum to the nucleus is usually low in direct reactions, therefore the outgoing proton has almost the same energy as the incoming one.

The reaction for the formation of a compound nucleus takes place in two different steps. In the first phase the projectile particle interacting strongly with the target nucleus will distribute all its energy on the target nucleons. A compound nucleus is formed in an excited state containing now both the nucleons of the projectile and of the target nucleus. A compound nucleus reaction can be represented as follows:



The nucleus created in the first stage of the reaction can have high excitation energy and be unstable. Fluctuations of the energy of the nucleons can make, in the second step, one or several nucleons, a fragment, get enough energy to escape from the nucleus, thus reducing the mass, charge and excitation energy. If the remaining nucleus has enough energy more nucleons or fragments are emitted until the excitation energy gets too low for further emission of nucleons and the nucleus decays by gamma or beta emission to the ground state. The analogy with water molecules boiling off heated water has given this process the name evaporation. Evaporation is the origin of most low energy nucleons and fragments emitted in the reactions. However, very low energy protons and fragments are, because of their electric charge, prevented from escaping the nucleus by the Coulomb barrier. A small number of light nuclei can tunnel through the potential barrier or be emitted by other processes, for instance fission in case of heavy nuclei [Ma06]. These fragments can carry valuable information on different reaction mechanisms other than evaporation. An interesting feature of evaporation is that the compound nucleus has no memory of the way it was formed, the decay is independent of the reaction in which it was created [Go50].

It is not absolutely necessary that the energy of the projectile to be distributed on “all” the nucleons in the target nucleus. It can also interact with several nucleons successively and transfer part of its energy in every collision and as a result the total energy transfer is large. The probability of many nucleon interactions is largest in central collisions. The energy transferred from the incoming particle to the target nucleons is shared evenly between them after many collisions among them. When this occurs the nucleus has reached equilibrium. Before equilibrium is reached nucleons can be emitted [Bl75] and they are called pre-equilibrium particles. The experimental signatures of these particles are the particles emitted with energies just below the nucleons coming from direct reactions [Sa80]. In all of the mentioned scenarios an excited nucleus, i.e. a compound nucleus, is left after the first stage of the reaction.

2. Over the entire energy range nuclear reactions can be classified as follows:

- low energy reactions, for energies up to 50 MeV
- intermediate energy reactions, for energies from around 200 MeV up to a few GeV
- high energy reactions, for energies higher than a few GeV

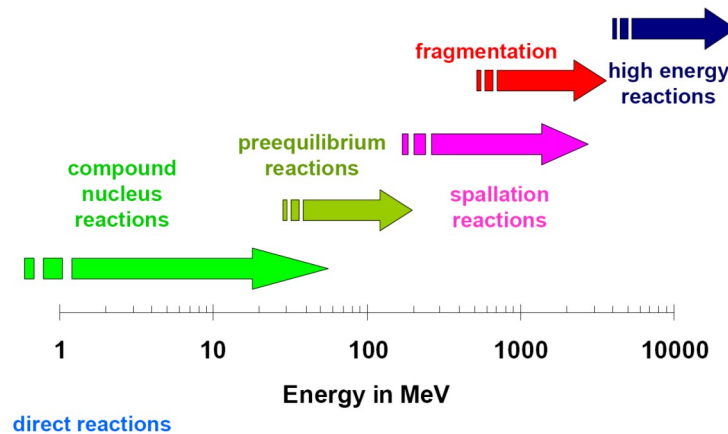


Figure 3.2: Dependence of the reaction mode on energy.

It must be emphasized that there is no strict definition for the term “medium energy reactions”. In this work is understood as reactions at energies above 50 MeV and below a few GeV (Figure 3.2 ). A detailed treatment of proton induced reactions at medium energies has to take into account a variety of phenomena such as spallation, fission and (multi)-fragmentation, the definitions and regimes of which overlap and are not well defined. Some details of the reactions mentioned will be shortly mentioned in what follows.

In “Nuclear Physics Academic Press ” the definition of **spallation** is the following: a type of nuclear reaction in which the high-energy level of incident particles causes the nucleus to eject more than three particles, thus changing both its mass number and its atomic number. In the context of ADS or high intense neutron sources spallation is seen as the desintegration of a nucleus by means of high energetic proton induced reactions. In this way approximately 40 neutrons per incident GeV proton are produced, a number that represents as much as 20 times as for a fission reaction in a conventional nuclear power plant with energy spectra of the neutrons similar up to the evaporation regime, but extending to higher energies up to the incident proton energies in case of spallation reactions. An energetic particle entering a massive target gives rise to a complex chain of interactions resulting in the emission of various particles, some of which are able to escape the target volume. The latter particles can be detected in the experiment

and provide information on the transport process involved. These processes can be viewed as a convolution of two types of cascades [Se47], such that particles released in a primary intra-nuclear cascade (INC) give rise to a inter-nuclear cascade of secondary and higher order reactions in the surrounding target material. A description of this reactions can be seen in Figure 3.3.

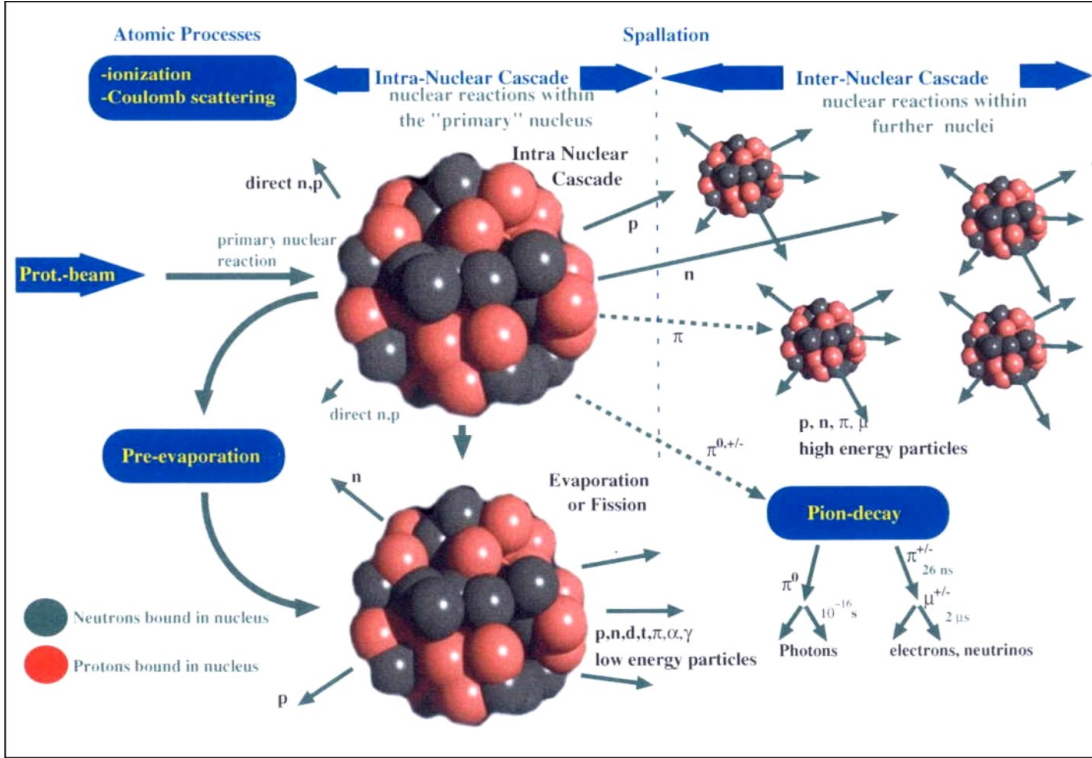


Figure 3.3: Illustration of particle interactions on the intra-, inter- and evaporation level, [Go04].

In the first stage the high energetic particle interacts with the individual nucleons instead of the formation of a compound nucleus as in low energy reactions. Initial collision leads to an ejection of nucleons and pions, which still have enough energy to produce a cascade reaction (intranuclear cascades). After this phase the nucleus is left in an excited state and goes to the ground state by evaporation of nucleons, mostly neutrons. In the secondary stage of the spallation reaction also **fission** may occur. Fission is the binary splitting of an excited nucleus into two approximately equal parts (Figure 3.4). It is understood as a consequence of the deformation when repelling electrostatic Coulomb forces on the proton overbalance the short ranging attractive nuclear forces. A ground-state-deformed nucleus is situated in the minimum of the potential energy which increases with increasing deformation towards the so-called saddle point deformation. Beyond the saddle point the potential energy declines due



to the decreasing Coulomb repulsion until the scission point is reached. Then the nucleus is constricted in such a way that fragmentation into two parts is likely.

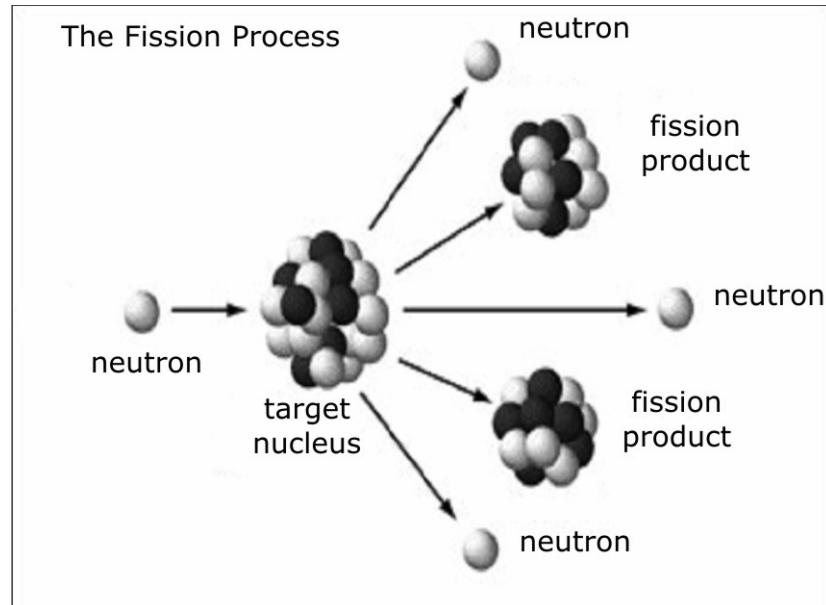


Figure 3.4: Illustration of a fission reaction

Another process occurs with the formation of intermediate mass fragments (IMFs) at higher temperatures as a consequence of increasing thermal motion linked with the increasing mean distance of the nucleons. An excited remnant achieves thermal equilibrium state and then expands, eventually reaching the freeze-out volume. At this point it fragments into neutrons, light charged particles and IMFs. This process is called **multi-fragmentation**. Due to the short ranging nuclear forces of nucleons the mean field collapses and IMFs are formed by condensation. For more details on the above described phenomena the reader is kindly referred to [Go04].

## 3.2 Experimental Approach

The measurement of integral cross-sections for the production of residual nuclides by proton induced reactions can be achieved using two different methods: classical kinematics and inverse kinematics. In what follows the two methods will be shortly described and the advantages and disadvantages of using them will be emphasized.

### 3.2.1 Classical kinematics

Classical kinematics consists in the irradiation of a target with protons or neutrons of the energy of interest and by analysing the produced species after irradiation

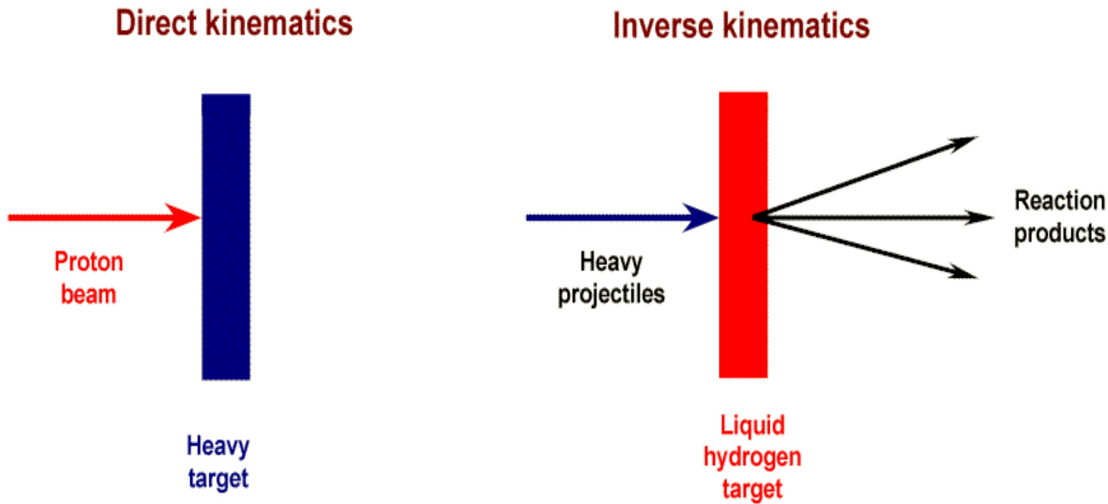


Figure 3.5: Classical kinematics versus Inverse kinematics

by means of off-line  $\gamma$ -spectrometry or by off-line and on-line mass spectrometry. The target can be irradiated either in the form of single foils or directly as a whole foil pile, called “stack”, hence the name of this method: “stacked-foil technique” (Figure 3.6). Both have advantages and disadvantages. During the irradiation of single foils unwanted reactions of secondarily produced particles in the target can be neglected, which is not always ensured in massive stacks. If many targets are to be examined, the irradiation of single foils is time consuming and not cost effective, so the stacked foil technique is preferred. This experimental approach allows the determination of cross-sections for several projectile energies because the primary particle meets the different targets with different energies, due to its deceleration in the stack. It provides very important information on the energy dependence of the production of specific nuclides which is extremely valuable for the understanding of the energy dependence of the different reaction mechanisms. Because of the time delay between the irradiation and measurement results are confined to residual nuclides with usually at least few hours half-lives which mostly reveal a cumulative production due to the decay of short lived progenitors. So this method can only give a limited insight into the reaction mechanism and information on the reaction kinematics is also not easily accessible.

### 3.2.2 Inverse kinematics

Inverse kinematics consists in the bombardment of an hydrogen target with heavy projectiles (Figure 3.7). In this case the heavy target nuclei acts as projectile. The

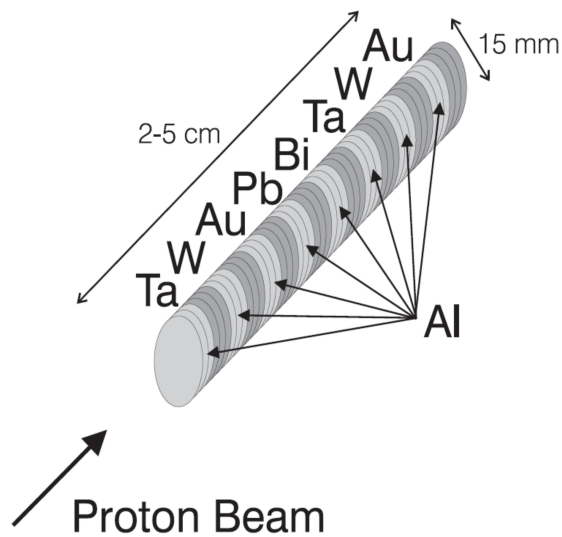


Figure 3.6: Example of an experimental setup for the stacked foil technique

reaction products are identified in-flight in a high resolution spectrometer and their mass and atomic number are determined. At the same time, information on the reaction kinematics is available, permitting to distinguish between fragmentation and fission products, due to their different kinematic properties. Using this technique all the primary residuals can be identified at certain energy points but not over the whole energy range desired, due to the efforts needed to perform this type of measurements. The combined information of these two experimental techniques, however, provide a basis for an improved understanding of nuclear reaction aspects and for improvements of the nuclear models, which now allow performing considerably more realistic calculations.

### 3.3 Determination of Cross-Sections for the Production of Residual Nuclides

#### 3.3.1 General case

Consider the nuclear reaction  $T(p,x)R$ , where a projectile  $p$  incident on the target nucleus  $T$  produces the residual  $R$  and an emitted particle  $x$ . Here  $\Phi$  is the projectile flux density. The cross-section  $\sigma$  represents the probability of occurring the reaction. The produced residual nuclide  $R$  with half-life  $T_{1/2}$  is also radioactive and is subject to the decay law  $N(t) = N_0 e^{-\lambda t}$  with decay constant  $\lambda = \frac{\ln(2)}{T_{1/2}}$ . The decay rate

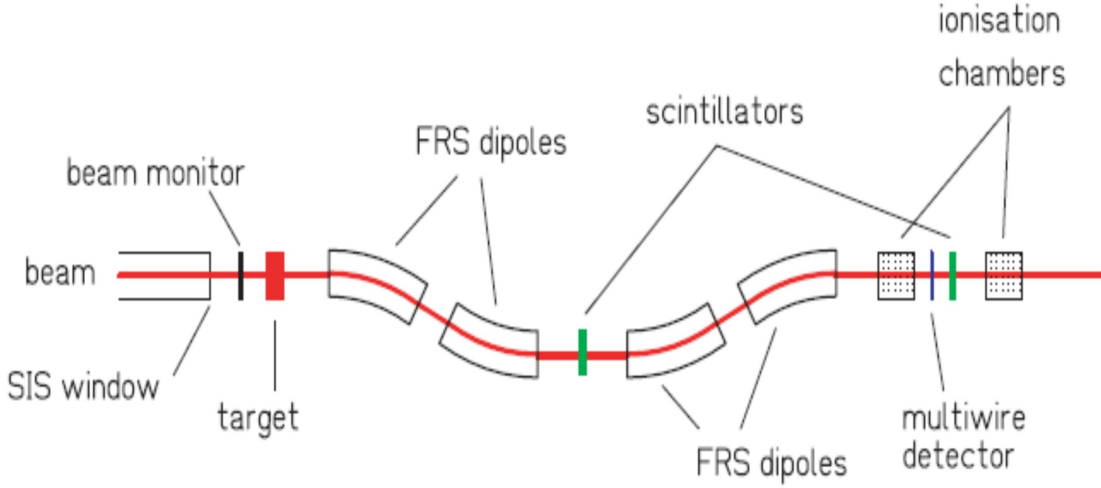


Figure 3.7: Example of an experimental setup for the inverse kinematics technique: Schematic view from above of the horizontal section of the experimental setup [Ri06] (FRS-fragment separator was used as a high resolution spectrometer)

for the residual is therefore:

$$\frac{dN_R}{dt} = \sigma_E \Phi_E N_T - \lambda N_R \quad (3.14)$$

which follows, with the initial condition  $N_R(t=0) = 0$ ,

$$N_R(t) = \frac{\sigma_E \Phi_E N_T}{\lambda} (1 - e^{-\lambda t}), t \leq t_{EOI} \quad (3.15)$$

At the end of the irradiation with the duration  $t_{irr}$  the activity becomes:

$$A(t_{EOI}) = \lambda N_R = \sigma_E \Phi_E N_T (1 - e^{-\lambda t_{irr}}) \quad (3.16)$$

In a measured  $\gamma$ -spectrum we obtain a number  $C$  of counts in a net full-energy peak at  $\gamma$  energy  $E_\gamma$  where a nuclide emits  $\gamma$ -quanta with an abundance  $I_\gamma(E_\gamma)$  which are detected with an efficiency  $\varepsilon_\gamma(E_\gamma)$ .  $C$  is related to the activity  $A$  of this nuclide between the beginning of the counting ( $BoC$ ) and the end of the counting ( $EOC$ ) according to

$$C = \int_{t_{BoC}}^{t_{EOC}} dt \varepsilon_\gamma(E_\gamma) I_\gamma(E_\gamma) A(t) \quad (3.17)$$

Integration of Eq. 3.17 yields for the activity at the end of irradiation ( $EOI$ )

$$A(t_{EOI}) = \frac{C\lambda}{I_\gamma \varepsilon_\gamma (1 - e^{-\lambda t_c})} e^{\lambda t_d} \quad (3.18)$$

with  $t_c = t_{EOC} - t_{BOC}$  being the counting time,  $t_d = t_{BOC} - t_{EOI}$  the decay time between end of irradiation ( $EOI$ ) and beginning of count ( $BOC$ ). The production and decay of the nuclide during the time of irradiation  $t_{irr}$  of a sample consisting of  $N_T$  target atoms with projectile of flux density  $\Phi$  is for negligible burn-up of the targets described by:

$$A(t) = N_T \sigma \Phi (1 - e^{-\lambda t}), 0 \leq t \leq t_{irr}, \quad (3.19)$$

with the cross section  $\sigma$  to be determined. Combining Eq. 3.18 and Eq. 3.19 yields:

$$\sigma = \frac{C\lambda}{I_\gamma \varepsilon_\gamma \Phi N_T} \frac{e^{\lambda t_d}}{(1 - e^{-\lambda t_c})(1 - e^{-\lambda t_{irr}})} \quad (3.20)$$

### 3.3.2 Independent and cumulative cross-sections

Equations 3.19 and 3.20 are strictly valid only for the so-called independently produced radionuclides because the only production mechanism assumed is the nuclear reaction leading to the produced nuclide. But in the majority of cases a further production by  $\beta^-$ ,  $\beta^+$ , EC or  $\alpha$ -decays of a radioactive precursor has to be taken into account. Since there are sometimes ambiguities existing about the terms independent and cumulative cross-sections some clarifications have to be given.

A cross-section for the production of a nuclide is denoted as independent if the nuclide can only be produced directly via the nuclear reaction between the projectile and the target nucleus and not via subsequent  $\beta^-$ ,  $\beta^+$ , EC or  $\alpha$ -decays. Such independent cross-sections are obtained if:

- either the nuclide is shielded by stable nuclides against  $\beta$  decay or by a long lived progenitor
- or the cross-section for the production of a progenitor is also measured so that the production via decay can be corrected for.

In all other cases the cross-sections are cumulative since they include also the production via decay of precursors. If we consider, e.g. the production of a nuclide  $D$ (aughter) on one hand by the nuclear reaction and on the other hand by decay of radioactive precursor  $M$ (other) then the solution of the differential equation

corresponding to Eq. 3.19 for the activity  $A_D(t)$  of  $D$  for times  $t > t_{irr}$

$$A_D(t) = N_T \Phi \left( \left( \sigma_D + \sigma_M \frac{\lambda_M}{\lambda_M - \lambda_D} \right) (1 - e^{-\lambda_D t_{irr}}) e^{-\lambda_D t} \right. \\ \left. + \sigma_M \frac{\lambda_D}{\lambda_M - \lambda_D} (1 - e^{-\lambda_M t_{irr}}) e^{-\lambda_M t} \right), \quad (3.21)$$

where  $\sigma_D, \sigma_M$  are the independent cross-sections for the mother  $M$  and the daughter  $D$ , respectively. Provided that the half-life of  $M$  is short compared to that of  $D$  ( $\lambda_M \gg \lambda_D$ ) we can neglect the second term in Eq. 3.21 for large  $t_d$ . This yields:

$$\sigma_{D,cum} = \sigma_D + \sigma_M \frac{\lambda_M}{\lambda_M - \lambda_D}, \quad (3.22)$$

with the cumulative cross-section  $\sigma_{D,cum}$  of the nuclide  $D$  calculated according to Eq. 3.20.

### 3.3.3 Corrections for radioactive progenitors

In the condition  $\lambda_M \gg \lambda_D$  under which we derived the cumulative cross-section  $\sigma_{D,cum}$  of  $D$  is fulfilled and we are able to measure  $\sigma_M$ , then we can derive the independent cross-section  $\sigma_D$  for the production of  $D$  from Eq. 3.22. However, there are some cases in which  $\lambda_M \gg \lambda_D$  is not satisfied. For such cases we proceed as follows. Assume a mother nuclide  $M$  of known activity  $A_M$  decaying with decay constant  $\lambda_M$  into the daughter  $D$  with  $\lambda_D$  for which wrong activities  $A_D^*$  are calculated according to Eq. 3.18. Solving the system of coupled differential equations describing the decay of the mother and the decay and buildup of the daughter after the end of irradiation ( $t=0$ ) we calculate the corrected activity according to Eq. 3.23 and obtain the independent cross-section of the daughter via Eq. 3.24:

$$A_D(t_{EoI}) = A_{t_{EoI}}^* + A_M(t_{EoI}) \frac{\lambda_D}{\lambda_D - \lambda_M} \left( 1 - \frac{\lambda_D}{\lambda_M} \frac{1 - e^{-\lambda_M t_c}}{1 - e^{-\lambda_D t_c}} e^{-(\lambda_M - \lambda_D t_d)} \right) \quad (3.23)$$

$$\sigma_D = \frac{A_{t_{EoI}}^*}{N_T \Phi (1 - e^{-\lambda_D t_{irr}})} - \sigma_M \left( 1 - \frac{\lambda_D}{\lambda_D - \lambda_M} \left( 1 - \frac{1 - e^{-\lambda_M t_{irr}}}{1 - e^{-\lambda_D t_{irr}}} \right) \right) \quad (3.24)$$

### 3.3.4 Corrections for $\gamma$ -interferences

From the very complex spectra we dealt with in this work, the cross-sections for some nuclides could only be determined after the correction of interfering  $\gamma$ -lines

from another nuclide which could not be resolved by our detectors. Assume that  $A_1(t_{EoI})$  and  $A_2(t_{EoI})$  are the activities of two nuclides at the end of irradiation which have interfering  $\gamma$ -lines with  $I_{\gamma_1}$  and  $I_{\gamma_2}$  being the abundances of the corresponding  $\gamma$ -quanta. Then first a wrong activity  $A_1^*(t_{EoI})$  is calculated according to Eq. 3.18 in our evaluation procedure under the assumption that the peak is only caused by nuclide 1. If  $A_2(t_{EoI})$  is known, e.g. from other  $\gamma$ -lines of nuclide 2, we can calculate the correct value of  $A_1(t_{EoI})$  to be:

$$A_1(t_{EoI}) = A_1^*(t_{EoI}) - A_2(t_{EoI}) \frac{\lambda_1 I_{\gamma_1}}{\lambda_2 I_{\gamma_2}} \frac{1 - e^{-\lambda_2 t_c}}{1 - e^{-\lambda_1 t_c}} e^{-(\lambda_2 - \lambda_1)t_d} \quad (3.25)$$

Although it is in principle possible to apply this scheme to more than only one interfering  $\gamma$ -line we limit ourselves to one correction term since the resulting uncertainty of the corrected activity quickly becomes rather high if the correction is large.





---

## 4 Experiments at TSL and LNS

### 4.1 Overview

Between 1993-1997 a number of experiments were performed at the SATURNE II synchrocyclotron of the Laboratoire National Saturne(LNS) at Saclay and at the cyclotron of the Svedberg Laboratory at Uppsala(TSL). At that time it was not possible to evaluate all the experiments. For some of the samples  $\gamma$ -spectrometric measurements were performed, but some of them were only irradiated and the  $\gamma$ -spectrometric measurements were left to be done at a later moment in time for long-lived radionuclides only. It is the case of experiments SACL0L, UPPS0H and UPPS0S, the subject of this work. These experiments were evaluated and the obtained results are presented in this work.

Integral cross-sections for the production of residual radionuclides were determined by off-line  $\gamma$ -spectrometry of irradiated thin targets. The experimental setup will be described shortly in the following sections. For more details see [Gl01], where the techniques used are described extensively.

### 4.2 Targets and Irradiations

To avoid additional production of nuclei by interaction of the protons with elemental impurities only high-purity materials were used as targets.

Each target was thoroughly cleaned and weighted before the irradiation. Typical weights of the individual targets with diameters of 15 mm were 10 or 33 mg/cm<sup>2</sup> for aluminum (99.999%). Targets were supplied by Goodfellow Metals Ltd., UK.

In order to allow the examination of many targets at different energy points, with a minimum requirement of beam-time, a stacked-foil technique was used at both locations LNS and TSL. Some details about the total experiments have to be mentioned at this point.

A large number of target elements was irradiated in each irradiation. This was done in order to check consistency of the new cross-sections with earlier results as well as to provide further targets of previously irradiated elements for further destructive investigations of long-lived radionuclides by accelerator mass spectrometry or of stable rare gas isotopes by conventional mass spectrometry. As a consequence, up to 36 elements scattered over the whole periodic system of elements from carbon to bismuth were irradiated in one experiment at LNS.

The proton irradiations were performed between 1995 and 1997 at the SATURNE II synchrocyclotron of the Laboratoire National Saturne at Saclay(LNS,  $E > 200$  MeV), France and at the Svedberg Laboratory at Uppsala(TSL,  $E < 200$  MeV). A detailed survey of the experiments performed at LNS and TSL can be found in Tables 4.1 and 4.2.

### Irradiations at TSL

At TSL the stacked foil technique was used, since the influences of secondary particles on the production of the residual nuclides studied here can be neglected in this energy range.

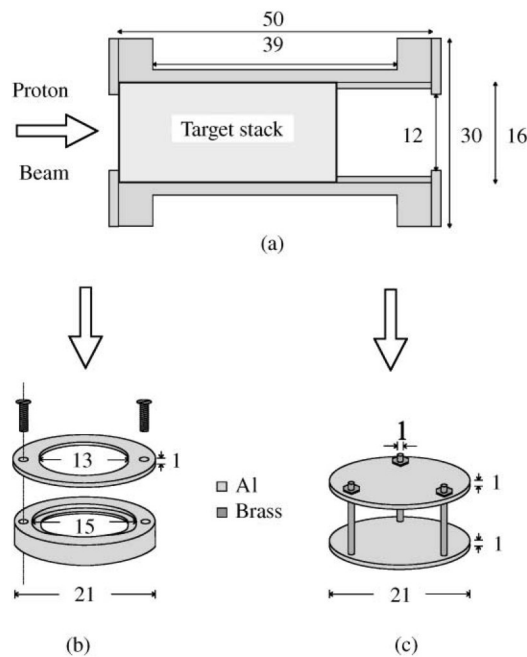


Figure 4.1: (a) Target containers used in experiments at TSL and LNS ; (b,c) the new and smaller target containers used in the experiments at LNS . At LNS the individual mini-stacks of type c were positioned in the beam by hanging them up on thin threads in the center of Al-frames which were not hit by the primary protons. Dimensions are given in mm [Gl98].

A variety of target elements were arranged in stack (in order of increasing mass) in different energy groups. In each group at least three different foils were put together in order to eliminate recoil effects for the foil in the middle which usually was analysed. Between these groups three Al monitor foils were inserted. The foils were used to further avoid recoil effects but also served for beam monitoring. Doing so, the flux densities were determined via the reaction  $^{27}\text{Al}(p, 3p3n)^{22}\text{Na}$  using the cross sections

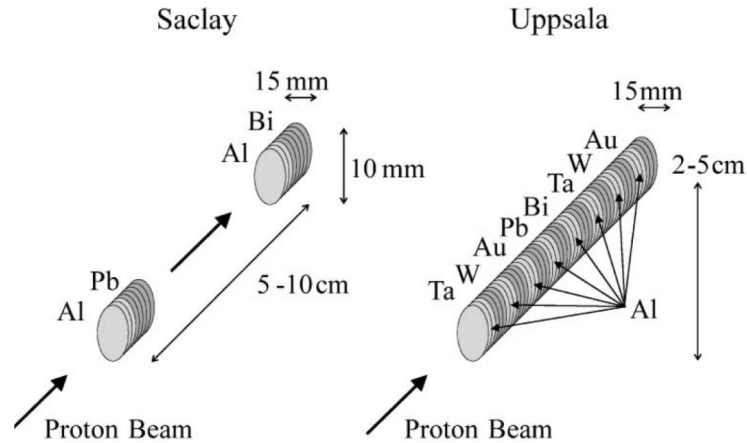


Figure 4.2: Schematic view of the target arrangements used (a) at LNS for energies above 200 MeV and (b) at TSL for energies below 180 MeV [Gl98].

given by [To81, St90]. The proton energy for each individual foil was calculated by means of the semiempirical approach given by Andersen and Ziegler [An77] using the update for the stopping power parameters given in the 1996 edition of the Table of Isotopes [Fi96].

### Irradiations at LNS

For the irradiations at LNS with energies above 200 MeV the mini-stack approach was used in order to reduce secondary particle effects [Gl01]. In this set-up three Al monitor foils and at least three target samples were put together in a so-called mini-stack. In each irradiation up to 30 individual mini-stacks were aligned in the beam with distances of 510 cm in-between. The final supports consisted of Al-frames which were not hit by the primary beam and in the center of which the ministacks were hanged by thin threads. The whole arrangement was optically adjusted using a laser beam to ensure that each mini-stack is in the beam line. The proton fluxes were again determined via the reaction  $^{27}\text{Al}(p, 3p3n)^{22}\text{Na}$  using the cross sections given by [To81, St90] and the proton energies were again calculated using the approach presented in [An77, Fi96]. For further information see [Mi97, Gl01]. The targets were arranged in a sequence of increasing atomic number along the beam. For light-target elements, several elements were packed together in one individual mini-stack. The irradiations were performed in air and lasted typically about twelve hours to get sufficient fluence. Though a stacked foil technique was used, only one energy point was investigated per irradiation for each target element.

<b>Experiment</b>	<b><math>E_{p,i}</math> [MeV]</b>	<b><math>E_{p,f}</math> [MeV]</b>	<b><math>t_{EoI}</math></b>	<b><math>t_{irr}</math> [s]</b>	<b><math>\xi</math> [g/cm<sup>2</sup>]</b>
SACL0C	1600	1565	14.10.1993 08 <sup>53</sup>	60180	22.9
SACL0D	1200	1161	15.10.1993 08 <sup>07</sup>	74040	21.1
SACL0E	800	752	19.05.1994 08 <sup>00</sup>	86940	29.5
SACL0F	600	545	20.05.1994 11 <sup>00</sup>	91260	31.0
SACL0G	400	309	06.10.1994 08 <sup>04</sup>	121200	39.7
SACL0H	330	228	07.10.1994 07 <sup>58</sup>	76200	38.5
SACL0K	280	119	10.07.1995 08 <sup>00</sup>	67320	49.7
<b>SACL0L</b>	<b>2600</b>	<b>2525</b>	<b>11.07.1995</b> <b>07<sup>17</sup></b>	<b>72180</b>	<b>48.5</b>
SACL0M	1400	1341	04.10.1995 14 <sup>07</sup>	70980	37.4
SACL0N	1000	938	05.10.1995 09 <sup>00</sup>	60480	38.1
SACL0P	280	188	22.05.1996 09 <sup>56</sup>	55500	31.1
SACL0R	2600	2541	23.05.1996 09 <sup>05</sup>	63600	37.7

Table 4.1: Survey on experiments performed at LNS

### 4.3 Measurements and evaluation of experimental data

#### 4.3.1 $\gamma$ Spectrometry

After the end of irradiation, the targets were transported to Cologne where the stacks and ministacks were dismantled and the individual targets separated. A part of them stayed at Cologne for measurement, another one was transported to Hanover for the same purpose. The  $\gamma$ -spectrometric measurements started about between 36 and 60 h after the end of irradiation, respectively. In the case of this work this is true for UPPS0H and SACL0L.

<b>Experiment</b>	<b><math>E_{p,i}</math></b> <b>[MeV]</b>	<b><math>E_{p,f}</math></b> <b>[MeV]</b>	<b><math>t_{EoI}</math></b>	<b><math>t_{irr}</math></b> <b>[s]</b>	<b><math>\xi</math></b> <b>[g/cm<sup>2</sup>]</b>
UPPS0B	176.5	64.1	17.11.1993 02 <sup>00</sup>	13380	30.4
UPPS0C	175.9	72.7	19.01.1994 23 <sup>10</sup>	25200	28.4
UPPS0D	178.2	105	29.11.1994 19 <sup>00</sup>	13380	17.8
UPPS0E	178.2	86.7	30.11.1994 07 <sup>00</sup>	21000	22.7
UPPS0F	136.1	61.4	22.02.1995 06 <sup>00</sup>	12180	15.2
UPPS0G	136.1	74.2	21.02.1995 21 <sup>30</sup>	12000	16.0
UPPS0H	137.0	59.1	10.10.1995 21 <sup>40</sup>	11400	16.7
UPPS0K	136.5	58.6	21.11.1995 20 <sup>10</sup>	-	19.3
UPPS0L	177.3	128.8	19.03.1996 23 <sup>30</sup>	12360	12.0
UPPS0M	177.3	130.0	20.03.1996 03 <sup>12</sup>	10320	13.8
UPPS0N	97.2	0	15.10.1996 19 <sup>53</sup>	14820	14.6
UPPS0P	97.2	0	16.10.1996 07 <sup>00</sup>	16200	12.0
UPPS0R	97.5	24.6	12.03.1997 07 <sup>22</sup>	19260	13.0
UPPS0S	97.5	38.6	11.03.1997 19 <sup>00</sup>	14400	9.8

Table 4.2: Survey on experiments performed at TSL

### $\gamma$ -spectrometric measurements

The  $\gamma$ -spectrometric measurements were performed using several high-purity germanium (HPGe) and germaniumlithium (Ge(Li)) detectors partially equipped with automatic sample changers to be used for the short-time measurements. Each detector was connected via pre- and spectroscopy amplifiers to computer-controlled multi-channel buffers whose built-in ADC digitized the pulses into spectra of usually 4096 channels. The amplification was chosen for the registration of  $\gamma$ -quanta with energies

between some tens of keV and about 2 MeV. Typical resolutions ranged from about 1 keV at 122 keV of  $^{57}\text{Co}$  to about 2 keV at 1332 keV of  $^{60}\text{Co}$ . The absolute calibration of the  $\gamma$ -spectrometers was performed for each geometry used by calibrated radionuclide sources ( $^{22}\text{Na}$ ,  $^{57}\text{Co}$ ,  $^{60}\text{Co}$ ,  $^{137}\text{Cs}$ ,  $^{133}\text{Ba}$ ,  $^{152}\text{Eu}$ , and  $^{241}\text{Am}$ ) with certified accuracies of  $\leq 2\%$  (PTB Braunschweig). Efficiency functions were obtained by fitting a double logarithmic linear function to the experimental efficiency data above 350 keV. Below this energy a fit function according to Gray and Ahmad [Gr85] was chosen. The efficiencies were repeatedly checked for each geometry for every detector.

Energy calibration was done using a least-squares fit to a second-order polynomial for the energies of the calibrated radionuclide sources. To avoid problems with too high dead-times and pile-up effects the distances between sample and detector window were varied between 5 and 60 cm. Thus it was possible to keep the dead-time below 10% with no detectable pile-up effects. The large distances were used especially for the short time measurements shortly after the irradiations because of the high activities of the samples. In these geometries no lead shielding of the detector was possible but interferences with background  $\gamma$ -lines were negligible anyway due to the short counting times as well as due to the high Compton-background caused by the measured samples themselves. Background spectra were taken for these measurements for about 3 days for each detector. These spectra were used in the data evaluation procedure to correct measured activities for background interferences. Measurement times ranged from 5 min in the beginning up to about 7 hours in some cases at the end of a measurement series.

### 4.3.2 Analysis of spectra

#### Stopping power and calculation of proton energies

Since a stacked-foil technique was applied the proton energies in all the different target foils had to be calculated. Although the energy degradation was small for the highest initial proton energies such calculations were performed for all irradiations at LNS and TSL. This was done by a computer program called “Stack”, originally based on the work of Andersen and Ziegler [An77]. An improved version with some updates [Fi96, Zi85] showed no significant difference to the older version [Mi97].

Stopping power is defined as the average energy loss of a charged particle per unit path length:

$$S = -\frac{dE}{ds} \quad (4.1)$$

The determination of the stopping power can be performed in many complex ways. Here is an example of the calculation of linear energy loss with the help of the Bethe-Bloch equation for heavy charged particles.

$$-\frac{dE}{ds} = \frac{4\pi z^2 e^4}{m_e \nu^2} N^V \cdot B, \quad (4.2)$$

$$B = Z \left[ \ln \frac{2m_e \nu^2}{I} - \ln(1 - \beta^2) - \beta^2 - \frac{c_k}{Z} \right], \quad (4.3)$$

$$\beta = \frac{\nu}{c}, \quad I = 11,5 \cdot Z \text{ (eV)}$$

where

- $-\frac{dE}{ds}$  Stopping power
- $z$  Atomic number of the heavy charged particle
- $m_e$  Rest mass of the electron
- $\nu$  Velocity of the heavy charged particle
- $N^V$  Number of nuclei of the absorber per  $\text{cm}^3$
- $B$  Atomic stopping number
- $Z$  Atomic number of the absorber
- $I$  Mean ionisation potential of the absorbers
- $c_k$  Correction factor for  $E < 4 \text{ MeV}$ ,  $0 < c_k < 1$ , charge exchange

At high energies ( $>1 \text{ MeV}$  per atomic mass unit) the stopping formula [An77] shows the dependence on two parameters, the mean ionization potential and the shell correction. These both parameters are different for different stopping materials. Experimental proton stopping power data are summarized by Anderson and Ziegler [An77]. Reliable data for many elements are available over a wide range of energies.

In Figure 4.3 is indirectly illustrated the dependence of the stopping power on the velocity of the charged particle by the representation of  $\frac{dE}{ds}$  as a function of traveled distance  $s$ . This behaviour is very important for applications in radiation therapy, when one needs to irradiate certain tumors with minimum damage to the external tissues.

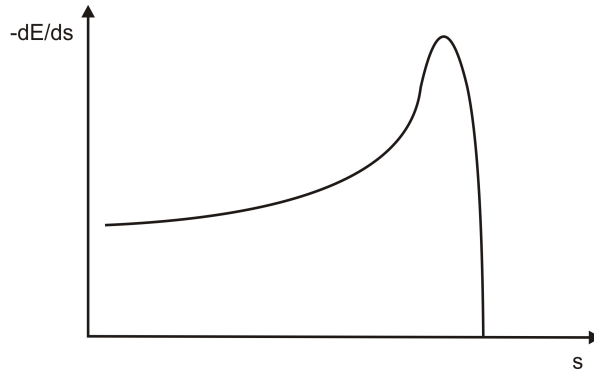


Figure 4.3: Bragg ionization curve

### Analysis of $\gamma$ spectra

The analysis of the  $\gamma$  was done by the commercially available code GAMMA-W [We95, We94]. GAMMA-W calculates net peak areas via an unfolding algorithm using a least-squares fit [We81]. For an evaluation, regions of a spectrum are defined in which all peaks are unfolded simultaneously after the background has been calculated according to [We81, We86]. Peak shapes are assumed to be Gaussian with a low-energy tailing. For each detector and measuring geometry, parameters were determined and supplied to the code which describe as function of energy or channel numbers the full-width at half-maximum of full-energy peaks and their tailings. The whole evaluation procedure can be done either in an automatic mode or interactively by the user. Although GAMMA-W is a sophisticated and successful code [B197], detailed tests showed in our case that for complex spectra the automatic mode is not reliable enough with respect to the necessary regioning of the spectrum, peak recognition, background determination, multiplet deconvolution and net-peak area calculation. Thus, we analyzed each spectrum interactively, making sure to get a maximum of information out of each spectrum. Proceeding in this way means, however, to give up the reproducibility of a spectrum analysis in contrast to the automatic and strict application of a mathematical algorithm.

### Nuclide identification

The spectrum analysis by Gamma-W code gives us an output file with net peak areas of the produced radionuclides as the parent decay. In the output file we have  $\gamma$ -energy with net peak area and also the uncertainty in it. Most codes and also Gamma-W offers such capabilities, but in general an algorithm which can be used with some confidence for complex spectra does not seem to exist. For identification of



residual nuclides we used the database provided by the Lund Nuclear Data Center [Lu08].

Product	Energy	I_gamma (%)	T <sub>1/2</sub>
Be-7	477,6	10,52	53.12d
Ca-47	1297,09	71	4.536d
Co-55	931,3	75	17.53h
Co-56	846,771	100	77.27d
	1238,282	67,6	77.27d
Co-57	122,06	85,6	271.79d
Co-58	810,775	99	70.86d
Co-60	1173,237	99,97	5.2714y
	1332,501	99,98	5.2714y
Cr-48	112,36	96	21.56h
	308,25	100	21.56h
Cr-51	320	10	27.70d
Cu-61	656,008	10,77	3.33h
Cu-64	1345,84	0,473	12.7h
Fe-59	1099,25	56	44.5d
	1291,597	43,2	44.5d
K-42	1524,7	18	12.36h
K-43	220,6	4,3	22.3h
	372,76	87	22.3h
	396,86	11,85	22.3h
	593,39	11,26	22.3h
	617,49	79,2	22.3h
Mg-28	400,56	36,6	20.91h
	941,72	38,3	20.91h
	1342,27	52,6	20.91h
Mn-52	744,23	90	5.59d
	935,538	94,5	5.59d
	1434,068	100	5.59d
Mn-54	834,848	99,97	312.3d
Na-22	1274,5	99,94	2.6019y
Na-24	1368,63	100	14.95h
	2754,028	99,94	14.95h
Ni-56	158,38	98,8	6.077d
	269,5	36,5	6.077d
	480,44	36,5	6.077d
	749,95	49,5	6.077d
	811,85	86	6.077d
	1561,8	14	6.077d
Ni-57	127,164	16,7	35.6h
	1377,63	81,7	35.6h
	1757,5	7,09	35.6h
	1919,52	12,26	35.6h
Sc-43	372,8	23	3.89h
Sc-44	1157	99	3.927h
Sc-44m	271,13	86,7	58.6h
Sc-46	889,277	99,984	83.76d
	1120,542	99,987	83.76d
Sc-47	159,377	68,3	3.34d
Sc-48	983,51	100	43.67h
	1037,599	97,6	43.67h
	1312,096	100	43.67h
V-48	983,51	99,98	15.97d
	1312,096	97,5	15.97d

Table 4.3: Nuclear data used in this work for the determination of experimental cross-sections

### 4.3.3 Contribution of uncertainties

#### Uncertainties of proton energies

Whereas the exact values of the contributions to the error of a result of a measurements are unknown and unknowable, the uncertainties associated with the random and systematic effects that give rise to error can be evaluated. But even if the evaluated uncertainties are small, there is no guarantee that the error in the measurement is small. The proton beam which falls on the target stack has three sources of uncertainties:

1. The first source is the uncertainty in the proton energy when the particles leaving the accelerator and is denoted by  $\Delta E_A$ .
2. The second source of uncertainty is that the protons are slowed down when they collide with the nuclei of the target. Thus if we represent the proton initial energy by  $E_{n,i}$  and hence after the interaction with the nuclide it is slowed down. As a result the energy turned into  $E_{n,f}$ . Thus in this case we have the energy difference in the form of kinetic energy of protons as  $\Delta E_{loss} = \frac{1}{2}(\Delta E_{n,i} - \Delta E_{n,f})$
3. Third source of uncertainty in the proton energy is the statistical nature of slowing down processes. There is an energy straggling which can be described according to [?] by Gaussian distribution with a characteristic width, the straggling parameter  $\alpha_i$ . The parameter  $\alpha$  we take from the output file of program Stack.

Combination of these uncertainties gives the uncertainty of proton energy  $E_n$  in the  $n^{th}$  target foil of a stack in the form

$$\Delta E_n = \sqrt{(\Delta E_A)^2 + (\Delta E_{loss})^2 + \left(\sum_{i=1}^n \alpha_i\right)^2} \quad (4.4)$$

#### Uncertainties of cross-sections

The following sources of uncertainties were considered for the cross-sections:

- Uncertainty in the determination of net peak areas:

This source of uncertainty is calculated by the evaluation code used for the spectrum analysis [To81]. It takes into account the Poisson uncertainties of the counts in the individual channels as well as the uncertainties of the background determination, propagating them according to the law of error propagation through the unfolding procedure. Sometime it is difficult to assign a peak to a nuclide,

because it is produced not only by a single nuclide. Now, if the contribution is not negligible, the activity of the contributing nuclide can be determined using another line or in later spectrum the interfering lines were corrected using this activity. If it seems that the contributions of other nuclides are very small then no correction is applied. Due to this procedure it has been assumed a maximum inaccuracy of 2% from the contribution of the other nuclides, but it must be pointed out that in the average this uncertainty should be smaller.

- Uncertainties of the half-lives:

Half-lives were taken from [Lu08]. Uncertainty of 1% were considered in the half-lives. Larger uncertainty may cause disagreements between different measurements due to the exponential dependence on time.

- Uncertainty of  $\gamma$ -abundances:

Intensities were also taken from [Lu08]. Those  $\gamma$ - lines which had high net peak areas were always considered and which were well-known, thus an uncertainty of only 2% were taken into account.

- Uncertainty of efficiency:

Standard calibration sources were supplied with an uncertainty  $\leq 2\%$ . Measurements with both detectors verified the uncertainty of full energy peak efficiency of 5 to 6%.

- Uncertainty of number of irradiated nuclei:

Each foil was weighted with an absolute uncertainty of  $\pm 0.4$  mg. In case of the aluminum catcher foils with typical weights of 60 mg, this resulted in an inaccuracy of about 1%.

- Uncertainty of flux density:

The flux densities were determined via the monitor reaction  $^{27}\text{Al}(p,3p3n)^{22}\text{Na}$  using cross-sections as described in detail in Refs. [Mi97, Bo96]. The uncertainty of flux density is mainly determined by the uncertainties of efficiency and of the mass of the catcher foil which sum up to be about 6%. No uncertainties were attributed to the monitor cross-sections. Moreover, an uncertainty in the monitor cross-section due to an uncertainty of the proton energy was not considered because the monitor excitation function does not vary in the energy region covered.

- Uncertainty of irradiation time, decay time and counting time:

For time scales determined by the half-lives of nuclides observed within this work,

it was assumed that uncertainties of the above-mentioned quantities are negligible.

- Uncertainty of impurities:

Due to the high purity of the target foils, contributions of other constituents were not considered.

- $\gamma$ - $\gamma$ -coincidences:

$\gamma$ - $\gamma$ -coincidences have to be taken into account at very small distances between sample and detector. Since distances from the detector down to 5 cm were used to get a sufficient counting statistics, it would have been necessary to correct them in some cases. But this was not done since the effects were visible only for some special nuclides. In these cases they caused an uncertainty in the determination of activity using different  $\gamma$ -lines of 45%. Consequently, this uncertainty had been taken as a general uncertainty due to  $\gamma$ - $\gamma$  coincidences in case of coincident  $\gamma$ -rays.

- Constancy of flux density over irradiation time:

The beam intensities were continuously monitored and recorded. Using these protocols, interruptions of the irradiations were taken into account using the following replacement in Eq. 3.20

$$\frac{1}{1 - \exp(-\lambda t_{irr})} \rightarrow \sum_{i=1}^n \frac{\exp(\lambda(t_{EoI} - t_{EoI,i}))}{1 - \exp(-\lambda t_{irr,i})} \quad (4.5)$$

Because the flux density itself may not be constant during irradiation we replaced  $\Phi$  in Eq. 3.20 and Eq. 3.21 by

$$\Phi \rightarrow \frac{1}{t_{EoI} - t_{BoI}} \int_{t_{BoI}}^{t_{EoI}} dt^* \Phi(t^*) \quad (4.6)$$

with  $\Phi(t^*)$  being the relative measurements of the beam current. Using these replacements the uncertainties due to fluctuations in the beam intensity become negligible. Moreover, they would affect only the cross-sections for very short-lived nuclides.

- Dead-time and pile-up losses in  $\gamma$ -spectrometry:

The dead-time of the detector systems was automatically corrected. Pile-up effects were not seen because the distances between samples and detector were

varied in the way that the counting rates were low enough to avoid both pile-up and failure of the automatic dead-time correction.

#### 4.4 Flux monitoring

The flux density in each sample was supposed to be the same as in the preceding aluminum catcher foils. Using the guarded Al targets in the middle, the flux density was determined by measuring the  $^{22}\text{Na}$ -activity via the  $\gamma$ -line at 1274.5 keV (I=99.9%). The monitor cross-sections used were those recommended by Tobailem and de Lassus St. Genies [To81] for energies above 200MeV and those measured by Steyn et al. [St90] below 200 MeV; see Ref. [Mi97] for a detailed discussion of the monitor cross-sections. At LNS, the fluences differed by a factor of up to 50 depending on the position of the mini-stack in the total arrangement, but also as a consequence of some variability of the beam currents delivered by the accelerator. At TSL, generally higher beam currents were available and the fluences were about a factor of 10 higher than the highest ones obtained at LNS. In spite of the extremely different experimental conditions, the results showed excellent consistency among the different experiments.

#### 4.5 Experimental results

Data needs for the development of accelerator driven system technologies include target elements like C, Mg, O, Si and Ca as components of building concrete, but also target elements like Cu, which can be found in the structure of the beam pipe or in the accelerator structural materials and Ni which is a component of stainless steel. The experimental results are discussed in this section. Altogether a number of 93 new cross sections were determined. Cross-sections for a nuclide were calculated for different gamma-energy lines in order to ensure the reliability of the work. The results were in good agreement with each other which proves the consistency of the obtained results.

### 4.5.1 Results from UPPS0H

During the UPPS0H experiment the following target elements were irradiated: C, O, Mg, Si, V, Ti, Co, Rb, Mo, In and Te. In this work we deal with C, O, Mg and Si only.

Experiment	Description	Target	Product
Uppsala H	$E_{p,i}=136$ MeV	Al	$^{24}\text{Na}$
	$E_{p,f}=59.1$ MeV	C	$^7\text{Be}$
	$t_{EOI}=10.10.1995/21:40$	Mg	$^7\text{Be}, ^{22}\text{Na}, ^{24}\text{Na}$
	$t_{irr}=11400\text{s}$	O	$^7\text{Be}$
		Si	$^7\text{Be}, ^{22}\text{Na}, ^{24}\text{Na}, ^{28}\text{Mg}$

Table 4.4: Survey on target-product combinations evaluated from UPPS0H

A survey on the details of the experiment and on the target-product combinations evaluated can be found in Tables 4.4 and 4.5. The numerical values of the newly determined cross-sections can be found in tabular form in Table 4.6.

Experiment	Target	Mass in mg	Energy in MeV	Flux density ( $\Phi$ ) in $\text{s}^{-1}\text{cm}^{-2}$	$u(\Phi)$ in $\text{s}^{-1}\text{cm}^{-2}$
Uppsala H	CCUH132	25.33	125.10	1.09E+11	2.10E+09
	CCUH312	25.3	106.40	1.06E+11	2.10E+09
	CCUH552	25.71	82.60	1.02E+11	2.10E+09
	MGUH142	40.21	124.60	1.09E+11	2.10E+09
	MGUH322	37.05	105.90	1.06E+11	2.10E+09
	MGUH572	39.59	82.00	1.01E+11	2.10E+09
	QQUH171	198.91	121.80	1.09E+11	2.10E+09
	QQUH411	201.39	97.45	1.04E+11	2.10E+09
	SIUH162	158.41	123.00	1.09E+11	2.10E+09
	SIUH402	159.26	98.80	1.05E+11	2.10E+09

Table 4.5: Survey on targets evaluated from UPPS0H

As the common product for all irradiated targets is  $^7\text{Be}$  the results for this residual nuclide have been chosen for exemplification and are displayed in Figure 4.4.

Target-Product	Target	Energy in MeV	Cross section in mb
$^{nat}\text{C}(\text{p},\text{x})^7\text{Be}$	CCUH132	125.1	$13.5\pm 1.1$
$^{nat}\text{C}(\text{p},\text{x})^7\text{Be}$	CCUH312	106.4	$12.8\pm 0.9$
$^{nat}\text{C}(\text{p},\text{x})^7\text{Be}$	CCUH552	82.6	$16.9\pm 1.2$
$^{nat}\text{Mg}(\text{p},\text{x})^7\text{Be}$	MGUH142	125	$2.37\pm 0.39$
$^{nat}\text{Mg}(\text{p},\text{x})^7\text{Be}$	MGUH322	105.9	$2.34\pm 0.12$
$^{nat}\text{Mg}(\text{p},\text{x})^7\text{Be}$	MGUH572	82	$1.96\pm 0.15$
$^{nat}\text{Mg}(\text{p},\text{x})^{22}\text{Na}$	MGUH142	125	$42.5\pm 2.9$
$^{nat}\text{Mg}(\text{p},\text{x})^{22}\text{Na}$	MGUH322	105.9	$48.9\pm 0.7$
$^{nat}\text{Mg}(\text{p},\text{x})^{22}\text{Na}$	MGUH572	82	$52.9\pm 1.2$
$^{nat}\text{Mg}(\text{p},\text{x})^{24}\text{Na}$	MGUH142	125	$6.10\pm 0.45$
$^{nat}\text{Mg}(\text{p},\text{x})^{24}\text{Na}$	MGUH322	105.9	$6.38\pm 0.95$
$^{nat}\text{Mg}(\text{p},\text{x})^{24}\text{Na}$	MGUH572	82	$6.89\pm 0.08$
$^{nat}\text{O}(\text{p},\text{x})^7\text{Be}$	QQUH171	121.8	$6.63\pm 0.65$
$^{nat}\text{O}(\text{p},\text{x})^7\text{Be}$	QQUH411	97.45	$6.74\pm 0.31$
$^{nat}\text{Si}(\text{p},\text{x})^7\text{Be}$	SIUH123	123	$141.1\pm 0.4$
$^{nat}\text{Si}(\text{p},\text{x})^7\text{Be}$	SIUH402	98.8	$1.16\pm 0.30$
$^{nat}\text{Si}(\text{p},\text{x})^{22}\text{Na}$	SIUH123	123	$16.6\pm 1.7$
$^{nat}\text{Si}(\text{p},\text{x})^{22}\text{Na}$	SIUH402	98.8	$18.04\pm 0.15$
$^{nat}\text{Si}(\text{p},\text{x})^{24}\text{Na}$	SIUH123	123	$3.46\pm 0.18$
$^{nat}\text{Si}(\text{p},\text{x})^{24}\text{Na}$	SIUH402	98.8	$3.35\pm 0.03$
$^{nat}\text{Si}(\text{p},\text{x})^{28}\text{Mg}$	SIUH123	123	$0.038\pm 0.002$
$^{nat}\text{Si}(\text{p},\text{x})^{28}\text{Mg}$	SIUH402	98.8	$0.033\pm 0.001$

Table 4.6: Cross sections determined for the production of residual nuclides by proton induced reactions in UPPS0H



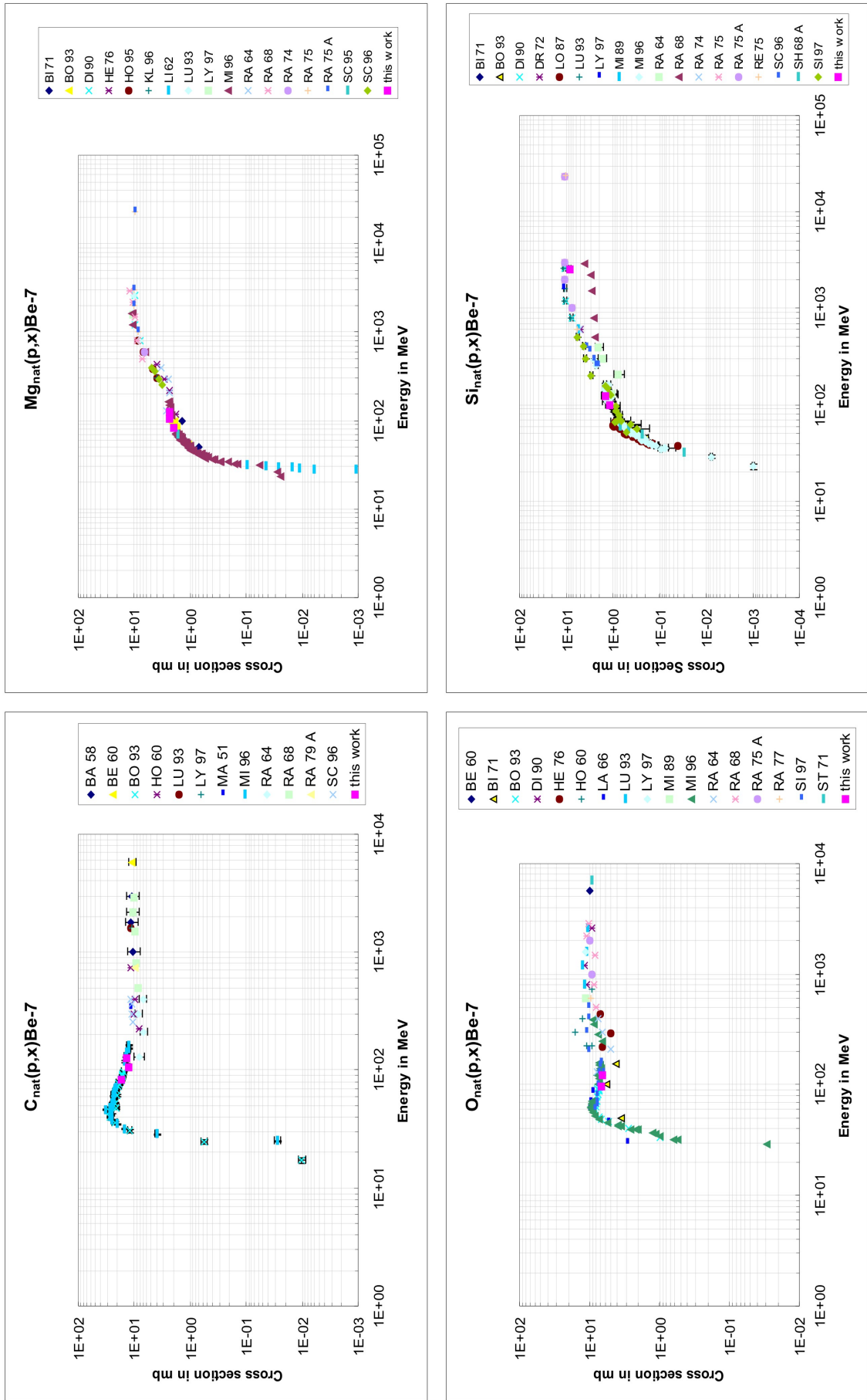


Figure 4.4: Experimental data for the production of  ${}^7\text{Be}$  from natural C, Mg, O and Si

As it will be discussed in the next chapter the production of  ${}^7\text{Be}$  from natural C and O is special because of the proximity in masses between target and product. This is nicely exhibited in the shape of the excitation function. For the target elements Mg and Si, below 100 MeV, contribution of low-energy production is observed and a change in slope can be noticed in the shape of the excitation function at about 200 MeV pointing to different formation modes as evaporation and pre-equilibrium emission at medium energies.

The data are exemplarily compared with earlier works. Our new cross-sections agree within errors with the large existing data base for the production of  ${}^7\text{Be}$ . A complete set of graphs presenting all the experimental data is given in Appendix F.

### 4.5.2 Results from SACL0L

The SACL0L experiment covered Ca, Cu, Ni and Si targets. The targets and the resulted residual nuclides together with a description of the parameters of the experiment can be found in Tables 4.7 and 4.8.

Experiment	Description	Target	Product
Saclay L	$E_{p,i}=2600$ MeV $E_{p,f}=2525$ MeV $t_{EOI}=11.07.1995/07:17$ $t_{irr}=72180$ s	Al	$^{24}\text{Na}$
		Ca	$^7\text{Be}$ , $^{24}\text{Na}$ , $^{43}\text{K}$
		Cu	$^{24}\text{Na}$ , $^{43}\text{K}$ , $^{44}\text{Sc}_m$ , $^{46}\text{Sc}$ , $^{47}\text{Sc}$ , $^{48}\text{Sc}$ , $^{48}\text{Cr}$ , $^{51}\text{Cr}$ , $^{52}\text{Mn}$ , $^{55}\text{Co}$ , $^{56}\text{Co}$ , $^{57}\text{Co}$ , $^{58}\text{Co}$ , $^{57}\text{Ni}$
		Ni	$^{24}\text{Na}$ , $^{43}\text{K}$ , $^{44}\text{Sc}_m$ , $^{48}\text{V}$ , $^{48}\text{Cr}$ , $^{51}\text{Cr}$ , $^{52}\text{Mn}$ , $^{55}\text{Co}$ , $^{56}\text{Co}$ , $^{57}\text{Co}$ , $^{56}\text{Ni}$ , $^{57}\text{Ni}$
		Si	$^7\text{Be}$ , $^{22}\text{Na}$ , $^{24}\text{Na}$ , $^{28}\text{Mg}$

Table 4.7: Survey on target-product combinations evaluated from SACL0L

Experiment	Target	Mass in mg	Energy in MeV	Flux density ( $\Phi$ ) in $\text{s}^{-1}\text{cm}^{-2}$	$u(\Phi)$ in $\text{s}^{-1}\text{cm}^{-2}$
Saclay L	NISL092	426.13	2553	6.10E+08	2.13E+07
	TISL062	107.82	2545	5.85E+08	2.28E+07
	CUSL102	190.88	2556	8.17E+08	3.45E+07
	CFSL052	570.21	2543	9.92E+08	7.04E+07
	SISL042	164.32	2540	9.92E+08	7.04E+07

Table 4.8: Survey on targets evaluated from UPPS0H

I have chosen to exemplify the production of  $^7\text{Be}$  from Ca and the production of  $^{24}\text{Na}$  from Ca, Cu and Si.

Target-Product	Target	Energy in MeV	Cross section in mb
$^{nat}\text{Ca}(p,x)^7\text{Be}$ $^{nat}\text{Ca}(p,x)^{24}\text{Na}$ $^{nat}\text{Ca}(p,x)^{43}\text{K}$	CFSL052	2540	$20.6\pm 1.3$ $2.51\pm 0.23$ $0.49\pm 0.03$
$^{nat}\text{Cu}(p,x)^{24}\text{Na}$ $^{nat}\text{Cu}(p,x)^{43}\text{K}$ $^{nat}\text{Cu}(p,x)^{44}\text{Sc}_m$ $^{nat}\text{Cu}(p,x)^{46}\text{Sc}$ $^{nat}\text{Cu}(p,x)^{47}\text{Sc}$ $^{nat}\text{Cu}(p,x)^{48}\text{Sc}$ $^{nat}\text{Cu}(p,x)^{48}\text{Cr}$ $^{nat}\text{Cu}(p,x)^{51}\text{Cr}$ $^{nat}\text{Cu}(p,x)^{52}\text{Mn}$ $^{nat}\text{Cu}(p,x)^{55}\text{Co}$ $^{nat}\text{Cu}(p,x)^{56}\text{Co}$ $^{nat}\text{Cu}(p,x)^{57}\text{Co}$ $^{nat}\text{Cu}(p,x)^{58}\text{Co}$ $^{nat}\text{Cu}(p,x)^{57}\text{Ni}$	CUSL102	2560	$2.96\pm 0.23$ $1.33\pm 0.18$ $5.25\pm 0.43$ $7.50\pm 0.98$ $2.75\pm 0.19$ $3.08\pm 0.02$ $0.36\pm 0.05$ $18.5\pm 3.2$ $5.96\pm 0.60$ $1.3\pm 0.06$ $7.98\pm 1.40$ $18.1\pm 0.5$ $24.3\pm 2.6$ $0.66\pm 0.06$
$^{nat}\text{Ni}(p,x)^{24}\text{Na}$ $^{nat}\text{Ni}(p,x)^{43}\text{K}$ $^{nat}\text{Ni}(p,x)^{44}\text{Sc}_m$ $^{nat}\text{Ni}(p,x)^{48}\text{Sc}$ $^{nat}\text{Ni}(p,x)^{48}\text{Cr}$ $^{nat}\text{Ni}(p,x)^{51}\text{Cr}$ $^{nat}\text{Ni}(p,x)^{48}\text{V}$ $^{nat}\text{Ni}(p,x)^{52}\text{Mn}$ $^{nat}\text{Ni}(p,x)^{56}\text{Ni}$ $^{nat}\text{Ni}(p,x)^{57}\text{Ni}$ $^{nat}\text{Ni}(p,x)^{55}\text{Co}$ $^{nat}\text{Ni}(p,x)^{56}\text{Co}$ $^{nat}\text{Ni}(p,x)^{57}\text{Co}$	NISL092	2553	$2.72\pm 0.20$ $0.61\pm 0.05$ $6.59\pm 0.33$ $0.50\pm 0.02$ $1.20\pm 0.01$ $31.8\pm 4.00$ $16.2\pm 0.8$ $11.2\pm 0.1$ $2.07\pm 0.15$ $13.1\pm 0.6$ $7.96\pm 0.10$ $31.6\pm 0.7$ $67.1\pm 3.3$
$^{nat}\text{Si}(p,x)^7\text{Be}$ $^{nat}\text{Si}(p,x)^{24}\text{Na}$	SISL042	2540	$8.16\pm 0.42$ $2.85\pm 0.22$

Table 4.9: Cross sections determined for the production of residual nuclides by proton induced reactions in SACL0L

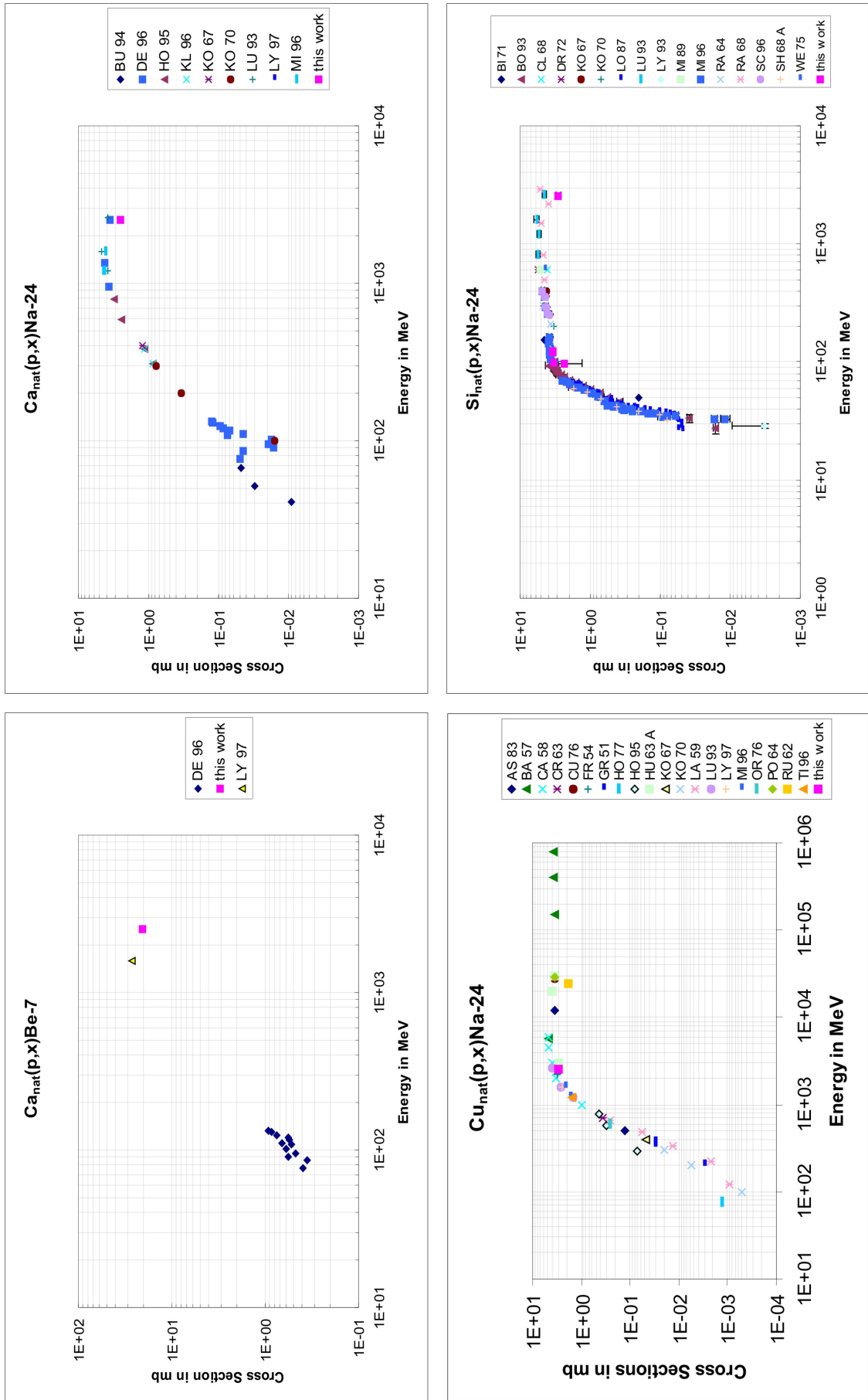


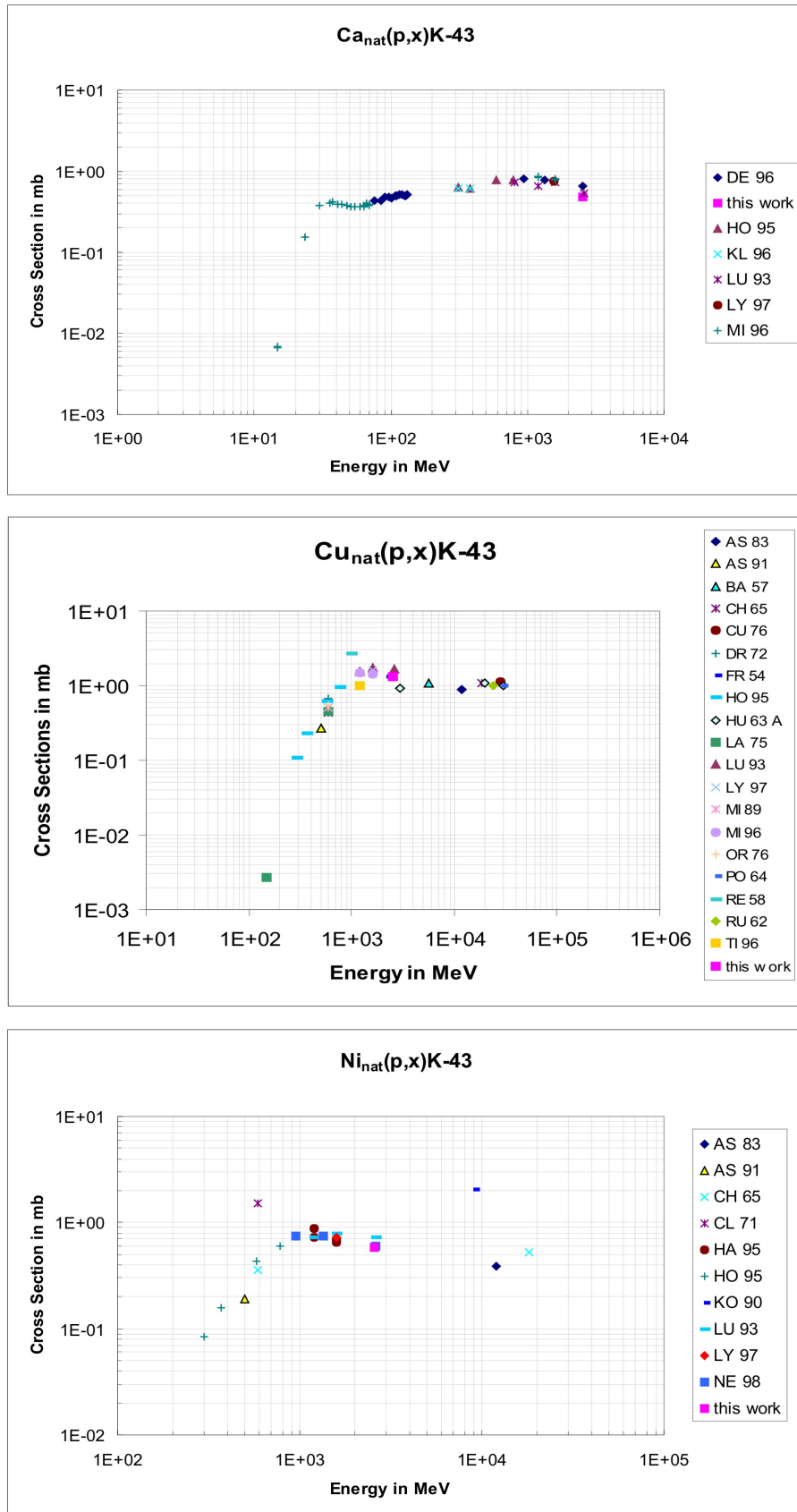
Figure 4.5: Experimental data for the production of  ${}^7\text{Be}$  from natural Ca and of  ${}^{24}\text{Na}$  from Ca, Cu and Si

As it can be seen in Figure 4.5 the data for the production of  ${}^7\text{Be}$  from Ca are scarce and far from giving a complete excitation function. Further measurements are needed for a better understanding of the production. In the case of the production of  ${}^{24}\text{Na}$  from Ca, Cu and Si consistent data basis exist and complete excitation functions are available. The shape of the excitation function suggest as production modes evaporation and pre-equilibrium emission at low energies and IMF production at medium energies.

For the production of  ${}^{43}\text{K}$  from Ca, Cu and Ni (Figure 4.6) not many experimental cross-sections were available for comparison. Further data are needed to describe these reactions completely.

The situation is much better for the production of  ${}^{55,56,57}\text{Co}$  from natural Cu (Figure 4.7). Complete and consistent excitation functions exist for these reactions for energies ranging from thresholds up to 2.6 GeV.

The data base for target element Ni allows a nearly complete description of the excitation functions for the production of radionuclides with masses above 43 (Figure 4.8 and Appendix F). For lower product masses the data base is less complete.

Figure 4.6: Experimental data for the production of  $^{43}\text{K}$  from Ca, Cu and Ni

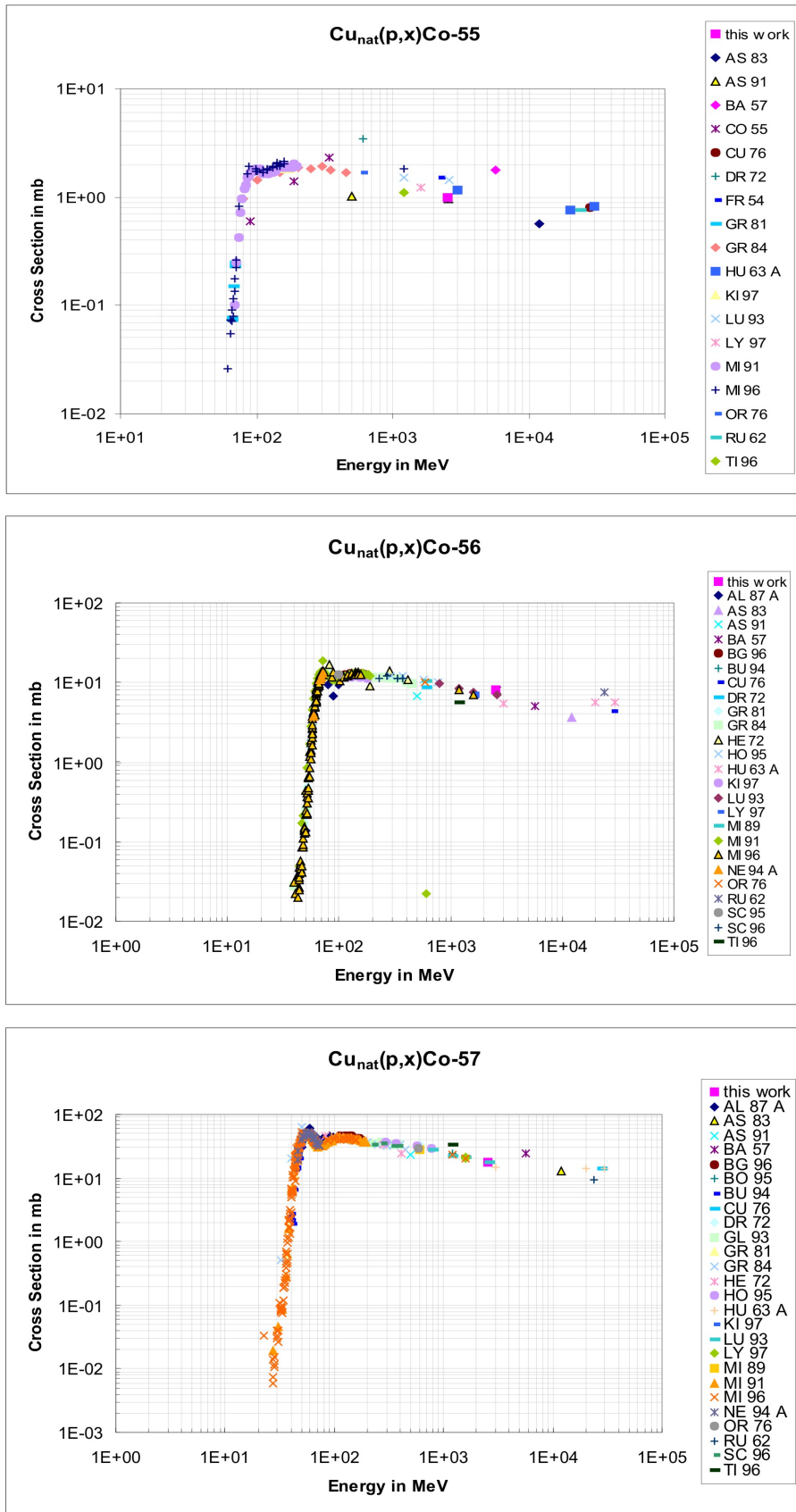
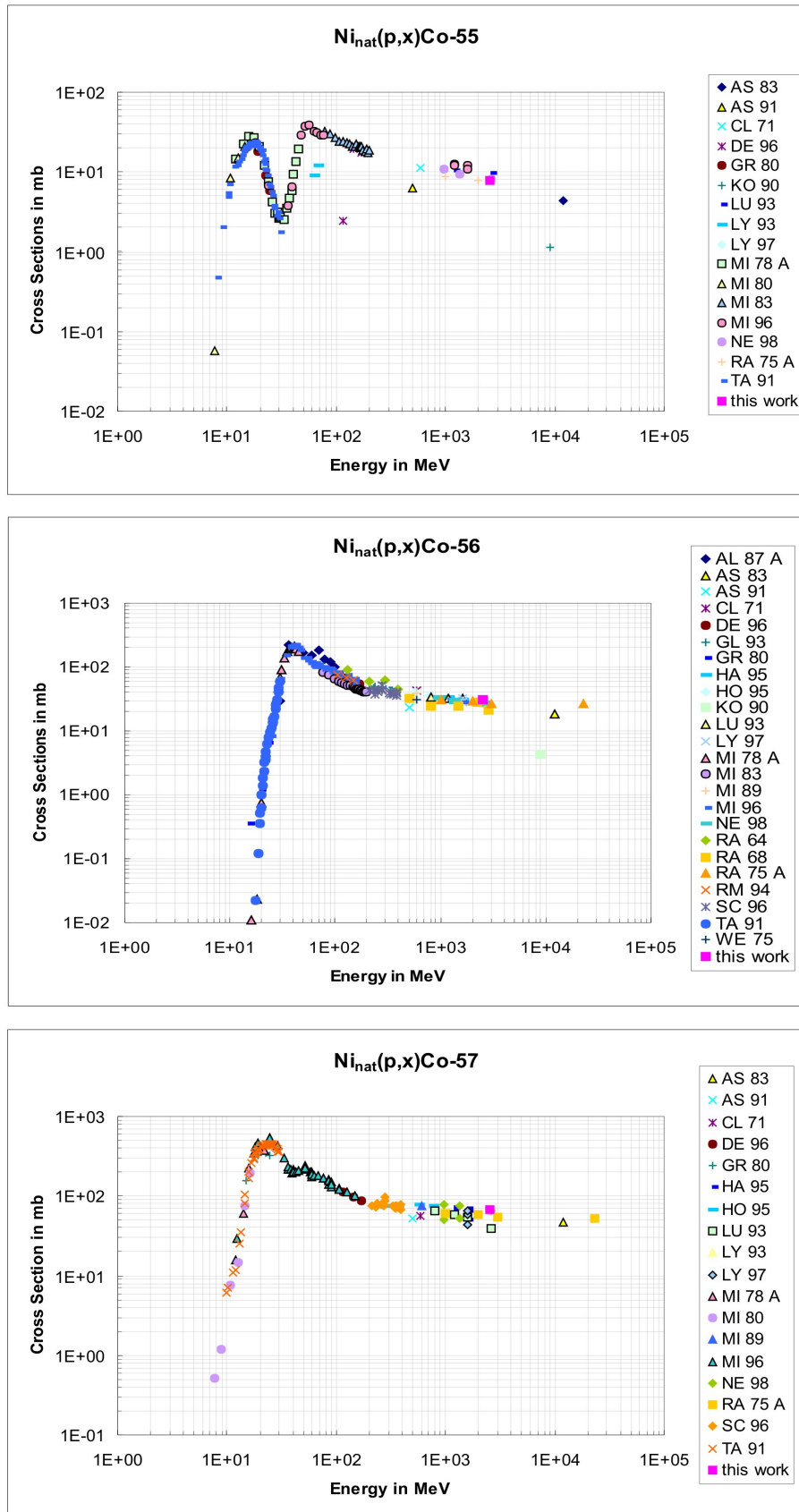


Figure 4.7: Experimental data for the production of  $^{55}\text{Co}$ ,  $^{56}\text{Co}$  and  $^{57}\text{Co}$  from Cu



Figure 4.8: Experimental data for the production of  $^{55}Co$ ,  $^{56}Co$  and  $^{57}Co$  from Ni

### 4.5.3 Results from UPPS0S

For targets irradiated during experiment UPPS0S first measurements were performed only recently. This is the reason why the determined cross-sections are confined to long-lived products. The parameters of the experiment can be found in Table 4.10 and a survey on irradiated targets, energies covered and flux densities is given in Table 4.11.

Experiment	Description	Target	Product
Uppsala S	$E_{p,i}=97.5$ MeV	Al	$^{24}\text{Na}$
	$E_{p,f}=38.6$ MeV	Fe	$^{54}\text{Mn}$
	$t_{EOI}=11.03.1997/19:00$	Mn	$^{54}\text{Mn}$
	$t_{irr}=14400\text{s}$	Ti	$^{44}\text{Ti}$
		Ag	$^{101}\text{Rh}, ^{102}\text{Rh}_m, ^{108}\text{Ag}_m$

Table 4.10: Survey on target-product combinations evaluated from UPPS0S

Experiment	Target	Mass in mg	Energy in MeV	Flux density ( $\Phi$ ) in $\text{s}^{-1}\text{cm}^{-2}$	$u(\Phi)$ in $\text{s}^{-1}\text{cm}^{-2}$
Uppsala S	FEUS032	134.31	95.77	8.11E+10	1.85E+10
	FEUS192	150.22	74.14	1.03E+11	2.36E+10
	FEUS322	141.49	53.84	1.23E+11	2.83E+10
	MNUS012	152.36	99.16	7.76E+10	1.78E+10
	MNUS172	149.48	77.05	1.00E+11	2.29E+10
	MNUS302	150.53	57.50	1.20E+11	2.75E+10
	MNUS372	154.2	45.20	1.32E+11	3.05E+10
	TIUS162	217.07	78.24	9.88E+10	2.26E+10
	TIUS202	219.9	72.66	1.04E+11	2.39E+10
	TIUS252	213.6	64.90	1.12E+11	2.57E+10
	TIUS292	216.96	59.14	1.18E+11	2.71E+10
	TIUS332	221.2	51.75	1.26E+11	2.89E+10
	AGUS043	211.82	93.84	8.30E+10	1.90E+10
	AGUS093	216.25	87.46	8.95E+10	2.05E+10
	AGUS113	211.09	84.08	9.29E+10	2.13E+10
	AGUS212	219.33	71.26	1.06E+11	2.43E+10
	AGUS232	210.92	68.07	1.09E+11	2.50E+10
	AGUS272	211.41	62.69	1.15E+11	2.63E+10
	AGUS342	219.7	49.74	1.28E+11	2.94E+10

Table 4.11: Survey on targets evaluated from UPPS0S

Target-Product	Target	Energy in MeV	Cross section in mb
$^{nat}\text{Fe}(p,x)^{54}\text{Mn}$	FEUS032	95.77	$109.2\pm 25.9$
$^{nat}\text{Fe}(p,x)^{54}\text{Mn}$	FEUS192	74.14	$59.3\pm 13.9$
$^{nat}\text{Fe}(p,x)^{54}\text{Mn}$	FEUS322	53.84	$86.3\pm 20.4$
$^{55}\text{Mn}(p,x)^{54}\text{Mn}$	MNUS012	99.16	$169.6\pm 39.9$
$^{55}\text{Mn}(p,x)^{54}\text{Mn}$	MNUS172	77.05	$170.8\pm 40.2$
$^{55}\text{Mn}(p,x)^{54}\text{Mn}$	MNUS302	57.50	$166.9\pm 39.8$
$^{55}\text{Mn}(p,x)^{54}\text{Mn}$	MNUS372	45.20	$211.6\pm 50.1$
$^{nat}\text{Ti}(p,x)^{44}\text{Ti}$	TIUS162	78.24	$5.62\pm 1.32$
$^{nat}\text{Ti}(p,x)^{44}\text{Ti}$	TIUS202	72.66	$4.88\pm 1.15$
$^{nat}\text{Ti}(p,x)^{44}\text{Ti}$	TIUS252	64.90	$3.76\pm 0.89$
$^{nat}\text{Ti}(p,x)^{44}\text{Ti}$	TIUS292	59.14	$3.36\pm 0.79$
$^{nat}\text{Ti}(p,x)^{44}\text{Ti}$	TIUS332	51.75	$3.13\pm 0.74$
$^{nat}\text{Ag}(p,x)^{101}\text{Rh}$	AGUS043	93.84	$18.2\pm 4.3$
$^{nat}\text{Ag}(p,x)^{101}\text{Rh}$	AGUS093	87.46	$15.4\pm 3.7$
$^{nat}\text{Ag}(p,x)^{101}\text{Rh}$	AGUS113	84.08	$13.5\pm 3.2$
$^{nat}\text{Ag}(p,x)^{101}\text{Rh}$	AGUS212	71.26	$6.89\pm 1.62$
$^{nat}\text{Ag}(p,x)^{101}\text{Rh}$	AGUS232	68.07	$6.99\pm 1.65$
$^{nat}\text{Ag}(p,x)^{101}\text{Rh}$	AGUS272	62.69	$7.80\pm 1.84$
$^{nat}\text{Ag}(p,x)^{101}\text{Rh}$	AGUS342	49.74	$0.67\pm 0.16$
$^{nat}\text{Ag}(p,x)^{102}\text{Rh}_m$	AGUS043	93.84	$10.2\pm 2.4$
$^{nat}\text{Ag}(p,x)^{102}\text{Rh}_m$	AGUS093	87.46	$9.40\pm 2.21$
$^{nat}\text{Ag}(p,x)^{102}\text{Rh}_m$	AGUS113	84.08	$9.11\pm 2.14$
$^{nat}\text{Ag}(p,x)^{102}\text{Rh}_m$	AGUS212	71.26	$7.12\pm 1.68$
$^{nat}\text{Ag}(p,x)^{102}\text{Rh}_m$	AGUS232	68.07	$5.51\pm 1.30$
$^{nat}\text{Ag}(p,x)^{102}\text{Rh}_m$	AGUS272	62.69	$2.94\pm 0.70$
$^{nat}\text{Ag}(p,x)^{102}\text{Rh}_m$	AGUS342	49.74	$2.05\pm 0.49$
$^{nat}\text{Ag}(p,x)^{108}\text{Ag}_m$	AGUS043	93.84	$18.6\pm 4.4$
$^{nat}\text{Ag}(p,x)^{108}\text{Ag}_m$	AGUS093	87.46	$18.9\pm 4.5$
$^{nat}\text{Ag}(p,x)^{108}\text{Ag}_m$	AGUS113	84.08	$18.8\pm 4.5$
$^{nat}\text{Ag}(p,x)^{108}\text{Ag}_m$	AGUS212	71.26	$18.8\pm 4.5$
$^{nat}\text{Ag}(p,x)^{108}\text{Ag}_m$	AGUS232	68.07	$18.8\pm 4.5$
$^{nat}\text{Ag}(p,x)^{108}\text{Ag}_m$	AGUS272	62.69	$18.5\pm 4.4$
$^{nat}\text{Ag}(p,x)^{108}\text{Ag}_m$	AGUS342	49.74	$17.9\pm 4.2$

Table 4.12: Cross sections determined for the production of residual nuclides by proton induced reactions in UPPS0S

A good data base was available for the production of  $^{54}\text{Mn}$  from natural Fe and Mn. The values of the cross-sections determined in this work seem to be slightly higher than the ones from earlier works, but still in agreement within errors (Figure 4.9).

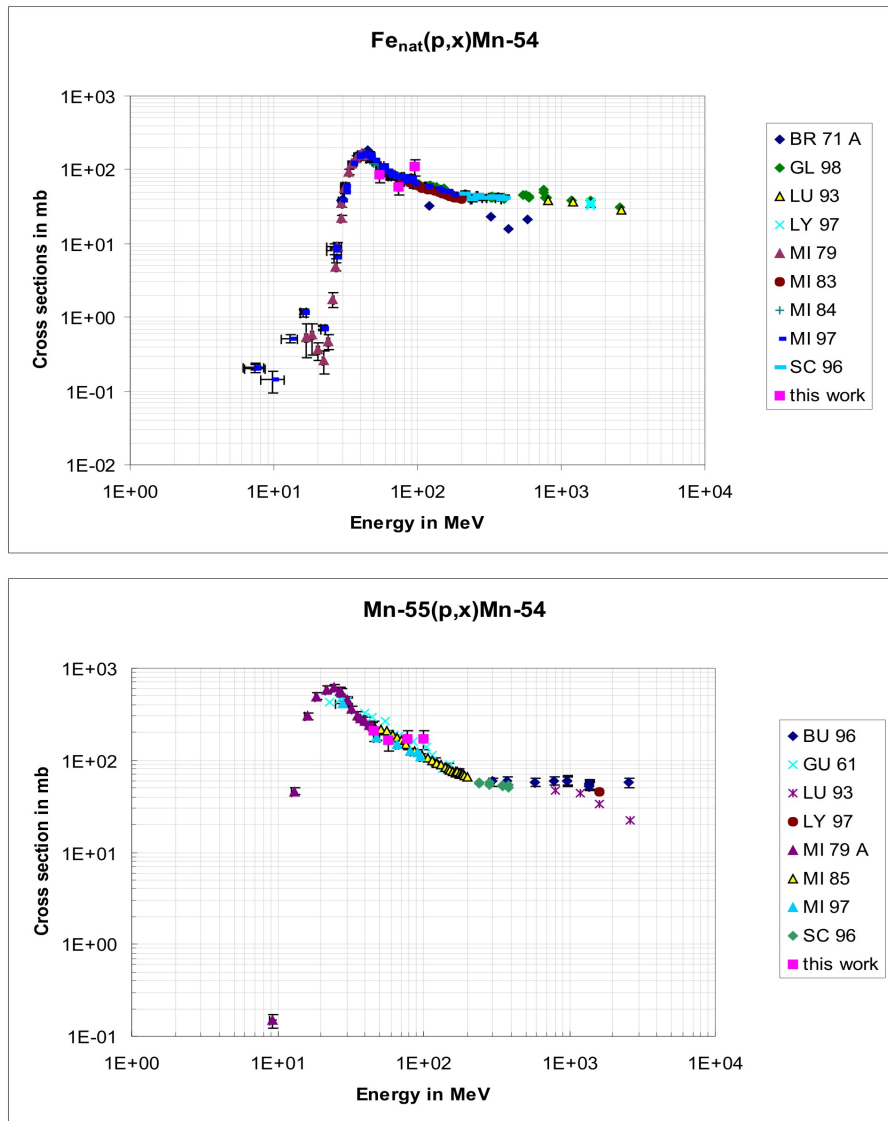


Figure 4.9: Experimental data for the production of  $^{54}\text{Mn}$  from natural Fe and Mn

The situation is the same also for  $^{44}\text{Ti}$  from natural Ti, but changes for the production of  $^{101}\text{Rh}$ ,  $^{102}\text{Rh}_m$  and  $^{108}\text{Ag}_m$ . Few data were available for comparison from [Bu96] and [Al94]. No data were found for  $^{108}\text{Ag}_m$ . Further measurements are needed to be able to give a complete description of the excitation functions.

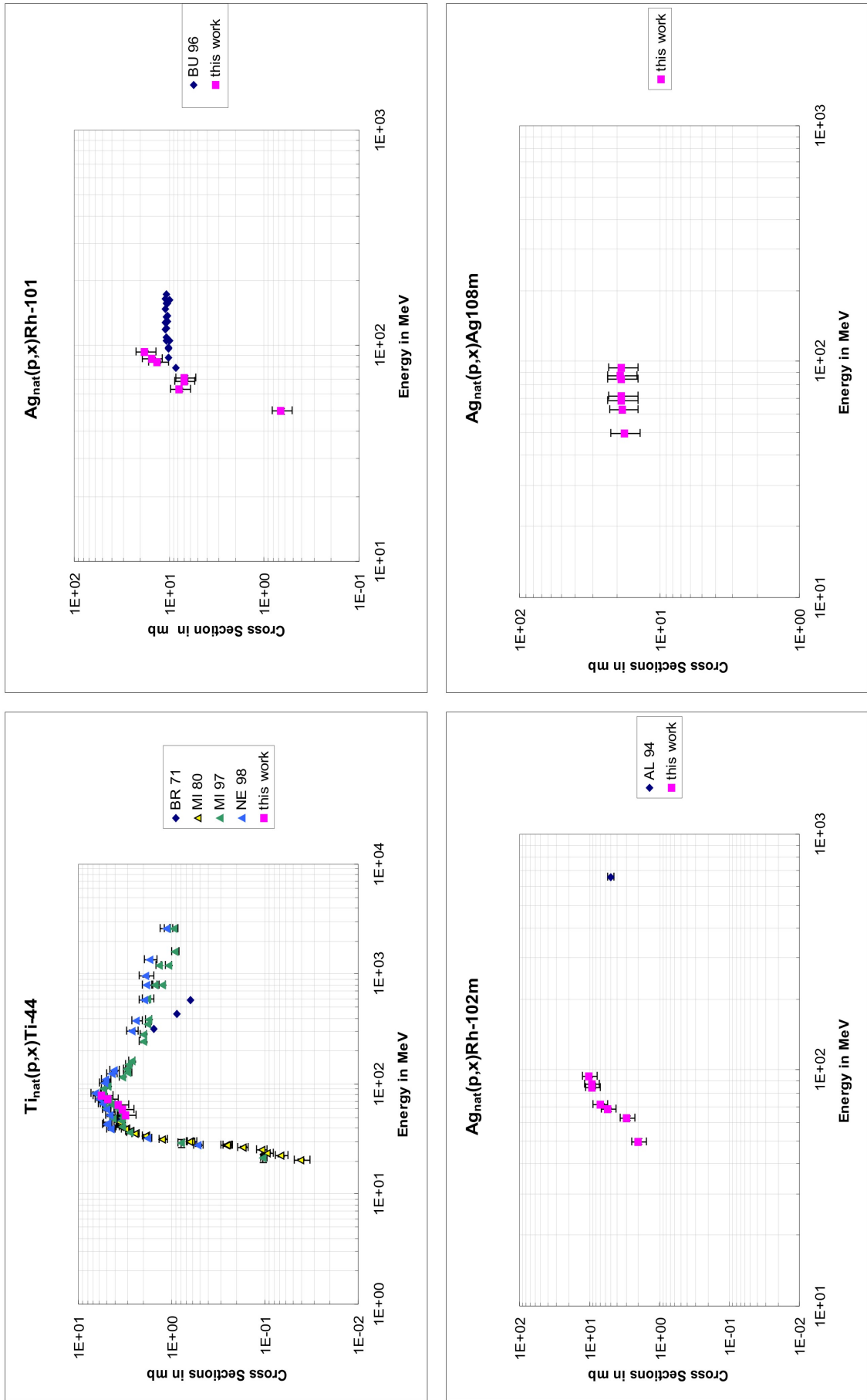


Figure 4.10: Experimental data for the production of  $^{44}Ti$  from natural Ti and of  $^{101}Rh$ ,  $^{102}Ti_m$  and of  $^{108}Ag_m$  from natural Ag

#### 4.5.4 Comparison with TALYS

Using TALYS code a comparison was made between our data for target elements Cu and Ni and the theoretical calculations. All the resulted graphs are displayed in Appendix G. For the production of  $^{46,47}\text{Sc}$  from natural Cu we observe an underestimation of the experimental cross-sections (Figure 4.11).

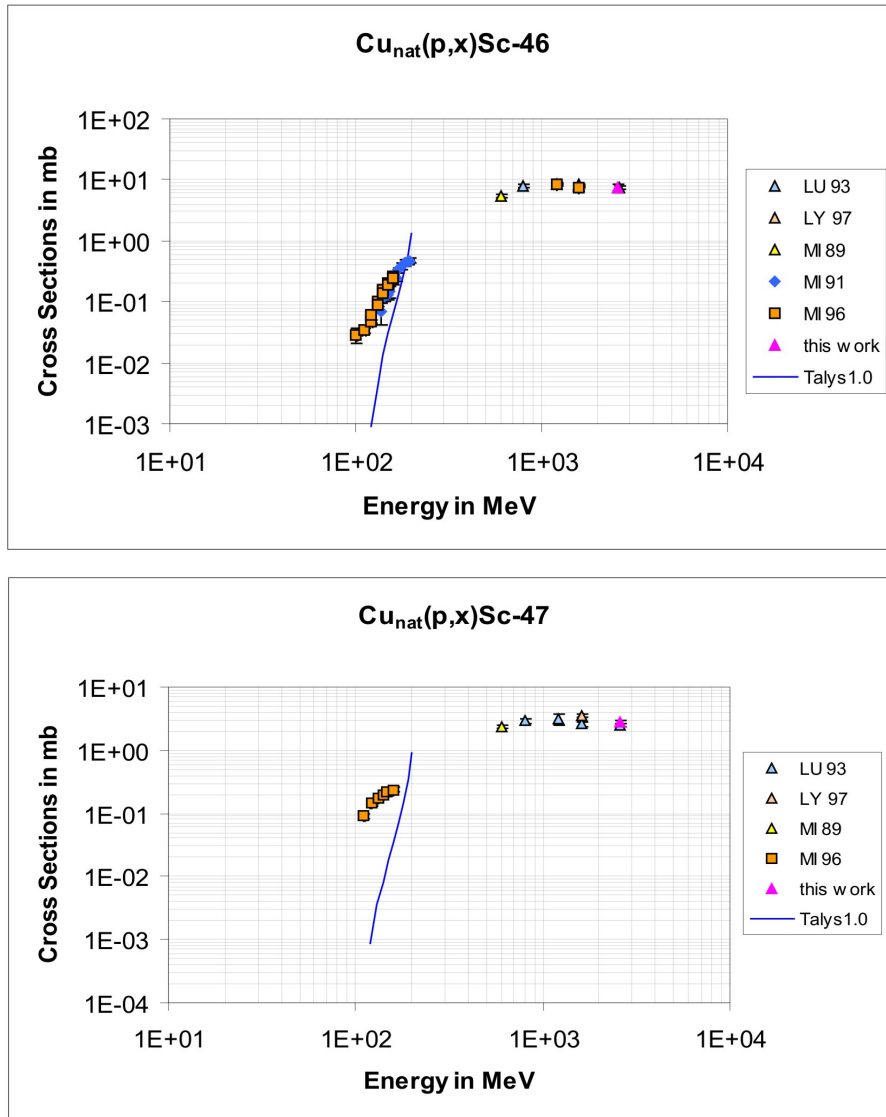


Figure 4.11: Production of  $^{46,47}\text{Sc}$  from natural Cu

We see a good agreement between TALYS and the experimental data for  $^{57,58}\text{Co}$  from natural Cu (Figure 4.12), although in the case of  $^{58}\text{Co}$  we observe a slight underestimation of the experimental data near the 200 MeV limit.

In the case of residual nuclide production from natural Ni an interesting behaviour is observed when comparing with the TALYS theoretical calculations. The

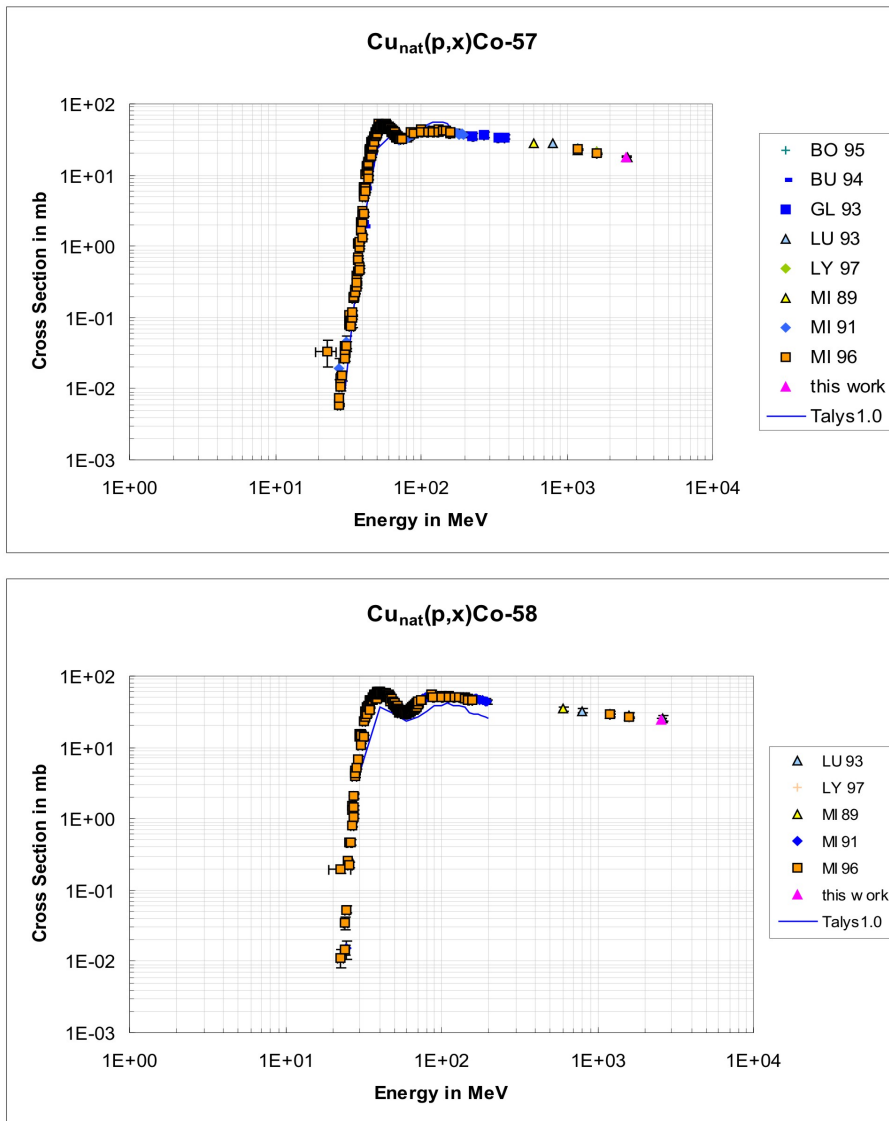


Figure 4.12: Production of  $^{57,58}\text{Co}$  from natural Cu

production is overestimated by orders of magnitude for  $^{48}\text{Cr}$  and underestimated for  $^{51}\text{Cr}$  (Figure 4.13).

For the rest of the products studied from natural Ni there is a good agreement between experiment and theory (Appendix G).

Theoretical calculations with TALYS show a good agreement up to about 100 MeV with the experimental data for the production of  $^{54}\text{Mn}$  from natural Fe and Mn (Figure 4.14). From 100 MeV up to 200 MeV the agreement exists no longer and the TALYS results are lower than the experimental ones. This is also true for  $^{101}\text{Rh}$  from natural silver (Figure 4.15). We observe an under-estimation of production for  $^{102}\text{Rh}_m$  and an over-estimation of the production for  $^{108}\text{Ag}_m$  (Figure 4.15).

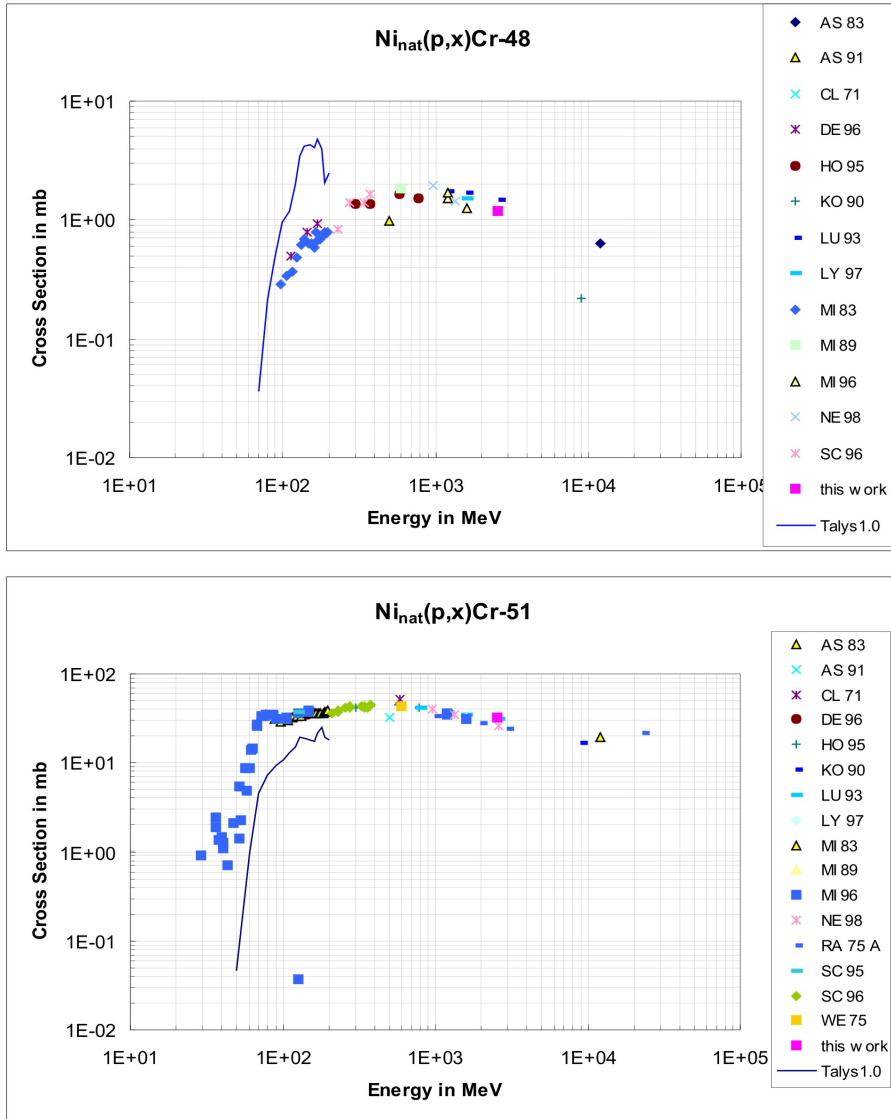


Figure 4.13: Production of  $^{48,51}Cr$  from natural Ni



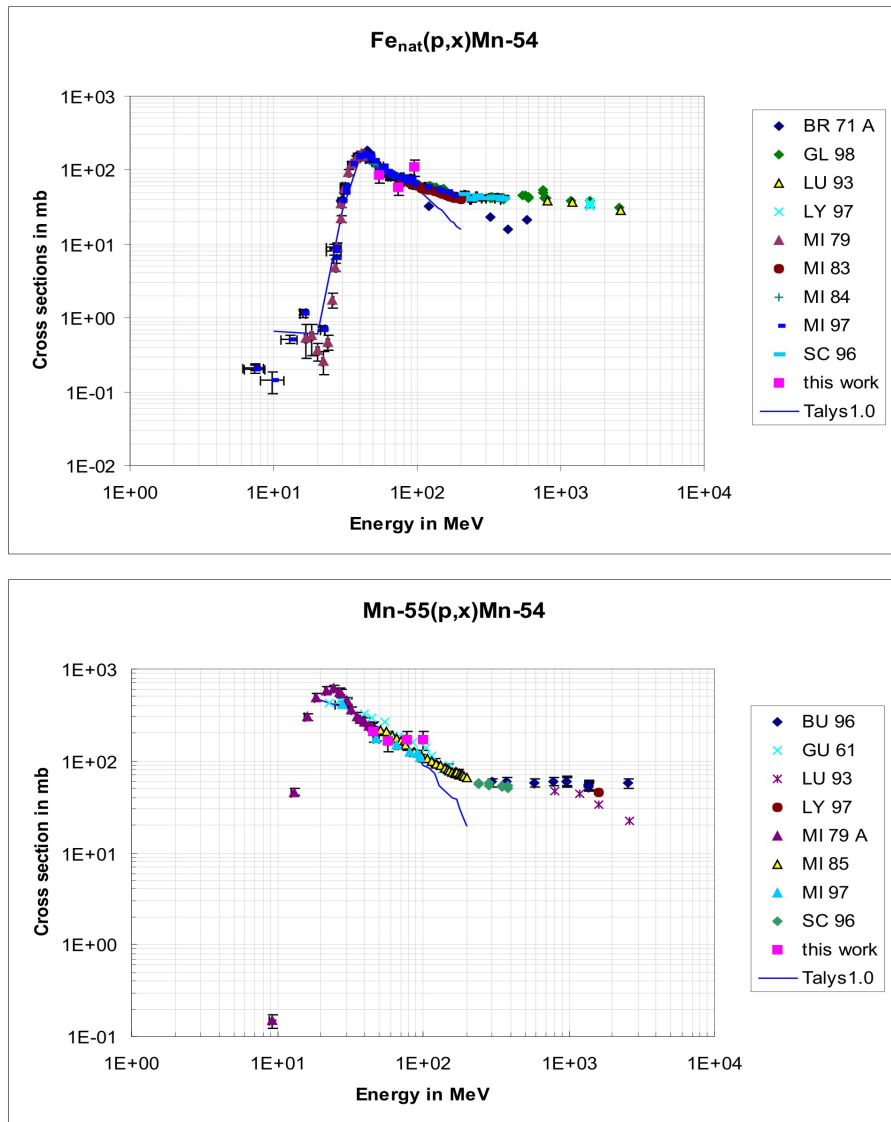


Figure 4.14: Experimental data for the production of  $^{54}\text{Mn}$  from natural Fe and Mn

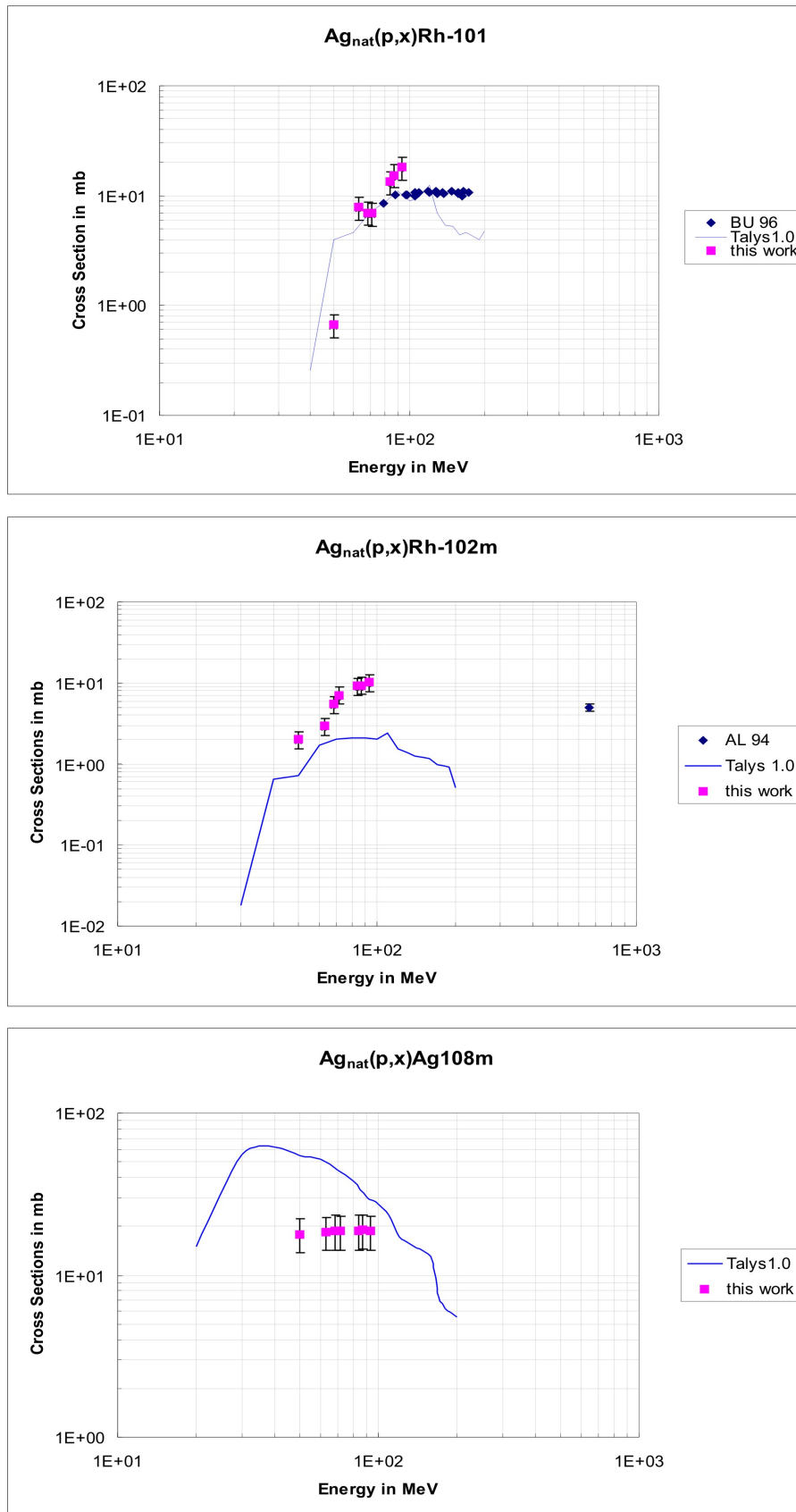


Figure 4.15: Experimental data for the production of  $^{101}Rh$ ,  $^{102}Rh_m$  and of  $^{108}Ag_m$  from natural Ag

## 5 NUDATRA Project

### 5.1 Overview

This work was performed as a contribution [Mi06] to the NUDATRA work package 5.4 "High Energy Experiments for Radioactivity, Chemical Modifications and Damage Assessment" for the EUROpean Research Programme for the TRANSmutation of High Level Nuclear Waste in an Accelerator Driven System (EUROTRANS).

In order to allow a systematic survey about the production of intermediate mass fragments by proton-induced reactions it was decided to cover all previous available and new data for the production of residual nuclides with masses between 3 and 30 over an energy range extending from thresholds up to 2.6 GeV.

The availability of experimental data differs considerably among the possible candidate nuclides. A criterion for inclusion into this work was that at least an estimate of the entire excitation function should be possible. It was further decided to include light- and intermediate-mass target elements where the residual nuclides are quite close in mass to the target element. This was done to allow a systematic description for targets spreading over the entire chart of nuclides and to survey whether or not there are peculiarities in the relevant reactions on heavy target elements.

In order to fulfill the task M5.19 within the NUDATRA project a number of recent and elder experiments were finally evaluated and the results are now available. Further evaluations are going on, as e.g. for proton-induced reactions on uranium and thorium between 200 MeV and 2.6 GeV. New measurements on the production of long-lived radionuclides and of stable rare gas isotopes were started. For some of them preliminary data are now available. In total, the now existing database allows a systematic survey on the production of intermediate mass fragments as functions of target element masses and energies and for comprehensive tests of models and codes describing medium-energy nuclear reactions.

## 5.2 Target and Product Nuclide Coverage

The availability of experimental data for the production of residual nuclides by proton-induced reactions depends widely on their application in various fields of basic and applied sciences; e.g. [Mi99, Mi00]. Already in the 1960's cross sections for the production of residual nuclides turned out to be the crucial quantities to understand cosmogenic nuclides in extraterrestrial matter and much work was done in the following decades dedicated to this issue.

By our group and a large number of collaborators a cross section database for the interpretation of cosmogenic nuclides was established in a series of thin-target and thick-target experiments during more than two decades. The database covers the target elements C, N, O, Mg, Al, Si, Ca, Ti, V, Mn, Fe, Co, Ni, Cu, Rb, Sr, Y, Zr, Nb, Mo, Rh, Ag, In, Te, Ba, and La for proton-induced reactions. In 1997, the database of cosmochemically relevant cross sections of proton-induced reactions covered nearly 550 target/product combinations with nearly 22,000 cross sections; [Mi95, Mi97] and references therein. More recent analyses covered the production of special long-lived radionuclides such as  $^{14}\text{C}$  [Ne96],  $^{36}\text{Cl}$  [Sc96a, Sc96b, Su97],  $^{41}\text{Ca}$  [Sc04],  $^{53}\text{Mn}$  [Me00], and  $^{129}\text{I}$  [Sc97] and of stable rare gas isotopes [Gi98, Gi98a, Ly98]. In addition, measurements of cosmochemically relevant cross sections were increasingly performed during recent years by other groups; see [Si97] for a review and references.

Today, such investigations are going on, focusing widely on the understanding of cosmogenic nuclides produced in-situ in the Earth's surface and consequently aiming more to neutron-induced rather than to proton-induced reactions. For accelerator technologies, production of residual nuclides at medium energies has to be modeled in order to describe the radioactive inventories of the spallation targets, the activation of accelerating structures, of the beam pipes and windows and of shielding materials, cooling materials and ambient air. Radionuclide inventories will determine the final disposal costs of spallation targets and will decide whether the burn-up of nuclear waste can be counterweighted or not by the creation of other activation products. Moreover, medium-energy cross sections of fission products and actinides are needed. Finally, the production of residual nuclides will cause chemical alteration of the irradiated components and, in particular, production of light complex particles such as  $^2\text{H}$ ,  $^3\text{H}$ ,  $^3\text{He}$ , and  $^4\text{He}$  will cause considerable material damage.

Integral excitation functions for the production of residual nuclides are basic quantities for the calculation of radioactive inventories of spallation targets in spallation neutron sources and in accelerator-driven devices for energy amplification or for

transmutation of nuclear waste. Due to the large range of relevant target elements and the vast amount of product nuclides it will not be possible to measure all the cross sections needed. Consequently, one will have to rely widely on models and codes to calculate the required cross sections and validation of such calculations will be a high priority issue. Since previous experiences with predictions of such excitation functions were not satisfying [Mi97a], two new code systems, namely TALYS [Ko05] and INCL4+ABLA [Bo02, Ju98], were developed within the HINDAS (High and Intermediate Energy Nuclear Data for Accelerator-Driven Systems) project [Ko92, Me05]. Experimental investigations of the HINDAS project provided consistent sets of nuclear data of all types to allow for comprehensive tests of these models; see ref. [Me05] for details.

Within the EC project HINDAS experimental investigations were extended to heavy target elements such as Ta, W, Pb, Bi [Gl01, Mi02, Ku01, Mi02a, Mi05], and U [Uo05]. These elements are under discussions as spallation-target materials in spallation neutron sources and in other accelerator based technologies. For the target element lead a comprehensive set of excitation functions published recently was completed by AMS-measurements of cross sections for the production of the long-lived radionuclides  $^{10}\text{Be}$ ,  $^{36}\text{Cl}$ , and  $^{129}\text{I}$ , [Sc05, Sc06]. For natural uranium, cross sections for the production of residual nuclides are available for p-energies from 21 MeV to 69 MeV [Uo05, Sh08, Sh09] and at 600 MeV [Ad05]. Further spin-offs of the HINDAS project were mass spectrometric measurements of cross sections for the production of stable and radioactive isotopes of He, Ne, Ar, Kr, and Xe from natural lead; [Ly05] and references therein.

Together with new and not previously published cross sections for the target elements Rb, Mo, Rh, Ag, In, Te, and La, the published cross sections for the production of residual nuclides for cosmochemically relevant target elements, and those measured within the HINDAS project for Fe, Ta, W, Au, Pb, Bi, and U, our consistent data base now contains data for nearly 1,500 nuclear reactions and more than 25,000 cross sections. Most of the data are available in EXFOR.

Our investigations made use of classical kinematics and, therefore, they are confined to residual nuclides with usually at least a few hours half-lives which mostly reveal a cumulative production due to the decay of short-lived progenitors. These investigations are complimentary to those using inverse kinematics where all the primary residuals can be studied at certain energy points but not over the whole energy range desired, e.g. [En01].

Products	Targets	Radioactive Progenitors
$^3\text{H}$	$^{\text{nat}}\text{Fe}, ^{\text{nat}}\text{Ni}, ^{\text{nat}}\text{Pb}$	
$^3\text{He}$	$^{\text{nat}}\text{Mg}, ^{\text{nat}}\text{Si}, ^{\text{nat}}\text{Fe}, ^{\text{nat}}\text{Ni}, ^{\text{nat}}\text{Pb}, ^{27}\text{Al}$	
$^3\text{He-c}$	$^{\text{nat}}\text{Fe}, ^{\text{nat}}\text{Ni}, ^{\text{nat}}\text{Pb}, ^{27}\text{Al}$	$^3\text{H}$
$^4\text{He}$	$^{\text{nat}}\text{Mg}, ^{\text{nat}}\text{Si}, ^{\text{nat}}\text{Fe}, ^{\text{nat}}\text{Ni}, ^{\text{nat}}\text{Pb}, ^{27}\text{Al}$	
$^6\text{Li}$	$^{14}\text{N}$	$^6\text{He}$
$^7\text{Li}$	$^{14}\text{N}, ^{16}\text{O}$	
$^7\text{Be}$	$^{\text{nat}}\text{C}, ^{\text{nat}}\text{N}, ^{\text{nat}}\text{O}, ^{\text{nat}}\text{Mg}, ^{\text{nat}}\text{Si}, ^{\text{nat}}\text{Ca},$ $^{\text{nat}}\text{Ti}, ^{\text{nat}}\text{V}, ^{\text{nat}}\text{Fe}, ^{\text{nat}}\text{Ni}, ^{\text{nat}}\text{Cu}, ^{\text{nat}}\text{Zr},$ $^{\text{nat}}\text{Mo}, ^{\text{nat}}\text{Ag}, ^{\text{nat}}\text{Ta}, ^{\text{nat}}\text{W}, ^{\text{nat}}\text{Pb}, ^{12}\text{C},$ $^{14}\text{N}, ^{16}\text{O}, ^{19}\text{F}, ^{27}\text{Al}, ^{55}\text{Mn}, ^{59}\text{Co}, ^{89}\text{Y},$ $^{93}\text{Nb}, ^{197}\text{Au}, ^{206}\text{Pb}, ^{207}\text{Pb}, ^{208}\text{Pb}, ^{209}\text{Bi}$	
$^9\text{Be}$	$^{14}\text{N}$	$^9\text{Li}, ^9\text{C}$
$^{10}\text{Be}$	$^{\text{nat}}\text{C}, ^{\text{nat}}\text{N}, ^{\text{nat}}\text{O}, ^{\text{nat}}\text{Mg}, ^{\text{nat}}\text{Si}, ^{\text{nat}}\text{Ti},$ $^{\text{nat}}\text{Fe}, ^{\text{nat}}\text{Ni}, ^{\text{nat}}\text{Cu}, ^{\text{nat}}\text{Ir}, ^{\text{nat}}\text{Pb}, ^{\text{nat}}\text{Bi},$ $^{12}\text{C}, ^{27}\text{Al}, ^{55}\text{Mn}, ^{59}\text{Co}$	
$^{10}\text{B}$	$^{14}\text{N}, ^{16}\text{O}$	$^{10}\text{Be}$
$^{11}\text{B}$	$^{14}\text{N}, ^{16}\text{O}$	$^{11}\text{Be}, ^{11}\text{Li}, ^{11}\text{C}$
$^{11}\text{C}$	$^{16}\text{O}$	
$^{14}\text{C}$	$^{\text{nat}}\text{O}, ^{\text{nat}}\text{Si}, ^{\text{nat}}\text{Fe}, ^{\text{nat}}\text{Ni}, ^{16}\text{O}$	$^{14}\text{B}, ^{14}\text{Be}$
$^{15}\text{O}$	$^{16}\text{O}$	
$^{18}\text{F}$	$^{\text{nat}}\text{Mg}, ^{\text{nat}}\text{Cu}, ^{\text{nat}}\text{Ag}, ^{\text{nat}}\text{Pb}, ^{23}\text{Na}, ^{27}\text{Al}$	$^{18}\text{Ne}$
$^{20}\text{Ne}$	$^{\text{nat}}\text{Mg}, ^{\text{nat}}\text{Si}, ^{\text{nat}}\text{Fe}, ^{\text{nat}}\text{Ni}, ^{27}\text{Al}$	$^{20}\text{F}, ^{20}\text{O}, ^{20}\text{N}, ^{20}\text{C}, ^{20}\text{Mg}, ^{20}\text{Ne}$
$^{21}\text{Ne}$	$^{\text{nat}}\text{Mg}, ^{\text{nat}}\text{Si}, ^{\text{nat}}\text{Fe}, ^{\text{nat}}\text{Ni}, ^{\text{nat}}\text{Pb}, ^{27}\text{Al}$	$^{21}\text{Mg}, ^{21}\text{Na}, ^{21}\text{N}, ^{21}\text{O}, ^{21}\text{F}$
$^{22}\text{Ne}$	$^{\text{nat}}\text{Mg}, ^{\text{nat}}\text{Si}, ^{\text{nat}}\text{Fe}, ^{\text{nat}}\text{Ni}, ^{\text{nat}}\text{Pb}, ^{27}\text{Al}$	$^{22}\text{Si}, ^{22}\text{Al}, ^{22}\text{Mg}, ^{22}\text{O}, ^{22}\text{F}$
$^{22}\text{Ne-c}$	$^{\text{nat}}\text{Mg}, ^{\text{nat}}\text{Si}, ^{\text{nat}}\text{Fe}, ^{\text{nat}}\text{Ni}, ^{\text{nat}}\text{Pb}, ^{27}\text{Al}$	$^{22}\text{Si}, ^{22}\text{Al}, ^{22}\text{Mg}, ^{22}\text{Na}, ^{22}\text{O}, ^{22}\text{F}$
$^{22}\text{Na}$	$^{\text{nat}}\text{Mg}, ^{\text{nat}}\text{Si}, ^{\text{nat}}\text{Ca}, ^{\text{nat}}\text{Ti}, ^{\text{nat}}\text{V}, ^{\text{nat}}\text{Fe},$ $^{\text{nat}}\text{Ni}, ^{\text{nat}}\text{Cu}, ^{\text{nat}}\text{Sr}, ^{\text{nat}}\text{Mo}, ^{\text{nat}}\text{Ag}, ^{\text{nat}}\text{Ta},$ $^{\text{nat}}\text{W}, ^{\text{nat}}\text{Pb}, ^{23}\text{Na}, ^{24}\text{Mg}, ^{25}\text{Mg}, ^{26}\text{Mg},$ $^{27}\text{Al}, ^{55}\text{Mn}, ^{59}\text{Co}, ^{89}\text{Y}, ^{93}\text{Nb}, ^{209}\text{Bi}$	$^{22}\text{Al}, ^{22}\text{Mg}, ^{22}\text{Si}$
$^{24}\text{Na}$	$^{\text{nat}}\text{Mg}, ^{\text{nat}}\text{Si}, ^{\text{nat}}\text{Ca}, ^{\text{nat}}\text{Ti}, ^{\text{nat}}\text{V}, ^{\text{nat}}\text{Fe},$ $^{\text{nat}}\text{Ni}, ^{\text{nat}}\text{Cu}, ^{\text{nat}}\text{Zr}, ^{\text{nat}}\text{Ag}, ^{\text{nat}}\text{Ta}, ^{\text{nat}}\text{Pb},$ $^{27}\text{Al}, ^{45}\text{Sc}, ^{48}\text{Ti}, ^{55}\text{Mn}, ^{59}\text{Co}, ^{197}\text{Au}$	$^{24}\text{O}, ^{24}\text{F}, ^{24}\text{Ne}$
$^{28}\text{Mg}$	$^{\text{nat}}\text{Si}, ^{\text{nat}}\text{Ca}, ^{\text{nat}}\text{Ti}, ^{\text{nat}}\text{V}, ^{\text{nat}}\text{Fe}, ^{\text{nat}}\text{Cu},$ $^{\text{nat}}\text{Pb}, ^{30}\text{Si}, ^{55}\text{Mn}, ^{59}\text{Co}, ^{209}\text{Bi}$	$^{28}\text{Na}, ^{28}\text{Ne}$
$^{26}\text{Al}$	$^{\text{nat}}\text{Mg}, ^{\text{nat}}\text{Si}, ^{\text{nat}}\text{Ca}, ^{\text{nat}}\text{Ti}, ^{\text{nat}}\text{Fe}, ^{\text{nat}}\text{Ni},$ $^{\text{nat}}\text{Pb}, ^{26}\text{Mg}, ^{27}\text{Al}, ^{55}\text{Mn}$	$^{26}\text{P}, ^{26}\text{Si}$

Table 5.1: Survey on the nuclear reactions dealt with in this report

This work gives the complete dataset in tabular form in Appendix A. A complete set of graphs presenting all the experimental data is given in Appendix C. The newly presented data are still labeled with their original experiments from which they were derived. They cover the following reference labels with respect to the radionuclide production: [Bo95, Bu94, Bu96, De96, Gl93, Ha95, Ho95, Kl96, Kr95, Ly93, Mi93, Ne94a, Pr97, Ro91, Re93, Sc91, Sc91a, Su95].

## 5.3 Experimental Data

One of the key issues in the construction of accelerator based technologies is the calculation of radioactive inventories of the spallation targets as well as activation of accelerator parts, shields, cooling media and ambient air. These calculations are important both for short lived radionuclides and long lived radionuclides since the latter decide about potential environmental impact and problems when such devices have to be decommissioned and disposed, but also for the production of stable nuclides, in particular gaseous elements, in medium energy nuclear reactions, in order to describe material damage in accelerator components. Having this in mind in this chapter we shall discuss some selected reactions to exemplify some features of the experimental excitation functions and to comment on some aspects of data consistency and quality.

### 5.3.1 $^3\text{He}$ and $^4\text{He}$

The production of light complex particles such as  $^2\text{H}$ ,  $^3\text{H}$ ,  $^3\text{He}$  and  $^4\text{He}$  will cause chemical alteration of the irradiated components. For example the accumulation of  $^3\text{He}$  and  $^4\text{He}$  influences the swelling (the He atoms are insoluble in most, if not, all metals; they tend to migrate and form large bubbles that at least embrittle the irradiated metal) of the lead spallation target and cooling system. The number of displacements per atom (dpa), which is an essential parameter for stability studies, is usually given as a function of the number of produced He atoms. Therefore, the quality of the  $^3\text{He}$  and  $^4\text{He}$  cross-sections directly affects the reliability of stability and design studies.

For the production of  $^3\text{He}$ , the experimental data have to be distinguished whether they describe the direct production of  $^3\text{He}$  or whether the production due to the decay of  $^3\text{H}$  is included. Therefore, we distinguish here cross sections for  $^3\text{He}$  (Figure 5.1) and  $^3\text{He}_c$  (Figure 5.2), the latter including the production via the decay of  $^3\text{H}$  which is usually assumed to equal the direct production of  $^3\text{He}$ . In total, sufficient data are available for the target elements Al, Mg, Si, Fe, Ni, Pb, and Bi.

For  $^4\text{He}$  (Figure 5.3), for which comprehensive data exist for the same target elements, the transition through two reaction modes from evaporation or PE-emission to production as IMF is more pronounced since the evaporation or PE-emission is more pronounced than for  $^3\text{He}$ . Also for the production of  $^4\text{He}$  the tendency for a decreasing importance of evaporation and PE-emission is seen with increasing mass number of the target elements. In Appendix C, Figures C.2 and C.3 further graphs can be studied for the production of  $^3\text{He}$ ,  $^3\text{He}_c$  and  $^4\text{He}$ .

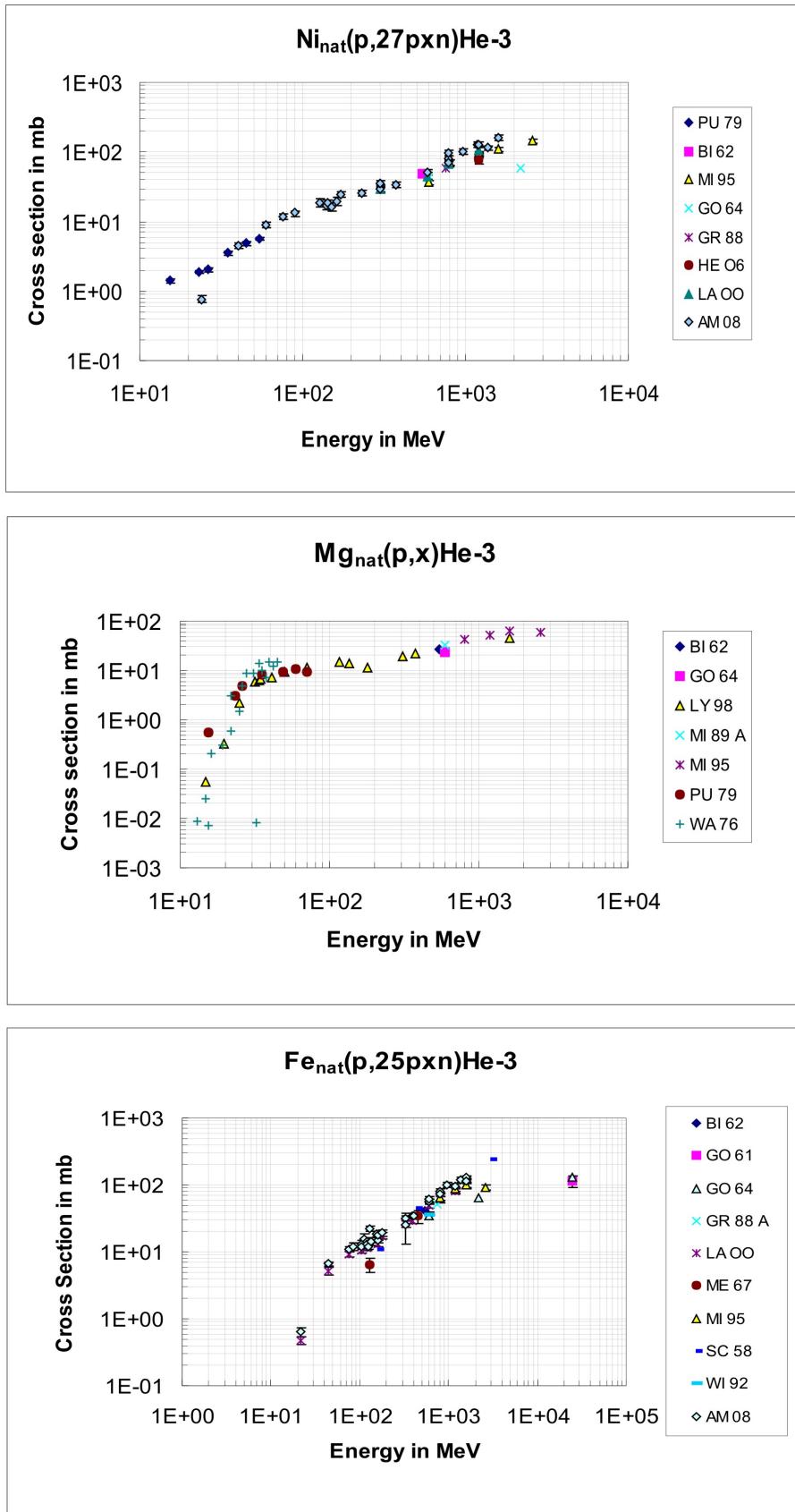


Figure 5.1: Excitation functions for the production of  $^3\text{He}$  by proton-induced reactions on natural magnesium, iron, and nickel



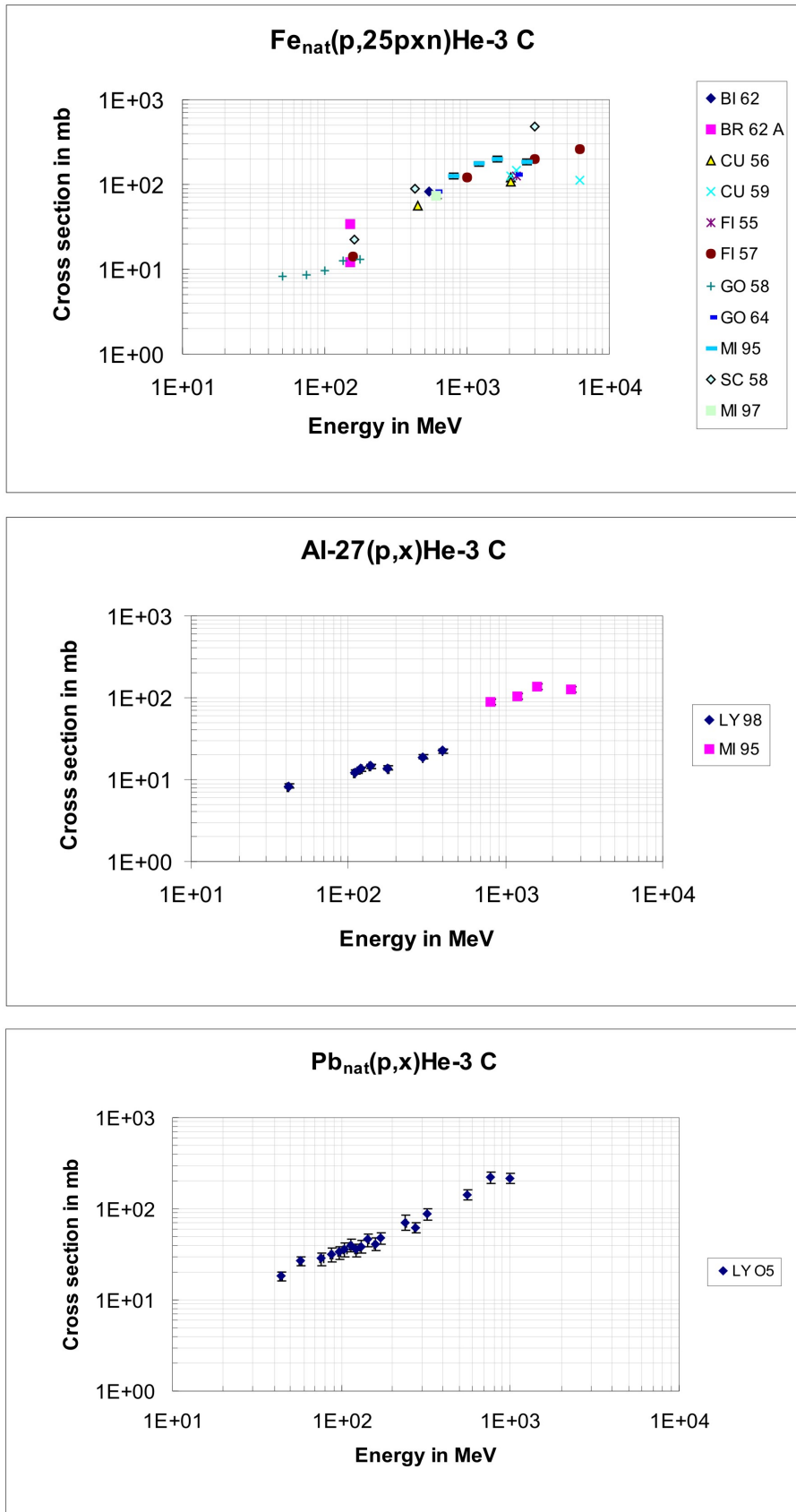


Figure 5.2: Excitation functions for the production of  ${}^3\text{He}_c$  on natural aluminum, iron, and lead.

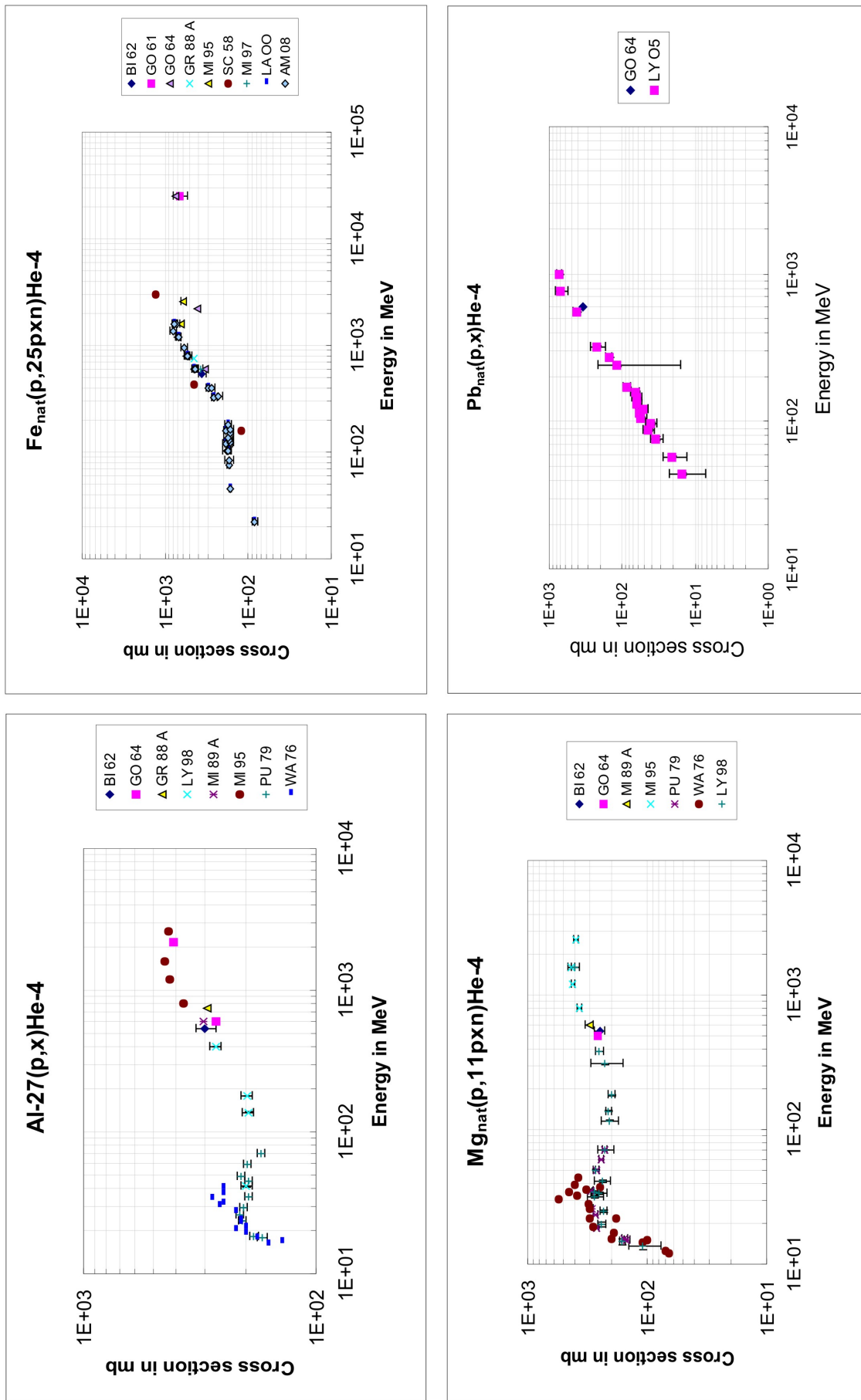


Figure 5.3: Excitation functions for the production of  ${}^4\text{He}$  by proton-induced reactions on natural magnesium, aluminum, iron, and lead.

### 5.3.2 ${}^7\text{Be}$ and ${}^{10}\text{Be}$

For heavier IMFs a really good data base exists for the production of  ${}^7\text{Be}$  (Figures 5.4 to 5.6 ). The situation for  ${}^{10}\text{Be}$  (Figures 5.8 and 5.11) is also not bad, but considerably less data exist than for  ${}^7\text{Be}$  because of the need of chemical separation and AMS-measurements.

In the case of  ${}^7\text{Be}$  and  ${}^{10}\text{Be}$  surely the target elements C, N, and O are particular because of their proximity in masses to the product nuclides. This is nicely exhibited by the structures of their excitation functions (see also Appendix C, Figures C.4 to C.10). For target elements from F to Bi the excitation functions for  ${}^7\text{Be}$  and  ${}^{10}\text{Be}$  run relatively smooth with energy. For the target elements from F to the iron group varying contributions of low energy production below 100 MeV are observed and the shapes of the excitation functions show a clear change in slopes above about 200 MeV pointing also for these product nuclides to different formation modes as evaporation or PE-emission residues and IMF-production at medium energies. For the heavy target elements above Ir only the production at energies above a few hundred MeV as IMFs can be experimentally observed. The measurements by Titarenko et al. [Ti04] do not exhibit significant differences between the cross sections for the production of  ${}^7\text{Be}$  from the different pure Pb isotopes. With respect to  ${}^{10}\text{Be}$ , it is to mention here that the data for  $\text{Bi}(p,X){}^{10}\text{Be}$  [Ta02] must still be regarded as preliminary. Further measurements are underway.

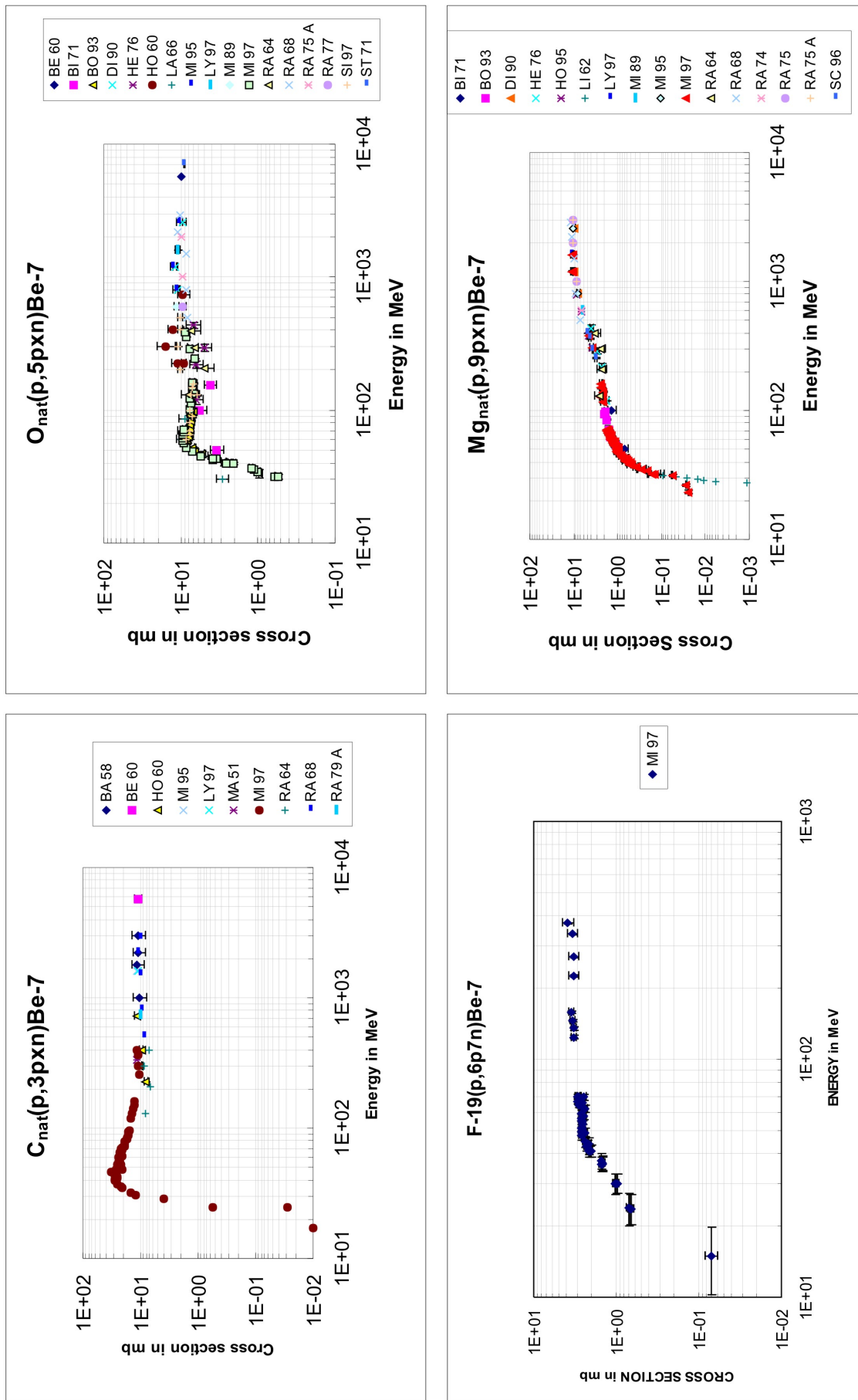


Figure 5.4: Excitation functions for the production of  ${}^7\text{Be}$  by proton-induced reactions on natural carbon, oxygen, fluorine, magnesium.

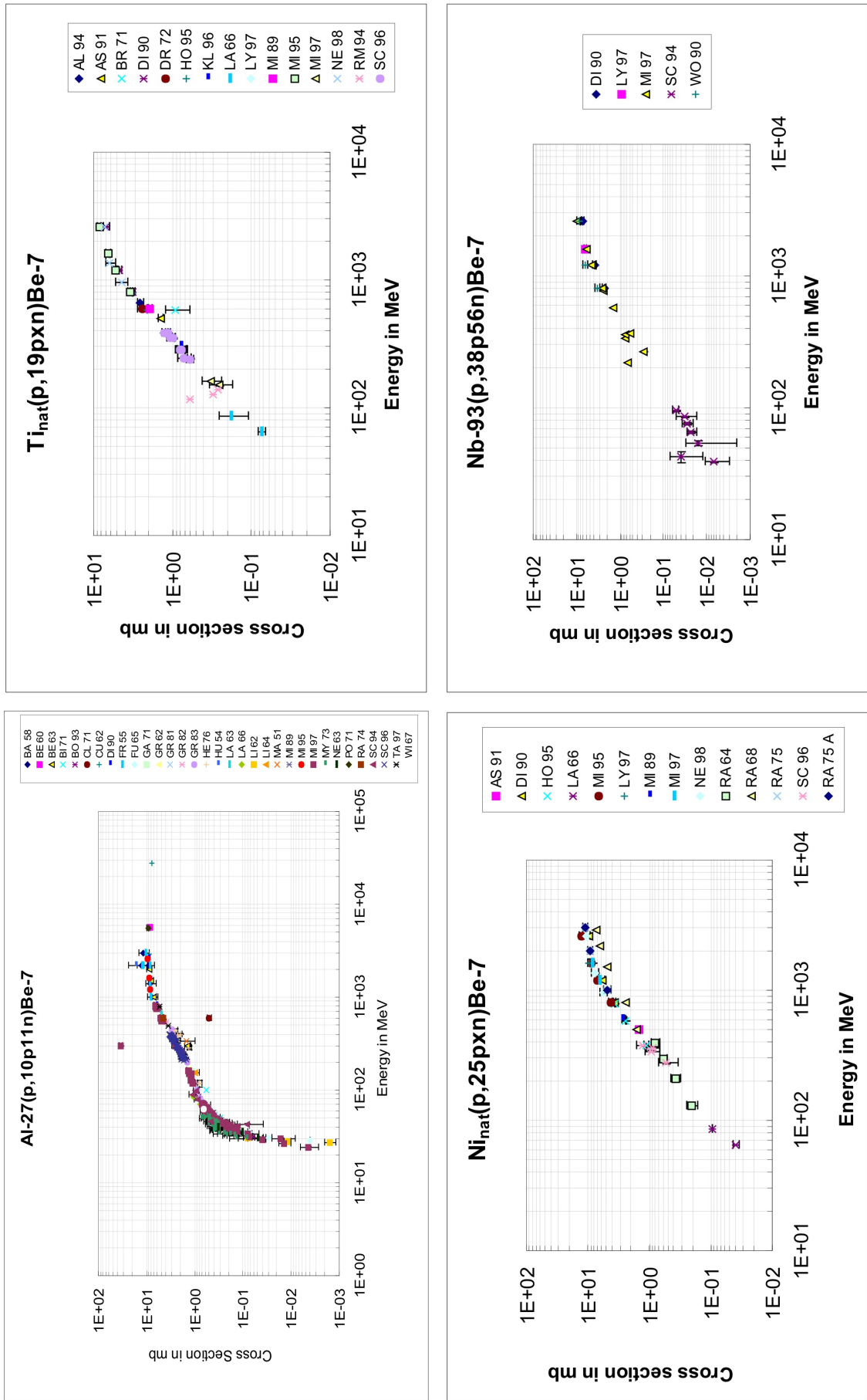


Figure 5.5: Excitation functions for the production of  ${}^7\text{Be}$  by proton-induced reactions on natural aluminum, titanium, nickel, and niobium.

### 5.3.3 $^{21}\text{Ne}$ , $^{22}\text{Na}$ , and $^{24}\text{Na}$

The situation becomes better for the neon isotopes (shown here for  $^{21}\text{Ne}$  in Figure 5.11) and for  $^{22}\text{Na}$  (Figure 5.12 and 5.13) and  $^{24}\text{Na}$  (Figure 5.14). It has to be mentioned that for  $^{22}\text{Ne}$  also the direct production and the cumulative one after the decay of  $^{22}\text{Na}$  is distinguished in the data, denominated as  $^{22}\text{Ne}$  and  $^{22}\text{Ne}_c$  (see Appendix C, Figures C.16 to C.25). For the stable neon isotopes sufficient experimental data exist to give complete excitation functions; see  $^{21}\text{Ne}$  in Figure 5.11). This is due to their importance as cosmogenic nuclides in extraterrestrial matter [Mi98, Mi99]. Consequently, the target elements investigated were Mg, Al, Si, Fe, and Ni. But, in the context of the HINDAS project [Me05] and thereafter systematic measurements for Pb and Bi were performed [Mi05] and further measurements are just going on by I. Leya and coworkers. Except for the product near target elements Mg, Al, and Si, the excitation functions are not much structured. They do not give indications of low-energy production by evaporation or PE-emission. So these products (and the heavier ones dealt with in this work) must be regarded as IMFs.

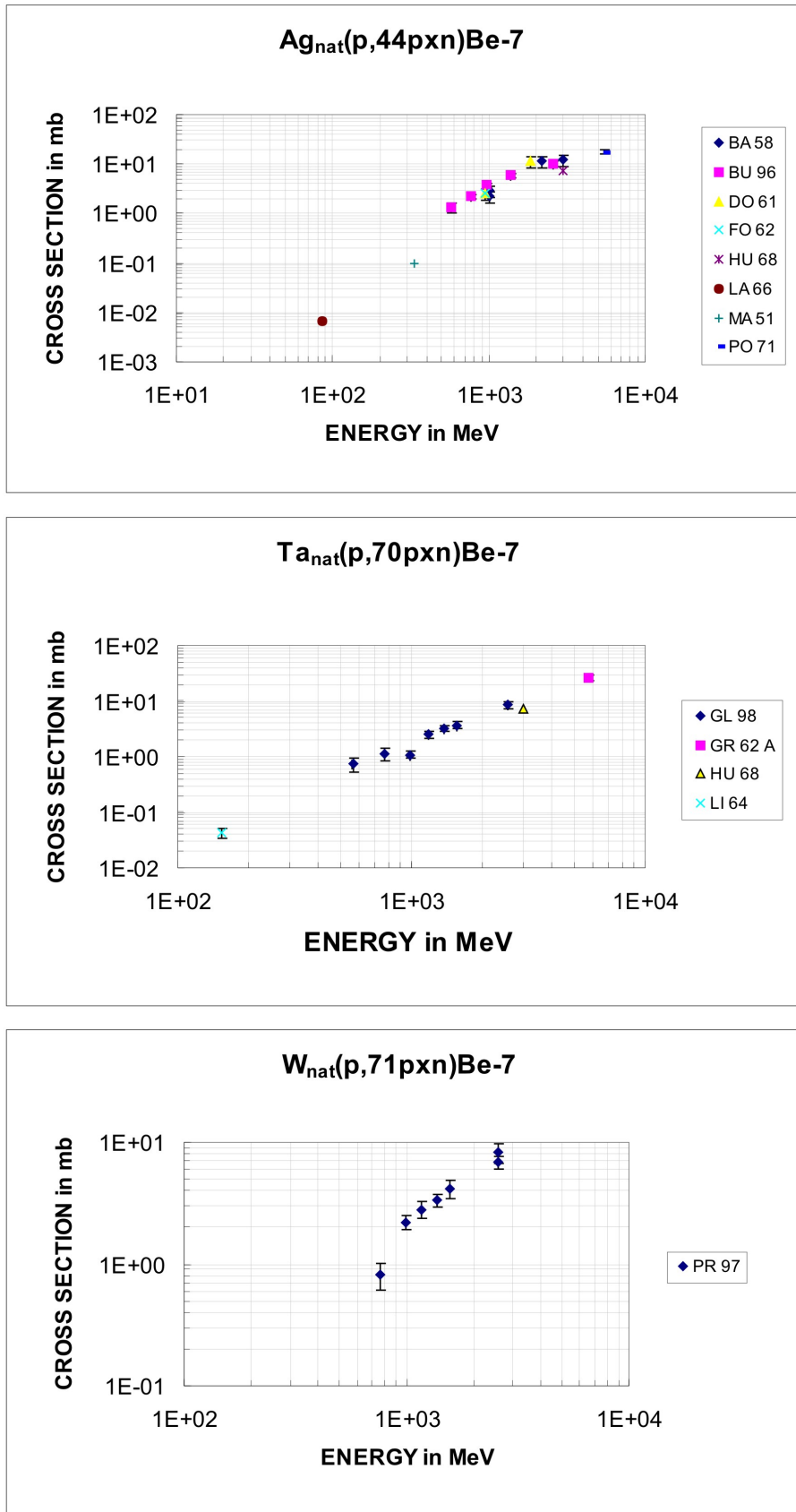


Figure 5.6: Excitation functions for the production of  ${}^7\text{Be}$  by proton-induced reactions on natural silver, tantalum and tungsten.

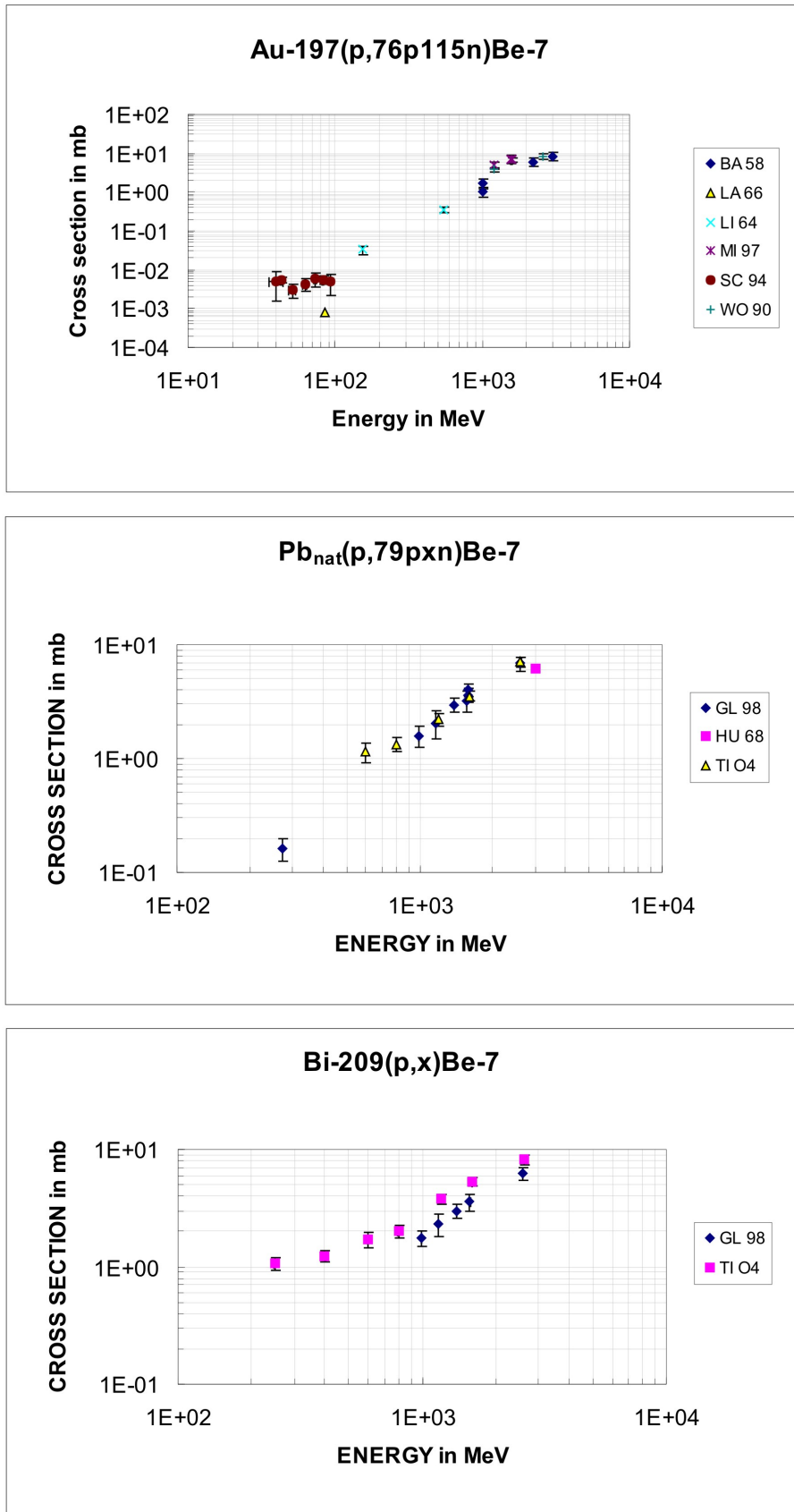


Figure 5.7: Excitation functions for the production of  ${}^7\text{Be}$  by proton-induced reactions on natural gold, lead, and bismuth.



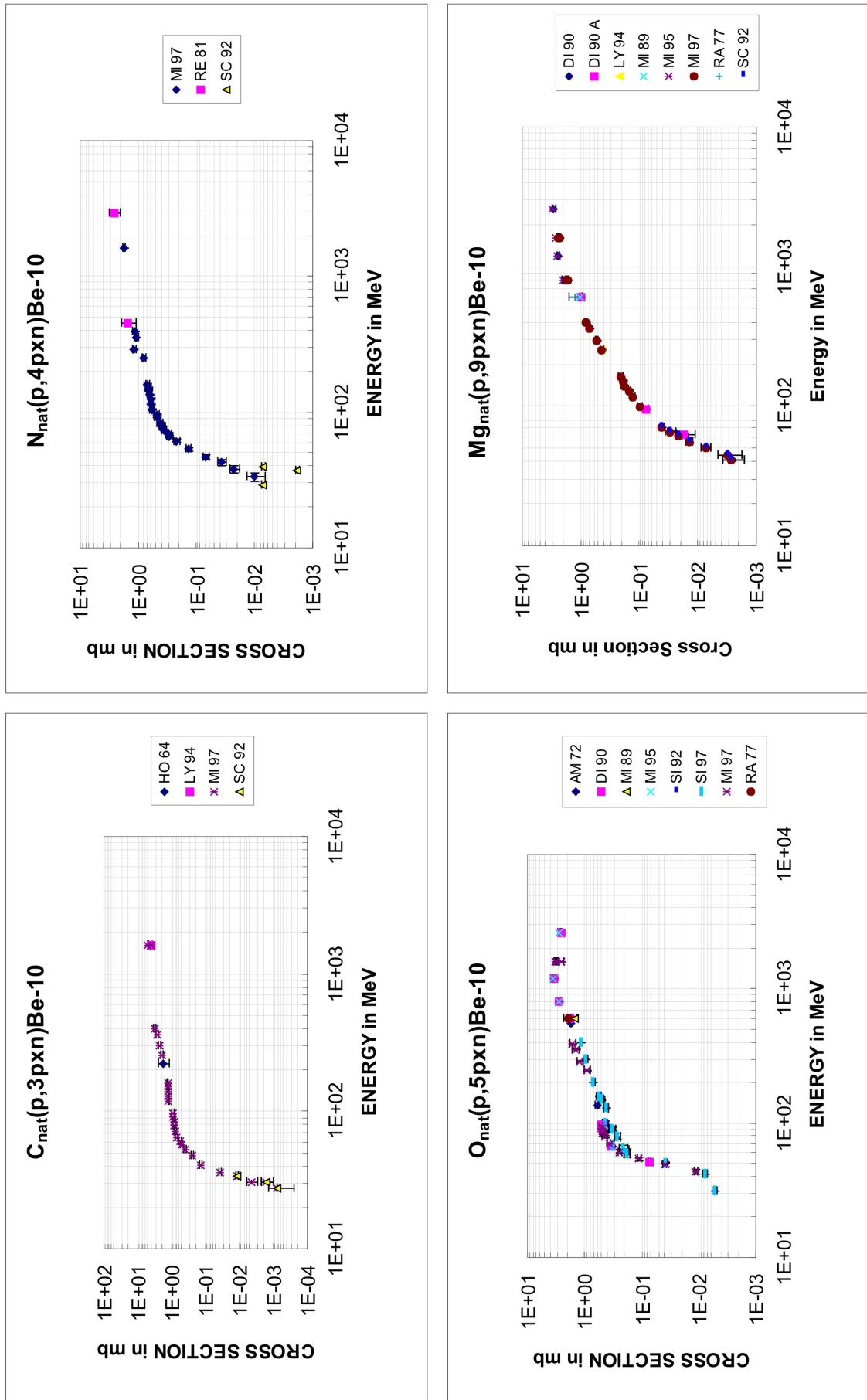


Figure 5.8: Excitation functions for the production of  $^{10}\text{Be}$  by proton-induced reactions on natural carbon, nitrogen, oxygen, magnesium.

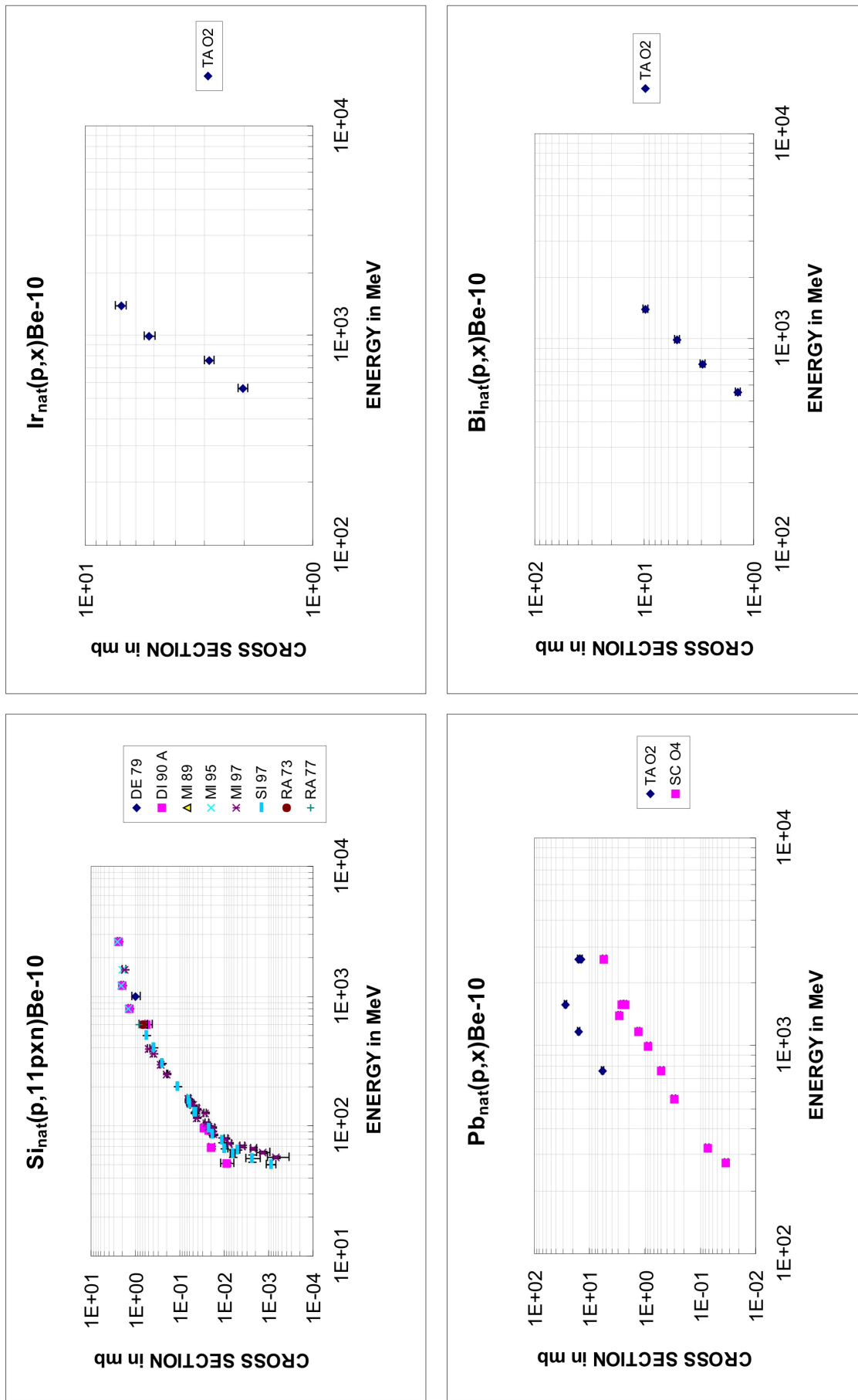


Figure 5.9: Excitation functions for the production of  $^{10}\text{Be}$  by proton-induced reactions on natural silicon, iridium, lead, and bismut.

By far most of the data exist for  $^{22}\text{Na}$  (Figure 5.12) from light and medium-mass target elements. Particular structures in the excitation functions are seen for target elements from Na to Ca, for all heavier target elements the excitation functions exhibit monotonous increases from thresholds to the highest energies investigated. In the case of the target element Mg, for mono-isotopic targets of  $^{24,25,26}\text{Mg}$  we see a nice distinction of the individual reaction channels contributing to the production of  $^{22}\text{Na}$  from natural magnesium (Figure 5.10). For  $^{24}\text{Na}$  (Figure 5.14) the phenomenology of the excitation functions does not differ from that of  $^{22}\text{Na}$ .

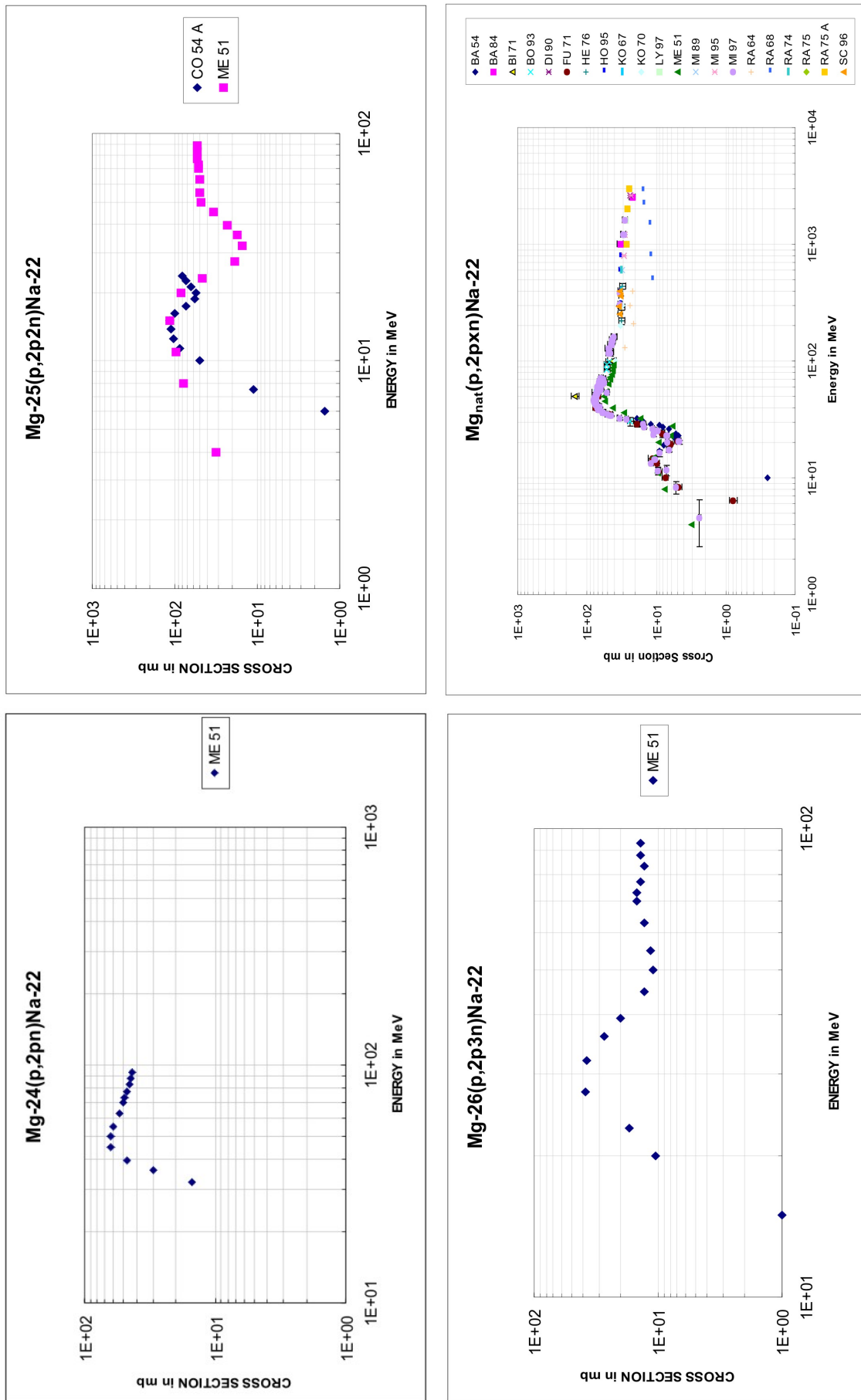


Figure 5.10: Excitation functions for the production of  $^{22}\text{Na}$  by proton-induced reactions on  $^{24,25,26}\text{natMg}$

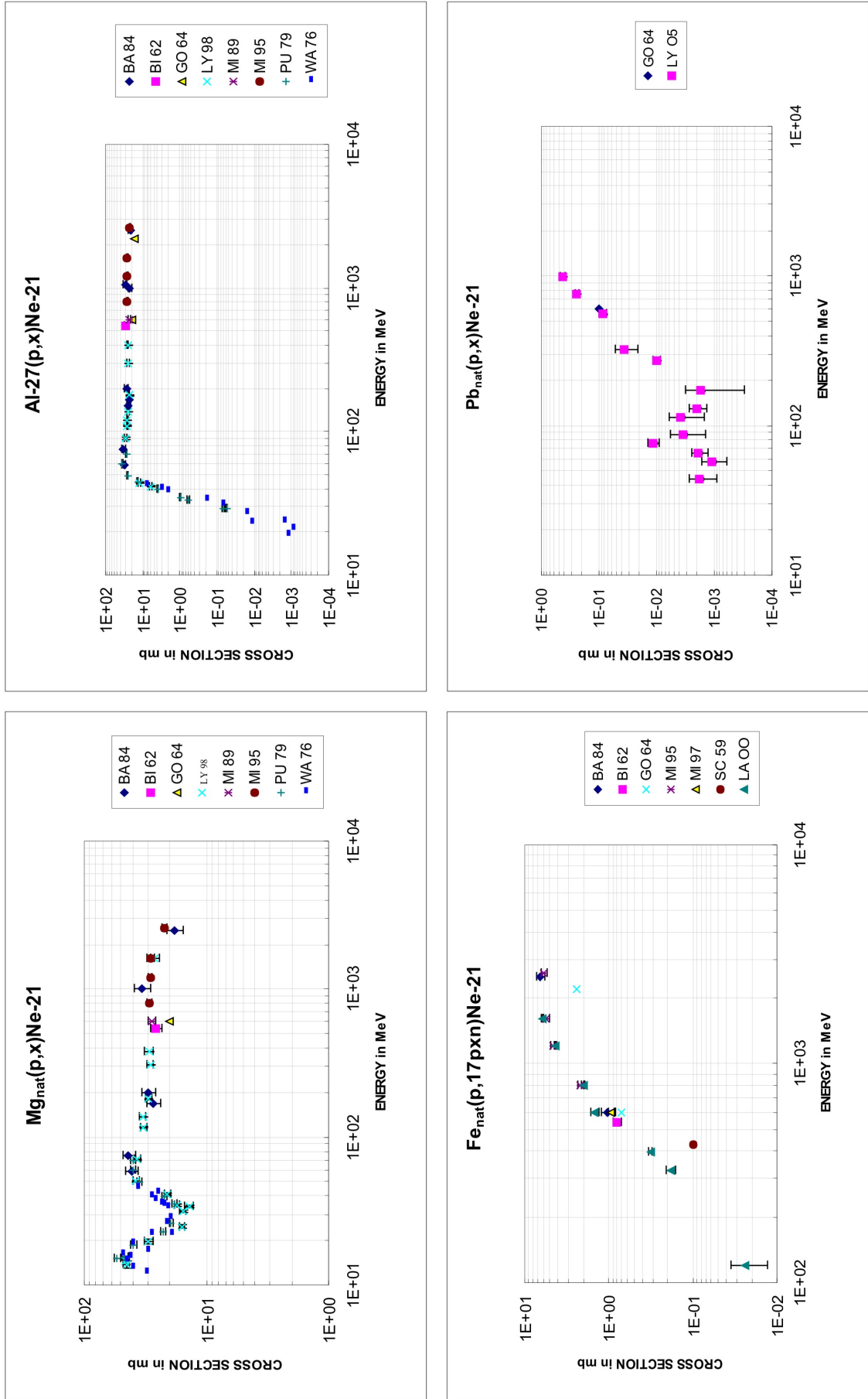


Figure 5.11: Excitation functions for the production of  $^{21}\text{Ne}$  by proton-induced reactions on natural magnesium, aluminum, iron, and lead.

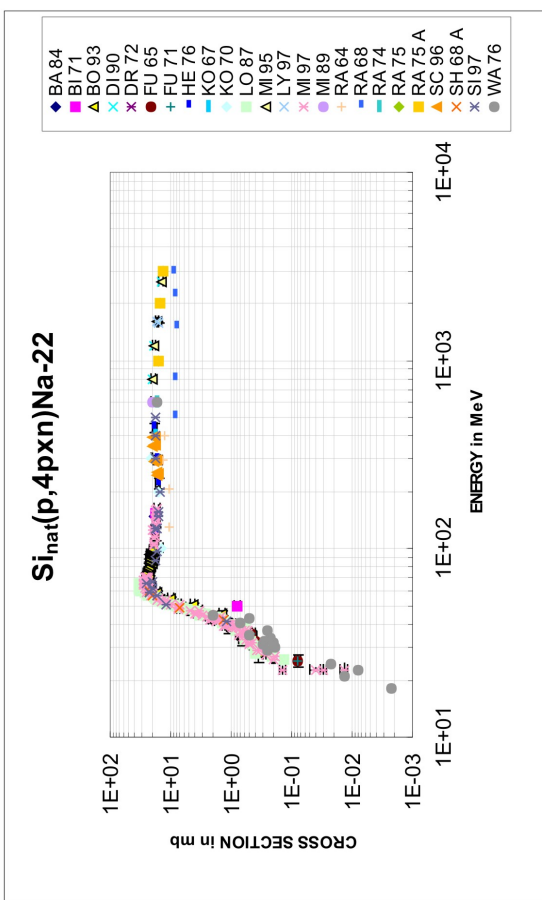
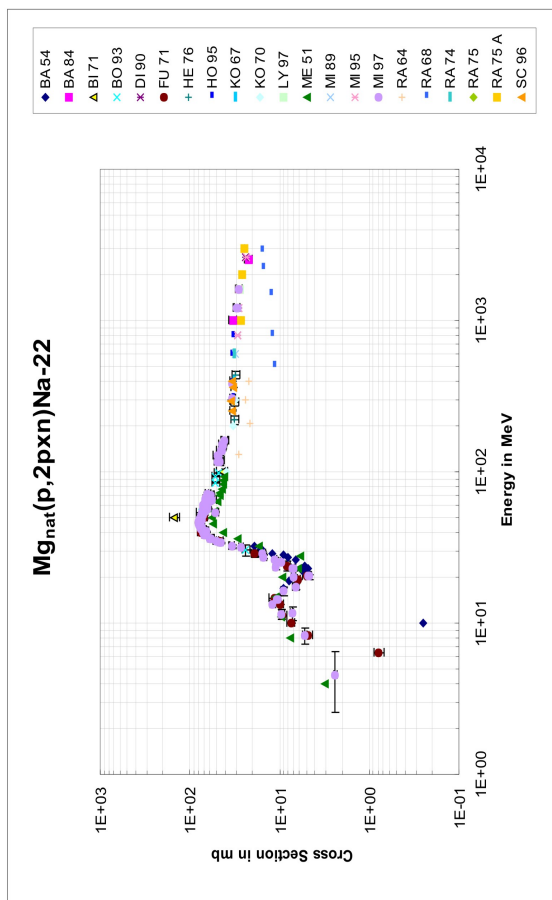
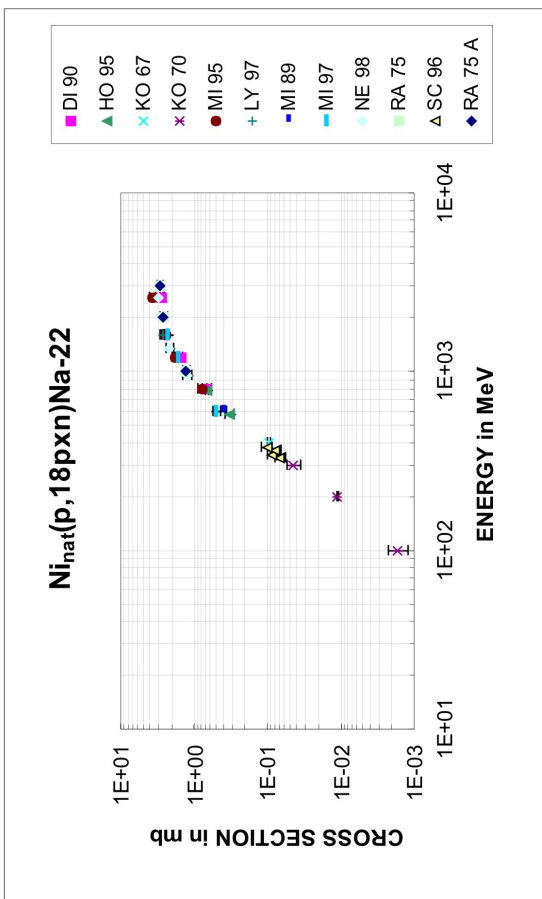
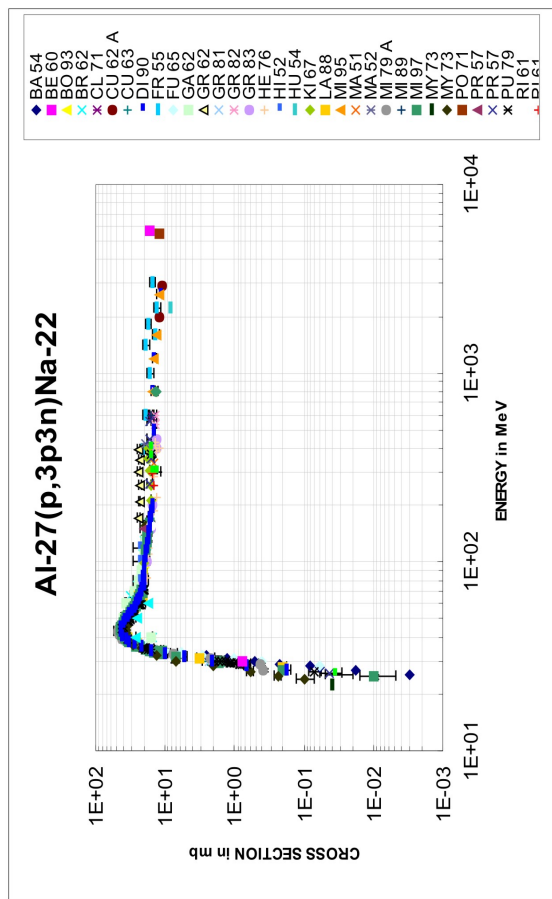


Figure 5.12: Excitation functions for the production of <sup>22</sup>Na by proton-induced reactions on natural magnesium, aluminum, silicon, nickel.

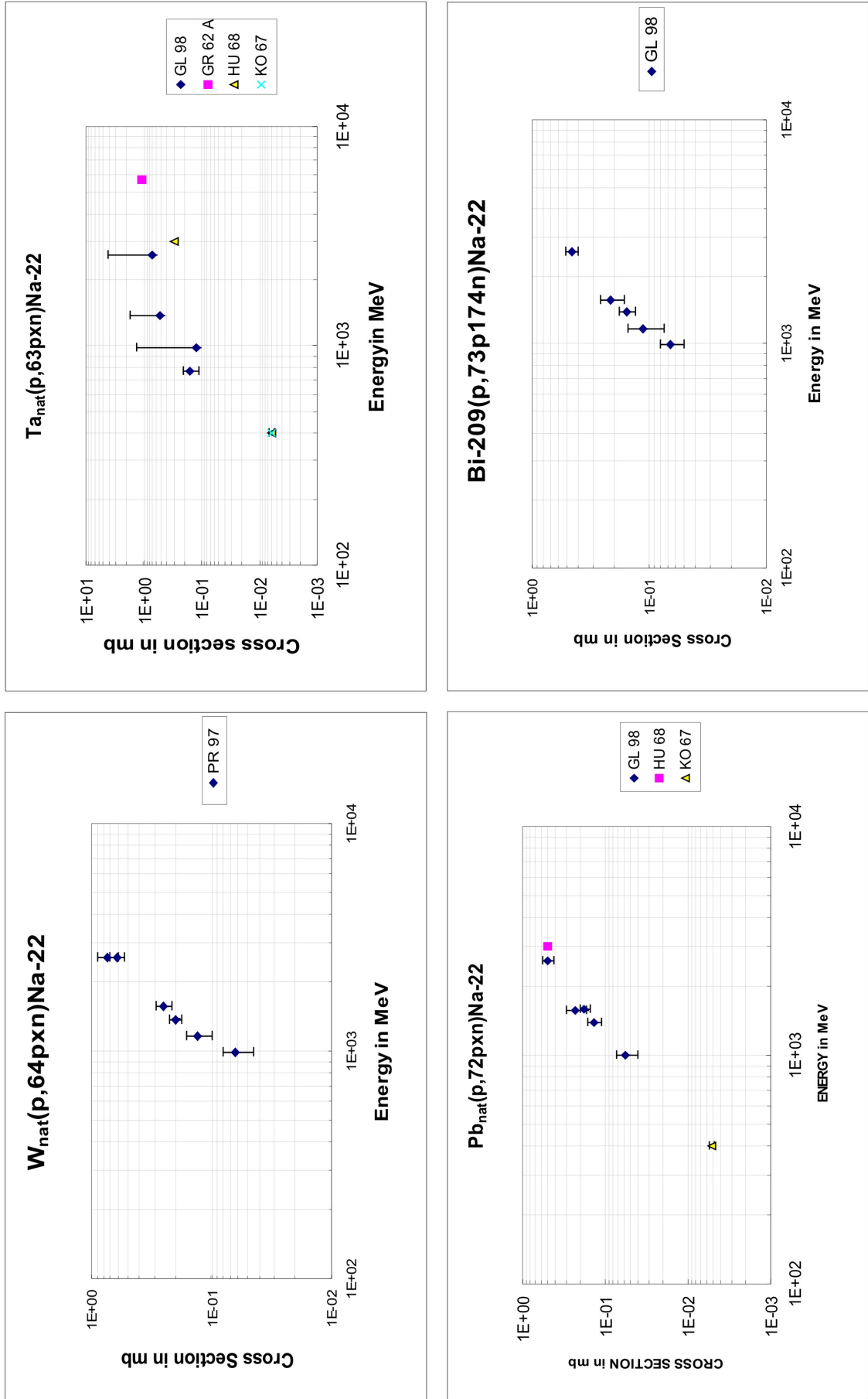


Figure 5.13: Excitation functions for the production of  $^{22}\text{Na}$  by proton-induced reactions on natural tantalum, lead and bismut.

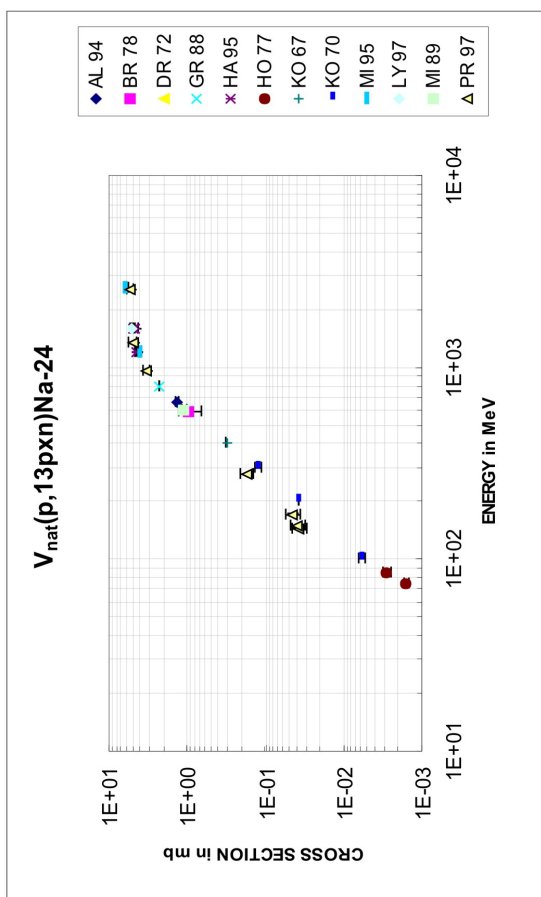
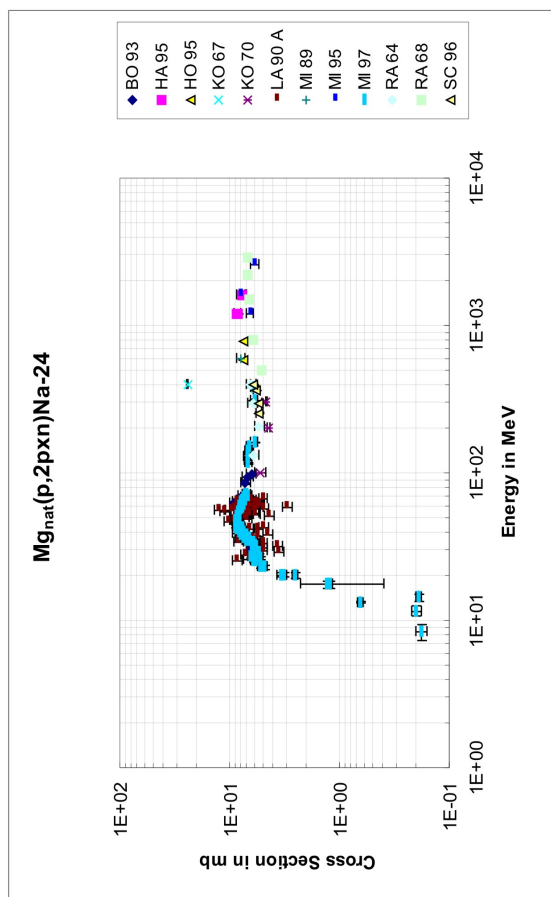
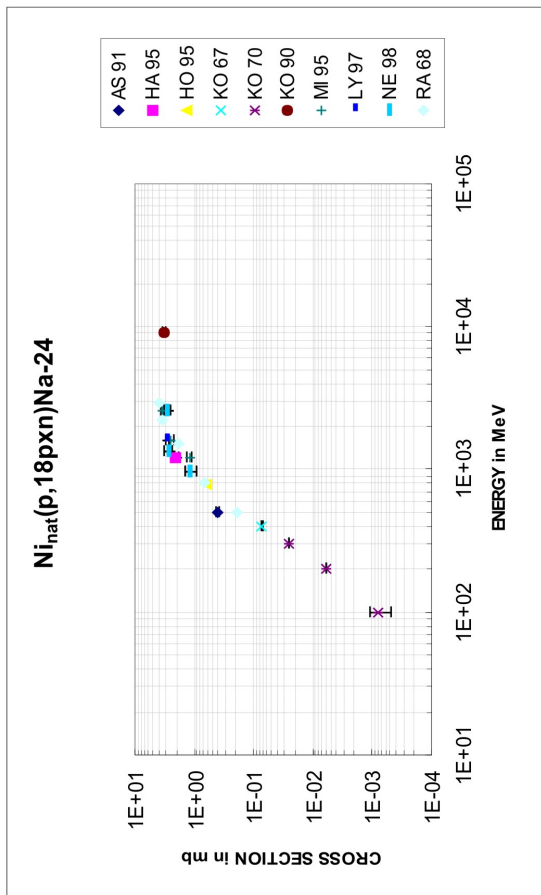
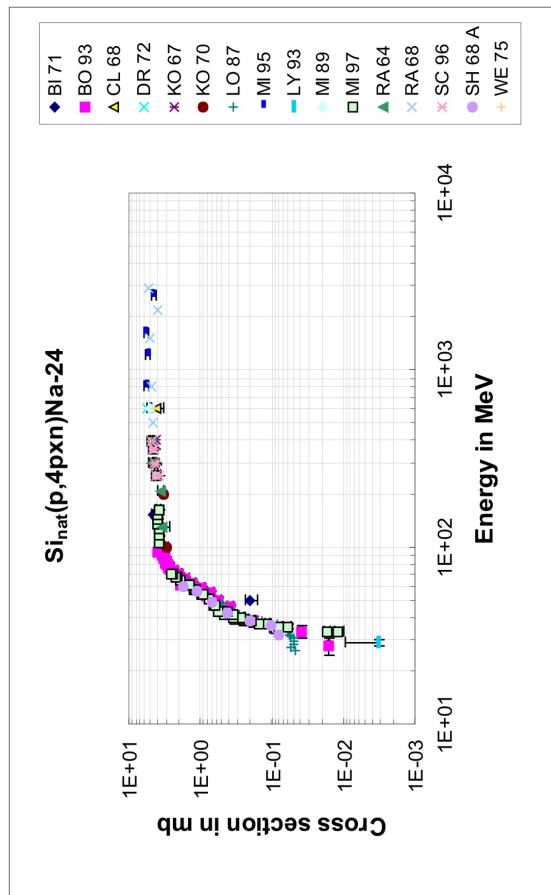


Figure 5.14: Excitation functions for the production of <sup>24</sup>Na by proton-induced reactions on natural magnesium, silicon, vanadium, nickel.



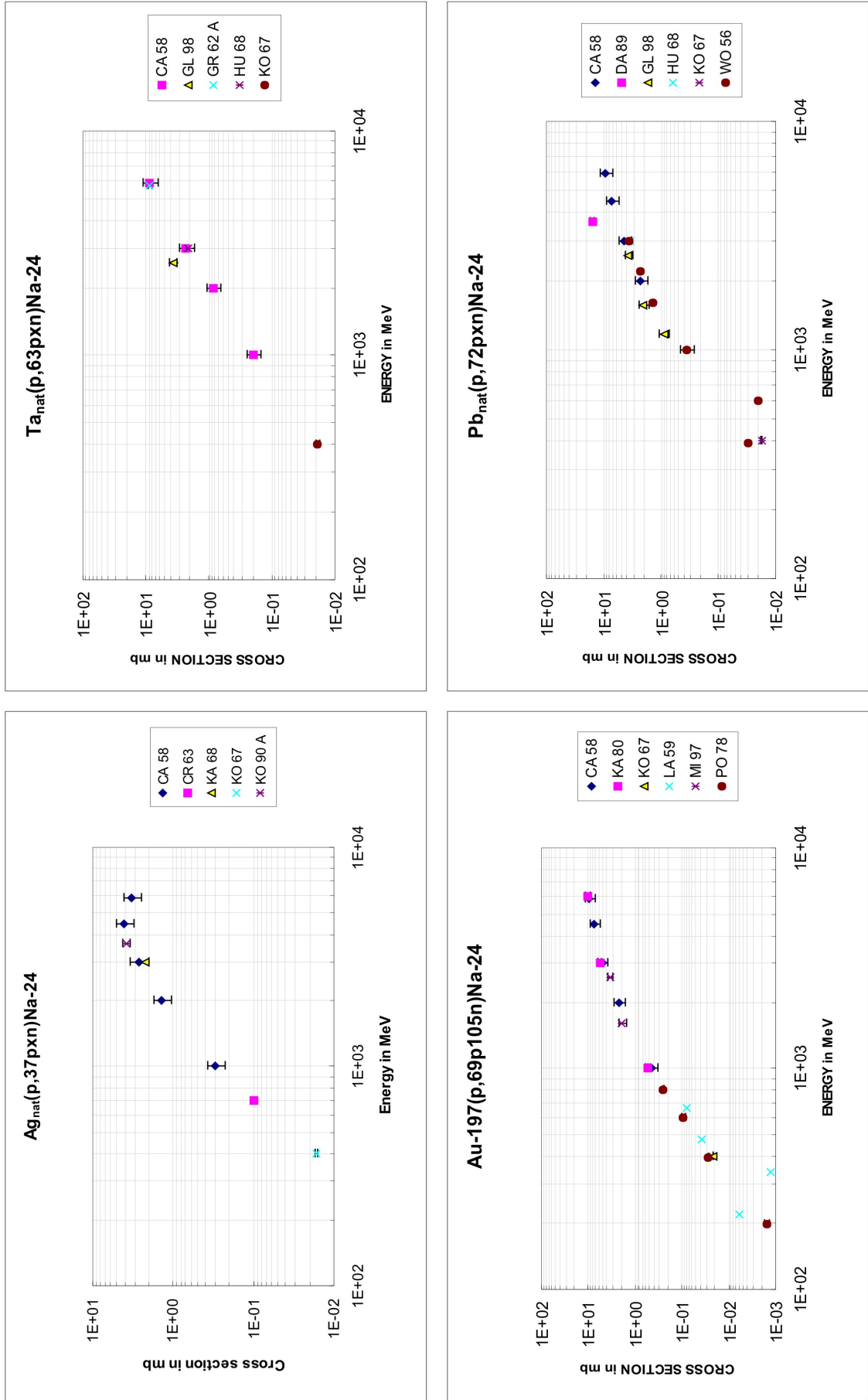


Figure 5.15: Excitation functions for the production of  $^{24}\text{Na}$  by proton-induced reactions on natural silver, tantalum, gold, and lead.

For the heaviest product nuclides dealt with in this thesis,  $^{28}\text{Mg}$  (Figure 5.16) and  $^{26}\text{Al}$  (Figure 5.17), just the target elements up to the iron group were systematically investigated. For heavier target elements just some data for Pb exist and ongoing measurements promise data for  $^{26}\text{Al}$  from lead and bismuth.

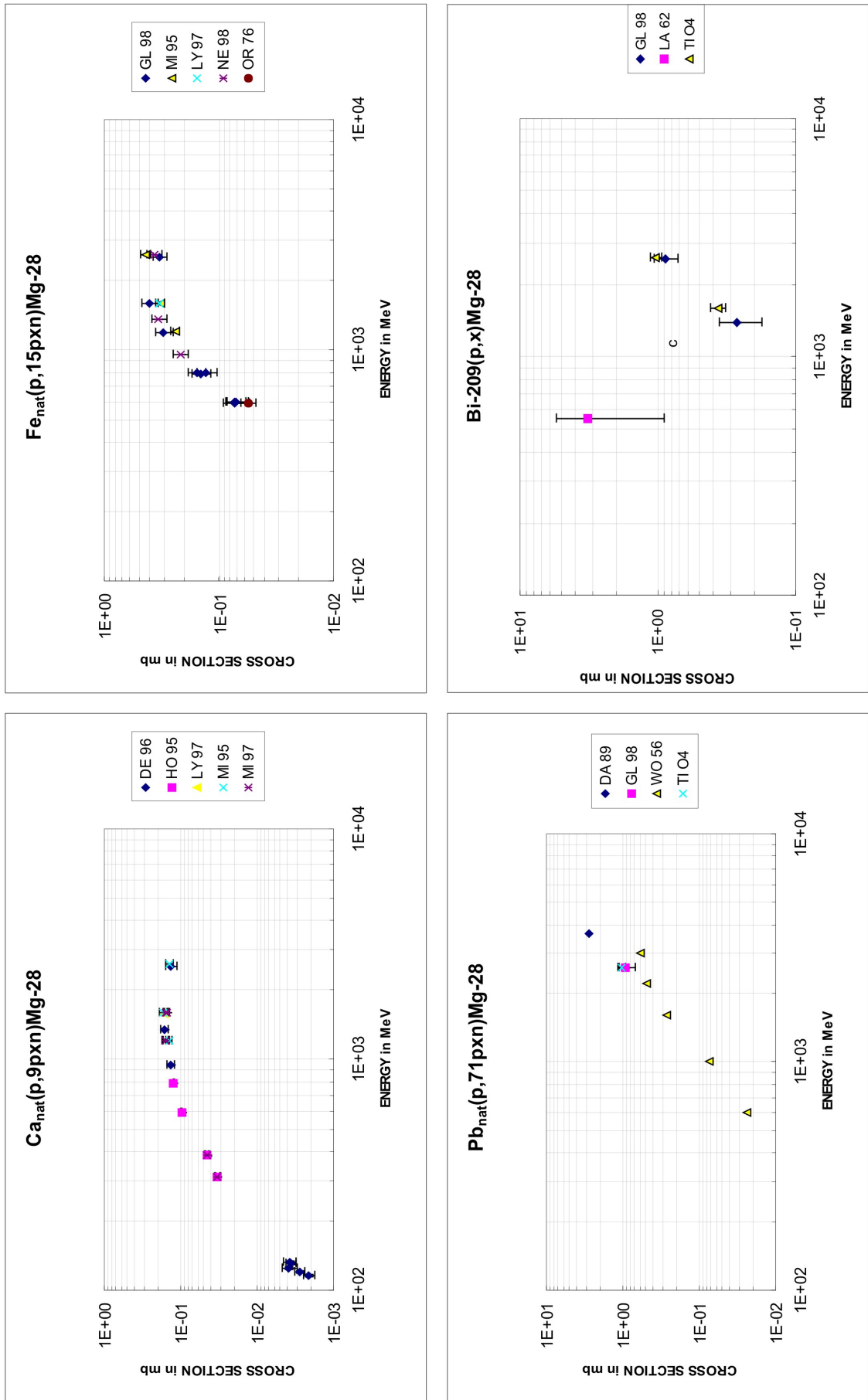


Figure 5.16: Excitation functions for the production of  $^{28}\text{Mg}$  by proton-induced reactions on natural calcium, iron, lead, and bismuth.

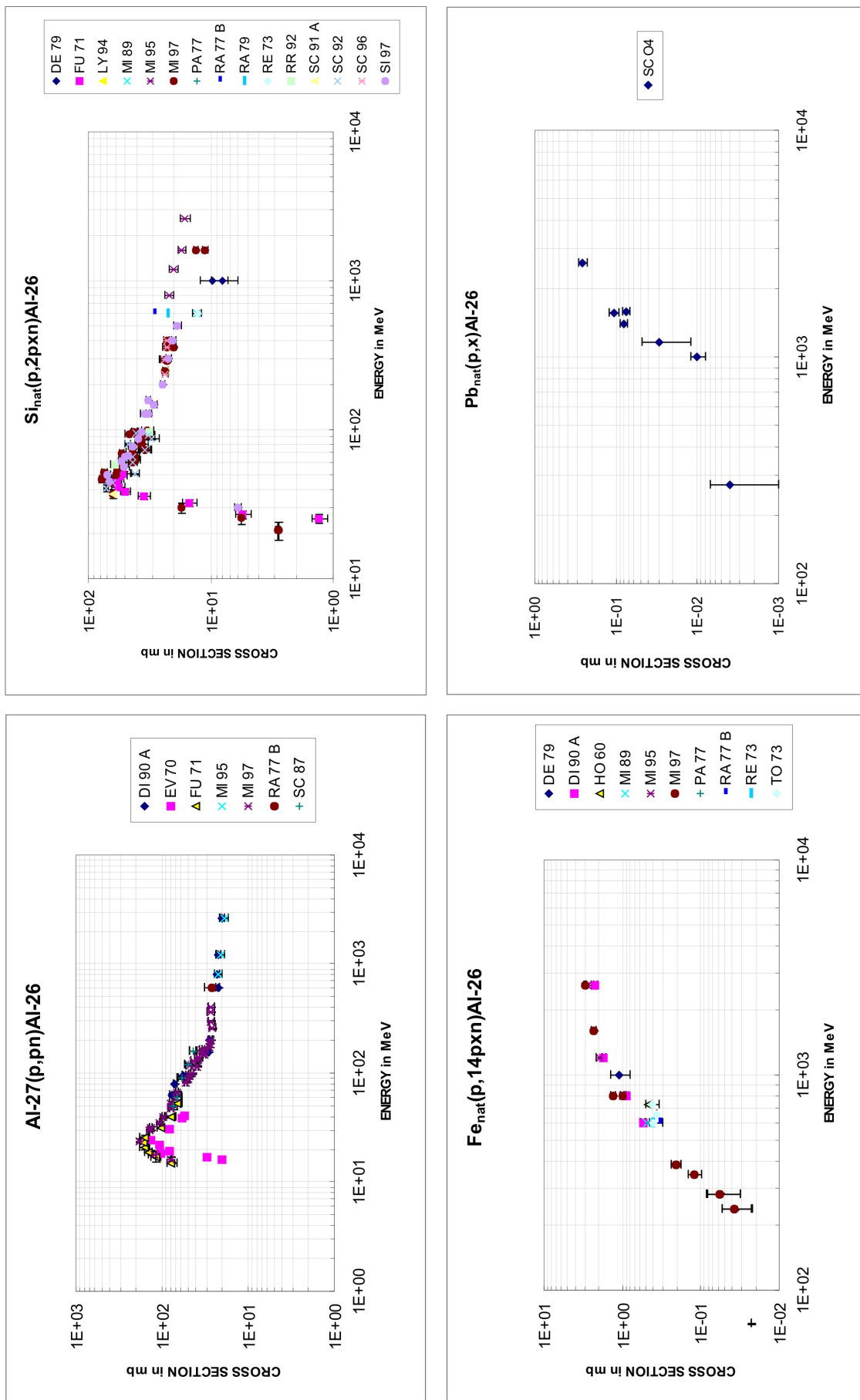


Figure 5.17: Excitation functions for the production of  $^{26}\text{Al}$  by proton-induced reactions on natural aluminum, silicon, iron, and lead.

Because of the particular importance of helium production in accelerator-driven facilities, the agreement among the experimental data is of outstanding importance. Such measurements were performed within the HINDAS project by direct measurement of light gas isotopes by the NESSI collaboration, e.g. [En99]. In addition and in order to test the consistency with earlier mass spectrometric measurements the production of stable and radioactive rare gas isotopes of He-, Ne-, Ar-, Kr-, and Xe from natural lead by proton-induced reactions was investigated from threshold up to 2.6 GeV by rare gas mass spectrometry [Ly05]. Apart from some exceptions the database for the proton-induced production of noble gas isotopes from lead is consistent and nearly complete. While for the production of He from Al and Fe, where the cross sections obtained by thin-target irradiation experiments are up to a factor of 2 higher than the NESSI data [En99], both datasets agree for the He production from lead (Figure 5.18). Figure 5.18 just contains the data by Leya and co-workers [Ly05] with respect to the mass spectrometric measurements. But for the cosmochemically important target elements Mg, Al, Si, Fe and Ni, considerably more data exist which were measured by different groups at different places. The recent ones of these measurements [Gi98, Gi98a] validate the measurements by Leya and co-workers [Ly98, Ly05]. Thus, our present conclusion is that some of the helium produced by evaporation and PE-emission from the light target elements must be missing in the NESSI measurements. This would explain that the cross sections for lead are well in agreement for the mass spectrometric and the NESSI measurements, but not for the light target elements.

Except for the NESSI measurements, all cross sections dealt with so far in this report were derived by off-line measurements after experiments in classical kinematics. The measurements with inverse kinematics performed at GSI, e.g. [En01], had not to be mentioned here because IMFs were not accessible in the past. However, in a recent experiment with U on protons in inverse kinematics, measurements of IMF down to masses of 15 were reported [Ri05]. Since we are not dealing with the target element uranium, this work is only mentioned for completeness here.

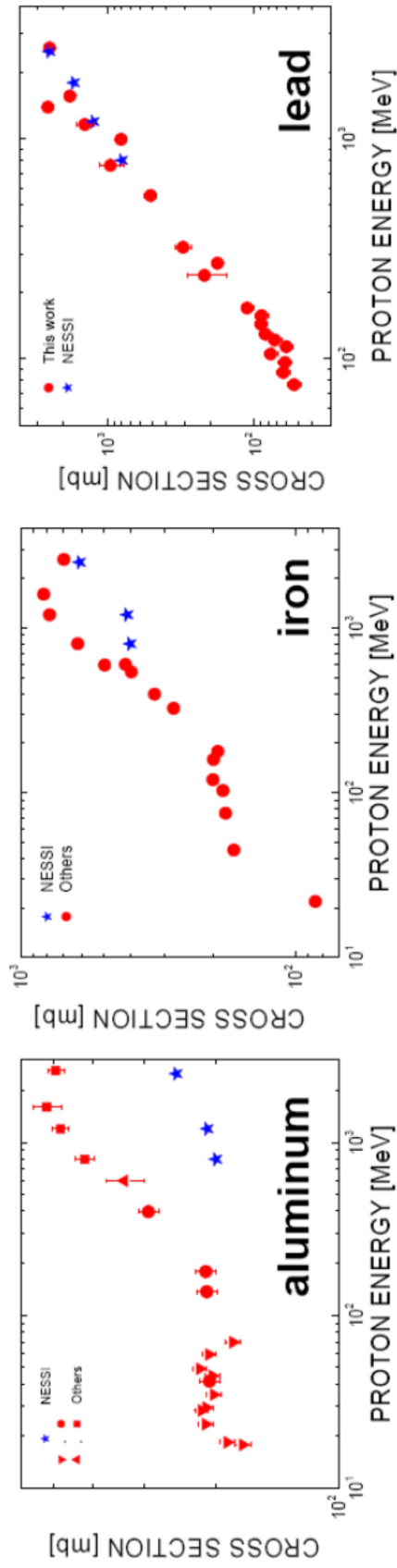


Figure 5.18: Production of He ( $=^3\text{He}+^4\text{He}$ ) from natural lead by proton-induced reactions; data are from [Ly05] (full circles) and [En99] (blue stars).

## 5.4 Empirical systematic

In order to emphasize the particularities of the phenomenology of IMF production some general considerations about the phenomenology of residual nuclide production at medium energies are necessary. In Serbers two-stage model [Se47] of nuclear reactions at intermediate energies the spallation process is described as a fast intra-nuclear cascade followed by a slow deexcitation shape of the highly excited intermediate system by evaporation. This view is valid still today. As a consequence of this model one expects the phenomenology of spallation reactions to be characterized by an exponential decrease of the isobaric mass yields with the mass difference between target and products. Figure 5.19 gives an example for the target element niobium where the upper envelope of the individual cross sections can serve as a first approximation of the isobaric mass yields. In early mathematical formulations this dependence was described by Rudstams formula [Ru66] which in addition to the exponential behavior of the isobaric mass yields described the residual nuclide distribution on an isobar by Gaussians or distorted semi-Gaussian functions. It was also observed that the slope of the exponential decrease of mass yields with target-product mass difference gets flatter with increasing particle energies.

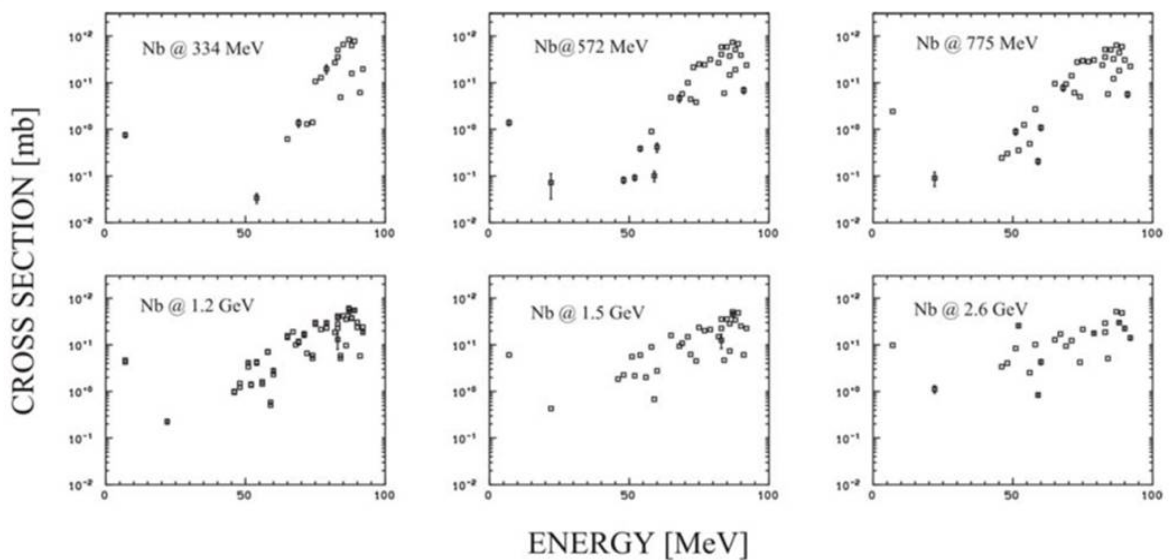


Figure 5.19: Cross sections for the production of residual nuclides from niobium as function of the product mass [Mi97].

At that time no experimental evidence existed that other evaporation processes than those of nucleons or light complex particles might contribute to the slow deexc-

tation process at the end of the intra-nuclear cascade. This lack of evidence originated from the fact that practically no experiments were performed to investigate proton-induced spallation reactions on heavy target elements. Already during the first two decades of spallation studies it was, however, observed that the isobaric yields and the individual cross sections for small residual nuclide masses increase again. In the example given in Figure 5.19 this effect is observed for mass 7, namely the production of  ${}^7\text{Be}$ . The increase of yields at low masses, which was also observed for other nuclides up to about mass 15, was attributed to fragmentation, e.g. in form of a Fermi break-up of the excited system after the intra-nuclear cascade. Whether or not this would lead to multifragmentation with enhanced multiplicities of IMFs was not discussed.

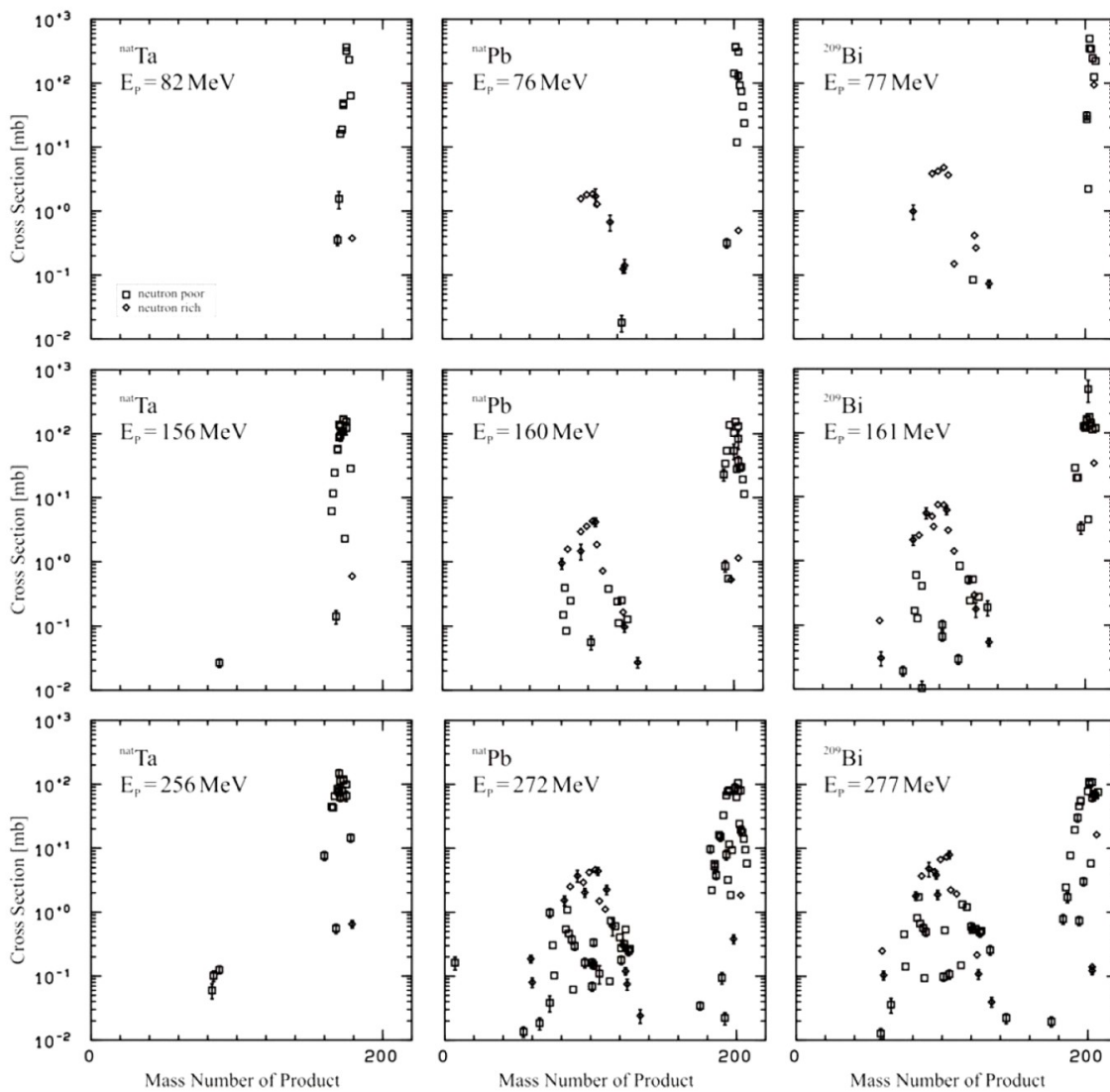


Figure 5.20: Cross sections for the production of residual nuclides from Ta, Pb, and Bi as function of the product mass [Gl98].



With the rising interest in accelerator-driven technologies intermediate-energy nuclear reactions with heavy target elements were systematically investigated and a new feature of spallation reactions was observed. The intermediate residuals at the end of intra-nuclear cascade could deexcite in addition to evaporation of nucleons and light complex particles via fission. This is exemplarily shown in Figures 5.20 - 5.22 for proton-induced reactions on Ta, Pb, and Bi. Already at about 200 MeV the fission channel is open for elements such as Ta, W (not shown), Au (not shown), Pb, and Bi.

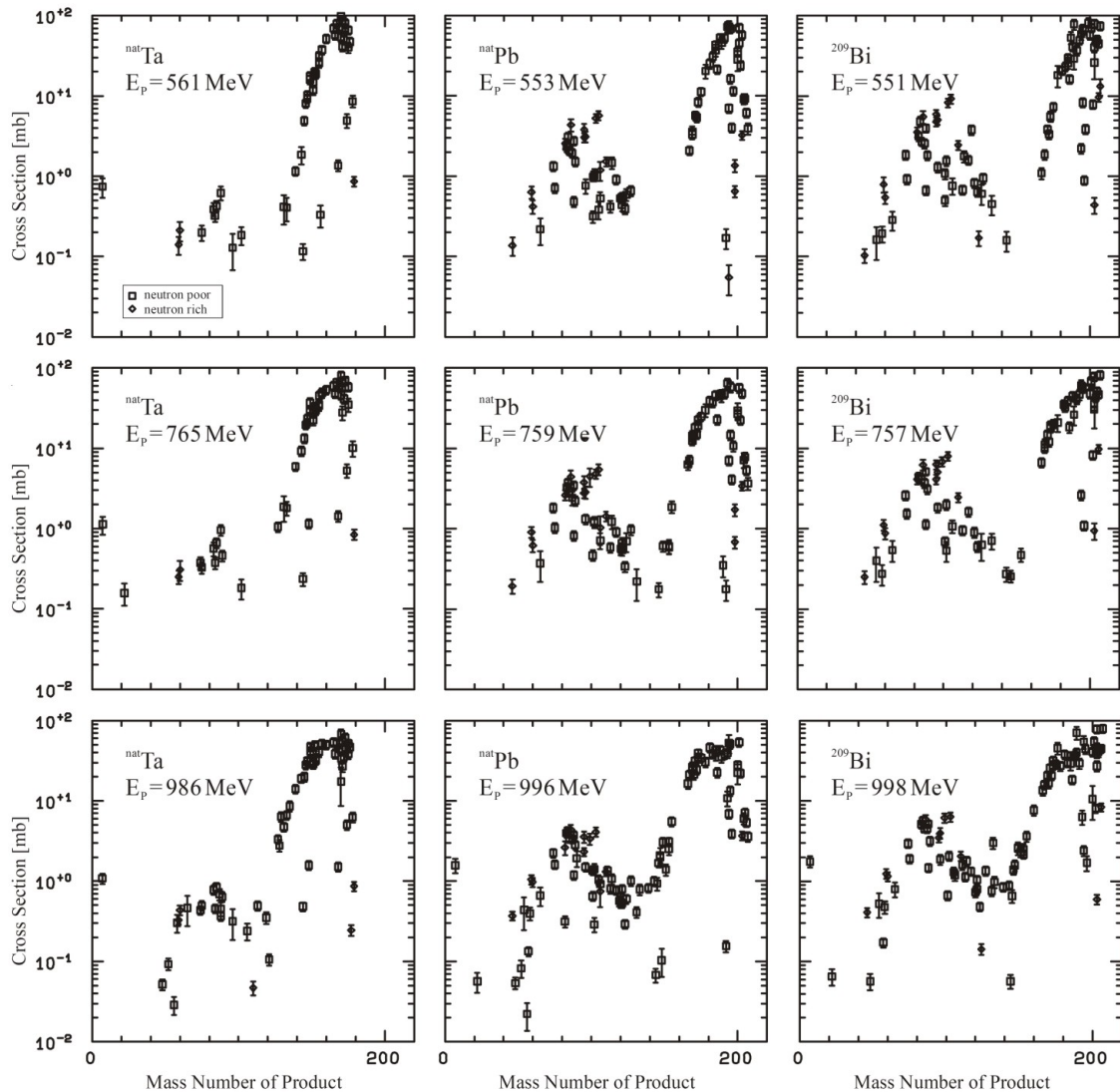


Figure 5.21: Cross sections for the production of residual nuclides from Ta, Pb, and Bi as function of the product mass [G198].

At energies of about 80 MeV fission products show up for Pb and Bi, but not for the lighter target elements. With increasing energies the fission channel becomes increasingly important. It dominates the mass distribution at about 1 GeV. However,

above masses of 140 the symmetric fission mass distribution shows a transition into the exponential mass distribution of "classical" spallation products for higher product masses. The flattening of the slope of isobaric yields of the "classical" spallation products tends to smear out the importance of the fission channel which, however, can be weakly distinguished even at 2.6 GeV (Figure 5.22). The knowledge about intermediate-energy proton-induced reactions with heavy target elements was strongly influenced by investigations using inverse kinematics, e.g. [En01], which allowed to measure complete distributions of residual nuclides for elements with atomic numbers above 20 in these reactions. These investigations are performed at particular energies and the efforts needed to perform these measurements do not allow for establishing complete excitation functions over large energy regions. Thus, the classical- and inverse-kinematics experiments are complementary with respect to the investigations of complete residual nuclide distributions at a particular energy with the measurement of the complete energy dependence for particular product nuclides.

One draw-back of the inverse kinematics was that low residual masses could not be observed and therefore no evidence about the IMFs could be obtained. Also in the intermediate-energy nuclear reactions of protons with heavy target elements an enhanced production of IMFs with masses below about 15 was observed in the experiments with classical kinematics (Figures 5.19 - 5.22). Only in recent experiments [Ri05] lower-mass residual nuclides were also observed using inverse kinematics. At present, we shall describe the phenomenology of IMF-production on the basis of the experimental data put together in the preceding section. This shall contribute to the discussion of the still open question whether the production of IMFs needs a particular production mode such as (multi-)fragmentation or whether the production of IMFs can be explained on the basis of deexcitation modes such as evaporation and fission in the second stage of spallation reactions. To this end we look at the systematic of cross sections at particular energies. Since not all the measurements were performed at the same energy points, we had to look at certain energy bins of  $\pm 100$  MeV width though for low energies this adds some scatter to the data because of the dependence of the individual cross sections on energy. This was done in Figures 5.23 - 5.33 in this section. Such a systematic was already used earlier [Mi00]. It can, however, now be discussed on the basis of much larger data base.

According to the shapes of the distributions of the residual nuclides (Figures 5.20 - 5.22), radionuclides with masses larger than 56 can be unambiguously recognized as being fission-products. The residual nuclide distributions indicate even that the fission products extend well beyond the maximum of the binding energy per nucleon curve.

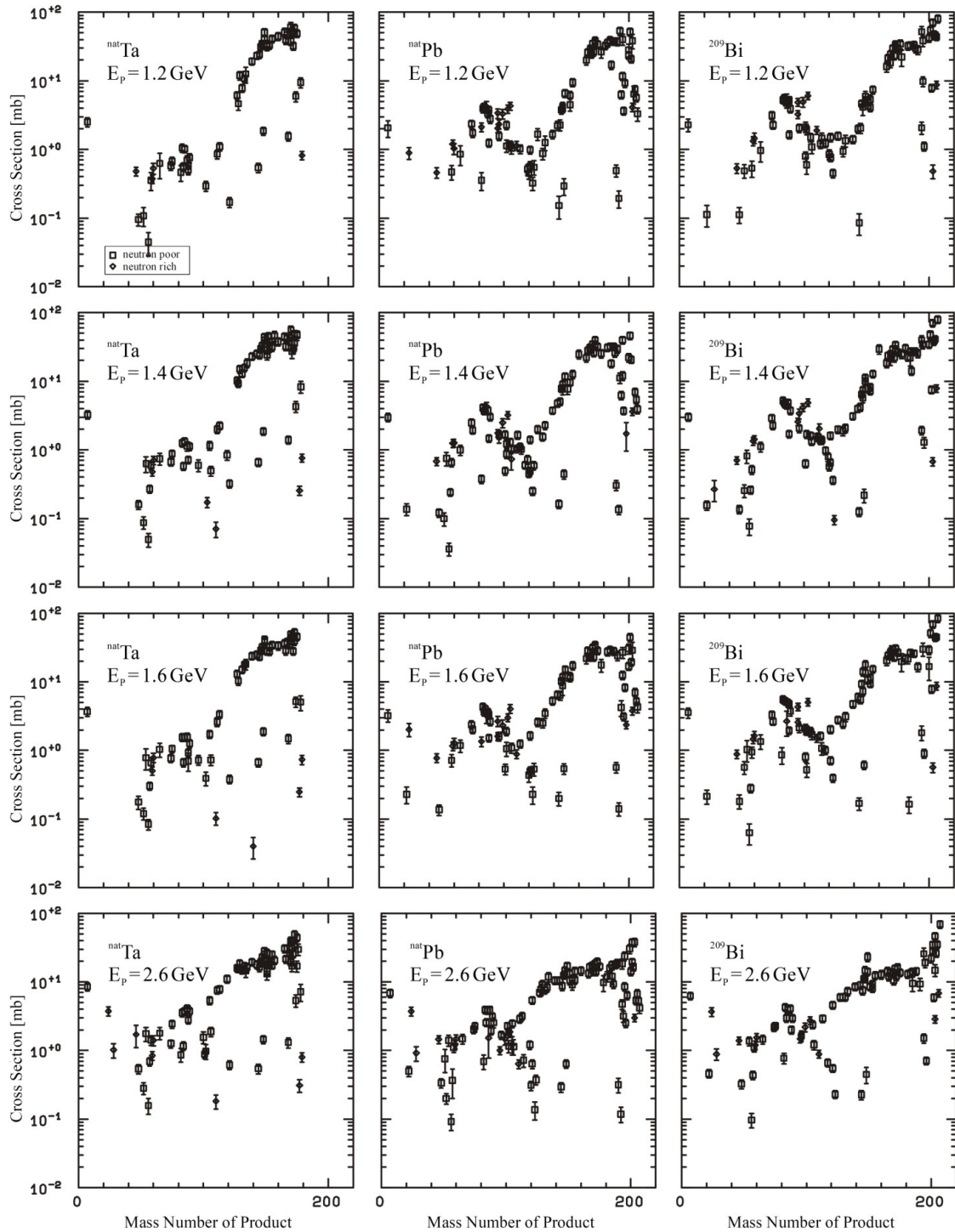


Figure 5.22: Cross sections for the production of residual nuclides from Ta, Pb, and Bi as function of the product mass [Gl98].

But, it will be easier to discuss first such nuclides above this maximum at mass 56. In Figure 5.23, the cross sections for the production of  $^{59}\text{Fe}$  and  $^{60}\text{Co}$  at energies of 0.8, 1.2, 1.6, and 2.6 GeV are plotted as function of the atomic numbers of the target

elements. One observes about an exponential decrease of the cross sections with increasing atomic number of the target element up to  $Z = 60$ . For higher atomic numbers  $Z > 73$  (Ta) the cross sections increase with atomic number of the target element also about exponentially.

For target elements between  $Z = 56$  and  $Z = 73$  no experimental data exist. The decrease of cross sections for targets with atomic numbers below 60 can be understood as the phenomenology of "classical" spallation reactions where the deexcitation in the stage of the reactions occurs solely via evaporation of nucleons and light composite particles. The increase for higher- $Z$  target elements points to an exponentially increasing importance of the fission channel in this second stage of the reaction. If the production of IMFs occurs in the context of the deexcitation via the fission channel, one would expect a similar behavior of IMF cross sections.

However, this is not the case as will be discussed below for all the residual nuclides dealt with in this work. In spite of the wealth of experimental data for the production of IMFs described in the preceding section, the systematic derived here remains not comprehensive for many residual nuclides. But, for some nuclides one obtains a rather comprehensive and consistent view of IMF production. Generally, we have plotted the cross sections for a particular residual nucleus as a function of the target mass number for energy bins centered around 600 MeV, 1200 MeV, 1600 MeV, 2000 MeV, 2200 MeV, and 2600 MeV for all the data available (Figures 5.24 - 5.33 and Appendix D). The center points of the energy bins were chosen to contain as many cross sections as possible and, at the same time, to give a systematic survey on all energies investigated. There is practically no dependence on target mass for the production of  $^3\text{He}$  and  $^4\text{He}$  for all energies (Figures 5.25 - 5.26). A slight increase with target mass of  $^3\text{He}$  and  $^4\text{He}$  production observed for high energies may be but is not necessarily significant.

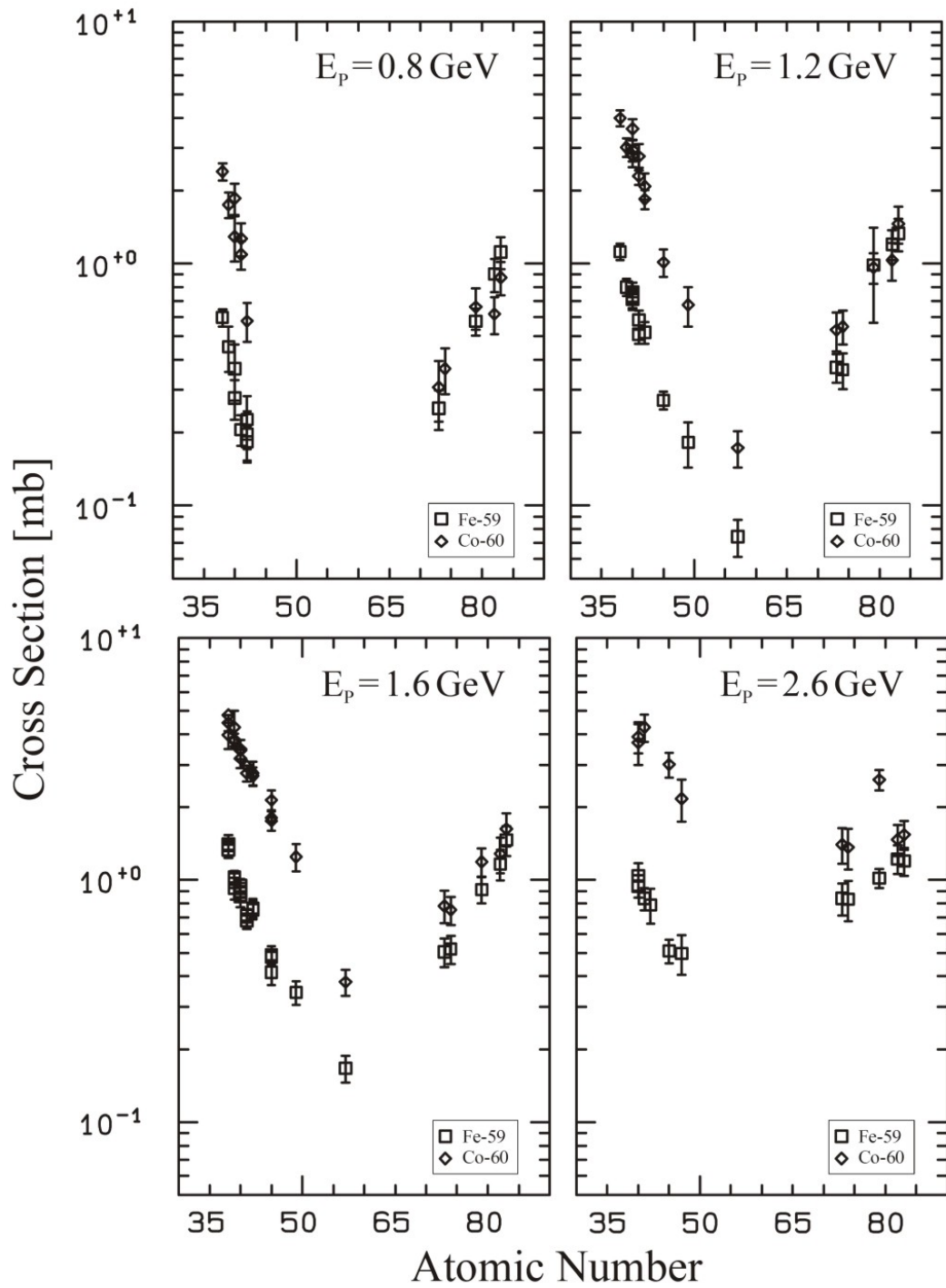


Figure 5.23: Systematic of the production of  $^{59}\text{Fe}$  and  $^{60}\text{Co}$  by proton-induced reactions as function of target atomic numbers according to [G198].

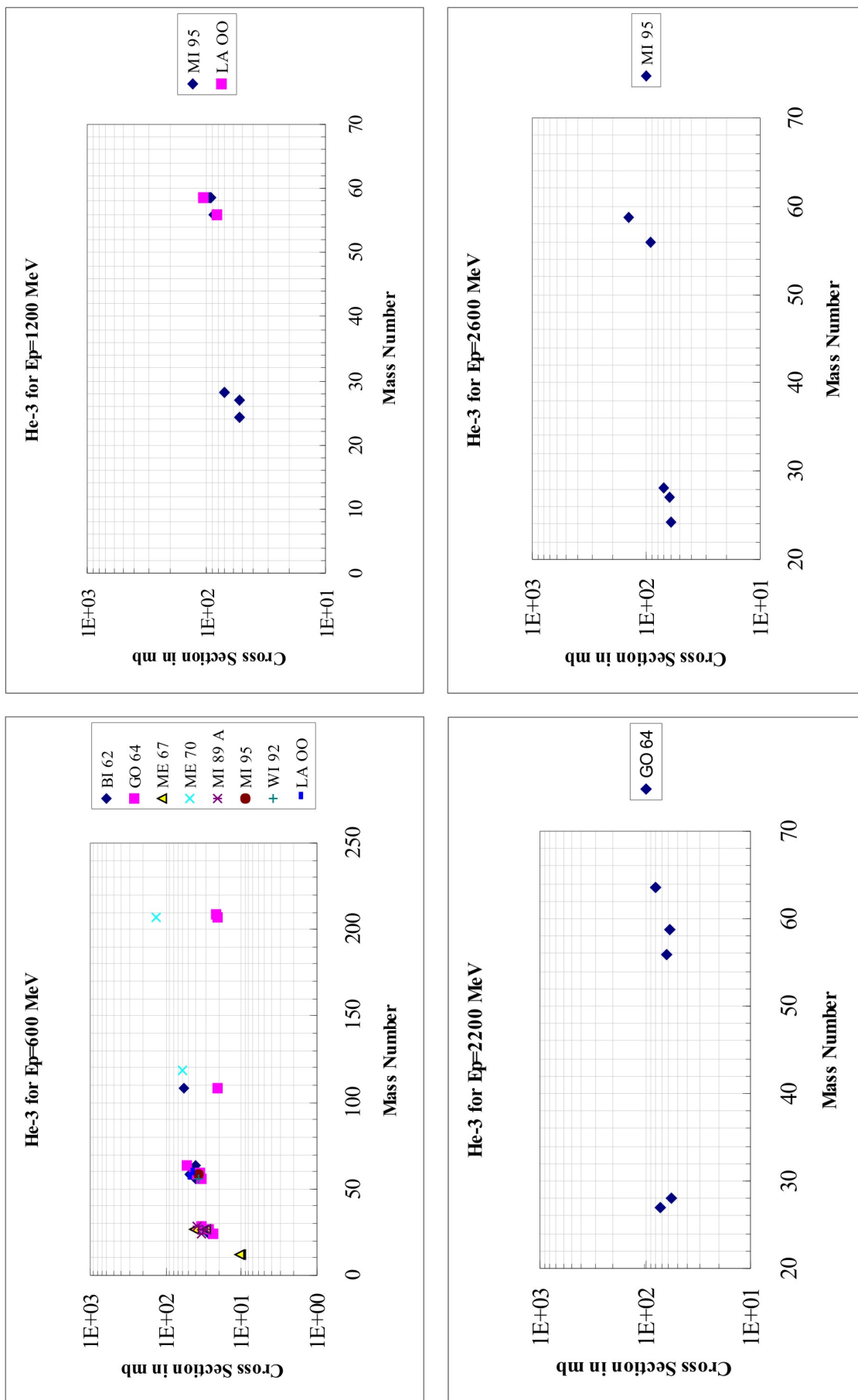


Figure 5.24: Systematic of the production of <sup>3</sup>He by proton-induced reactions as function of target mass numbers.

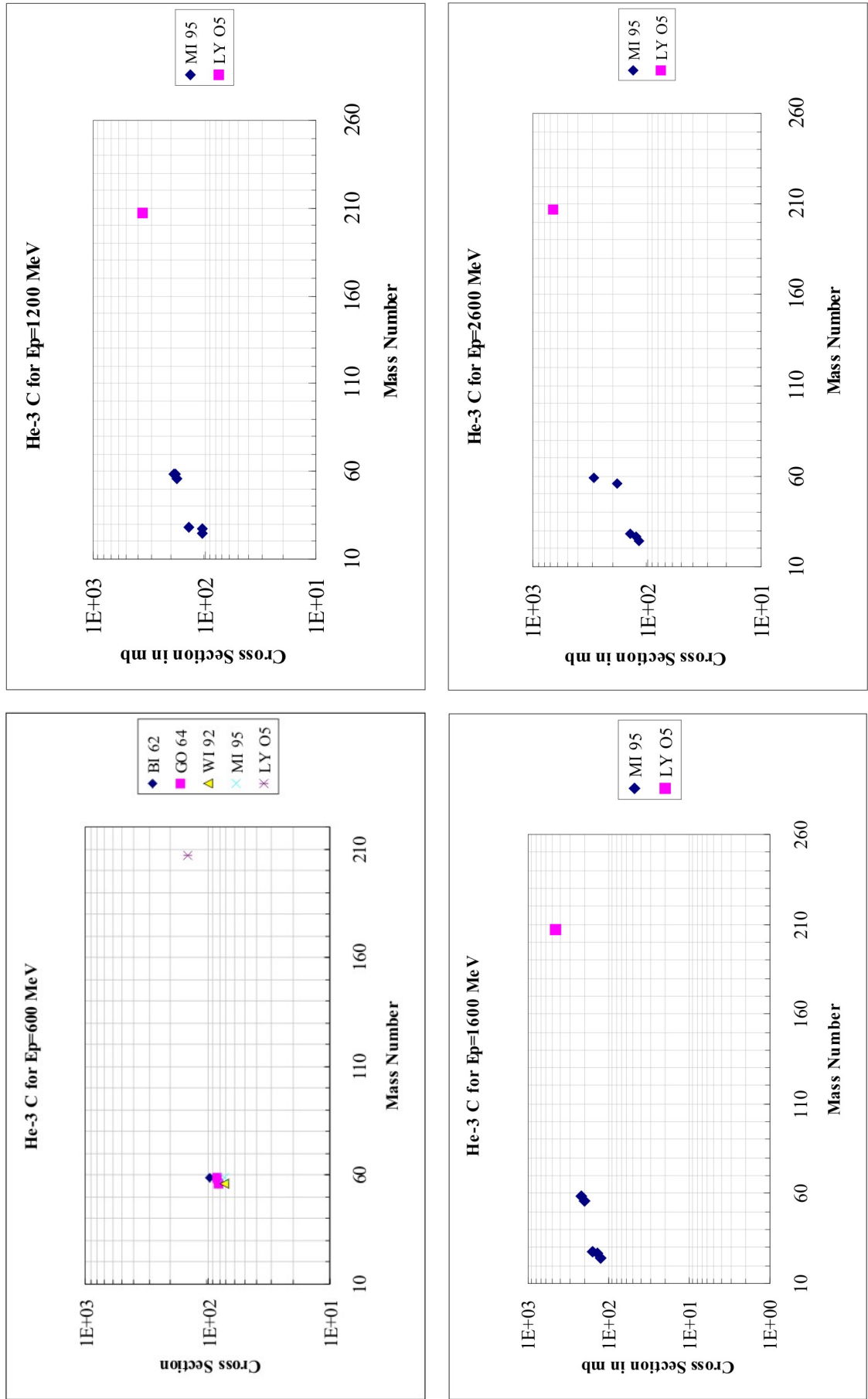


Figure 5.25: Systematic of the production of  $^3\text{He}_c$  by proton-induced reactions as function of target mass numbers.

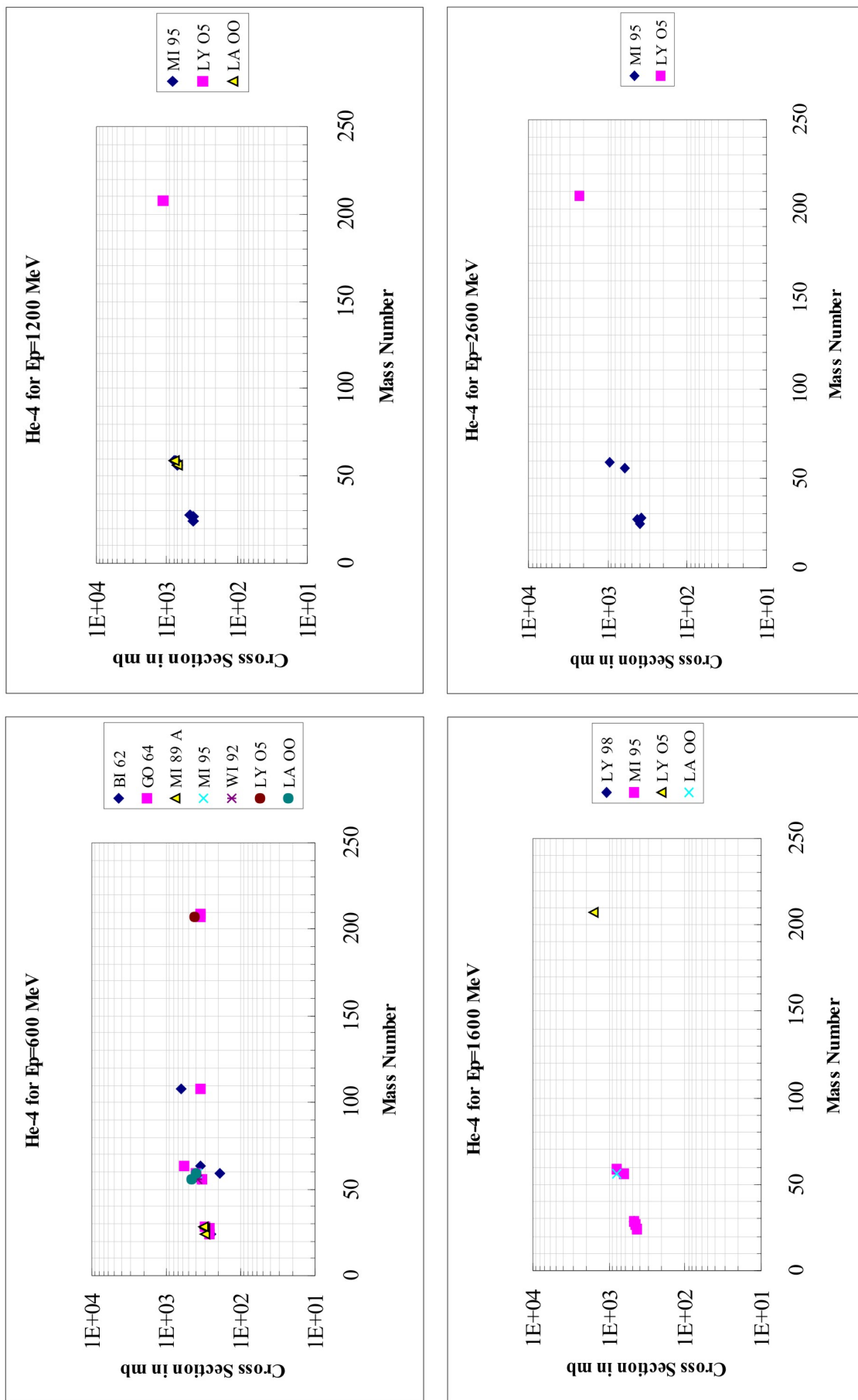


Figure 5.26: Systematic of the production of  $^4\text{He}$  by proton-induced reactions as function of target mass numbers.



For the production of  ${}^7\text{Be}$  (Figure 5.27) and  ${}^{10}\text{Be}$  (Figure 5.28) the systematic looks similar but shows slight differences. For  ${}^7\text{Be}$  at 500 MeV and target elements up to iron, the cross sections decrease with increasing target mass. Naturally, the production from C, N, and O is somewhat particular because of the small mass-distance of targets and products. For higher target masses the cross sections stay essentially constant over the entire higher mass region. For an energy of 1000 MeV, there is a general trend of decrease of the cross sections with target mass, however, with a change in slope for target elements heavier than iron. At 1500 MeV, 2000 MeV and 2600 MeV, the cross sections for the production of  ${}^7\text{Be}$  practically depend slightly linear on a logarithmic scale over the entire target mass region with tendency of lower decreases with increasing energy.

For  ${}^{10}\text{Be}$ , the situation is not so clear cut, mainly because of a still persistent lack of data. In particular, the preliminary data by Tarabishi [Ta02] need urgently to be confirmed by independent measurements. Such measurements are underway. In general, one can conclude for  ${}^{10}\text{Be}$  that there appears not to be a significantly different trend in the data than observed for  ${}^7\text{Be}$ .

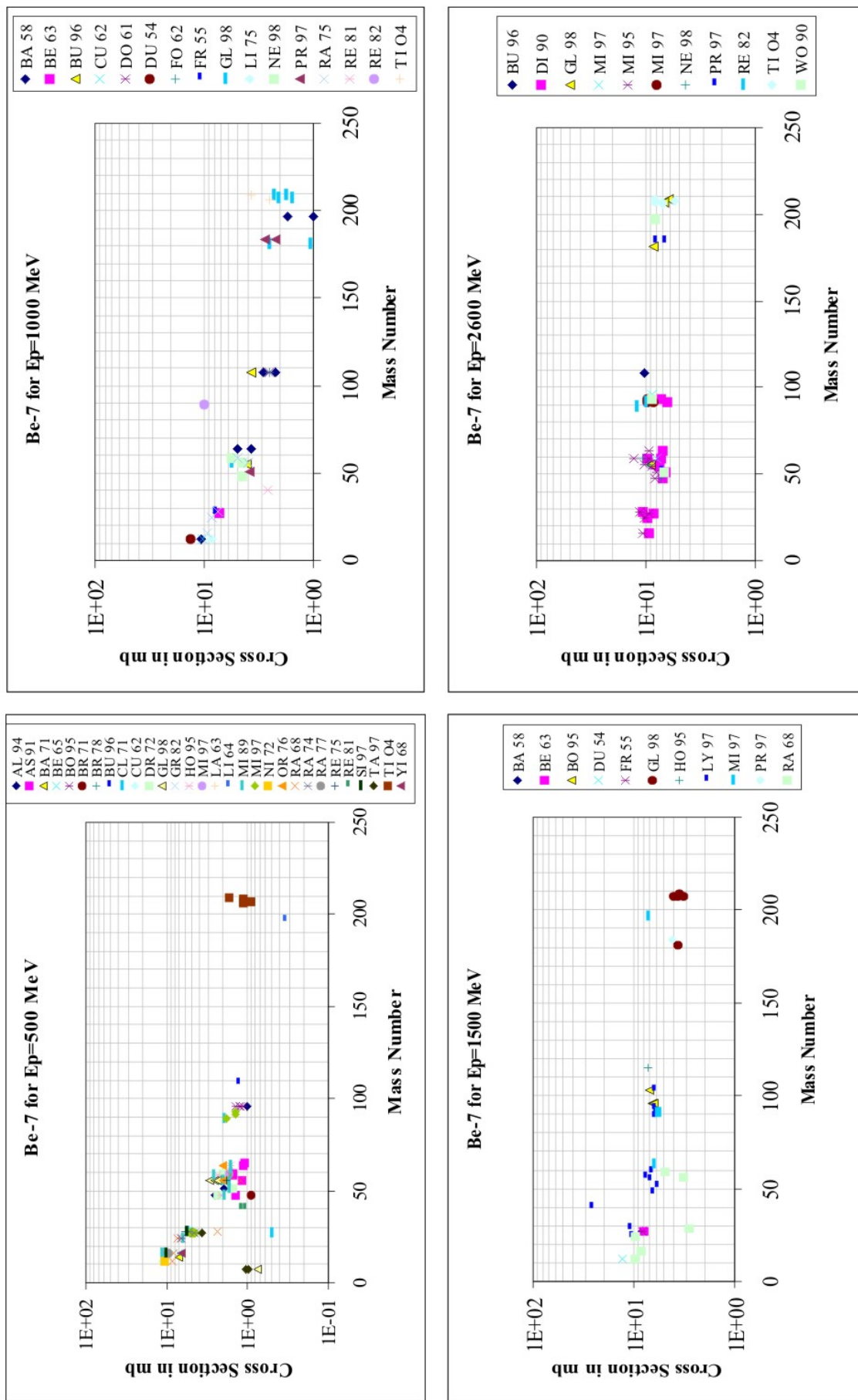


Figure 5.27: Systematic of the production of  ${}^7\text{Be}$  by proton-induced reactions as function of target mass numbers.

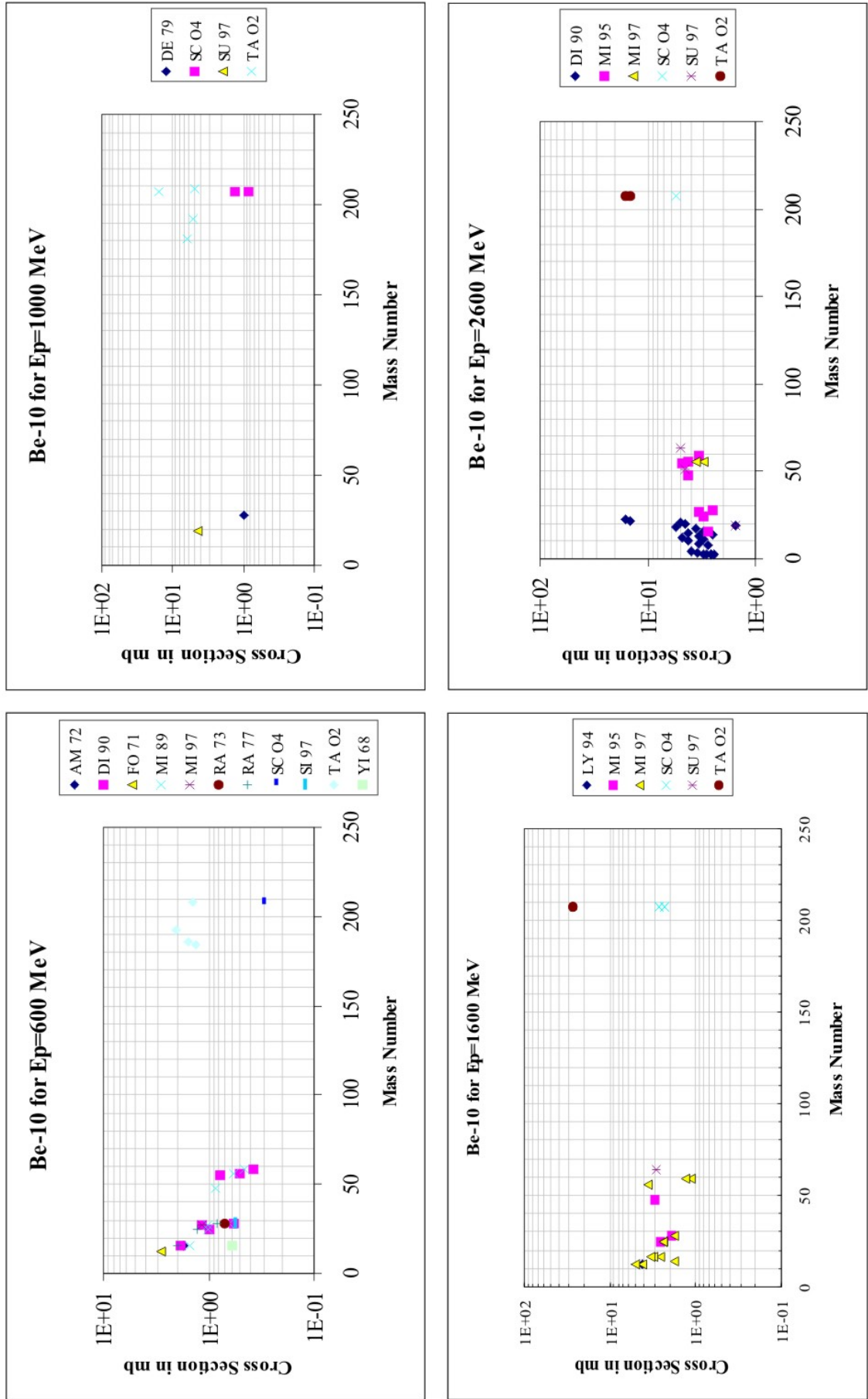


Figure 5.28: Systematic of the production of  $^{10}\text{Be}$  by proton-induced reactions as function of target mass numbers.

A clearer picture is obtained for the heavier IMFs, such as the neon isotopes,  $^{22}\text{Na}$ ,  $^{24}\text{Na}$ ,  $^{28}\text{Mg}$ , and  $^{26}\text{Al}$ .

For  $^{21}\text{Ne}$  at 600 MeV, one observes an exponential decrease of the cross sections with target mass up to mass 60. For higher masses this decrease becomes much less steep: only about a factor of two between mass 60 and 200 (Figure 5.29).

For  $^{22}\text{Na}$  (Figure 5.30) most data exist in this product mass region. At 500 MeV the cross sections decrease exponentially over the entire target mass region. Above mass 100 no  $^{22}\text{Na}$  could be measured. For energies above 1000 MeV  $^{22}\text{Na}$  could be observed for all target masses. As in the case of  $^{21}\text{Ne}$ , one observes for  $^{22}\text{Na}$  a composite curve for the dependence of its production as a function of target mass. It is composed from two exponentials, a steep one up to a target mass of about 100 and a flatter decreasing one up to lead and bismuth. This holds also true at the highest energy of 2600 MeV.

For  $^{24}\text{Na}$  (Figure 5.31) the picture is similar, but shows some differences for higher target masses. The picture at about 500 MeV, which actually includes also the early 600 MeV data with considerable scatter, the steep exponential decrease up to mass 60 of the target elements is again observed. For higher target masses there is considerable ambiguity due to unacceptable scatter of many old data which is still enhanced by the strong dependence on energy of the cross sections in this energy bin. But for higher energies, the systematic becomes clearer because also the old data appear to be more consistent. We observe generally a flattening of the steep exponential decrease of the cross sections for target masses up to 100. For heavier target masses, however, there is practically no decrease and the production cross sections remain more or less constant. There might even be a slight increase with target masses at 2600 MeV.

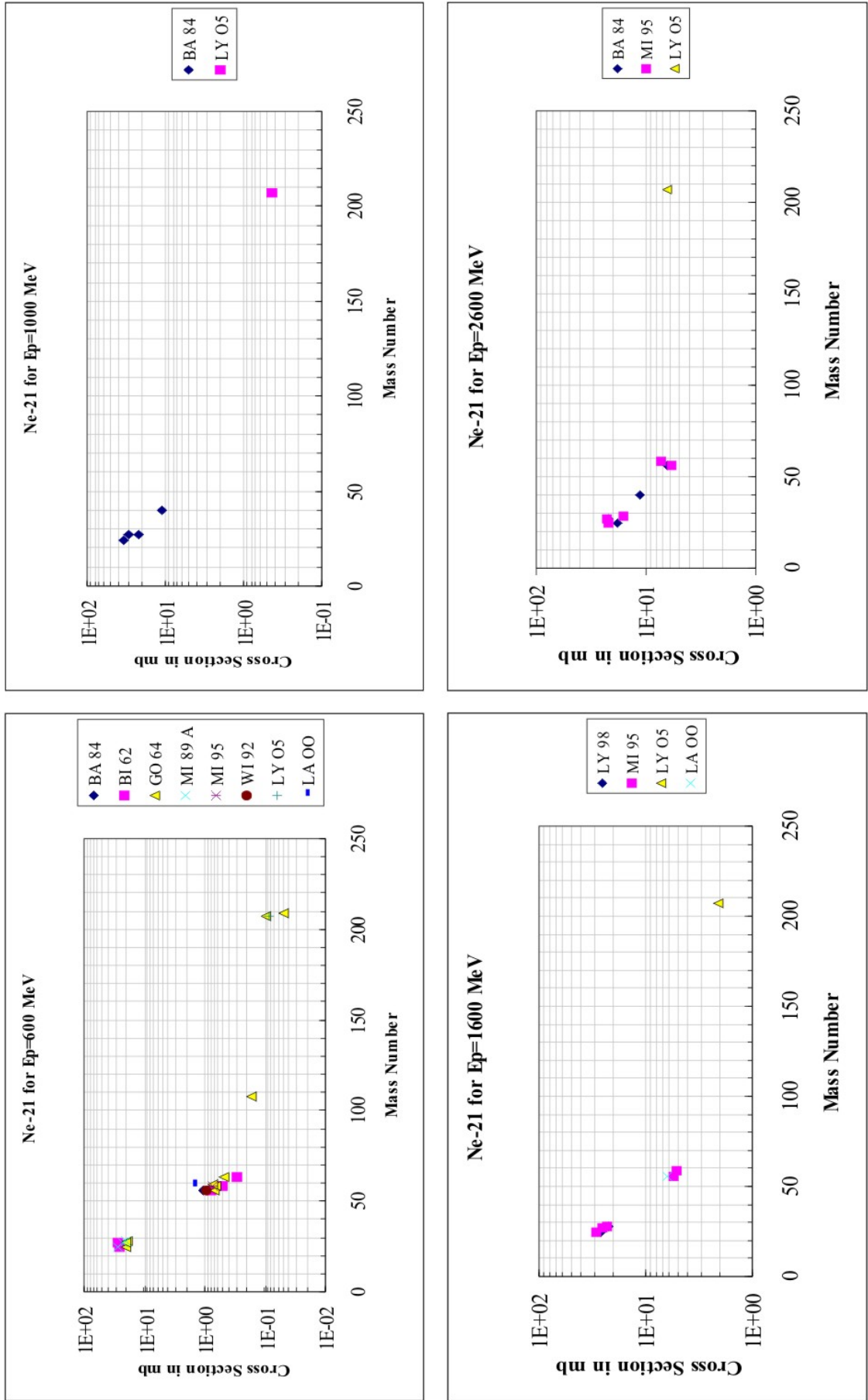


Figure 5.29: Systematic of the production of  $^{21}\text{Ne}$  by proton-induced reactions as function of target mass numbers.

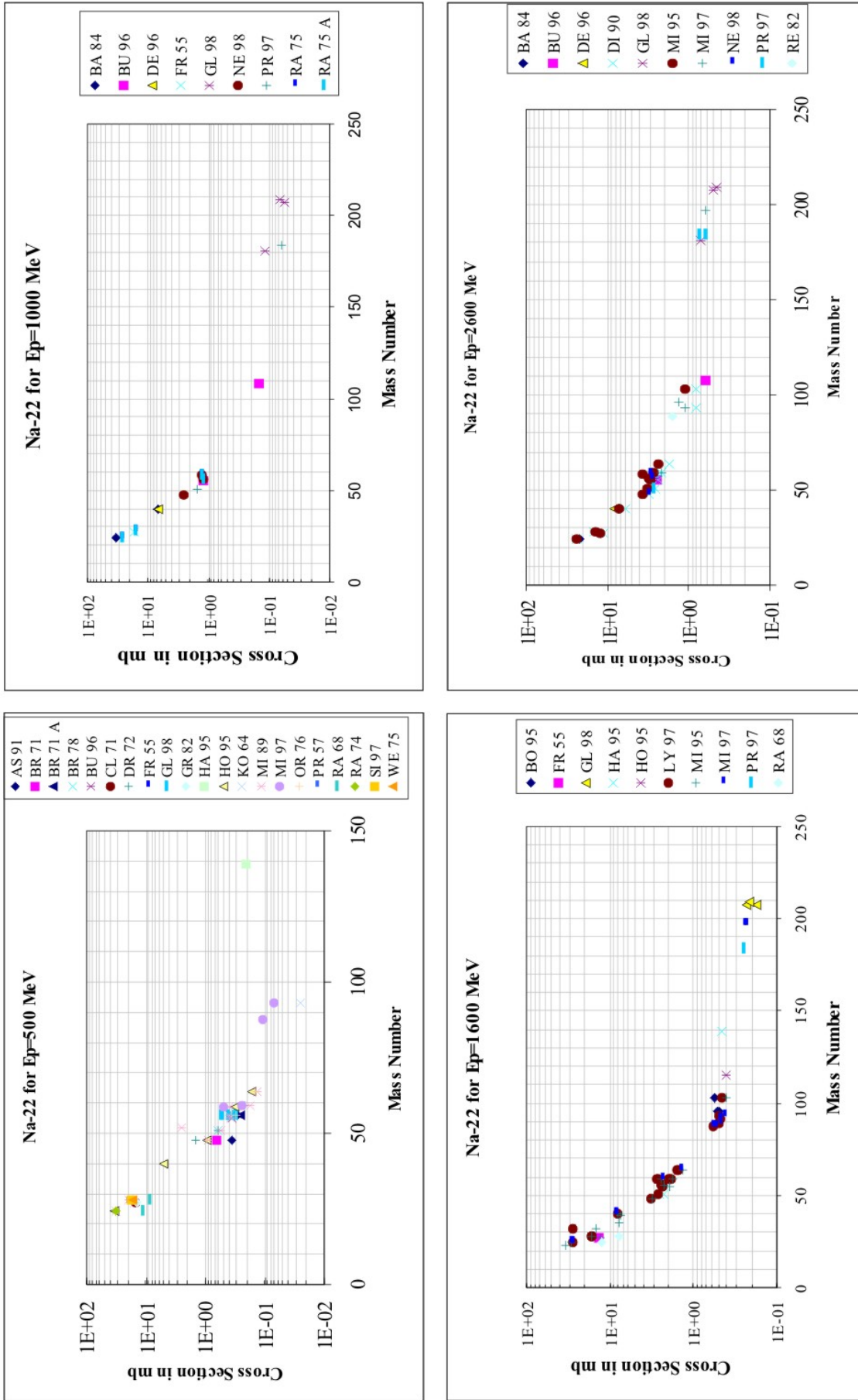


Figure 5.30: Systematic of the production of  $^{22}\text{Na}$  by proton-induced reactions as function of target mass numbers.

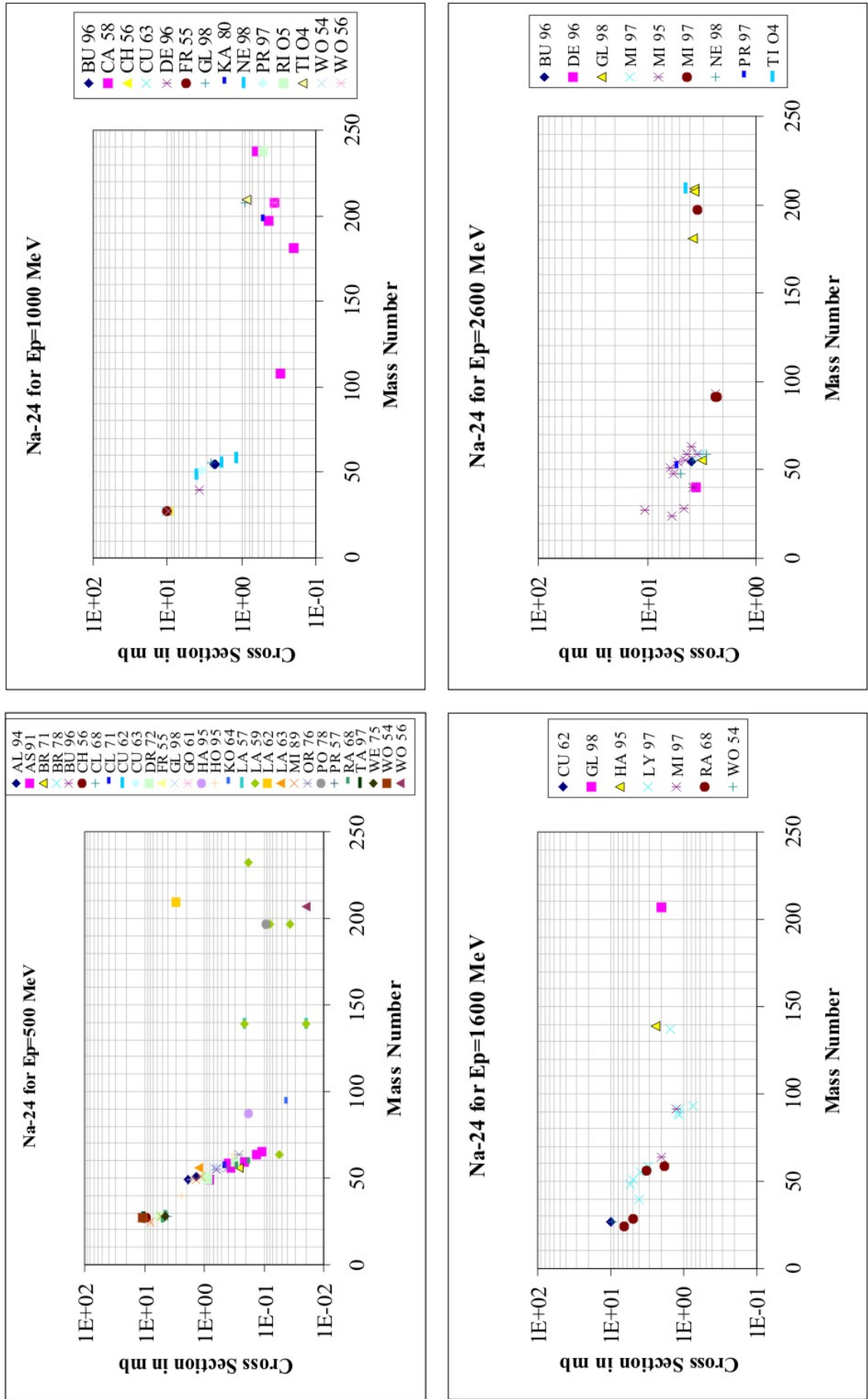


Figure 5.31: Systematic of the production of  $^{24}\text{Na}$  by proton-induced reactions as function of target mass numbers.

For  $^{28}\text{Mg}$  (Figure 5.32), the data base is not as comprehensive as for  $^{22}\text{Na}$  (and  $^{24}\text{Na}$ ). In spite of that there are strong indications that after some structure in the systematic for target elements quite close to the product mass, the production of  $^{26}\text{Mg}$  remains practically constant for higher target masses. For  $^{26}\text{Al}$  (Figure 5.33), the situation is again not yet satisfactory because of lack of data because of the big efforts needed for chemistry and AMS. But, the available data point to a dependence on target mass similar to that observed for the other products with product masses above 20.

So one may conclude that the systematic of the production of the radionuclides, dealt with in this work as IMFs, have scarcely something in common with the dependence on target element exhibited by the established fission products  $^{59}\text{Fe}$  and  $^{60}\text{Co}$ . It must also be emphasized that their behavior shows no difference depending on whether or not a fission channel is open. It is, however, natural that a phenomenology as here described cannot decide about the actual reaction modes. This can only be done on the basis of model calculations based on a sound theory of nuclear reactions at intermediate energies. However, such model calculations must be able to describe the trends with energies and the dependencies on target masses described in this thesis. Consequently, the data base described here and the systematic discussed in this section provides a basis for testing models and codes describing the production of IMFs in intermediate energy nuclear reactions.



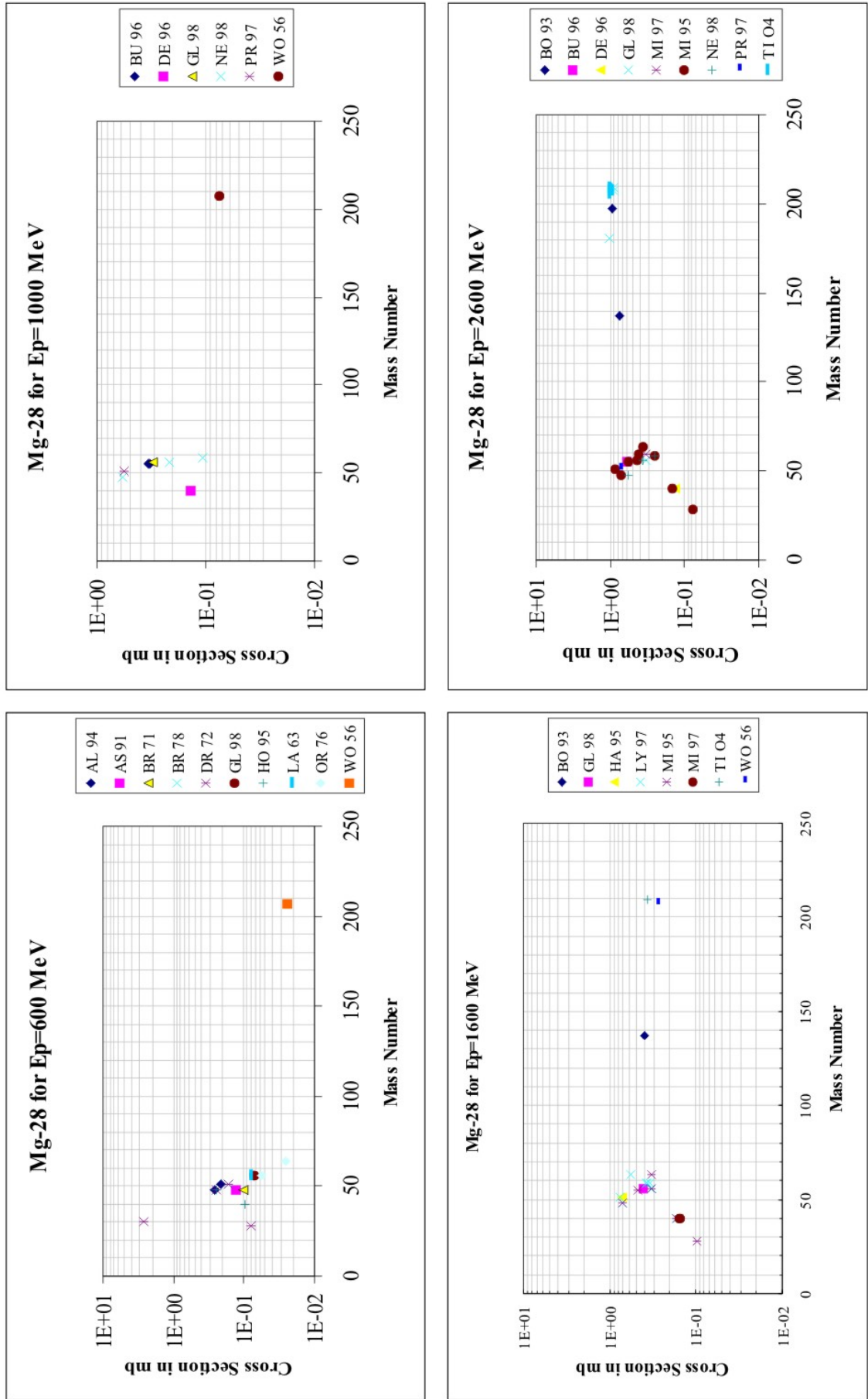


Figure 5.32: Systematic of the production of  $^{28}\text{Mg}$  by proton-induced reactions as function of target mass numbers.

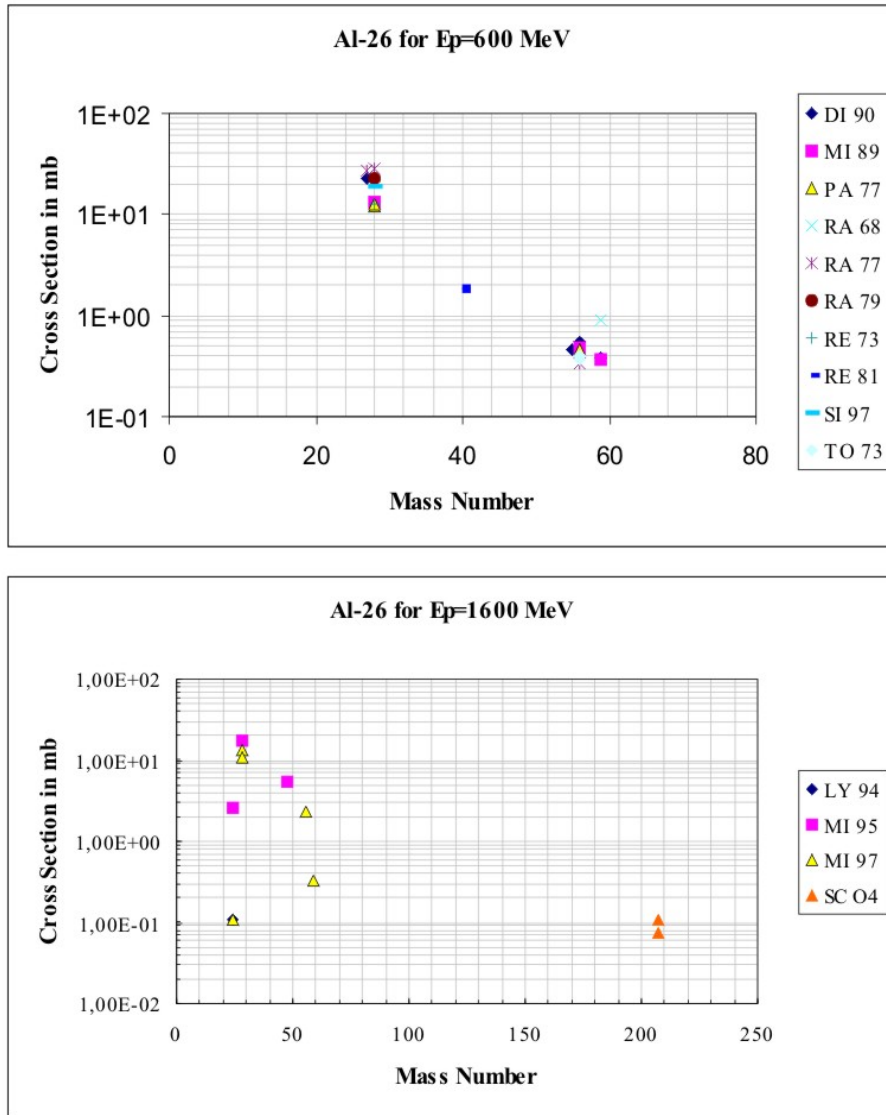


Figure 5.33: Systematic of the production of  $^{26}\text{Al}$  by proton-induced reactions as function of target mass numbers.

## 5.5 Comparison between experiment and theory

### 5.5.1 Modeling of residual nuclide production at medium energies

Apart from the experimentally accessible measurement of production cross-sections, the theoretical modeling is necessary in order to understand the nuclear reactions. Beyond that it is also necessary to formulate a model, which is capable in all aspects to describe a reaction.

A variety of theoretical models are in general use at this time for calculating nuclear reaction cross sections. To put these models in perspective, an overview is presented here of the physical features that they emphasize. Since the nature of the nuclear force is not fully understood, and since nuclei consist of nucleons interacting through complicated many-body interactions, a comprehensive theory of nuclear reactions and nuclear structure derived from fundamental principles, with good predictive abilities, does not yet exist. Instead, nuclear physics researchers often develop models which typically emphasize one or more physical features over others, depending on the context of the investigation. Examples include compound nucleus, direct, and various preequilibrium nuclear reaction theories, including exciton and intranuclear cascade semiclassical models and quantum mechanical multistep approaches. The drawbacks inherent in emphasizing certain physical aspects over others are partly compensated by a corresponding insight, and mathematical simplicity, exhibited by a model.

Many different interaction mechanisms can occur when a nucleon of a few hundred MeV and below strikes a target nucleus. At low incident energies (a few MeV, say), nuclear reactions take place by the compound nucleus process, in which the incident particle is captured by the target nucleus, and its energy is shared statistically among all the nucleons of the compound system. After a time much greater than the interaction time, the compound nucleus emits one or more particles and generally attains its ground state by gamma-ray emission. As the incident energy increases, it becomes more likely that particle emission will take place in the first stage of the reaction, when the incident particle interacts with the target nucleus as a whole (for example, a collective excitation) or a nucleon within it. Many theories have been developed to enable the cross sections of these direct reactions to be calculated, and they facilitate an understanding of elastic and inelastic scattering and particle transfer reactions. However, experimental and theoretical research in the last few decades has shown that particle emission can take place with a time scale longer than the very rapid direct reactions (about  $10^{-22}$ ) but much much shorter than the slower compound nucleus reactions (about  $10^{-16}$  to  $10^{-18}$  sec). These emission processes are known as preequilibrium or

multistep reactions, and they are characterized by particles emitted with relatively high energies and with angular distributions that are peaked in the forward direction. One of the problems in nuclear reaction theory is a proper treatment of the scattering at energies where two or more reaction mechanisms apply.

The demand for reliable theoretical predictions of production cross sections is by no means satisfied by the models and codes which are available today. In this context it is essential that reliable and comprehensive databases to exist which can serve as benchmarks for code development and validation.

We will shortly discuss the different modes of proton induced production of residual nuclides at intermediary energies and we will see how these modes manifest in the excitation functions and whether they are capable of explaining all their features.

R. Serber describes spallation as a fast intra-nuclear cascade of nucleon-nucleon interactions followed by a slow de-excitation in statistical equilibrium.

Accepting the general validity of Serber's two step process, the first phase is a quick sequence of nucleon-nucleon collisions since the wavelength of the incoming particle is small compared with the distances of the nucleons inside the target nucleus. This phase is called the intranuclear cascade (INC) and comprises collisions of primary and secondary fast nucleons with other nucleons of the composite system and the creation of pi-mesons. During this phase nucleons and light clusters are emitted from the composite system. The particles emitted during the INC have high energies and they are preferably emitted in the beam direction. The energy distribution of the INC particles and the residual system at the end of the INC, called prefragment, depends on the mass of the target, the incident energy and the impact parameter. It also should be noted that for light- and medium-mass targets the nature of the incoming particle (proton or neutron) significantly influences the neutron excess of the composite system and of the prefragments.

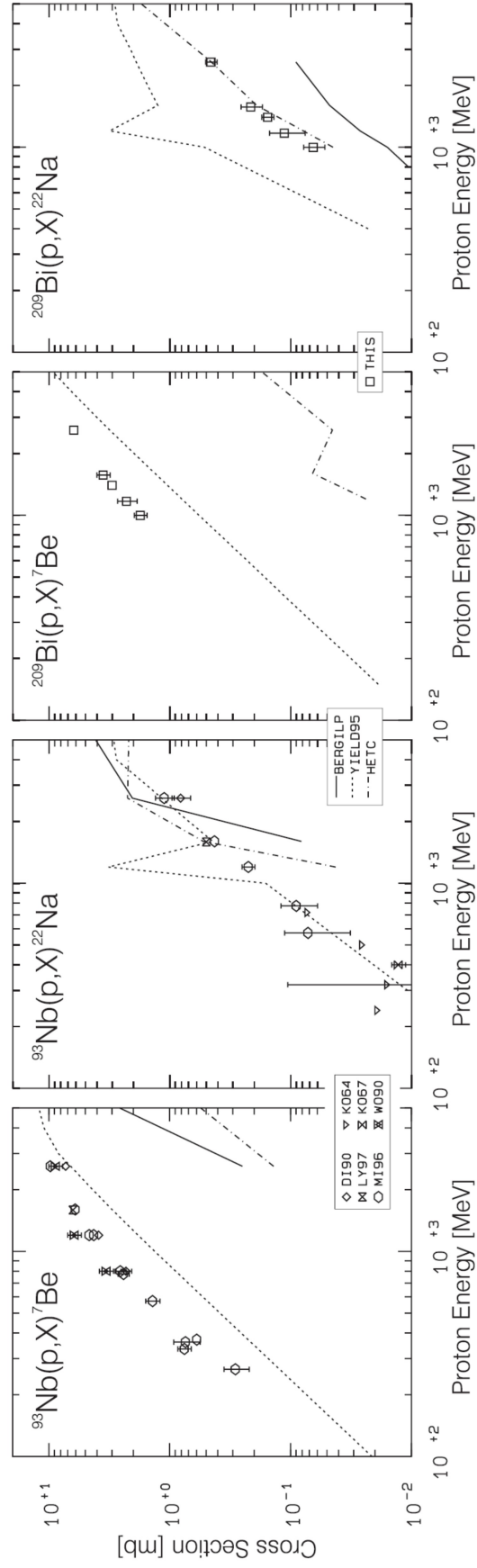


Figure 5.34: Experimental cross sections for the production of  $^7\text{Be}$  and  $^{22}\text{Na}$  from niobium and bismuth compared with theoretical ones calculated by the LAHET code system [Pr94, Pr89] using the Bertini-Gilbert-Cameron options, the HETC in form of the HET-KFA2 code [Cl88] and a semiempirical formula according to the YIELD code [Si73a, Si73b]; according to [Gl98].

Depending on the above mentioned parameters, the number of baryon-baryon collisions show a steady increase with time which then suddenly flattens, when equipartition of energies is attained. At this time the fast intranuclear cascade ends and the second, slow step of the reaction begins, in which the highly excited prefragment deexcites. Deexcitation of the prefragment can occur principally in two ways, by evaporation of nucleons and nucleon clusters or by the breakup of the unstable prefragment into two or more fragments, which themselves may still release their excitation energies by evaporation of nucleons and nucleon clusters. The first of these deexcitation paths is called the classical evaporation phase as invented in Serber's model, the second is called multifragmentation. For heavy target elements at least two different types of fission have to be added to this scenario.

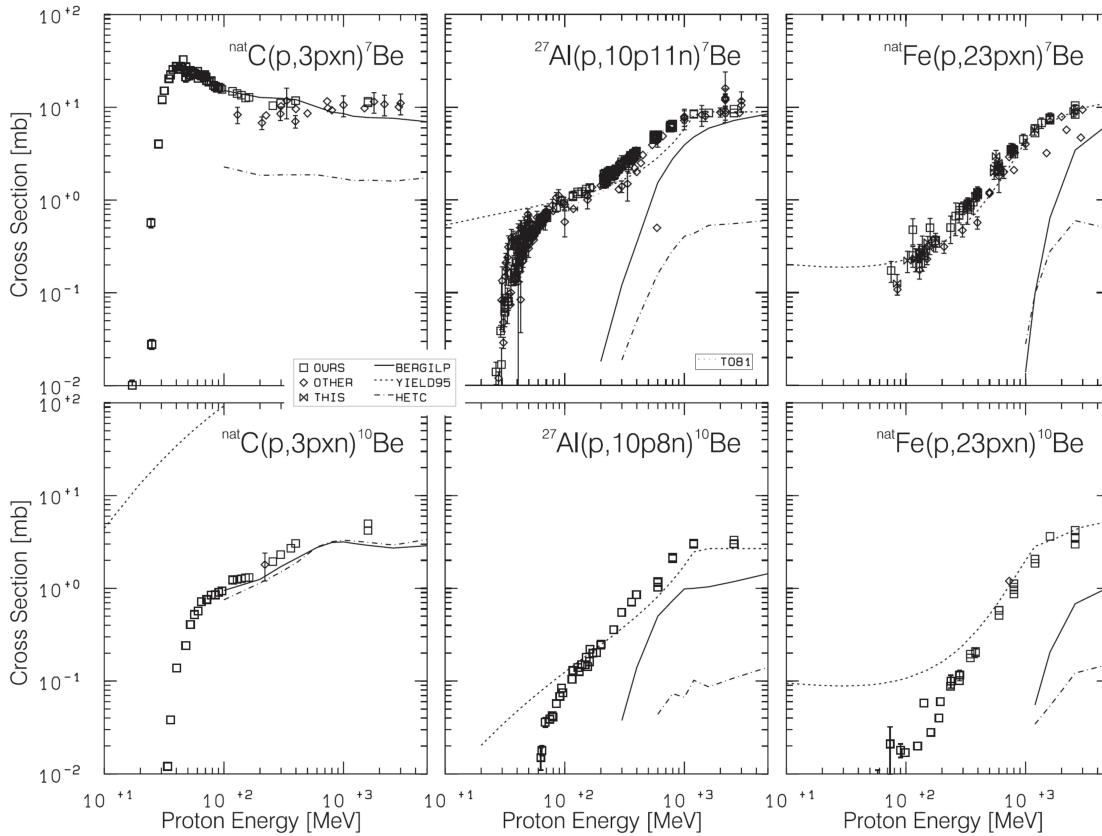


Figure 5.35: Experimental cross sections for the production of  ${}^7\text{Be}$  and  ${}^{10}\text{Be}$  from carbon, aluminum, and iron compared with theoretical ones calculated by the LAHET code system [Pr94, Pr89] using the Bertini-Gilbert-Cameron options, the HETC in form of the HET-KFA2 code [Cl88] and a semiempirical formula according to the YIELD code [Si73a, Si73b]; according to [Gl98].

Generally, a reliable a priori calculation of cross sections for the production of residual nuclides at intermediate energies is a demanding task which up today has

many open questions. On the basis of our extensive data base many models and codes have been tested in this respect; see [Mi97] and references therein. A general survey on the predictive capabilities of a wide variety of models and codes was performed in a NEA model and code Intercomparison [Mi97a]. The result of this intercomparison was that the best codes just were capable to calculate residual nuclide production cross sections within a factor of two on the average. In many cases average deviations exceeded an order of magnitude. For intermediate energies and heavy target elements the LAHET code system (LCS) [Pr89, Pr94] and the HET-KFA2 [Cl88] were tested in particular using always the Bertini INC model [Be69] for the calculation of the intranuclear cascade. The HET model which was originally developed by Armstrong and Chandler [Ar72] is included in both code systems. Also these models turned out to fail widely [Gl01]. It was a general observation in all those tests that for fission products and for the IMFs dealt within this work the results were inadequate. In Figures 5.35 - 5.36 some examples are given. Aside of the LAHET and HET-KFA2 codes also semiempirical formulas were tested [Gl98, Gl01]. The result for such formulas was in a nutshell that they worked fairly well if experimental data were known, but that they frequently failed when extrapolating to reactions for which no data were known before (Figure 5.35).

In order to improve this unsatisfactory situation two codes systems were developed during the HINDAS project [Me05] to satisfy the needs for modeling nuclear reaction data at intermediate and high energies. The TALYS code includes the optical model, direct, pre-equilibrium, fission and statistical models and thereby gives a prediction for all the open reaction channels for energies up to about 200 MeV [Ko05]. The INCL4+ABLA code system is a combination of the codes INCL4 [BO02] for the intra-nuclear cascade and ABLA [Ju98] for the nucleus de-excitation. The experimental data base established during the HINDAS project offers an excellent chance for the validation of the new codes.

During the HINDAS project [Me05] and in a recent paper [Mi05] “blind” calculations were performed for Fe, W, Ta, Pb, Bi, and U and the results were compared with the new experimental data in order to validate these code systems with respect to their capabilities to predict cross sections for the production of residual nuclides respective. Figure 5.37 gives an example for such a comparison for the production of  $^{52m+g}\text{Mn}$  from natural iron. A more systematic survey on the capabilities of the TALYS and INCL4+ABLA codes and on still pertaining problems is given in Figure 5.39 for the target element bismuth. Generally, the results of these comparisons were quite good. For a wide range masses from target-near to spallation products, both codes, TALYS

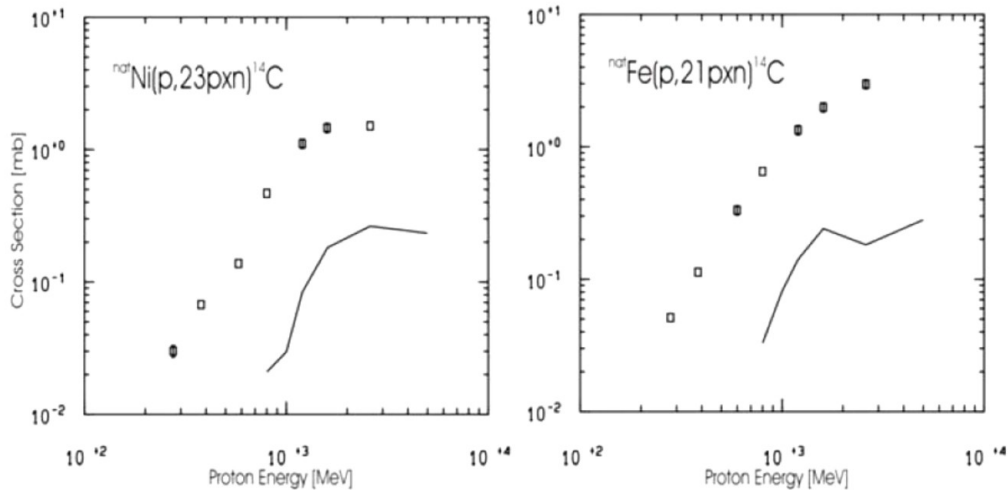


Figure 5.36: Experimental cross sections for the production of  $^{14}\text{C}$  from natural iron and nickel compared with theoretical ones calculated with the HET-KFA2 code within the HERMES code system [Cl88].

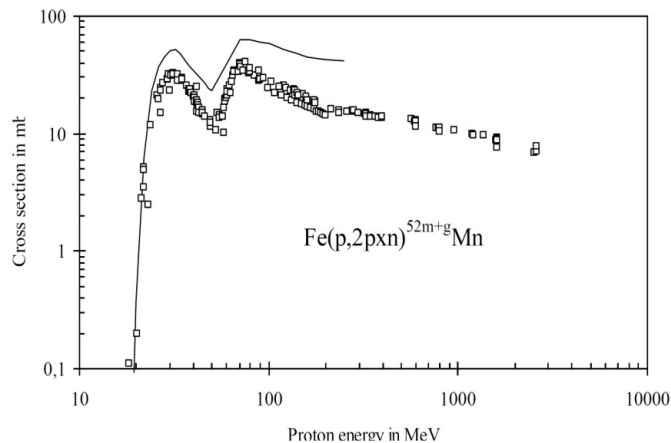


Figure 5.37: Experimental cross sections (squares) for the production of  $^{52m+g}\text{Mn}$  from natural iron by proton-induced reactions in comparison with TALYS results (solid line) [Mi05].

and INCL4+ABLA, adequately reproduce the experimental cross sections varying by 5 orders of magnitude over the entire range of energies for. In contrast to earlier evaluations [Mi97, Gl01, Ku01, Mi02, Mi02a], the new codes also give reasonable results for all fission products.

In general both codes performed quite satisfactorily, though some problems remained to be solved. With respect to the production of IMFs, however, the problem of grossly underestimating their production by the INCL4+ABLA code remained. In Figure 5.37, this is already seen for the production of  $^{22}\text{Na}$  from Bi, which is underes-



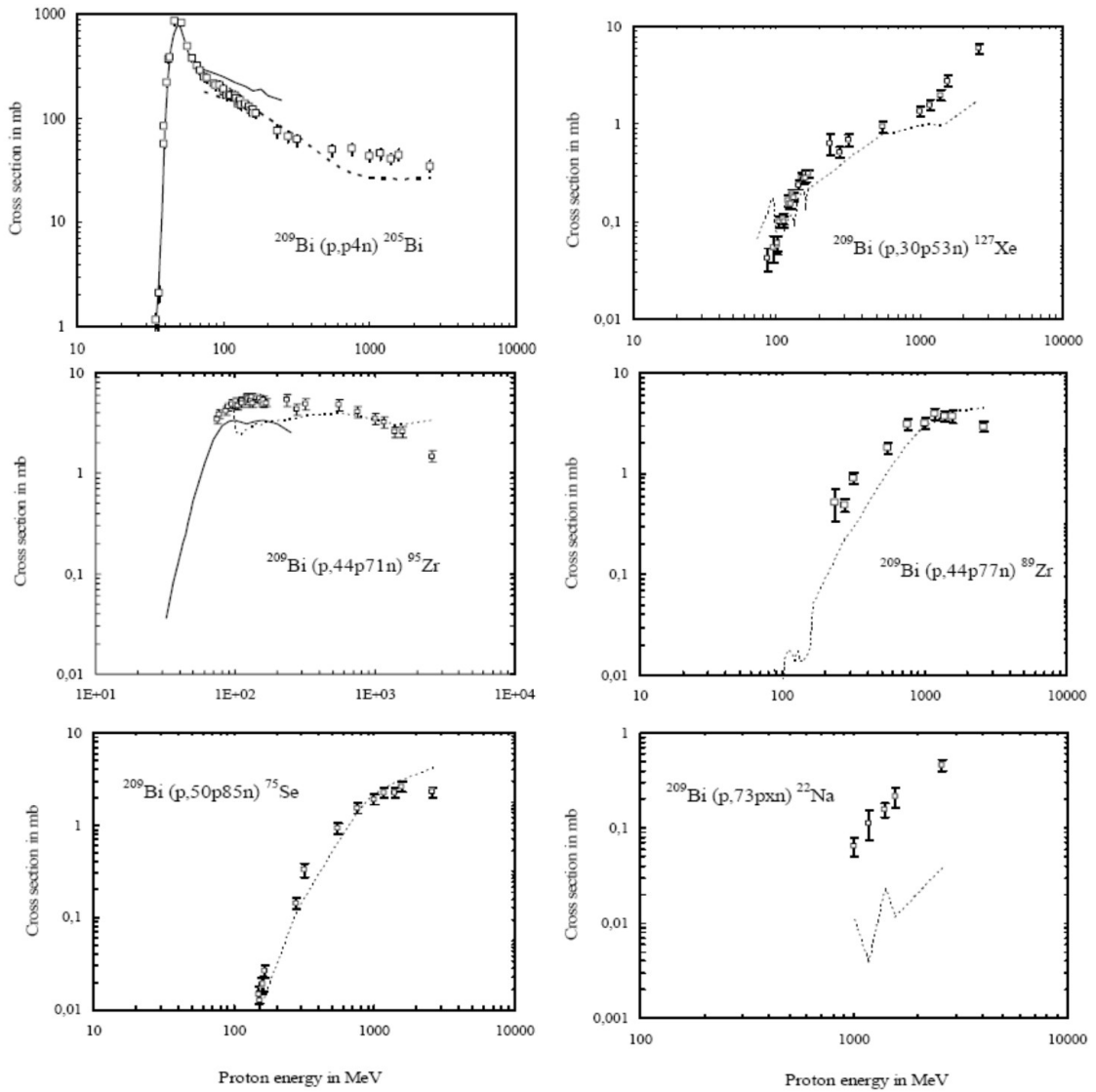


Figure 5.38: Comparison of experimental cross sections [Mi02] with model calculations using the TALYS (solid lines) and INCL4+ABLA (broken lines) codes; from [Mi05].

timated by about an order of magnitude. This failure was attributed at that time to the neglect of multi-fragmentation in the existing codes [Mi05].

### 5.5.2 TALYS

Model calculations were performed for the production of residual nuclides using the TALYS code [Ko05] with standard options for energies up to 200 MeV. Created at NRG Petten (Netherlands) and CEA Bruyères-le-Châtel (France), TALYS is a computer code system for the analysis and prediction of nuclear reactions. The basic objective behind its construction is the simulation of nuclear reactions that involve neutrons, photons, protons, deuterons, tritons,  $^3\text{He}$ - and alpha-particles, in the 1 keV - 200 MeV energy range and for target nuclides of mass 12 and heavier. To achieve this, a set of nuclear reaction models (see Table 5.5.2) are implemented into a single code system in order to enable the evaluation of nuclear reactions from the unresolved resonance range up to intermediate energies.

An additional advantage of TALYS is the option of fine tuning the adjustable parameters of the various reaction models to available experimental data. However, this option was not used in the present work, but it could be used to adapt the theoretical calculation to the experimental data.

Table 5.2: Nuclear models and structure information implemented in TALYS 0.72 (released 21.dez.06)

#### Optical Model:

- Optical model potential (OMP) calculations are performed with ECIS-2003
- Neutrons/protons: Koning-Delaroche phenomenological spherical OMP (local / global), Soukhovitskii deformed OMP for actinides, and user-defined OMP's
- Complex particles: Simplified Watanabe folding approach

#### Direct Reactions:

- Direct reaction calculations are performed with ECIS-2003
- DWBA for (near) spherical nuclei
- Coupled-channels for deformed nuclei (symmetric rotational / harmonic vibrational / vibration-rotational / asymmetric rotational)
- Weak-coupling model for odd nuclei
- Giant resonances (Kalbach macroscopic phenomenological model)

**Compound Reactions:**

- Hauser-Feshbach
- Width-fluctuation models (Moldauer / GOE triple integral / HRTW)
- Blatt-Biedenharn formalism for angular distributions

**Pre-equilibrium Reactions:**

- Two-component excitation model
- Photon exciton model (Akkermans and Gruppelaar)
- Continuum stripping, pick-up and knock-out (Kalbach phenomenological model)
- Angular distribution (Kalbach systematics)

**Multiple Emission:**

- Multiple pre-equilibrium emission for any number of particles
- Multiple Hauser-Feshbach emission for any number of particles

**Fission:**

- Hill-Wheeler transmission coefficients
- single / double / triple humped barriers
- Class II (III) states
- Experimental barrier parameters
- Rotating-Liquid-Drop model
- Rotating-Finite-Range model
- Microscopic barrier parameters
- Fission fragment mass distributions (Multi-Model Random-Neck-Rupture model)
- Fission fragment charge distributions (scission-point model)

**Gamma-Ray Transmission Coefficients:**

- Brink-Axel Lorentzian
- Kopecky-Uhl Generalised Lorentzian
- photoabsorption cross sections: (GDR + quasi-deuteron (Chadwick))

**Nuclear Structure Database (based on RIPL-2):**

- Abundancies
- Discrete levels
- Deformations
- Masses
- Level density parameters
- Resonance parameters
- Fission barrier parameters
- Thermal cross sections
- Microscopic level densities
- Precission shapes

The nuclear models that are adjusted in this manner can be used to obtain further information about the nuclear properties. Specific features of TALYS and a full description of all implemented nuclear models are given by A.J. Koning, S. Hilaire and M. Duijvestijn [Ko07].

Radioactive progenitors were considered in the calculations according to Table 5.3 if necessary. Selected results are presented in Figures 5.39-5.44, all the results are listed in Appendix D. The theoretical curves are only given for the energy regions covered by the experimental data.

Except for the light product nuclides with masses below 20 the calculations describe the experimental data fairly well. For the lightest product nuclides, i.e.  $^{14}\text{C}$  and  $^{15}\text{O}$  from oxygen (Figure 5.39), we see severe over- and underestimation of the experimental cross sections and also for the production of  $^{18}\text{F}$  from sodium and magnesium the calculations fail widely to reproduce the experimental data (Figure 5.40).

<b>Target</b>	<b>Product</b>	<b>Considered Progenitors</b>
<sup>nat</sup> O	<sup>14</sup> C	<sup>14</sup> B
<sup>nat</sup> Si	<sup>14</sup> C	independent
<sup>16</sup> O	<sup>14</sup> C	independent
<sup>16</sup> O	<sup>15</sup> O	independent
<sup>nat</sup> Mg	<sup>18</sup> F	<sup>18</sup> Ne
<sup>23</sup> Na	<sup>18</sup> F	<sup>18</sup> Ne
<sup>27</sup> Al	<sup>18</sup> F	<sup>18</sup> Ne
<sup>nat</sup> Mg	<sup>20</sup> Ne	<sup>20</sup> F, <sup>20</sup> O, <sup>20</sup> Na, <sup>20</sup> Mg
<sup>nat</sup> Si	<sup>20</sup> Ne	<sup>20</sup> F, <sup>20</sup> O, <sup>20</sup> Na, <sup>20</sup> Mg
<sup>27</sup> Al	<sup>20</sup> Ne	<sup>20</sup> F, <sup>20</sup> O, <sup>20</sup> Na, <sup>20</sup> Mg
<sup>nat</sup> Mg	<sup>21</sup> Ne	<sup>21</sup> F, <sup>21</sup> O, <sup>21</sup> Na, <sup>21</sup> Mg
<sup>nat</sup> Si	<sup>21</sup> Ne	<sup>21</sup> F, <sup>21</sup> O, <sup>21</sup> Na, <sup>21</sup> Mg
<sup>27</sup> Al	<sup>21</sup> Ne	<sup>21</sup> F, <sup>21</sup> O, <sup>21</sup> Na, <sup>21</sup> Mg
<sup>nat</sup> Mg	<sup>22</sup> Ne	<sup>22</sup> Mg, <sup>22</sup> Al, <sup>22</sup> F, <sup>22</sup> O
<sup>nat</sup> Si	<sup>22</sup> Ne	<sup>22</sup> Mg, <sup>22</sup> Al, <sup>22</sup> F
<sup>27</sup> Al	<sup>22</sup> Ne	<sup>22</sup> Mg, <sup>22</sup> Al, <sup>22</sup> F
<sup>nat</sup> Mg	<sup>22</sup> Ne-C	<sup>22</sup> Na, <sup>22</sup> Mg, <sup>22</sup> Al, <sup>22</sup> F, <sup>22</sup> O
<sup>nat</sup> Si	<sup>22</sup> Ne-C	<sup>22</sup> Na, <sup>22</sup> Mg, <sup>22</sup> Al, <sup>22</sup> F
<sup>27</sup> Al	<sup>22</sup> Ne-C	<sup>22</sup> Na, <sup>22</sup> Mg, <sup>22</sup> Al, <sup>22</sup> F
<sup>nat</sup> Mg	<sup>22</sup> Na	<sup>22</sup> Mg, <sup>22</sup> Al
<sup>nat</sup> Si	<sup>22</sup> Na	<sup>22</sup> Mg
<sup>nat</sup> Ca	<sup>22</sup> Na	<sup>22</sup> Mg
<sup>24</sup> Mg	<sup>22</sup> Na	<sup>22</sup> Mg, <sup>22</sup> Al
<sup>25</sup> Mg	<sup>22</sup> Na	<sup>22</sup> Mg, <sup>22</sup> Al
<sup>26</sup> Mg	<sup>22</sup> Na	<sup>22</sup> Mg
<sup>27</sup> Al	<sup>22</sup> Na	<sup>22</sup> Mg, <sup>22</sup> Al
<sup>nat</sup> Mg	<sup>24</sup> Na	<sup>24</sup> Ne
<sup>nat</sup> Si	<sup>24</sup> Na	<sup>24</sup> Ne
<sup>27</sup> Al	<sup>24</sup> Na	<sup>24</sup> Ne
<sup>nat</sup> Si	<sup>28</sup> Mg	independent
<sup>nat</sup> Mg	<sup>26</sup> Al	independent
<sup>nat</sup> Si	<sup>26</sup> Al	<sup>26</sup> Si
<sup>26</sup> Mg	<sup>26</sup> Al	independent
<sup>27</sup> Al	<sup>26</sup> Al	<sup>26</sup> Si

Table 5.3: Product nuclides determined and radioactive progenitors considered for the calculations

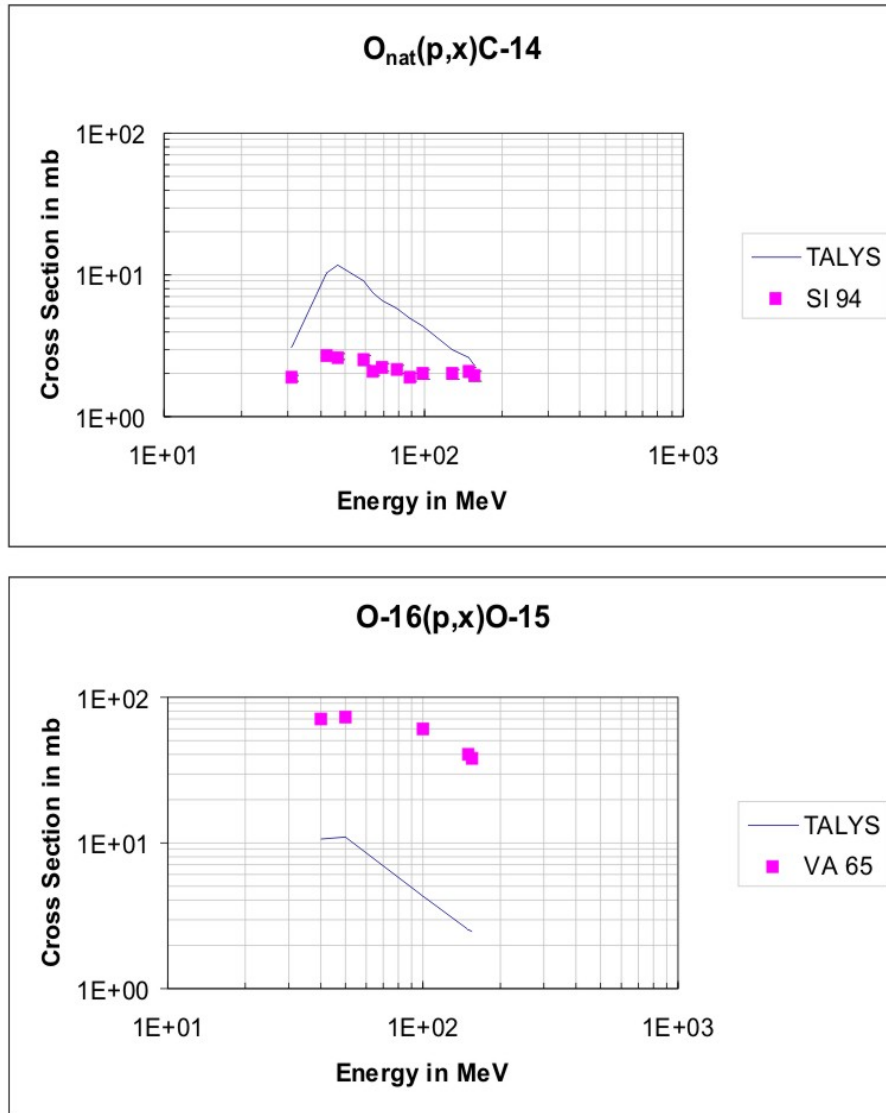


Figure 5.39: Comparison of experimental cross sections for the production  $^{14}\text{C}$  from natural oxygen and  $^{15}\text{O}$  from  $^{16}\text{O}$  with model calculations using the TALYS code.

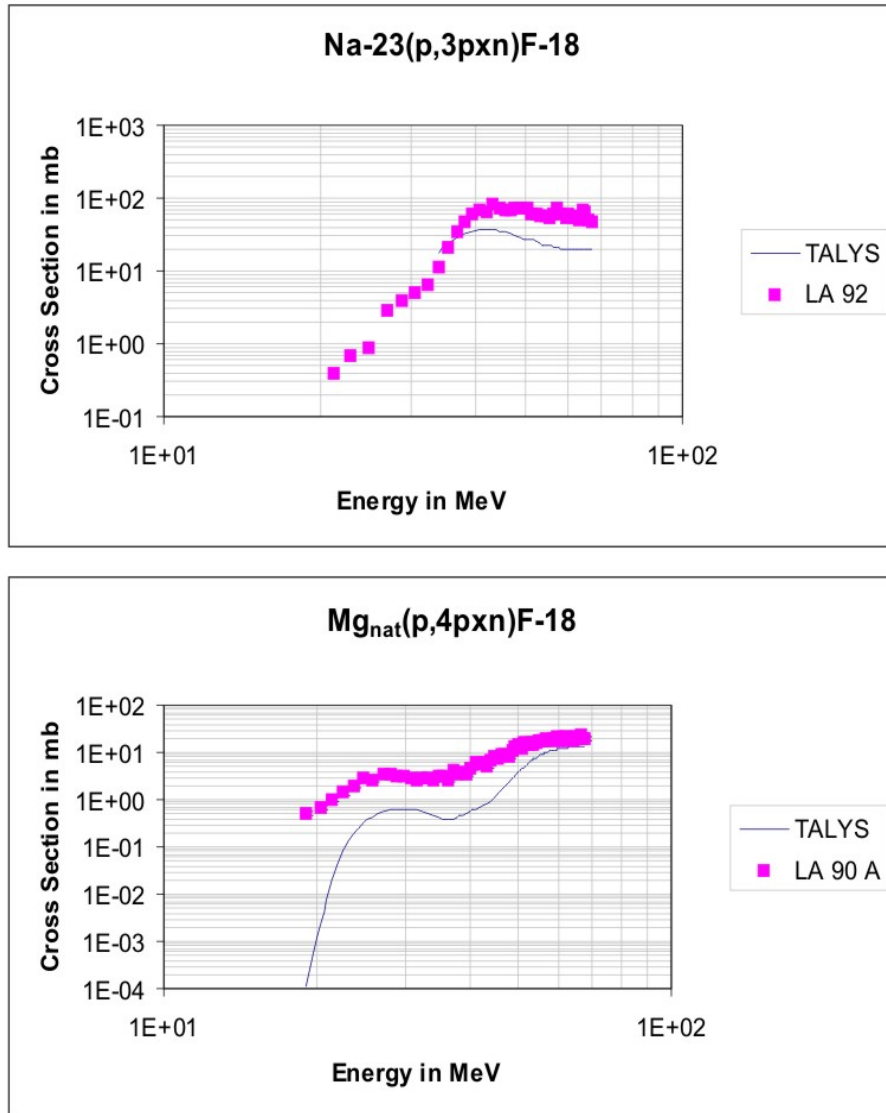


Figure 5.40: Comparison of experimental cross sections for the production  $^{18}\text{F}$  from sodium and natural magnesium with model calculations using the TALYS code

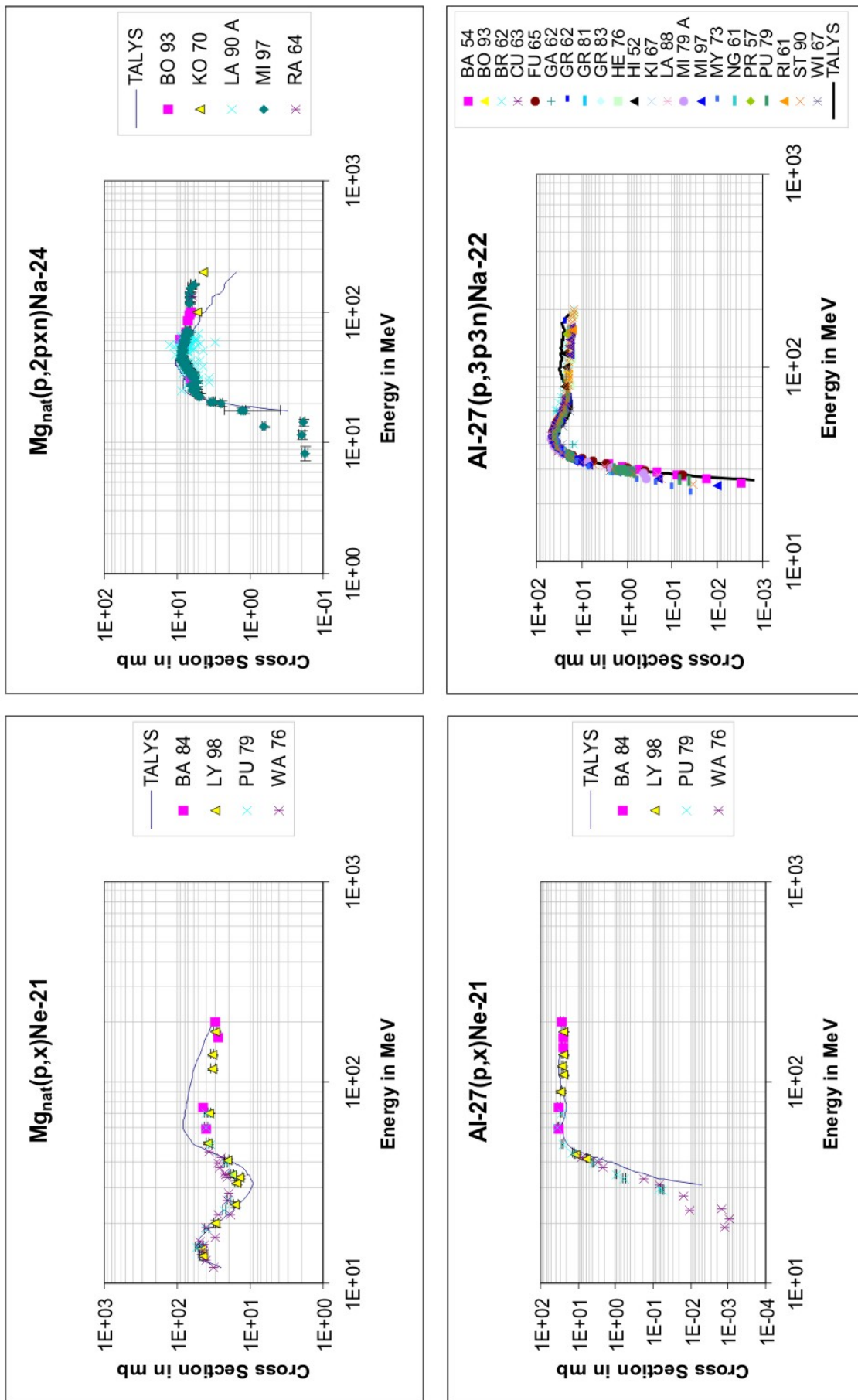


Figure 5.41: Comparison of experimental cross sections for the production of  $^{21}Ne$  and  $^{24}Na$  from natural  $Mg$  and of  $^{21}Ne$  and  $^{22}Na$  from  $^{27}Al$  with model calculations using the TALYS code



The production of  $^{28}\text{Mg}$  from natural silicon has actually an unique reaction path, namely  $^{30}\text{Si}(p,3p)^{28}\text{Mg}$ . This reaction tends to be increasingly underestimated with increasing proton energy.

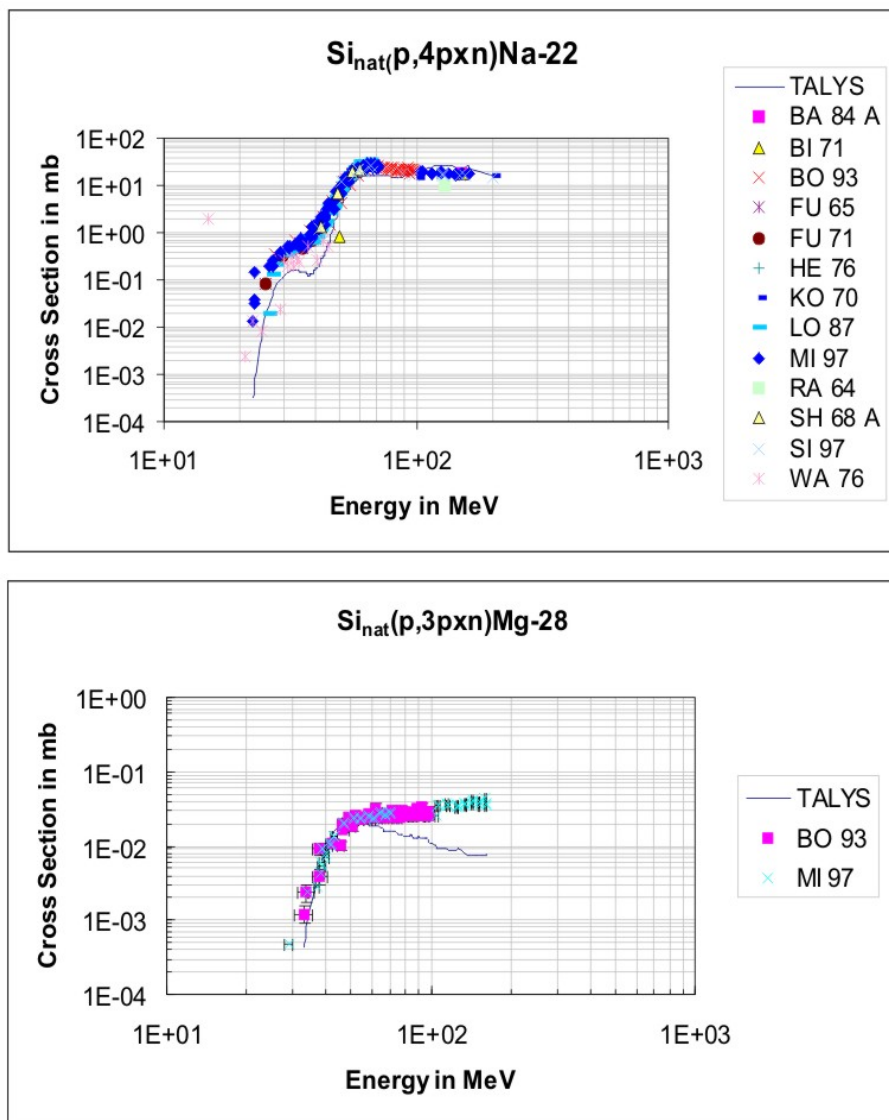


Figure 5.42: Comparison of experimental cross sections for the production of  $^{22}\text{Na}$  and  $^{28}\text{Mg}$  from natural silicon with model calculations using the TALYS code

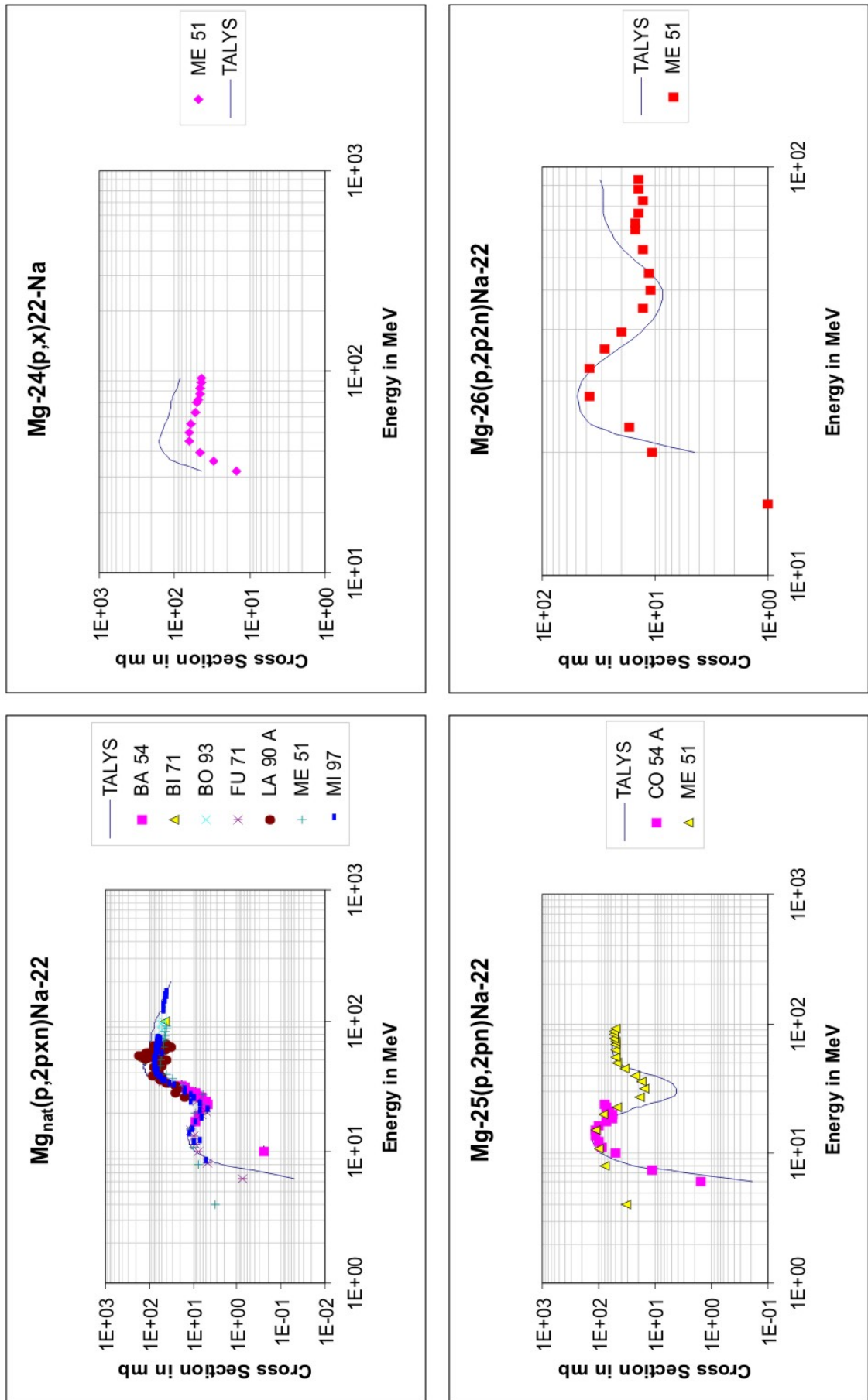


Figure 5.43: Comparison of experimental cross sections for the production of  $^{22}\text{Na}$  from natural magnesium and from individual magnesium isotopes with model calculations using the TALYS code

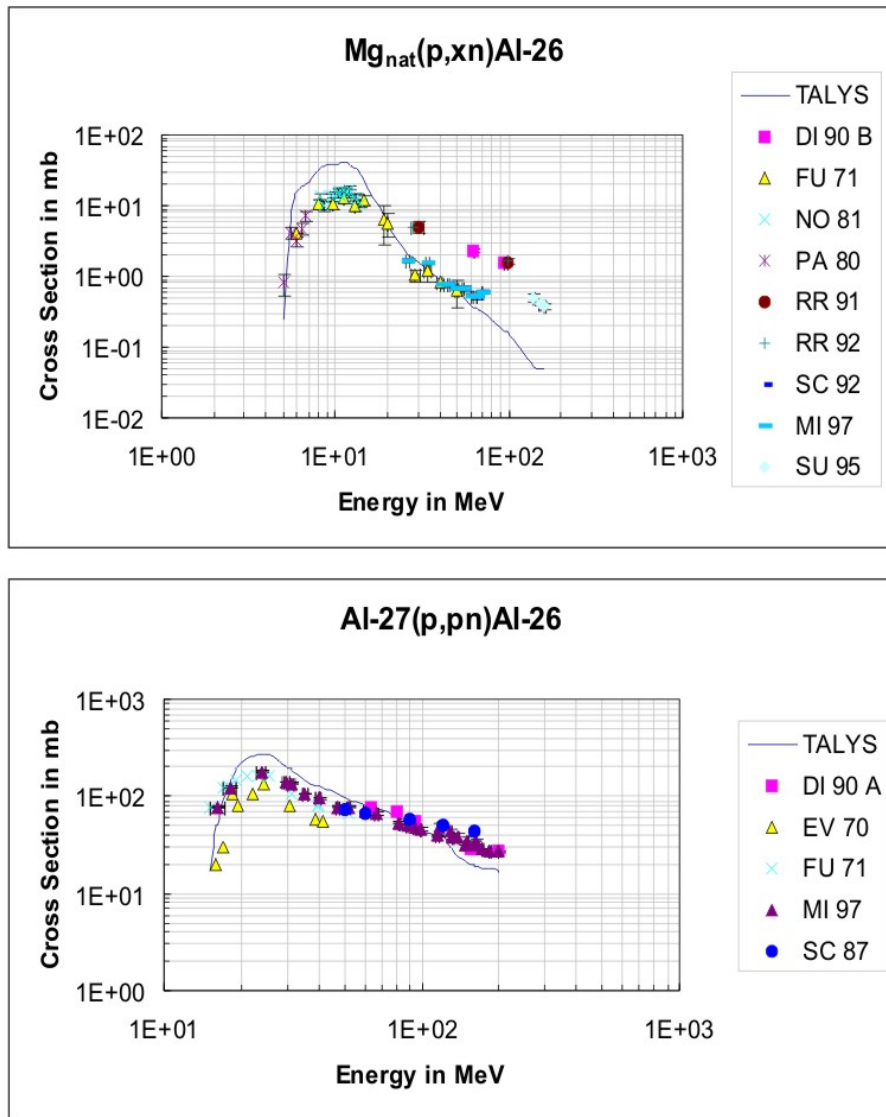


Figure 5.44: Comparison of experimental cross sections for the production of  $^{26}Al$  from magnesium and aluminium with model calculations using the TALYS code.

### 5.5.3 INCL4+ABLA

As already pointed out before, all earlier available models and codes fail to reproduce the production of IMFs like  ${}^7\text{Be}$  and  ${}^{10}\text{Be}$ . This is also true for the INCL4+ABLA calculations as well as for the Bertini-Gilbert-Cameron calculations (Figure 5.46). The calculations underestimate the experimental data by orders of magnitude. It is, however, a new observation that also the production of neon and sodium isotopes is grossly underestimated (Figure 5.47). Mostly, the INCL4+ABLA calculations perform a little bit better. Just for  ${}^{28}\text{Mg}$  and  ${}^{26}\text{Al}$  examples can be shown for which the order of magnitude of the experimental cross sections is met (Figure 5.47).

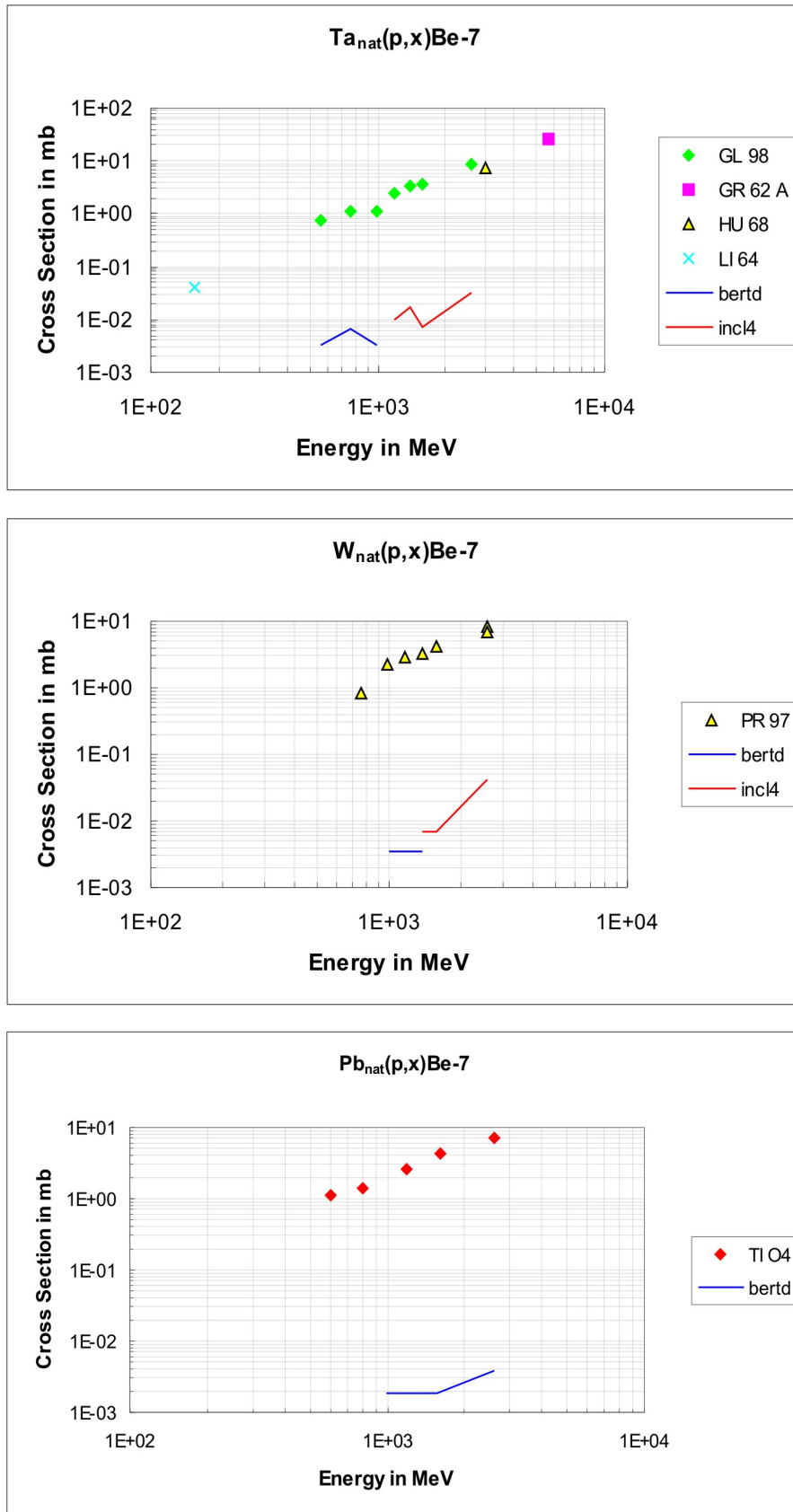


Figure 5.45: Comparison of experimental cross sections for the production of  ${}^7\text{Be}$  from natural tantalum, tungsten, and lead with model calculations using the INCL4+ABLA code and with Bertini-Gilbert-Cameron calculations.

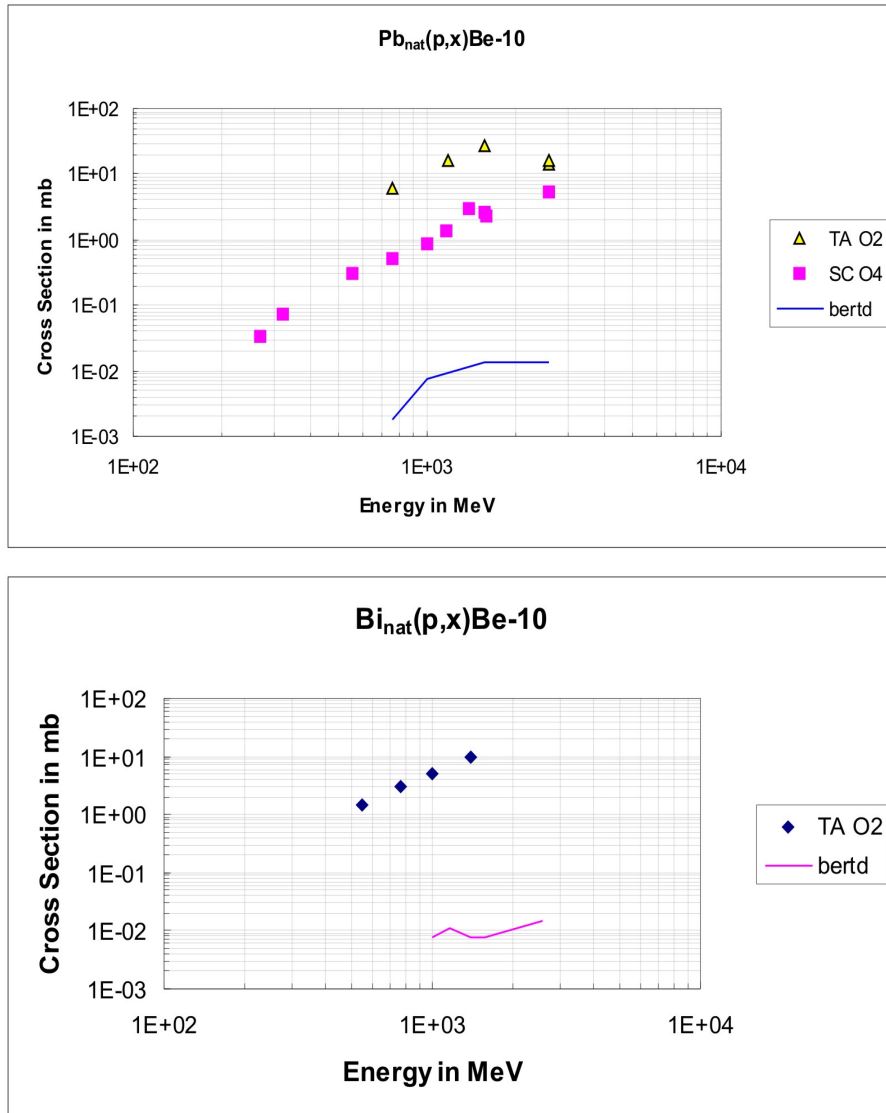


Figure 5.46: Comparison of experimental cross sections for the production of  $^{10}Be$  from natural lead and bismuth with model calculations using the INCL4+ABLA code and with Bertini-Gilbert-Cameron calculations.

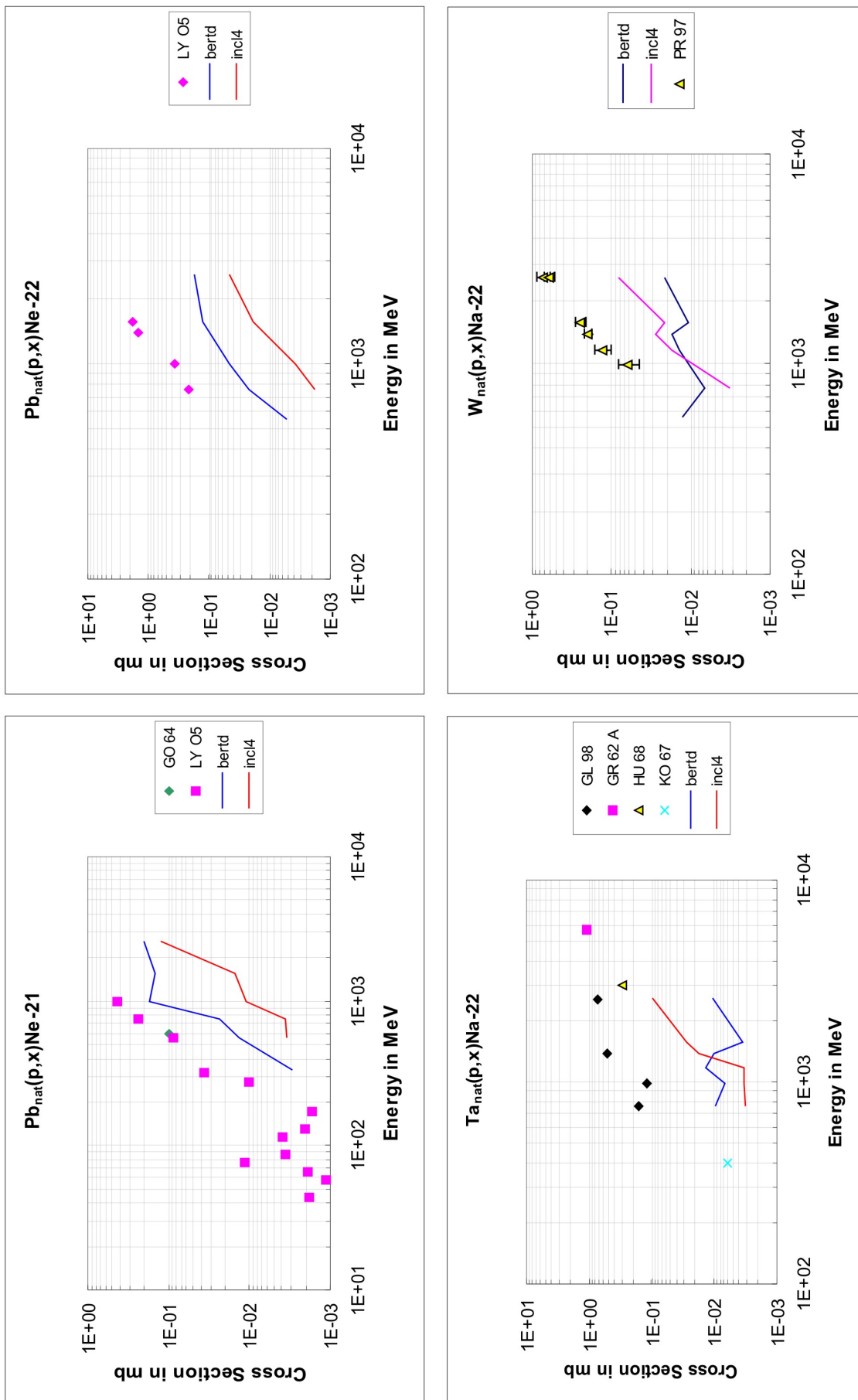


Figure 5.47: Comparison of experimental cross sections for the production of  $^{21}Ne$  and  $^{22}Ne$  from natural lead, of  $^{23}Na$  from natural tantalum and tungsten with model calculations using the INCL4+ABLA code and with Bertini-Gilbert-Cameron calculations.



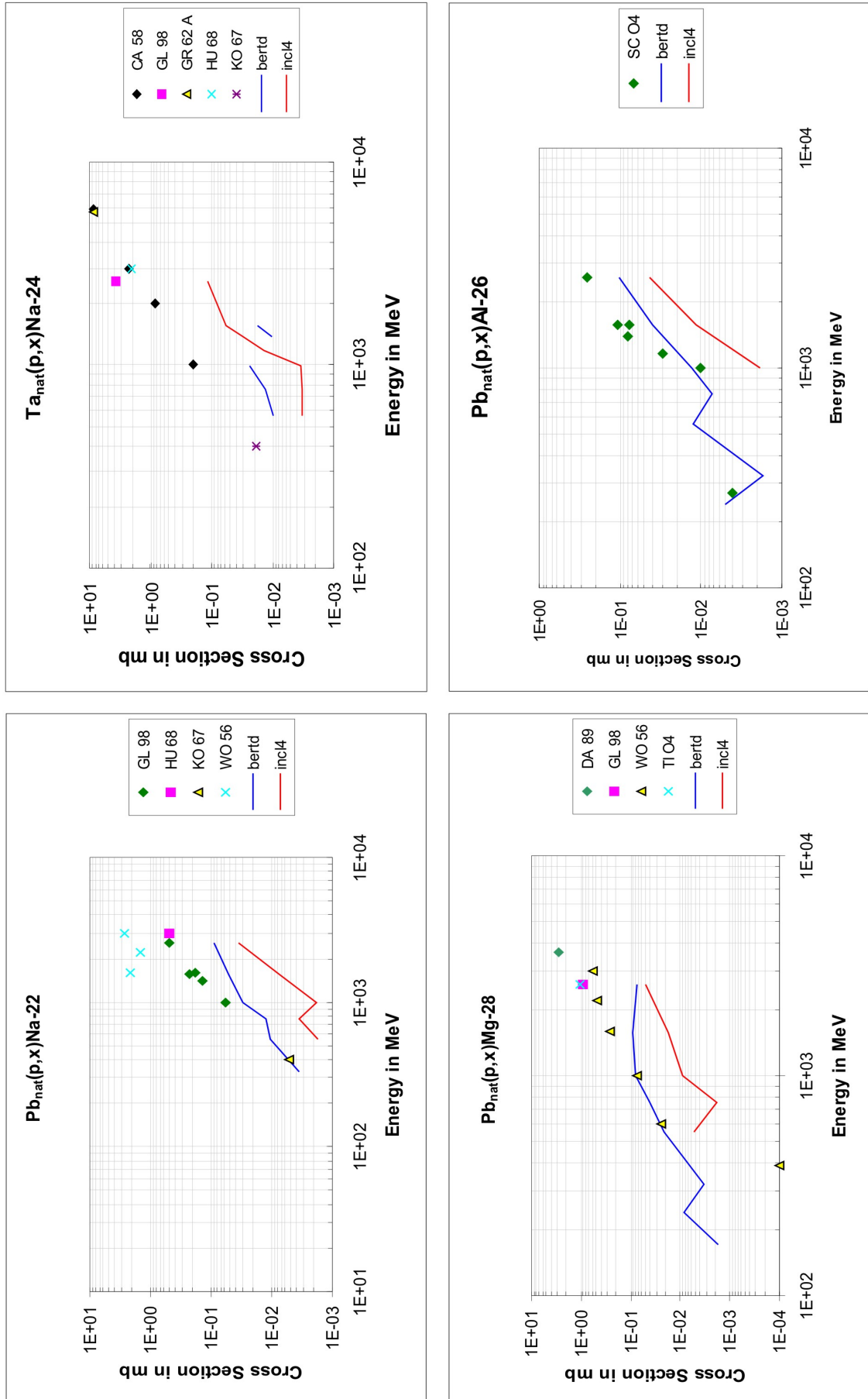


Figure 5.48: Comparison of experimental cross sections for the production of  $^{22}\text{Na}$  from natural lead, of  $^{24}\text{Na}$  from natural tantalum, of  $^{28}\text{Mg}$  and of  $^{26}\text{Al}$  from natural lead with model calculations using the INCL4+ABLA code and with Bertini-Gilbert-Cameron calculations.



---

## 6 Conclusions

By the evaluation of previous  $\gamma$ -spectrometric measurements and by the measurement of long-lived radioactive progenitors in targets of earlier experiments: UPPS0H, UPPS0S and SACL0L this work is contributing to the cross-sections database for proton induced reactions with a number of new cross sections covering target elements Si, Ca, Ti, Mn, Fe, Ni, Cu and Ag, which are relevant for research studies concerning accelerator driven technologies.

For the NUDATRA project a number of 173 excitation functions were studied for the production of residual nuclides with masses between 3 and 30, over an energy range extending from thresholds up to 2.6 GeV with targets spreading over the entire chart of nuclides. The results have been compared with TALYS and INCL4+ABLA codes. While TALYS describes fairly well the shapes of the excitation functions, with a few exceptions which were discussed in the proceeding chapters, INCL4+ABLA fails to describe the experimental data by orders of magnitude.

The present work provides the necessary data and empirical systematic to allow consistent and comprehensive testing of model calculations describing the production of light intermediate mass fragments in proton-induced reactions. It covers sufficient residuals and a wide energy range to contribute to the crucial question whether or not the production of intermediate mass fragments are an extreme case of fission and evaporation or whether a separate fragmentation mode is needed to explain the experimental data.

The existing codes are not capable to predict reliably the experimental data. As a consequence, for accelerator based technologies, it will be necessary to provide extensive experimental database for radionuclide production which have to contain all relevant nuclides for technological development, environment protection or other reasons.



---

## 7 Acknowledgements

There are a lot of people who directly or indirectly contributed to the completion of this work and whom I want to thank.

I will start first by thanking Prof. Dr. Rolf Michel who welcomed me at the ZSR and who directed me towards the successful completion of this thesis. Thank you for your constant guiding and the time spent in helpful and inspiring discussions.

I take this opportunity to thank Dr. Ingo Leya for the time spent to review my dissertation.

I would also like to express my thanks to all my colleagues at ZSR for creating such a friendly working atmosphere. My special thanks go to Dr. Michael Täschner who helped me through the first steps of getting accustomed to a new working environment and to a new country, to Dr. Carsten Wanke for his help with the measuring system , and to Frau Monika Gorny for her friendship and for her patient German lessons.

I thank my family in Romania, my parents and my brother, for their unconditional support over the years we have been apart.

Last, but not least, i would like to thank my husband Daniel for his love, patience and support and for never letting me quit on anything.



---

## References

- [Ad05] J. Adam et al., in: R.C. Haight et al. (eds). *AIP Conf. Proc. Melville NY vol. 769* (2005), 1043–1046.
- [Ai91] J. Aichelin. *Phys. Rep. 202* (1991), 233.
- [Al62] G. Albouy et al. *Phys. Lett. 2* (1962), 306.
- [Al62a] G. Albouy et al. *J. Phys. et Radium 23* (1962), 1000.
- [Al63] G. Albouy et al. *J. Phys. et Radium 24* (1963), 67.
- [Al94] Y.V. Aleksandrov et al. *Proc. Int. Conf. Nuclear Data for Science and Tech., Gatlinburg vol.1* (1994), 371.
- [Am72] B.S. Amin. *Nucl. Phys. A 195* (1972), 311.
- [An77] H.H. Andersen and J.F. Ziegler. *Hydrogen Stopping Power and Range in all Elements* in *Stopping and Ranges of Ions in Matter*, vol. 3. Pergamon Press, 1997.
- [Ar72] T.W. Armstrong and K.C. Chandler. *Nucl. Sci. Eng. 49* (1972), 110.
- [As83] T. Asano et al. *Phys. Rev. C 28* (1983), 1718.
- [As91] Y. Asano et al. *J. Phys. Soc. Jap. 60* (1991), 107.
- [Ba51] R.E. Batzel and G.T. Seaborg. *Phys. Rev. 82* (1951), 607.
- [Ba51a] R.E. Batzel, D.R. Miller and G.T. Seaborg. *Phys. Rev. 84* (1951), 671.
- [Ba54] R.E. Batzel and G.H. Coleman. *Phys. Rev. 93* (1954), 280.
- [Ba58] E. Baker et al. *Phys. Rev. 112* (1958), 1319.
- [Ba71] M. Barbier and S. Regnier. *J. Inorg. Nucl. Chem. 33* (1971), 2720.
- [Ba84] F. Baros and S. Regnier. *J. Phys. 45* (1984), 855.
- [Be00] J. Benlliure et al. *GSI Annual Report, GSI 2000-1*, 29.
- [Be03] M. Bernas et al. *Nucl. Phys. A 725* (2003), 213.
- [Be54] E. Belmont and J.M. Miller. *Phys. Rev. 95* (1954), 1554.
- [Be60] P.A. Benioff. *Phys. Rev. 119* (1960), 316.

- [Be69] H.W. Bertini. *Phys. Rev.* *188* (1969), 1711.
- [Be98] J. Benlliure et al. *Nucl. Phys. A* *628* (1998), 458.
- [Bi62] R.H. Bieri and W. Rutsch. *Compt. Rend. Reun. Soc. Suisse Phys.* *35* (1962), 553.
- [Bi71] R. Bimbot and H. Gauvin. *Compt. Rend. Ser. B* *273* (1971), 1054.
- [Bi71a] C. Birattari et al. *Nucl. Phys. A* *166* (1971), 605.
- [Bl75] M. Blann. *Ann. Rev. Nucl. Sci.* *25* (1975), 25–123.
- [Bl97] M. Blaauw. *Nucl. Instrum. Methods Phys. Res., Sect. A* *387* (1997), 416.
- [Bo02] A. Boudard et al. *Phys. Rev. C* *66* (2002).
- [Bo93] R. Bodemann et al. *Nucl. Instrum. Methods Phys. Res., Sect. B* *82* (1993), 9.
- [Bo95] L. Bornschein. Diplomarbeit, Universität Hannover, ZSR, 1995.
- [Bo95a] J.P. Bondorf et al. *Phys. Rep.* *257* (1995), 133.
- [Bo96] R. Bodemann et al. *TSL Progress Report 1994-1995* (1996), 36–38.
- [Br62] C. Brun. *J. Phys. Rad* *23* (1962), 371.
- [Br62a] C. Brun. *J. Phys. Rad* *23* (1962), 167.
- [Br71] R.L. Brodzinski et al. *Phys. Rev. C* *4* (1971), 1250.
- [Br71a] R.L. Brodzinski et al. *Phys. Rev. C* *4* (1971), 1257.
- [Br78] H. O'Brien et al. *Prog. Nucl. Med.* *4* (1978), 93.
- [Bu94] H. Busemann. Diplomarbeit, Universität Hannover, ZSR, 1994.
- [Bu96] A. Busse. Diplomarbeit, Universität Hannover, ZSR, 1996.
- [Ca58] A.A. Caretto et al. *Phys. Rev.* *110* (1958), 1130.
- [Ca58a] A.A. Caretto and G. Friedland. *Phys. Rev.* *110* (1958), 1169.
- [Ch56] G.A. Chackett et al. *Proc. Phys. Soc. London A* *69* (1956), 43.
- [Cl68] J.E. Cline et al. *IN-1218* (1968), 135–138.



- [Cl71] J.E. Cline and E.B. Nieschmidt. *Nucl. Phys. A* 169 (1971), 437.
- [Cl88] P. Cloth et al. *Juel-2203* (1988).
- [Co54] B.L. Cohen and T.H. Handley. *Phys. Rev.* 93 (1954), 514.
- [Co54a] B.L. Cohen et al. *Phys. Rev.* 96 (1954), 1617.
- [Co55] B.L. Cohen and E. Newman. *Phys. Rev.* 99 (1955), 718.
- [Co55a] B.L. Cohen et al. *Phys. Rev.* 99 (1955), 723.
- [Co55b] B.L. Cohen. *Phys. Rev.* 100 (1955), 206.
- [Cu58] J.B. Cumming et al. *Phys. Rev.* 111 (1958), 1386.
- [Cu59] L.A. Currie. *Phys. Rev.* 114 (1959), 878.
- [Cu62] J.B. Cumming et al. *Phys. Rev.* 127 (1962), 950.
- [Cu62a] J.B. Cumming et al. *Phys. Rev.* 128 (1962), 2392.
- [Cu63] J.B. Cumming. *Nucl. Phys.* 49 (1963), 417.
- [Cu63a] J.B. Cumming. *Ann. Rev. Nucl. Sci.* 13 (1963), 261.
- [Cu81] J.B. Cumming et al. *Nucl. Instrum. Methods Phys. Res.* 180 (1981), 37.
- [De96] D. Deubel. Diplomarbeit, Universität Hannover, ZSR, 1996.
- [Di51] K.M. Dickson and T.C. Randle. *Proc. Phys. Soc. London* 64 (1951), 902.
- [Di90] B. Dittrich et al. *Radiochimica Acta* 50 (1990), 11.
- [Di90a] B. Dittrich et al. *Nucl. Instrum. Methods Phys. Res., Sect. B* 52 (1990), 588.
- [Di90b] B. Dittrich. PhD thesis, Univ. zu Köln, 1990.
- [Do61] I. Dostrovsky et al. *Phys. Rev.* 123 (1961), 1452.
- [En01] T. Enqvist. *Nucl. Phys. A* 686 (2001), 481.
- [En99] M. Enke. *Nucl. Phys. A* 657 (1999), 317.
- [Ep71] M. Epherre and C. Seide. *Phys. Rev. C* 3 (1971), 2167.
- [Ep71a] M. Epherre and C. Seide. *Phys. Rev. C* 3 (1971), 2167.

- [Fi55] E.L. Fireman. *Tritium Phys. Rev.* 97 (1955), 1303.
- [Fi57] E.L. Fireman and J. Zähringer. *Phys. Rev.* 107 (1957), 1695.
- [Fi96] R.B. Firestone and V.S. Shirley (eds.). *Table of Isotopes, 8th edition.* Wiley, New York (1996).
- [Fo62] W.A. Fowler et al. *Geophys. J.* 6 (1962), 148.
- [Fo71] P. Fontes et al. *Nucl. Phys. A* 165 (1971), 405.
- [Fo75] P. Fontes. PhD thesis, Univ. de Paris-Sued, Centre D'orsay, 1975.
- [Fr54] G. Friedlander et al. *Phys. Rev.* 94 (1954), 727.
- [Fr55] G. Friedlander et al. *Phys. Rev.* 99 (1955), 263.
- [Fu65] M. Furukawa et al. *Nucl. Phys.* 69 (1965), 362.
- [Fu71] M. Furukawa et al. *Nucl. Phys. A* 174 (1971), 539.
- [Ga62] H. Gauvin et al. *Nucl. Phys.* 39 (1962), 447.
- [Ga91] J.-J. Gaimard and K.-H. Schmidt. *Nucl. Phys. A* 531 (1991), 709.
- [Ge06] D.F. Geesaman et al. *Annu. Rev. Nucl. Part. Sci.* 56 (2006), 53.
- [Gi98] E. Gilabert et al. *Nucl. Instrum. Methods Phys. Res., Sect. B* 145 (1998), 293.
- [Gi98a] E. Gilabert et al. *Meteoritics and Planetary Science No. 4 Supplement A* 33 (1998), 58.
- [Gl01] M. Gloris et al. *Nucl. Instrum. Methods Phys. Res., Sect. A* 463 (2001), 593.
- [Gl93] M. Gloris. Diplomarbeit, Universität Hannover, ZSR, 1993.
- [Gl98] M. Gloris. Dissertation, Universität Hannover, 1998.
- [Go04] F. Goldenbaum. *The Physics of Spallation Processes; Theory, Experiments and Applications.* Forschungszentrum Jülich GmbH, 2004.
- [Go50] S.N. Goshal et al. *Phys. Rev.* 80 (1950), 939.
- [Go60] J. Gonzalez-Vidal and W.H. Wade. *Phys. Rev.* 120 (1960), 1354.
- [Go61] K. Goebel et al. *Nucl. Phys.* 24 (1961), 28.

- [Go61a] K. Goebel. *Z. Naturforschg. 16a* (1961), 231.
- [Gr60] E. Gradsztajn. *J. Phys. Rad 21* (1960), 761.
- [Gr62a] J.R. Grover. *Phys. Rev. 126* (1962), 1540.
- [Gr81] A. Gruetter. *Nucl. Phys. A 383* (1981), 98.
- [Gr82] A. Gruetter. *Int. J. Appl. Radiat. Isot. 33* (1982), 725.
- [Gr85] P.W. Gray and A. Ahmad. *Nucl. Instrum. Methods Phys. Res., Sect. A 237* (1985), 577.
- [Gr88a] S.L. Green et al. *J. Nucl. Mat. 155-157* (1988), 1350.
- [Gu83] K.K. Gudima et al. *Nucl. Phys. A 401* (1983), 329.
- [Ha87] A.A. Harms. *Principle of Nuclear Sciences and Engineering*. Research Studies Press, England, 1987.
- [Ha95] S. Hasse. Diplomarbeit, Universität Hannover, ZSR, 1995.
- [He06] C.-M. Herbach, J. Toke et al. *Nucl. Phys. A 756* (2006), 426.
- [He56] C.G. Heininger and E.O. Wiig. *Phys. Rev. 101* (1956), 1074.
- [He76] H.R. Heydegger et al. *Phys. Rev. C 14* (1976), 1506.
- [Hi52] N.M. Hintz and N.F. Ramsey. *Phys. Rev. 88* (1952), 19.
- [Hi56] H.G. Hicks, P.C. Stevenson and W.E. Nervik. *Phys. Rev. 102* (1956), 1390.
- [Ho60] M. Honda and P. Lal. *Phys. Rev. 118* (1960), 1618.
- [Ho64] M. Honda and D. Lal. *Nucl. Phys. 51* (1964), 363.
- [Ho77] R. Holub et al. *Nucl. Phys. A 288* (1977), 291.
- [Ho78] J.J. Hogan and E. Gadioli. *Nuovo Cimento 45A* (1978), 341.
- [Ho95] A. Howering. Diplomarbeit, Universität Hannover, ZSR, 1995.
- [Hu54] J. Hudis et al. *Phys. Rev. 94* (1954), 775.
- [Hu63] R.M. Humes et al. *Phys. Rev. 130* (1963), 1522.
- [Hu63a] J. Hudis et al. *Phys. Rev. 129* (1963), 434.

- [Hu68] J. Hudis and S. Tanaka. *Phys. Rev.* *171* (1968), 1297.
- [Hu68a] J. Hudis. *Phys. Rev.* *171* (1968), 1301.
- [Ja74] W.W. Jacobs et al. *Phys. Rev. C* *9* (1974), 2134.
- [Ju70] M. Jung et al. *Phys. Rev. C* *1* (1970), 435.
- [Ju98] A.R. Junghans et al. *Nucl. Phys. A* *629* (1998), 635.
- [Ka68] S. Katcoff et al. *Phys. Rev.* *166* (1968), 1147.
- [Ka80] S.B. Kaufmann and E.P. Steinberg. *Phys. Rev. C* *22* (1980), 167.
- [Ki67] F.M. Kiely. PhD thesis, Carnegie Inst. of Technology, Pittsburgh, 1998.
- [Kl96] B. Klug. Diplomarbeit, Universität Hannover, ZSR, 1996.
- [Ko05] A.J. Koning et al., in: R.C. Haight et al. (eds). *AIP Conf. Proc. Melville NY* *769* (2005), 1154.
- [Ko07] A.J. Koning, S. Hilaire and M. Duijvestijn. *TALYS-1.0, A nuclear reaction program, User manual, December 21. 2007.*
- [Ko64] R.G. Korteling and E.K. Hyde. *Phys. Rev.* *136B* (1964), 425.
- [Ko67] R.G. Korteling and A.A. Caretto. *J. Inorg. Nucl. Chem.* *29* (1967), 2863.
- [Ko70] R.G. Korteling and A.A. Caretto. *Phys. Rev. C* *1* (1970), 1960.
- [Ko70a] R.G. Korteling and R. Kiefer. *Phys. Rev. C* *2* (1970), 957.
- [Ko88] P. Kozma et al. *Czech. J. Phys. B* *38* (1988), 973.
- [Ko90] P. Kozma and J. Klimann. *J. Phys. G* *16* (1990), 45.
- [Ko90a] P. Kozma and B. Tumendemberel. *Czech. J. Phys. B* *40* (1990), 29.
- [Ko91] P. Kozma et al. *J. Phys. G, Nucl. Part. Phys.* *17* (1991), 675.
- [Ko92] A.J. Koning et al. *Nucl. Science Technology, Supplement* *769* (1992), 1154.
- [Ko98] A.J. Koning et al. *NEA-REPORT NEA/WPEC-13, ECN-RX-98-014* (1998).
- [Kr77] S. Krämer et al. *J. Inorg. Nucl. Chem. Lett.* *13* (1977), 205.
- [Kr95] A. Krins. Diplomarbeit, Universität Hannover, ZSR, 1995.

- [Ku01] J. Kuhnenn et al. *Radiochimica Acta* 89 (2001), 697.
- [La57] A.K. Lavrukhina et al. *At. Energ.* 3 (1957), 285.
- [La59] A.K. Lavrukhina et al. *J. Nucl. Energy II* 8 (1959), 231.
- [La63] A.K. Lavrukhina et al. *Sov. Phys. JETP* 16 (1963), 1.
- [La63a] A.K. Lavrukhina et al. *Sov. Phys. JETP* 17 (1963), 960.
- [La66] M.S. Laffleur et al. *Can. J. Chem.* 44 (1966), 2749.
- [La73] H. Laumer et al. *Phys. Rev. C* 8 (1973), 483.
- [La74] H. Laumer et al. *Phys. Rev. C* 10 (1974), 1045.
- [La88] M.C. Lagunas-Solar et al. *Appl. Rad. Isot.* 39 (1988), 41.
- [La90a] M.C. Lagunas-Solar and O.F. Carvacho. *Appl. Rad. Isot.* 41 (1990), 349.
- [La90b] M.C. Lagunas-Solar et al. *Appl. Rad. Isot.* 41 (1990), 521.
- [La92] M.C. Lagunas-Solar et al. *Appl. Rad. Isot.* 43 (1992), 1005.
- [Le04] M. Leino and F.P. Hessberger. *Annu. Rev. Nucl. Part. Sci.* 54 (2004), 175.
- [Le61] M. Lefort et al. *Nucl. Phys.* 25 (1961), 216.
- [Li62] R.H. Lindsay and E.F. Neuzil. *Phys. Rev.* 127 (1962), 1269.
- [Li64] M. Ligonniere et al. *Comptes Rendus Acad. Soc. Paris* 259 (1964), 1406.
- [Li75] P.J. Lindstrom et al. *Report LBL 3650* (1975).
- [Lo87] Y.N. Lobach. *Atomnaya Energiya* 63 (1987), 30.
- [Lu08] <http://nucleardata.nuclear.lu.se/nucleardata/>.
- [Lu93] M. Luepke. Thesis, Uni. Hannover, 1993.
- [Ly05] I. Leya. *Nucl. Instrum. Methods Phys. Res., Sect. B* 229 (2005), 1.
- [Ly93] A. Krins. Diplomarbeit, Universität Hannover, ZSR, 1995.
- [Ly97] I. Leya. Dissertation, Uni. Hannover, 1997.
- [Ly98] I. Leya. *Nucl. Instrum. Methods Phys. Res., Sect. B* 145 (1998), 449.

- [Ma06] H. Matchner et al. *Phys. Rev. C* 73 (2006), 044606.
- [Ma51] L. Marquez and I. Perlman. *Phys. Rev.* 81 (1951), 953.
- [Ma52] L. Marquez. *Phys. Rev.* 86 (1952), 405.
- [Ma69] P. Marmier and E. Sheldon. *Physics of Nuclei and Particles*, vol. 1. Academic Press, London, 1969.
- [Me00] S. Merchel et al. *Nucl. Instrum. Methods Phys. Res., Sect. B* 172 (2000), 144.
- [Me05] J.P. Meulders et al. *HINDAS, High and Intermediate Energy Nuclear Data for Accelerator-Driven Systems, Final Technical Report, January 2005*.
- [Me51] J.W. Meadows and R.B. Holt. *Phys. Rev.* 83 (1951), 1257.
- [Me51a] J.W. Meadows and R.B. Holt. *Phys. Rev.* 83 (1951), 47.
- [Me62] S. Meghir. Thesis, Montreal, 1962.
- [Me67] V.N. Mekhedov. *Sov. J. Nucl. Phys.* 5 (1967), 24.
- [Me70] B.N. Mekhedov and V.N. Mekhedov. *Sov. J. Nucl. Phys.* 11 (1975), 397.
- [Mi00] R. Michel, in: D. Filges et al.(eds.). *Proc. of the Fifth Workshop on Simulating Accelerator Irradiation Environments (SARE-5)*, July 17-18, 2000, OECD Headquarters Paris, ISSN 1433-559X, ESS 112-01-T, April 2001, 27–53.
- [Mi02] R. Michel et al. *Nucl. Science Technology, Supplement 2* (2002), 242.
- [Mi02a] M.M.H. Miah et al. *Nucl. Science Technology, Supplement 2* (2002), 369.
- [Mi05] R. Michel et al., in: R.C. Haight et al. (eds). *AIP Conf. Proc. Melville NY 769* (2005), 1551.
- [Mi06] R. Michel and M. Tutuc. *Production of Light and Intermediate Mass Residues, Report for EUROTRANS/NUDATRA Milestone M5.19, November 2006*.
- [Mi79] R. Michel et al. *Nucl. Phys. A* 322 (1979), 40.
- [Mi85] R. Michel et al. *Nucl. Phys. A* 441 (1985), 617.
- [Mi89] R. Michel et al. *Analyst* 114 (1989), 295.
- [Mi93] R. Michel et al. *J. Radioanal. Nucl. Chem.* 169 (1993), 13.

- [Mi95] R. Michel et al. *Nucl. Instrum. Methods Phys. Res., Sect. B* 103 (1995), 183.
- [Mi97] R. Michel et al. *Nucl. Instrum. Methods Phys. Res., Sect. B* 129 (1997), 153.
- [Mi97a] R. Michel and P. Nagel. *International Codes and Model Intercomparison for Intermediate Energy Activation Yields*, NSC/DOC(97)-1, NEA/OECD, Paris (1997).
- [Mi98] R. Michel and S. Neumann. *Proc. Indian Acad. Sci. (Earth Planet. Sci.)* 107 No. 4 (1998), 441.
- [Mi99] R. Michel et al. *Radiochim. Acta* 87 (1999), 47.
- [Mo62] D.L. Morris and A.A. Caretto. *Phys. Rev.* 127 (1962), 1731.
- [Mo70] L.P. Moskaleva et al. *Sov. J. Nucl. Phys.* 12 (1971), 472.
- [My73] K. Miyano. *J. Phys. Soc. Jap.* 34 (1973), 853.
- [Ne55] W.E. Nervik and G.T. Seaborg. *Phys. Rev.* 97 (1955), 1092.
- [Ne60] D.R. Nethaway and L. Winsberg. *Phys. Rev.* 119 (1960), 1375.
- [Ne63] E.F. Neuzil and R.H. Lindsay. *Phys. Rev.* 131 (1963), 1697.
- [Ne94] B. Neumaier et al. *Radiochim. Acta* 65 (1994), 1.
- [Ne94a] S. Neumann. Dissertation, Universität Hannover, ZSR, 1994.
- [Ne96] U. Neupert. Thesis, Universität Hannover, 1996.
- [Ne97] U. Neupert. Thesis, Uni.Hannover, 1997.
- [Ne98] S. Neumann. Thesis, Uni.Hannover, 1998.
- [Ng61] Nguyen-Long-Den. *Comptes Rendus Academie de Sciences* 253 (1961), 2919.
- [Ni95] K. Niita et al. *Phys. Rev. C* 52 (1995), 2620.
- [No81] E.B. Norman et al. *Nucl. Phys. A* 357 (1981), 228.
- [Or76] C.J. Orth et al. *J. Inorg. Nuc. Chem.* 38 (1976), 13.
- [Pa60] V. Parikh. *Nucl. Phys.* 18 (1960), 646.
- [Pa60a] V. Parikh. *Nucl. Phys.* 18 (1960), 638.

- [Pa77] P. Paillard. Thesis, Bordeaux, 1977.
- [Pa80] M. Paul et al. *Phys. Lett. 94b* (1980), 303.
- [Po71] A.M. Poskanzer et al. *Phys. Rev. C 3* (1971), 882.
- [Po78] N.T. Porile et al. *Phys. Rev. C 18* (1978), 2231.
- [Po79] N.T. Porile, G.D. Cole and C.R. Rudy. *Phys. Rev. C 19* (1979), 2288.
- [Pr57] D.I. Prokoshkin and A.A. Tiapkin. *Sov. Phys. JEPT 5* (1957), 148.
- [Pr89] R.E. Prael. *LA-UR-89-3347, Los Alamos National Laboratory* (1989).
- [Pr94] R.E. Prael, in. *Proc. of a Specialists' Meeting*, Issy-les-Moulineaux, France, 30 May - 1 June (1994).
- [Pr97] J. Protoschill. Diplomarbeit, Universität Hannover, ZSR, 1997.
- [Pu79] P. Pulfer. Thesis, Uni.Bern, 1979.
- [Ra64] G.V.S. Rayudu. *Can. J. Chem. 42* (1964), 1149.
- [Ra68] G.V.S. Rayudu. *J. Inorg. Nucl. Chem. 30* (1969), 2311.
- [Ra73] G.M. Raisbeck and F. Yiou. *13<sup>th</sup> Int. Cosmic Rays Conf. Denver 1* (1973), 494.
- [Ra74] G.M. Raisbeck and F. Yiou. *Phys. Rev. C 9* (1974), 1385.
- [Ra75] G.M. Raisbeck and F. Yiou. *Phys. Rev. C 12* (1975), 915.
- [Ra75a] G.M. Raisbeck and F. Yiou. *14<sup>th</sup> Int. Cosmic Rays Conf. Munich 2* (1975), 495.
- [Ra77] G.M. Raisbeck and F. Yiou. *15<sup>th</sup> Int. Cosmic Rays Conf. Ploudiv 2* (1977), 203.
- [Ra77a] G.M. Raisbeck and F. Yiou. *15<sup>th</sup> Int. Cosmic Rays Conf. Ploudiv 2* (1977), 112.
- [Ra77b] G.M. Raisbeck and F. Yiou. *15<sup>th</sup> Int. Cosmic Rays Conf. Ploudiv 2* (1977), 116.
- [Ra79] G.M. Raisbeck and F. Yiou. *16<sup>th</sup> Int. Cosmic Rays Conf. Kyoto 2* (1979), 207.



- [Re58] P. Reasbeck and J.E. Warren. *J. Inorg. Nucl. Chem.* 7 (1958), 343.
- [Re63] L.P. Remsberg and J.M. Miller. *Phys. Rev.* 130 (1963), 2069.
- [Re65] J.B.J. Read and J.M. Miller. *Phys. Rev.* 140 (1965), 623.
- [Re65a] P.L. Reeder. *J. Inorg. Nucl. Chem.* 27 (1965), 1879.
- [Re73] S. Regnier et al. *Earth Planet. Sci. Lett.* 18 (1973), 9.
- [Re75] S. Regnier et al. *C.R.Acad. Sc. Paris B280* (1975), 513.
- [Re81] J.-L. Reyss et al. *Earth Planet. Sci. Lett.* 53 (1981), 203.
- [Re82] S. Regnier et al. *Phys. Rev. C* 26 (1982), 931.
- [Re93] H. Reinhardt. Diplomarbeit, Universität Hannover, ZfS, 1993.
- [Ri05] M.V. Ricciardi et al. *GSI Report* (2005).
- [Ri06] M.V. Ricciardi et al. *Phys. Rev. C* 73 (2006), 014607.
- [Ri61] K.W. Rind. Thesis, New York, 1961.
- [Ro76] C.T. Roche et al. *Phys. Rev. C* 14 (1976), 410.
- [Ro91] R. Roesel. Priv. comm. to R. Michel.
- [Ru66] G. Rudstam. *Z. Naturforsch.* 21a (1966), 1027.
- [Sa80] G.R. Satchler. *Introduction to Nuclear Reactions*. Oxford University Press, 1980.
- [Sc04] Ch. Schnabel et al. *Nucl. Instrum. Methods Phys. Res., Sect. B* 223-224 (2004), 812.
- [Sc05] D. Schumann et al., in: R.C. Haight et al. (eds). *AIP Conf. Proc. Melville NY* 769 (2005), 1517.
- [Sc06] D. Schumann et al. *Nucl. Instrum. Methods Phys. Res., Sect. A* 562 (2006), 1057.
- [Sc58] O.A. Schaffer and J. Zaehring. *Z. Naturforsch.* 13a (1958), 346.
- [Sc59] O.A. Schaffer and J. Zaehring. *Phys. Rev.* 113 (1959), 674.

- [Sc87] R.J. Schneider et al. *Nucl. Instrum. Methods Phys. Res., Sect. B* 29 (1987), 271.
- [Sc91] M. Schnatz. Diplomarbeit, Universität Hannover, 1991.
- [Sc91a] T. Schiekel. Diplomarbeit, Universität Köln, 1991.
- [Sc94] B. Scholten et al. *Radiochim. Acta* 748 (1994), 1.
- [Sc95] T. Schiekel. Thesis, Universität zu Köln, 1995.
- [Sc96] Th. Schiekel et al. *Nucl. Instrum. Methods Phys. Res., Sect. B* 114 (1996), 91.
- [Sc96a] T. Schiekel et al. *Nucl. Instrum. Methods Phys. Res., Sect. B* 114 (1996), 91.
- [Sc96b] T. Schiekel et al. *Nucl. Instrum. Methods Phys. Res., Sect. B* 113 (1996), 484.
- [Sc97] Ch. Schnabel et al., in: G. Reffo et al. (eds). *Conf. Proc. Nuclear Data for Science and Technology*, Societa Italiana di Fisica, Bologna, vol. 59 (1997), 1559.
- [Se47] R. Serber. *Phys. Rev.* 72 (1947), 1114.
- [Sh08] Shams A.M. Issa et al, in. *Proc. of IX Radiation Physics and Protection Conference, 15-19 Nov. 2008, Nasr City-Cairo, Egypt* (2008).
- [Sh09] Shams A.M. Issa. Ph.d thesis, Al-Azhar University, Faculty of Science, Assiut, Egypt, 2009.
- [Sh68a] D.W. Sheffey et al. *Phys. Rev.* 172 (1968), 1094.
- [Sh93] S. Shibata et al. *Phys. Rev. C* 48 (1993), 2617.
- [Si73a] R. Silberberg and C.H. Tsao. *Astrophys. J. Suppl. Ser.* 220(I) 25 (1973), 315.
- [Si73b] R. Silberberg and C.H. Tsao. *Astrophys. J. Suppl. Ser.* 220(I) 25 (1973), 335.
- [Si91] J.M. Sisterson et al. *LPSC XXII* (1991), 1267.
- [Si91a] J.M. Sisterson et al. *Meteoritics* (1991), 395.
- [Si92] J.M. Sisterson et al. *LPSC XXIII* (1992).
- [Si94] J.M. Sisterson et al. *Nucl. Instrum. Methods Phys. Res., Sect. B* 92 (1994), 510.
- [Si97] J.M. Sisterson et al. *Nucl. Instrum. Methods Phys. Res., Sect. B* 123 (1997), 324.

- [St68] A.F. Stehney and E.P. Steinberg. *Nucl. Instrum. Methods Phys. Res.* 59 (1968), 102.
- [St68a] A.F. Stehney and E.P. Steinberg. *Nucl. Phys. B* 5 (1968), 188.
- [St71] G.B. Stapleton and R.H. Thomas. *Nucl. Phys. A* 175 (1971), 124.
- [St90] G.F. Steyn et al. *Appl. Radiat. Isot.* 41 (1990), 315.
- [Su95] F. Sudbrock. Priv. comm. to R. Michel.
- [Su97] F. Sudbrock et al., in: G. Reffo et al. (eds). *Conf. Proc. Nuclear Data for Science and Technology*, Societa Italiana di Fisica, Bologna vol. 59 (1997), 1534–1536.
- [Su97a] F. Sudbrock et al., in. *Progress Report on Nuclear Data Research in the Federal Republic of Germany for the Period April, 1st, 1996 to March, 31th, 1997*, NEA/NSC/DOC(97) 13, INDC(Ger)-043/LN, Jül-3410 (1997), 40–42.
- [Ta02] A. Tarabischi. Thesis, Universität zu Köln, 2002.
- [Ta03] J. Taieb et al. *Nucl. Phys. A* 724 (2003), 413.
- [Ta61] M.A. Tamers and G. Delibrias. *Compt. Rend. Acad. Sci.* 253 (1961), 1202.
- [Ta97] T.N. Taddeucci et al. *Phys. Rev. C* 55 (1997), 1551.
- [Ti04] Y.E. Titarenko. *Experimental and Theoretical Studies of the Yields of Residual Product Nuclei Produced in Thin Pb and Bi Targets Irradiated by 40-2600 MeV Protons*, Final Technical Report on the ISTC Project 2002 (2004).
- [Ti96] Y.E. Titarenko et al. *Proc. 2nd Int. Conf. on Accelerator-Driven Transmutation Technologies and Applications*, Kalmar, 3-7 June (1996).
- [To73] J. Tobailem et al. *Rapport CEA-R-4441* (1973).
- [To81] J. Tobailem and C.H. de Lassus St. Genies. *Report CEA-N-1466* (1981), 5.
- [Uo05] M.A.M. Uosif et al., in: R.C. Haight et al. (eds). *AIP Conf. Proc. Melville NY* vol. 769 (2005), 1547–1550.
- [Va63] L. Valentin et al. *Phys. Lett.* 7 (1963), 15.
- [Va65] L. Valentin. *Nucl. Phys.* 62 (1965), 81.
- [Vi06] V.E. Viola et al. *Phys. Rep.* 434 (2006), 1.

- [Vo94] H. Vonach. Priv. comm. to R. Michel.
- [Wa54] G.D. Wagner and E.O. Wiig. *Phys. Rev.* *96* (1954), 1100.
- [Wa76] J.R. Walton et al. *J. Geophys. Res.* *81* (1976), 5689.
- [Wa86] C.F. Wang and N.T. Porile. *Phys. Rev. C* *33* (1986), 2183.
- [We75] H. Weigel et al. *Radiochem. Radioanal. Lett* *21* (1975), 293.
- [We81] W. Westmeier. *Nucl. Instrum. Methods Phys. Res.* *180* (1981), 205.
- [We86] W. Westmeier. *Nucl. Instrum. Methods Phys. Res., Sect. A* *242* (1986), 437.
- [We94] W. Westmeier. *Comercially available code GAMMA-W, ver. 15.03* (1994).
- [We95] W. Westmeier. *GAMMA-W manual, Ebsdorfergrund-Mölln* (1995).
- [Wi67] I.R. Williams and C.B. Fulmer. *Phys. Rev.* *162* (1967), 1055.
- [Wi67a] I.R. Williams and C.B. Fulmer. *Phys. Rev.* *154* (1967), 1005.
- [Wo54] R.L. Wolfgang and G. Friedlander. *Phys. Rev.* *96* (1954), 199.
- [Wo55] R.L. Wolfgang and G. Friedlander. *Phys. Rev.* *98* (1955), 1871.
- [Wo56] R.L. Wolfgang et al. *Phys. Rev.* *103* (1956), 394.
- [Yi69] F. Yiou et al. *J. Geophys. Res.* *74* (1969), 2447.
- [Yu60] H.P. Yule and A. Turkevich. *Phys. Rev.* *118* (1960), 1591.
- [Zi85] J.F. Ziegler, J.P. Biersack and U. Littmark. *The Stopping Power and Range of Ions in Solids* in *Stopping and Ranges of Ions in Matter*, vol. 1. Pergamon Press, 1985.

## List of Tables

1.1	Examples for applications of nuclear data. . . . .	3
4.1	Survey on experiments performed at LNS . . . . .	26
4.2	Survey on experiments performed at TSL . . . . .	27
4.3	Nuclear data used in this work for the determination of experimental cross-sections . . . . .	32
4.4	Survey on target-product combinations evaluated from UPPS0H . . . .	37
4.5	Survey on targets evaluated from UPPS0H . . . . .	37
4.6	Cross sections determined for the production of residual nuclides by proton induced reactions in UPPS0H . . . . .	38
4.7	Survey on target-product combinations evaluated from SACL0L . . . .	41
4.8	Survey on targets evaluated from UPPS0H . . . . .	41
4.9	Cross sections determined for the production of residual nuclides by proton induced reactions in SACL0L . . . . .	42
4.10	Survey on target-product combinations evaluated from UPPS0S . . . .	48
4.11	Survey on targets evaluated from UPPS0S . . . . .	48
4.12	Cross sections determined for the production of residual nuclides by proton induced reactions in UPPS0S . . . . .	49
5.1	Survey on the nuclear reactions dealt with in this report . . . . .	60
5.2	Nuclear models and structure information implemented in TALYS 0.72 (released 21.dez.06) . . . . .	112
5.3	Product nuclides determined and radioactive progenitors considered for the calculations . . . . .	115



## List of Figures

3.1	Schematical drawing of an outgoing particle spectrum. The energy regions to which direct (D), pre-equilibrium (P) and compound (C) mechanisms contribute are indicated. The dashed curve distinguishes the compound contribution from the rest in the transitional energy region, [Ko07]. . . . .	11
3.2	Dependence of the reaction mode on energy. . . . .	13
3.3	Illustration of particle interactions on the intra-, inter- and evaporation level, [Go04]. . . . .	14
3.4	Illustration of a fission reaction . . . . .	15
3.5	Classical kinematics versus Inverse kinematics . . . . .	16
3.6	Example of an experimental setup for the stacked foil technique . . . .	17
3.7	Example of an experimental setup for the inverse kinematics technique: Schematic view from above of the horizontal section of the experimental setup [Ri06] (FRS-fragment separator was used as a high resolution spectrometer) . . . . .	18
4.1	(a) Target containers used in experiments at TSL and LNS ; (b,c) the new and smaller target containers used in the experiments at LNS . At LNS the individual mini-stacks of type c were positioned in the beam by hanging them up on thin threads in the center of Al-frames which were not hit by the primary protons. Dimensions are given in mm [Gl98]. . .	24
4.2	Schematic view of the target arrangements used (a) at LNS for energies above 200 MeV and (b) at TSL for energies below 180 MeV [Gl98]. . .	25
4.3	Bragg ionization curve . . . . .	30
4.4	Experimental data for the production of ${}^7\text{Be}$ from natural C, Mg, O and Si . . . . .	39
4.5	Experimental data for the production of ${}^7\text{Be}$ from natural Ca and of ${}^{24}\text{Na}$ from Ca, Cu and Si . . . . .	43
4.6	Experimental data for the production of ${}^{43}\text{K}$ from Ca, Cu and Ni . . .	45
4.7	Experimental data for the production of ${}^{55}\text{Co}$ , ${}^{56}\text{Co}$ and ${}^{57}\text{Co}$ from Cu .	46
4.8	Experimental data for the production of ${}^{55}\text{Co}$ , ${}^{56}\text{Co}$ and ${}^{57}\text{Co}$ from Ni .	47
4.9	Experimental data for the production of ${}^{54}\text{Mn}$ from natural Fe and Mn	50
4.10	Experimental data for the production of ${}^{44}\text{Ti}$ from natural Ti and of ${}^{101}\text{Rh}$ , ${}^{102}\text{Ti}_m$ and of ${}^{108}\text{Ag}_m$ from natural Ag . . . . .	51
4.11	Production of ${}^{46,47}\text{Sc}$ from natural Cu . . . . .	52

4.12 Production of  $^{57,58}\text{Co}$  from natural Cu . . . . . 53

4.13 Production of  $^{48,51}\text{Cr}$  from natural Ni . . . . . 54

4.14 Experimental data for the production of  $^{54}\text{Mn}$  from natural Fe and Mn 55

4.15 Experimental data for the production of  $^{101}\text{Rh}$ ,  $^{102}\text{Rh}_m$  and of  $^{108}\text{Ag}_m$   
 from natural Ag . . . . . 56

5.1 Excitation functions for the production of  $^3\text{He}$  by proton-induced reac-  
 tions on natural magnesium, iron, and nickel . . . . . 62

5.2 Excitation functions for the production of  $^3\text{He}_c$  on natural aluminum,  
 iron, and lead. . . . . 63

5.3 Excitation functions for the production of  $^4\text{He}$  by proton-induced reac-  
 tions on natural magnesium, aluminum, iron, and lead. . . . . 64

5.4 Excitation functions for the production of  $^7\text{Be}$  by proton-induced reac-  
 tions on natural carbon, oxygen, fluorine, magnesium. . . . . 66

5.5 Excitation functions for the production of  $^7\text{Be}$  by proton-induced reac-  
 tions on natural aluminum, titanium, nickel, and niobium. . . . . 67

5.6 Excitation functions for the production of  $^7\text{Be}$  by proton-induced reac-  
 tions on natural silver, tantalum and tungsten. . . . . 69

5.7 Excitation functions for the production of  $^7\text{Be}$  by proton-induced reac-  
 tions on natural gold, lead, and bismuth. . . . . 70

5.8 Excitation functions for the production of  $^{10}\text{Be}$  by proton-induced reac-  
 tions on natural carbon, nitrogen, oxygen, magnesium. . . . . 71

5.9 Excitation functions for the production of  $^{10}\text{Be}$  by proton-induced reac-  
 tions on natural silicon, iridium, lead, and bismut. . . . . 72

5.10 Excitation functions for the production of  $^{22}\text{Na}$  by proton-induced reac-  
 tions on  $^{24,25,26,nat}\text{Mg}$  . . . . . 74

5.11 Excitation functions for the production of  $^{21}\text{Ne}$  by proton-induced reac-  
 tions on natural magnesium, aluminum, iron, and lead. . . . . 75

5.12 Excitation functions for the production of  $^{22}\text{Na}$  by proton-induced reac-  
 tions on natural magnesium, aluminum, silicon, nickel. . . . . 76

5.13 Excitation functions for the production of  $^{22}\text{Na}$  by proton-induced reac-  
 tions on natural tantalum, lead and bismut. . . . . 77

5.14 Excitation functions for the production of  $^{24}\text{Na}$  by proton-induced reac-  
 tions on natural magnesium, silicon, vanadium, nickel. . . . . 78

5.15 Excitation functions for the production of  $^{24}\text{Na}$  by proton-induced reac-  
 tions on natural silver, tantalum, gold, and lead. . . . . 79



5.16	Excitation functions for the production of $^{28}\text{Mg}$ by proton-induced reactions on natural calcium, iron, lead, and bismuth. . . . .	81
5.17	Excitation functions for the production of $^{26}\text{Al}$ by proton-induced reactions on natural aluminum, silicon, iron, and lead. . . . .	82
5.18	Production of He ( $=^3\text{He}+^4\text{He}$ ) from natural lead by proton-induced reactions; data are from [Ly05] (full circles) and [En99] (blue stars). . . .	84
5.19	Cross sections for the production of residual nuclides from niobium as function of the product mass [Mi97]. . . . .	85
5.20	Cross sections for the production of residual nuclides from Ta, Pb, and Bi as function of the product mass [Gl98]. . . . .	86
5.21	Cross sections for the production of residual nuclides from Ta, Pb, and Bi as function of the product mass [Gl98]. . . . .	87
5.22	Cross sections for the production of residual nuclides from Ta, Pb, and Bi as function of the product mass [Gl98]. . . . .	89
5.23	Systematic of the production of $^{59}\text{Fe}$ and $^{60}\text{Co}$ by proton-induced reactions as function of target atomic numbers according to [Gl98]. . . . .	91
5.24	Systematic of the production of $^3\text{He}$ by proton-induced reactions as function of target mass numbers. . . . .	92
5.25	Systematic of the production of $^3\text{He}_e$ by proton-induced reactions as function of target mass numbers. . . . .	93
5.26	Systematic of the production of $^4\text{He}$ by proton-induced reactions as function of target mass numbers. . . . .	94
5.27	Systematic of the production of $^7\text{Be}$ by proton-induced reactions as function of target mass numbers. . . . .	96
5.28	Systematic of the production of $^{10}\text{Be}$ by proton-induced reactions as function of target mass numbers. . . . .	97
5.29	Systematic of the production of $^{21}\text{Ne}$ by proton-induced reactions as function of target mass numbers. . . . .	99
5.30	Systematic of the production of $^{22}\text{Na}$ by proton-induced reactions as function of target mass numbers. . . . .	100
5.31	Systematic of the production of $^{24}\text{Na}$ by proton-induced reactions as function of target mass numbers. . . . .	101
5.32	Systematic of the production of $^{28}\text{Mg}$ by proton-induced reactions as function of target mass numbers. . . . .	103
5.33	Systematic of the production of $^{26}\text{Al}$ by proton-induced reactions as function of target mass numbers. . . . .	104

5.34 Experimental cross sections for the production of  ${}^7\text{Be}$  and  ${}^{22}\text{Na}$  from niobium and bismuth compared with theoretical ones calculated by the LAHET code system [Pr94, Pr89] using the Bertini-Gilbert-Cameron options, the HETC in form of the HET-KFA2 code [Cl88] and a semiempirical formula according to the YIELD code [Si73a, Si73b]; according to [Gl98]. . . . . 107

5.35 Experimental cross sections for the production of  ${}^7\text{Be}$  and  ${}^{10}\text{Be}$  from carbon, aluminum, and iron compared with theoretical ones calculated by the LAHET code system [Pr94, Pr89] using the Bertini-Gilbert-Cameron options, the HETC in form of the HET-KFA2 code [Cl88] and a semiempirical formula according to the YIELD code [Si73a, Si73b]; according to [Gl98]. . . . . 108

5.36 Experimental cross sections for the production of  ${}^{14}\text{C}$  from natural iron and nickel compared with theoretical ones calculated with the HET-KFA2 code within the HERMES code system [Cl88]. . . . . 110

5.37 Experimental cross sections (squares) for the production of  ${}^{52m+g}\text{Mn}$  from natural iron by proton-induced reactions in comparison with TALYS results (solid line) [Mi05]. . . . . 110

5.38 Comparison of experimental cross sections [Mi02] with model calculations using the TALYS (solid lines) and INCL4+ABLA (broken lines) codes; from [Mi05]. . . . . 111

5.39 Comparison of experimental cross sections for the production  ${}^{14}\text{C}$  from natural oxygen and  ${}^{15}\text{O}$  from  ${}^{16}\text{O}$  with model calculations using the TALYS code. . . . . 116

5.40 Comparison of experimental cross sections for the production  ${}^{18}\text{F}$  from sodium and natural magnesium with model calculations using the TALYS code . . . . . 117

5.41 Comparison of experimental cross sections for the production of  ${}^{21}\text{Ne}$  and  ${}^{24}\text{Na}$  from natural Mg and of  ${}^{21}\text{Ne}$  and  ${}^{22}\text{Na}$  from  ${}^{27}\text{Al}$  with model calculations using the TALYS code . . . . . 118

5.42 Comparison of experimental cross sections for the production of  ${}^{22}\text{Na}$  and  ${}^{28}\text{Mg}$  from natural silicon with model calculations using the TALYS code . . . . . 120

5.43 Comparison of experimental cross sections for the production of  ${}^{22}\text{Na}$  from natural magnesium and from individual magnesium isotopes with model calculations using the TALYS code . . . . . 121

5.44	Comparison of experimental cross sections for the production of $^{26}\text{Al}$ from magnesium and aluminium with model calculations using the TALYS code. . . . .	122
5.45	Comparison of experimental cross sections for the production of $^7\text{Be}$ from natural tantalum, tungsten, and lead with model calculations using the INCL4+ABLA code and with Bertini-Gilbert-Cameron calculations. . .	124
5.46	Comparison of experimental cross sections for the production of $^{10}\text{Be}$ from natural lead and bismuth with model calculations using the INCL4+ABLA code and with Bertini-Gilbert-Cameron calculations. . .	125
5.47	Comparison of experimental cross sections for the production of $^{21}\text{Ne}$ and $^{22}\text{Ne}$ from natural lead, of $^{22}\text{Na}$ from natural tantalum and tungsten with model calculations using the INCL4+ABLA code and with Bertini-Gilbert-Cameron calculations. . . . .	126
5.48	Comparison of experimental cross sections for the production of $^{22}\text{Na}$ from natural lead, of $^{24}\text{Na}$ from natural tantalum, of $^{28}\text{Mg}$ and of $^{26}\text{Al}$ from natural lead with model calculations using the INCL4+ABLA code and with Bertini-Gilbert-Cameron calculations. . . . .	127
C.1	Experimental data for the production of $^3\text{H}$ from natural Fe, Ni and Pb and of $^3\text{He}$ from natural Si . . . . .	164
C.2	Experimental data for the production of $^3\text{He}$ from natural Pb and $^{27}\text{Al}$ , of $^3\text{He}_c$ from natural Ni and of $^4\text{He}$ from natural Si . . . . .	165
C.3	Experimental data for the production of $^4\text{He}$ from natural Ni, of $^6\text{Li}$ from $^{14}\text{N}$ and of $^7\text{Li}$ from $^{14}\text{N}$ and $^{16}\text{O}$ . . . . .	166
C.4	Experimental data for the production of $^7\text{Be}$ from natural N, Si, Ca and V	167
C.5	Experimental data for the production of $^7\text{Be}$ from natural Fe, Cu, Zr and Mo . . . . .	168
C.6	Experimental data for the production of $^7\text{Be}$ from $^{12}\text{C}$ , $^{14}\text{N}$ , $^{16}\text{O}$ and $^{55}\text{Mn}$	169
C.7	Experimental data for the production of $^7\text{Be}$ from $^{59}\text{Co}$ , $^{89}\text{Y}$ , $^{206}\text{Pb}$ and $^{207}\text{Pb}$ . . . . .	170
C.8	Experimental data for the production of $^7\text{Be}$ from $^{208}\text{Pb}$ , of $^9\text{Be}$ from $^{14}\text{N}$ and of $^{10}\text{Be}$ from natural Ti and Fe . . . . .	171
C.9	Experimental data for the production of $^{10}\text{Be}$ from natural Ni, Cu, $^{12}\text{Cu}$ and $^{27}\text{Al}$ . . . . .	172
C.10	Experimental data for the production of $^{10}\text{Be}$ from $^{55}\text{Mn}$ , $^{59}\text{Co}$ and $^{10}\text{B}$ from $^{14}\text{N}$ and $^{16}\text{O}$ . . . . .	173

C.11 Experimental data for the production of  $^{11}\text{B}$  from  $^{14}\text{N}$  and  $^{16}\text{O}$ , of  $^{11}\text{C}$  from  $^{16}\text{O}$  and of  $^{14}\text{C}$  from natural O . . . . . 174

C.12 Experimental data for the production of  $^{14}\text{C}$  from natural Si, Fe, Ni and  $^{16}\text{O}$  . . . . . 175

C.13 Experimental data for the production of  $^{15}\text{O}$  from  $^{16}\text{O}$  and of  $^{18}\text{F}$  from natural Mg, Cu and Ag . . . . . 176

C.14 Experimental data for the production of  $^{18}\text{F}$  from Pb,  $^{23}\text{Na}$  and  $^{27}\text{Al}$  and of  $^{20}\text{Ne}$  from natural Mg . . . . . 177

C.15 Experimental data for the production of  $^{20}\text{Ne}$  from natural Si, Fe, Ni and  $^{27}\text{Al}$  . . . . . 178

C.16 Experimental data for the production of  $^{21}\text{Ne}$  from natural Si and Ni and of  $^{22}\text{Ne}$  from natural Mg and Si . . . . . 179

C.17 Experimental data for the production of  $^{22}\text{Ne}$  from natural Fe, Ni, Pb and  $^{27}\text{Al}$  . . . . . 180

C.18 Experimental data for the production of  $^{22}\text{Ne}_c$  from natural Mg, Si, Fe and Ni . . . . . 181

C.19 Experimental data for the production of  $^{22}\text{Ne}_c$  from Pb and  $^{27}\text{Al}$  and of  $^{22}\text{Na}$  from natural Ca and Ti . . . . . 182

C.20 Experimental data for the production of  $^{22}\text{Na}$  from natural V, Fe, Cu and Sr . . . . . 183

C.21 Experimental data for the production of  $^{22}\text{Na}$  from natural Mo and Ag,  $^{23}\text{Na}$  and  $^{55}\text{Mn}$  . . . . . 184

C.22 Experimental data for the production of  $^{22}\text{Na}$  from  $^{59}\text{Co}$ ,  $^{89}\text{Y}$ ,  $^{93}\text{Nb}$  and of  $^{24}\text{Na}$  from natural Ca . . . . . 185

C.23 Experimental data for the production of  $^{24}\text{Na}$  from natural Ti, Fe, Cu and Zr . . . . . 186

C.24 Experimental data for the production of  $^{24}\text{Na}$  from  $^{27}\text{Al}$ ,  $^{45}\text{Sc}$ ,  $^{48}\text{Ti}$  and  $^{55}\text{Mn}$  . . . . . 187

C.25 Experimental data for the production of  $^{24}\text{Na}$  from  $^{59}\text{Co}$  and of  $^{28}\text{Mg}$  from natural Si, Ti and V . . . . . 188

C.26 Experimental data for the production of  $^{28}\text{Mg}$  from natural Cu,  $^{30}\text{Si}$ ,  $^{55}\text{Mn}$  and  $^{59}\text{Co}$  . . . . . 189

C.27 Experimental data for the production of  $^{26}\text{Al}$  from natural Ca, Mg, Ti and Ni . . . . . 190

C.28 Experimental data for the production of  $^{26}\text{Al}$  from  $^{26}\text{Mg}$  and  $^{55}\text{Mn}$  . . . 191

E.1	Data for the production of $^{14}\text{C}$ from natural Si and $^{16}\text{O}$ , of $^{18}\text{F}$ from $^{27}\text{Al}$ and of $^{20}\text{Ne}$ from natural Mg . . . . .	196
E.3	Data for the production of $^{22}\text{Ne}$ from natural Si and $^{27}\text{Al}$ , of $^{22}\text{Ne}$ from $^{27}\text{Al}$ and of $^{22}\text{Ne}_c$ from natural Mg and Si . . . . .	197
E.4	Data for the production of $^{22}\text{Ne}_c$ from $^{27}\text{Al}$ , of $^{22}\text{Na}$ from natural Ca and Si and of $^{24}\text{Na}$ from natural Si and $^{27}\text{Al}$ . . . . .	198
E.5	Data for the production of $^{26}\text{Al}$ from natural Si and $^{26}\text{Mg}$ . . . . .	199
F.1	Experimental data for the production of $^{44}\text{Sc}_m$ , $^{46}\text{Sc}$ , $^{47}\text{Sc}$ and $^{48}\text{Sc}$ from natural Cu . . . . .	202
F.2	Experimental data for the production of $^{48}\text{Cr}$ , $^{51}\text{Cr}$ , $^{52}\text{Mn}$ and $^{58}\text{Co}$ from natural Cu . . . . .	203
F.3	Experimental data for the production of $^{57}\text{Ni}$ from natural Cu and of $^{24}\text{Na}$ , $^{44}\text{Sc}_m$ and of $^{48}\text{V}$ from natural Ni . . . . .	204
F.4	Experimental data for the production of $^{48}\text{Cr}$ , $^{51}\text{Cr}$ , $^{52}\text{Mn}$ and of $^{56}\text{Ni}$ from natural Ni . . . . .	205
F.5	Experimental data for the production of $^{57}\text{Ni}$ from natural Ni and of $^7\text{Be}$ , $^{22}\text{Na}$ and $^{28}\text{Mg}$ from natural Si . . . . .	206
F.6	Experimental data for the production of $^{22}\text{Na}$ and of $^{24}\text{Na}$ from Mg . . . . .	207
G.1	Experimental data for the production of $^{48}\text{Sc}$ , $^{48}\text{Cr}$ , $^{51}\text{Cr}$ and of $^{52}\text{Mn}$ from natural Cu . . . . .	210
G.2	Experimental data for the production of $^{55}\text{Co}$ , $^{56}\text{Co}$ and of $^{57}\text{Ni}$ from natural Cu . . . . .	211
G.3	Experimental data for the production of $^{48}\text{V}$ , $^{52}\text{Mn}$ , $^{55}\text{Co}$ and of $^{56}\text{Co}$ from natural Ni . . . . .	212
G.4	Experimental data for the production of $^{57}\text{Co}$ , $^{56}\text{Ni}$ and of $^{57}\text{Ni}$ from natural Ni . . . . .	213



## A Studied reactions for NUDATRA project

	Target		Reaction	Product		
1.	Fe	0	p,26pxn	H	3	
2.	Ni	0	p,28pxn	H	3	
3.	Pb	0	p,82pxn	H	3	
4.	Mg	0	p,11pxn	He	3	
5.	Si	0	p,13pxn	He	3	
6.	Fe	0	p,25pxn	He	3	
7.	Ni	0	p,27pxn	He	3	
8.	Pb	0	p,81pxn	He	3	
9.	Al	27	p,12p13n	He	3	
10.	Fe	0	p,25pxn	He	3	C
11.	Ni	0	p,28pxn	He	3	C
12.	Pb	0	p,81pxn	He	3	C
13.	Al	27	p,12p13n	He	3	C
14.	Mg	0	p,11pxn	He	4	
15.	Si	0	p,13pxn	He	4	
16.	Fe	0	p,25pxn	He	4	
17.	Ni	0	p,27pxn	He	4	
18.	Pb	0	p,81pxn	He	4	
19.	Al	27	p,12p12n	He	4	
20.	N	14	p,5p4n	Li	6	
21.	N	14	p,5p3n	Li	7	
22.	O	16	p,6p4n	Li	7	
23.	C	0	p,3pxn	Be	7	
24.	N	0	p,4pxn	Be	7	
25.	O	0	p,5pxn	Be	7	
26.	Mg	0	p,9pxn	Be	7	
27.	Si	0	p,11pxn	Be	7	
28.	Ca	0	p,17pxn	Be	7	
29.	Ti	0	p,19pxn	Be	7	
30.	V	0	p,20pxn	Be	7	
31.	Fe	0	p,23pxn	Be	7	
32.	Ni	0	p,25pxn	Be	7	
33.	Cu	0	p,26pxn	Be	7	
34.	Zr	0	p,37pxn	Be	7	
35.	Mo	0	p,39pxn	Be	7	
36.	Ag	0	p,44pxn	Be	7	
37.	Ta	0	p,70pxn	Be	7	
38.	W	0	p,71pxn	Be	7	
39.	Pb	0	p,79pxn	Be	7	
40.	C	12	p,3p3n	Be	7	
41.	N	14	p,4p4n	Be	7	
42.	O	16	p,5p5n	Be	7	
43.	F	19	p,6p7n	Be	7	
44.	Al	27	p,10p11n	Be	7	
45.	Mn	55	p,22p27n	Be	7	
46.	Co	59	p,24p29n	Be	7	
47.	Y	89	p,36p47n	Be	7	
48.	Nb	93	p,38p56n	Be	7	
49.	Au	197	p,76p115n	Be	7	
50.	Pb	206	p,79p121n	Be	7	

## STUDIED REACTIONS FOR NUDATRA PROJECT

51.	Pb	207	p,79p122n	Be	7	
52.	Pb	208	p,79p123n	Be	7	
53.	Bi	209	p,80p123n	Be	7	
54.	N	14	p,4p2n	Be	9	
55.	C	0	p,3pxn	Be	10	
56.	N	0	p,4pxn	Be	10	
57.	O	0	p,5pxn	Be	10	
58.	Mg	0	p,9pxn	Be	10	
59.	Si	0	p,11pxn	Be	10	
60.	Ti	0	p,19pxn	Be	10	
61.	Fe	0	p,23pxn	Be	10	
62.	Ni	0	p,25pxn	Be	10	
63.	Cu	0	p,26pxn	Be	10	
64.	Ir	0	p,74pxn	Be	10	
65.	Pb	0	p,79pxn	Be	10	
66.	Bi	0	p,80pxn	Be	10	
67.	C	12	p,3p	Be	10	
68.	Al	27	p,10p8n	Be	10	
69.	Mn	55	p,22p24n	Be	10	
70.	Co	59	p,24p26n	Be	10	
71.	N	14	p,3p2n	B	10	
72.	O	16	p,4p3n	B	10	
73.	N	14	p,3pn	B	11	
74.	O	16	p,4p2n	B	11	
75.	O	16	p,3p3n	C	11	
76.	O	0	p,3pxn	C	14	
77.	Si	0	p,9pxn	C	14	
78.	Fe	0	p,21pxn	C	14	
79.	Ni	0	p,23pxn	C	14	
80.	O	16	p,3p	C	14	
81.	O	16	p,pn	O	15	
82.	Mg	0	p,4pxn	F	18	
83.	Cu	0	p,21pxn	F	18	
84.	Ag	0	p,39pxn	F	18	
85.	Pb	0	p,74pxn	F	18	
86.	Na	23	p,3pxn	F	18	
87.	Al	27	p,5pxn	F	18	
88.	Mg	0	p,3pxn	Ne	20	
89.	Si	0	p,5pxn	Ne	20	
90.	Fe	0	p,17pxn	Ne	20	
91.	Ni	0	p,19pxn	Ne	20	
92.	Al	27	p,4p4n	Ne	20	
93.	Mg	0	p,3pxn	Ne	21	
94.	Si	0	p,5pxn	Ne	21	
95.	Fe	0	p,17pxn	Ne	21	
96.	Ni	0	p,19pxn	Ne	21	
97.	Pb	0	p,73pxn	Ne	21	
98.	Al	27	p,4p3n	Ne	21	
99.	Mg	0	p,3pxn	Ne	22	
100.	Si	0	p,5pxn	Ne	22	
101.	Fe	0	p,17pxn	Ne	22	
102.	Ni	0	p,19pxn	Ne	22	



103.	Pb	0	p,73pxn	Ne	22	
104.	Al	27	p,4p2n	Ne	22	
105.	Mg	0	p,3pxn	Ne	22	C
106.	Si	0	p,5pxn	Ne	22	C
107.	Fe	0	p,17pxn	Ne	22	C
108.	Ni	0	p,19pxn	Ne	22	C
109.	Pb	0	p,73pxn	Ne	22	C
110.	Al	27	p,4p2n	Ne	22	C
111.	Mg	0	p,2pxn	Na	22	
112.	Si	0	p,4pxn	Na	22	
113.	Ca	0	p,10pxn	Na	22	
114.	Ti	0	p,12pxn	Na	22	
115.	V	0	p,13pxn	Na	22	
116.	Fe	0	p,16pxn	Na	22	
117.	Ni	0	p,18pxn	Na	22	
118.	Cu	0	p,19pxn	Na	22	
119.	Sr	0	p,28pxn	Na	22	
120.	Mo	0	p,32pxn	Na	22	
121.	Ag	0	p,37pxn	Na	22	
122.	Ta	0	p,63pxn	Na	22	
123.	W	0	p,x	Na	22	
124.	Pb	0	p,72pxn	Na	22	
125.	Na	23	p,pn	Na	22	
126.	Mg	24	p,2pn	Na	22	
127.	Mg	25	p,2p2n	Na	22	
128.	Mg	26	p,2p3n	Na	22	
129.	Al	27	p,3p3n	Na	22	
130.	Mn	55	p,15p19n	Na	22	
131.	Co	59	p,17p21n	Na	22	
132.	Y	89	p,29p39p	Na	22	
133.	Nb	93	p,31p63n	Na	22	
134.	Bi	209	p,73p115n	Na	22	
135.	Mg	0	p,2pxn	Na	24	
136.	Si	0	p,4pxn	Na	24	
137.	Ca	0	p,10pxn	Na	24	
138.	Ti	0	p,12pxn	Na	24	
139.	V	0	p,13pxn	Na	24	
140.	Fe	0	p,16pxn	Na	24	
141.	Ni	0	p,18pxn	Na	24	
142.	Cu	0	p,19pxn	Na	24	
143.	Zr	0	p,30pxn	Na	24	
144.	Ag	0	p,37pxn	Na	24	
145.	Ta	0	p,63pxn	Na	24	
146.	Pb	0	p,72pxn	Na	24	
147.	Al	27	p,3pn	Na	24	
148.	Sc	45	p,11p11n	Na	24	
149.	Ti	48	p,12p13n	Na	24	
150.	Mn	55	p,15p17n	Na	24	
151.	Co	59	p,17p19n	Na	24	
152.	Au	197	p,69p105n	Na	24	
153.	Si	0	p,3pxn	Mg	28	
154.	Ca	0	p,9pxn	Mg	28	

155.	Ti	0	p,11pxn	Mg	28	
156.	V	0	p,12pxn	Mg	28	
157.	Fe	0	p,15pxn	Mg	28	
158.	Cu	0	p,18pxn	Mg	28	
159.	Pb	0	p,71pxn	Mg	28	
160.	Si	30	p,3p	Mg	28	
161.	Mn	55	p,14p14n	Mg	28	
162.	Co	59	p,16p16n	Mg	28	
163.	Bi	209	p,72p110n	Mg	28	
164.	Mg	0	p,xn	Al	26	
165.	Si	0	p,2pxn	Al	26	
166.	Ca	0	p,8pxn	Al	26	
167.	Ti	0	p,10pxn	Al	26	
168.	Fe	0	p,14pxn	Al	26	
169.	Ni	0	p,16pxn	Al	26	
170.	Pb	0	p,70pxn	Al	26	
171.	Mg	26	p,xn	Al	26	
172.	Al	27	p,pn	Al	26	
173.	Mn	55	p,13p17n	Al	26	

## B Product-target overview for NUDATRA data

Products	Targets	Radioactive Progenitors
$^3\text{H}$	$^{\text{nat}}\text{Fe}, ^{\text{nat}}\text{Ni}, ^{\text{nat}}\text{Pb}$	
$^3\text{He}$	$^{\text{nat}}\text{Mg}, ^{\text{nat}}\text{Si}, ^{\text{nat}}\text{Fe}, ^{\text{nat}}\text{Ni}, ^{\text{nat}}\text{Pb}, ^{27}\text{Al}$	
$^3\text{He-c}$	$^{\text{nat}}\text{Fe}, ^{\text{nat}}\text{Ni}, ^{\text{nat}}\text{Pb}, ^{27}\text{Al}$	$^3\text{H}$
$^4\text{He}$	$^{\text{nat}}\text{Mg}, ^{\text{nat}}\text{Si}, ^{\text{nat}}\text{Fe}, ^{\text{nat}}\text{Ni}, ^{\text{nat}}\text{Pb}, ^{27}\text{Al}$	
$^6\text{Li}$	$^{14}\text{N}$	$^6\text{He}$
$^7\text{Li}$	$^{14}\text{N}, ^{16}\text{O}$	
$^7\text{Be}$	$^{\text{nat}}\text{C}, ^{\text{nat}}\text{N}, ^{\text{nat}}\text{O}, ^{\text{nat}}\text{Mg}, ^{\text{nat}}\text{Si}, ^{\text{nat}}\text{Ca}, ^{\text{nat}}\text{Ti}, ^{\text{nat}}\text{V}, ^{\text{nat}}\text{Fe}, ^{\text{nat}}\text{Ni}, ^{\text{nat}}\text{Cu}, ^{\text{nat}}\text{Zr}, ^{\text{nat}}\text{Mo}, ^{\text{nat}}\text{Ag}, ^{\text{nat}}\text{Ta}, ^{\text{nat}}\text{W}, ^{\text{nat}}\text{Pb}, ^{12}\text{C}, ^{14}\text{N}, ^{16}\text{O}, ^{19}\text{F}, ^{27}\text{Al}, ^{55}\text{Mn}, ^{59}\text{Co}, ^{89}\text{Y}, ^{93}\text{Nb}, ^{197}\text{Au}, ^{206}\text{Pb}, ^{207}\text{Pb}, ^{208}\text{Pb}, ^{209}\text{Bi}$	
$^9\text{Be}$	$^{14}\text{N}$	$^9\text{Li}, ^9\text{C}$
$^{10}\text{Be}$	$^{\text{nat}}\text{C}, ^{\text{nat}}\text{N}, ^{\text{nat}}\text{O}, ^{\text{nat}}\text{Mg}, ^{\text{nat}}\text{Si}, ^{\text{nat}}\text{Ti}, ^{\text{nat}}\text{Fe}, ^{\text{nat}}\text{Ni}, ^{\text{nat}}\text{Cu}, ^{\text{nat}}\text{Ir}, ^{\text{nat}}\text{Pb}, ^{\text{nat}}\text{Bi}, ^{12}\text{C}, ^{27}\text{Al}, ^{55}\text{Mn}, ^{59}\text{Co}$	
$^{10}\text{B}$	$^{14}\text{N}, ^{16}\text{O}$	$^{10}\text{Be}$
$^{11}\text{B}$	$^{14}\text{N}, ^{16}\text{O}$	$^{11}\text{Be}, ^{11}\text{Li}, ^{11}\text{C}$
$^{11}\text{C}$	$^{16}\text{O}$	
$^{14}\text{C}$	$^{\text{nat}}\text{O}, ^{\text{nat}}\text{Si}, ^{\text{nat}}\text{Fe}, ^{\text{nat}}\text{Ni}, ^{16}\text{O}$	$^{14}\text{B}, ^{14}\text{Be}$
$^{15}\text{O}$	$^{16}\text{O}$	
$^{18}\text{F}$	$^{\text{nat}}\text{Mg}, ^{\text{nat}}\text{Cu}, ^{\text{nat}}\text{Ag}, ^{\text{nat}}\text{Pb}, ^{23}\text{Na}, ^{27}\text{Al}$	$^{18}\text{Ne}$
$^{20}\text{Ne}$	$^{\text{nat}}\text{Mg}, ^{\text{nat}}\text{Si}, ^{\text{nat}}\text{Fe}, ^{\text{nat}}\text{Ni}, ^{27}\text{Al}$	$^{20}\text{F}, ^{20}\text{O}, ^{20}\text{N}, ^{20}\text{C}, ^{20}\text{Mg}, ^{20}\text{Ne}$
$^{21}\text{Ne}$	$^{\text{nat}}\text{Mg}, ^{\text{nat}}\text{Si}, ^{\text{nat}}\text{Fe}, ^{\text{nat}}\text{Ni}, ^{\text{nat}}\text{Pb}, ^{27}\text{Al}$	$^{21}\text{Mg}, ^{21}\text{Na}, ^{21}\text{N}, ^{21}\text{O}, ^{21}\text{F}$
$^{22}\text{Ne}$	$^{\text{nat}}\text{Mg}, ^{\text{nat}}\text{Si}, ^{\text{nat}}\text{Fe}, ^{\text{nat}}\text{Ni}, ^{\text{nat}}\text{Pb}, ^{27}\text{Al}$	$^{22}\text{Si}, ^{22}\text{Al}, ^{22}\text{Mg}, ^{22}\text{O}, ^{22}\text{F}$
$^{22}\text{Ne-c}$	$^{\text{nat}}\text{Mg}, ^{\text{nat}}\text{Si}, ^{\text{nat}}\text{Fe}, ^{\text{nat}}\text{Ni}, ^{\text{nat}}\text{Pb}, ^{27}\text{Al}$	$^{22}\text{Si}, ^{22}\text{Al}, ^{22}\text{Mg}, ^{22}\text{Na}, ^{22}\text{O}, ^{22}\text{F}$
$^{22}\text{Na}$	$^{\text{nat}}\text{Mg}, ^{\text{nat}}\text{Si}, ^{\text{nat}}\text{Ca}, ^{\text{nat}}\text{Ti}, ^{\text{nat}}\text{V}, ^{\text{nat}}\text{Fe}, ^{\text{nat}}\text{Ni}, ^{\text{nat}}\text{Cu}, ^{\text{nat}}\text{Sr}, ^{\text{nat}}\text{Mo}, ^{\text{nat}}\text{Ag}, ^{\text{nat}}\text{Ta}, ^{\text{nat}}\text{W}, ^{\text{nat}}\text{Pb}, ^{23}\text{Na}, ^{24}\text{Mg}, ^{25}\text{Mg}, ^{26}\text{Mg}, ^{27}\text{Al}, ^{55}\text{Mn}, ^{59}\text{Co}, ^{89}\text{Y}, ^{93}\text{Nb}, ^{209}\text{Bi}$	$^{22}\text{Al}, ^{22}\text{Mg}, ^{22}\text{Si}$
$^{24}\text{Na}$	$^{\text{nat}}\text{Mg}, ^{\text{nat}}\text{Si}, ^{\text{nat}}\text{Ca}, ^{\text{nat}}\text{Ti}, ^{\text{nat}}\text{V}, ^{\text{nat}}\text{Fe}, ^{\text{nat}}\text{Ni}, ^{\text{nat}}\text{Cu}, ^{\text{nat}}\text{Zr}, ^{\text{nat}}\text{Ag}, ^{\text{nat}}\text{Ta}, ^{\text{nat}}\text{Pb}, ^{27}\text{Al}, ^{45}\text{Sc}, ^{48}\text{Ti}, ^{55}\text{Mn}, ^{59}\text{Co}, ^{197}\text{Au}$	$^{24}\text{O}, ^{24}\text{F}, ^{24}\text{Ne}$
$^{28}\text{Mg}$	$^{\text{nat}}\text{Si}, ^{\text{nat}}\text{Ca}, ^{\text{nat}}\text{Ti}, ^{\text{nat}}\text{V}, ^{\text{nat}}\text{Fe}, ^{\text{nat}}\text{Cu}, ^{\text{nat}}\text{Pb}, ^{30}\text{Si}, ^{55}\text{Mn}, ^{59}\text{Co}, ^{209}\text{Bi}$	$^{28}\text{Na}, ^{28}\text{Ne}$
$^{26}\text{Al}$	$^{\text{nat}}\text{Mg}, ^{\text{nat}}\text{Si}, ^{\text{nat}}\text{Ca}, ^{\text{nat}}\text{Ti}, ^{\text{nat}}\text{Fe}, ^{\text{nat}}\text{Ni}, ^{\text{nat}}\text{Pb}, ^{26}\text{Mg}, ^{27}\text{Al}, ^{55}\text{Mn}$	$^{26}\text{P}, ^{26}\text{Si}$



---

## C Excitation functions for the NUDATRA experimental data

The graphs are displayed in increasing order of the atomic number of the products:

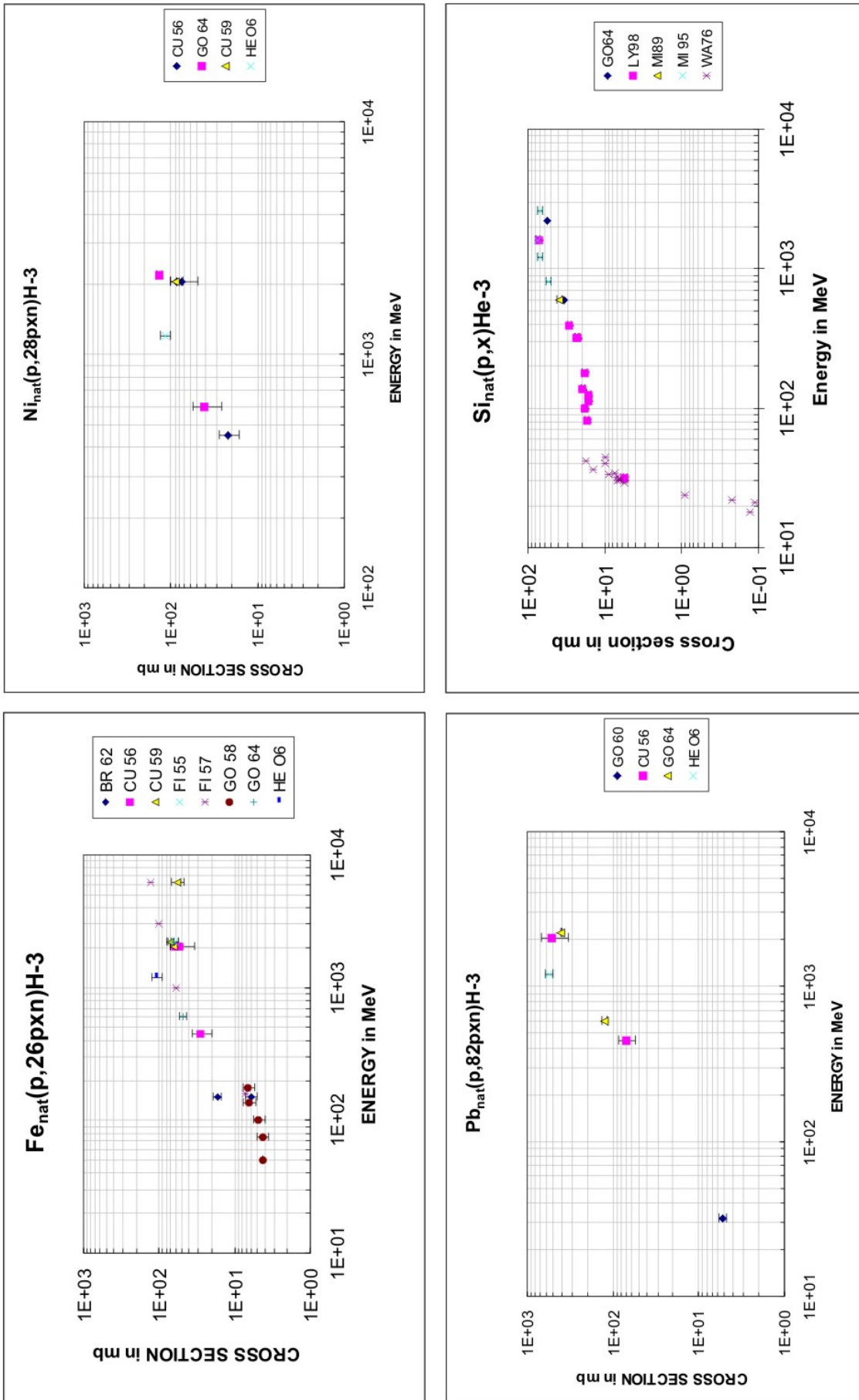


Figure C.1: Experimental data for the production of  $^3\text{H}$  from natural Fe, Ni and Pb and of  $^3\text{He}$  from natural Si

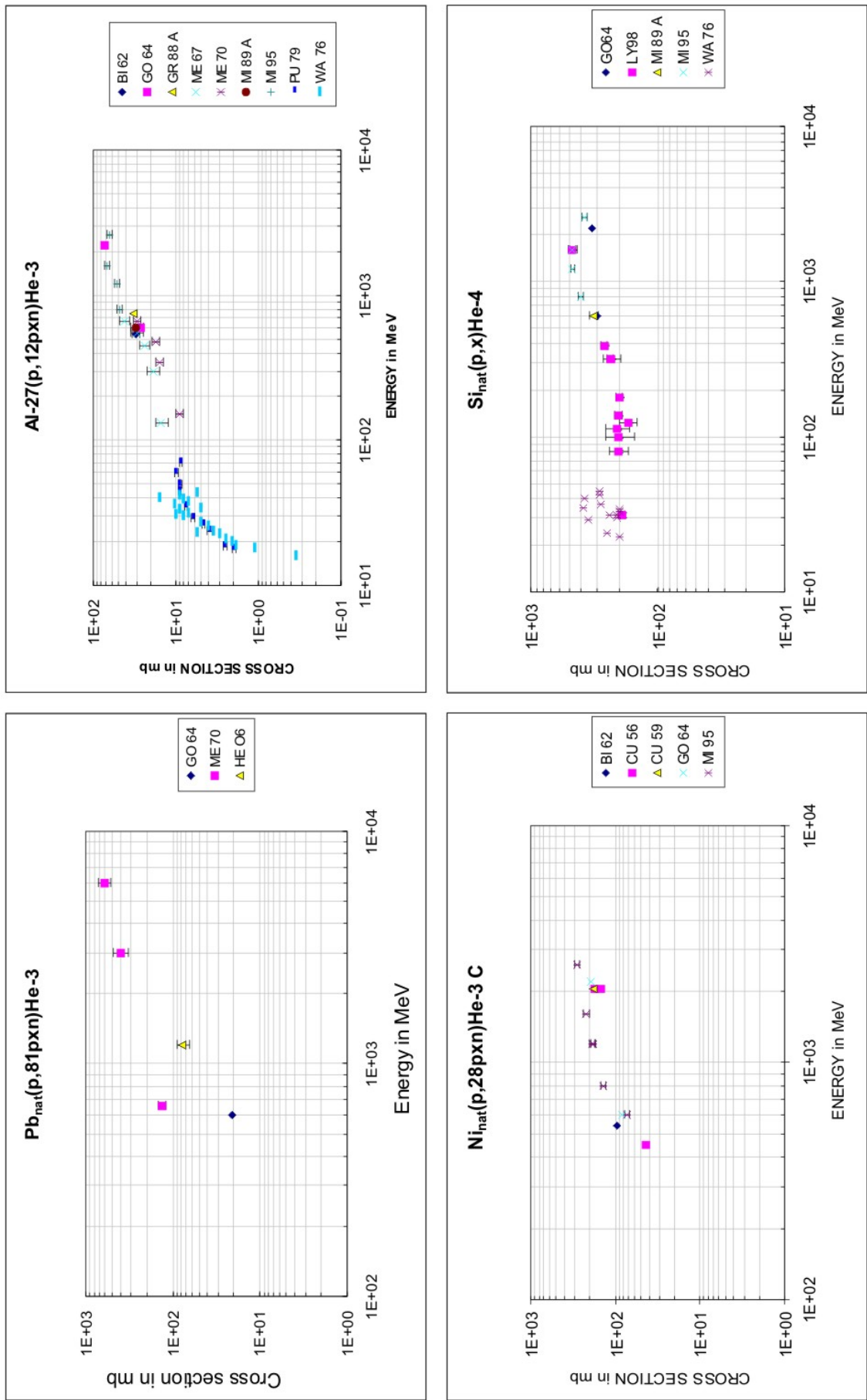


Figure C.2: Experimental data for the production of  $^3\text{He}$  from natural Pb and  $^{27}\text{Al}$ , of  $^3\text{He}_c$  from natural Ni and of  $^4\text{He}$  from natural Si

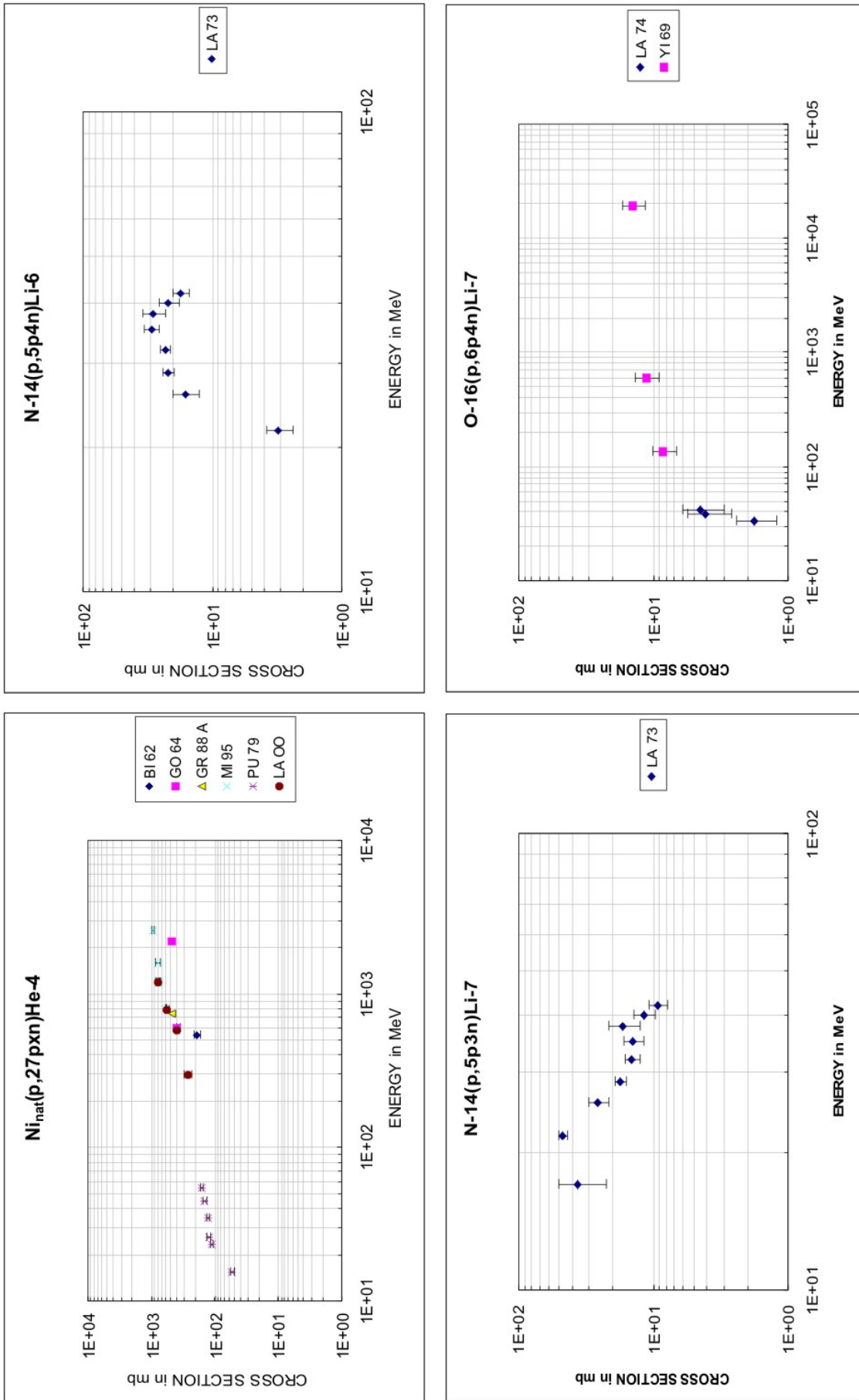


Figure C.3: Experimental data for the production of  $^4He$  from natural Ni, of  $^6Li$  from  $^{14}N$  and of  $^7Li$  from  $^{16}O$



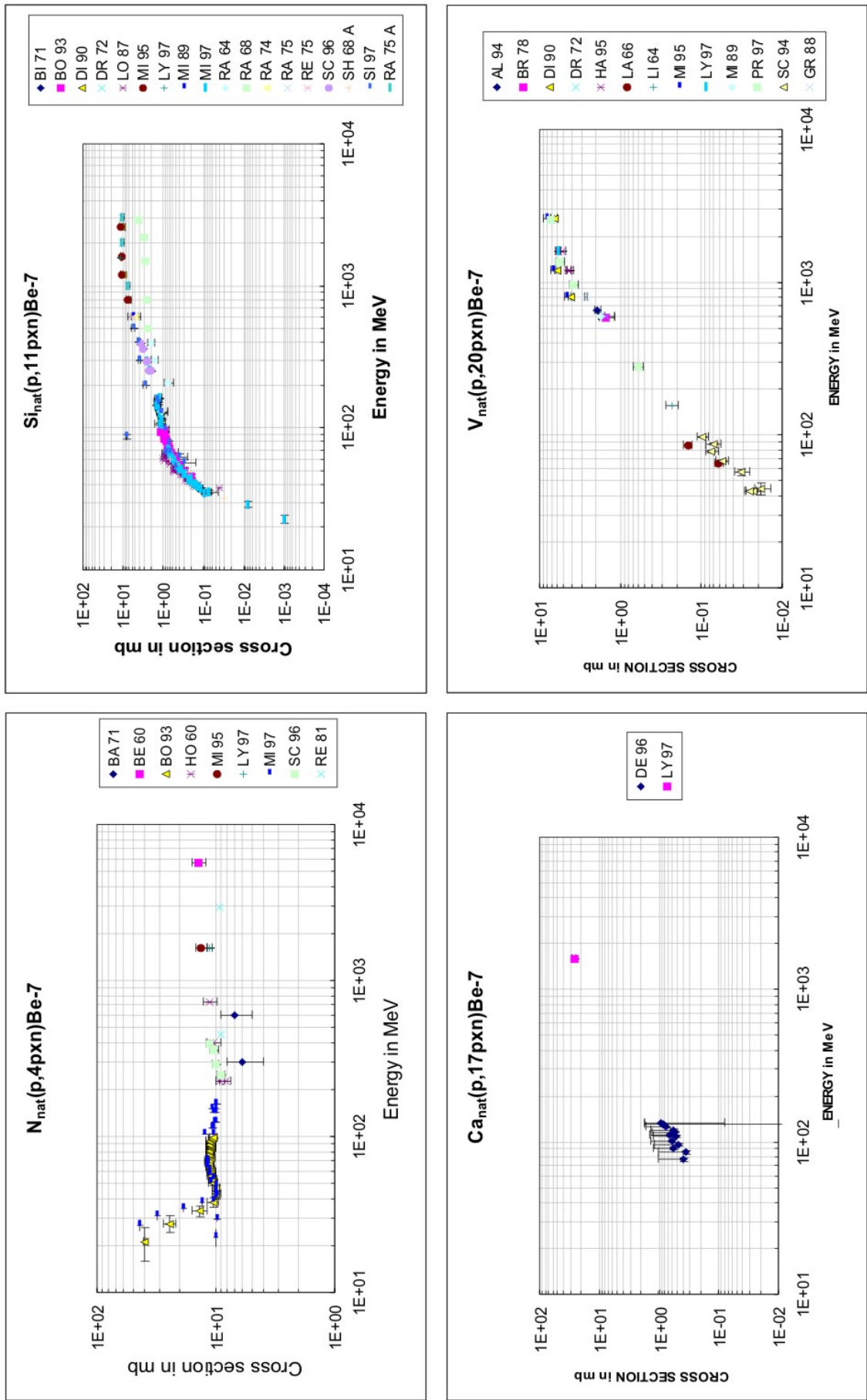


Figure C.4: Experimental data for the production of  ${}^7\text{Be}$  from natural N, Si, Ca and V

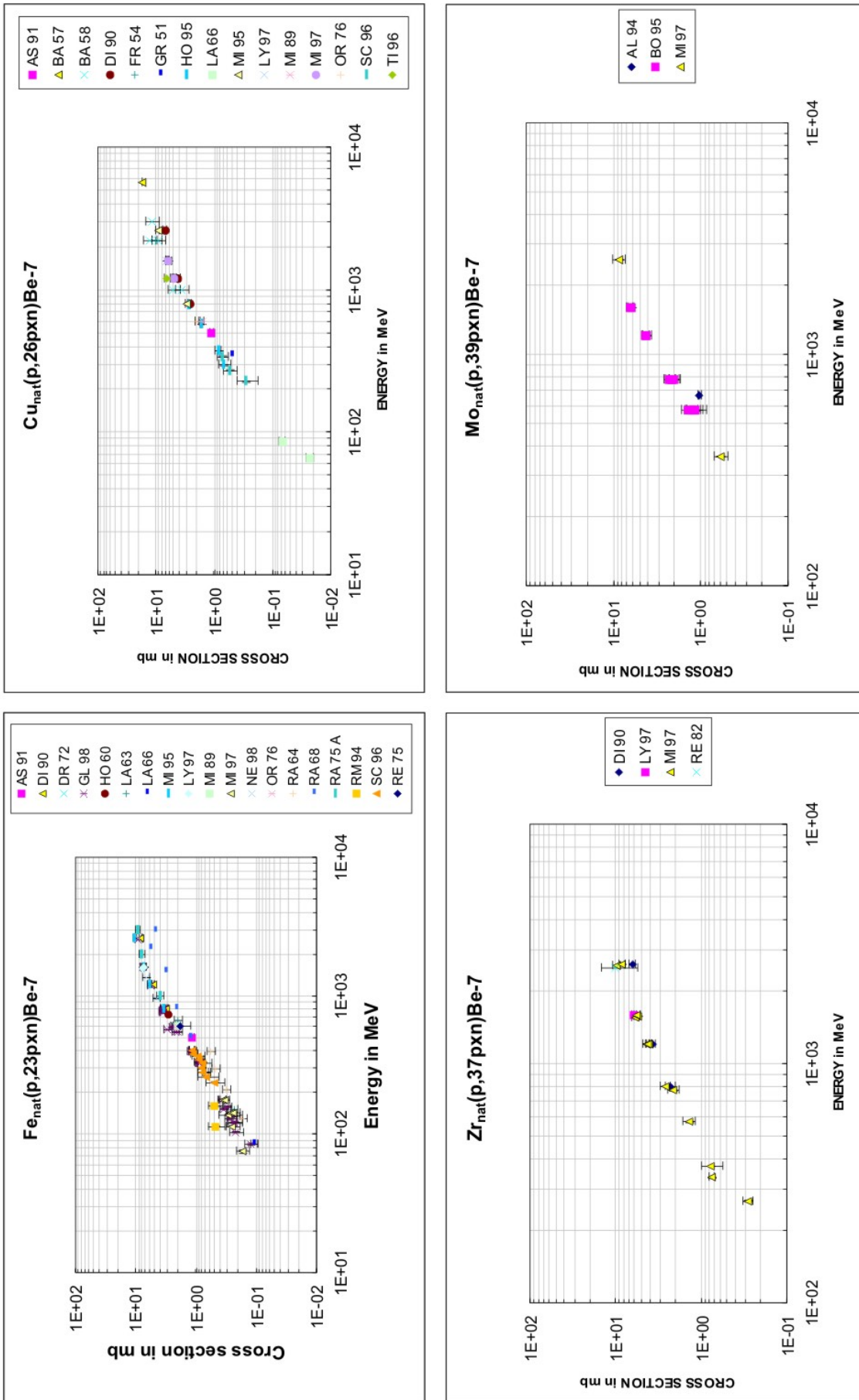


Figure C.5: Experimental data for the production of  ${}^7\text{Be}$  from natural Fe, Cu, Zr and Mo

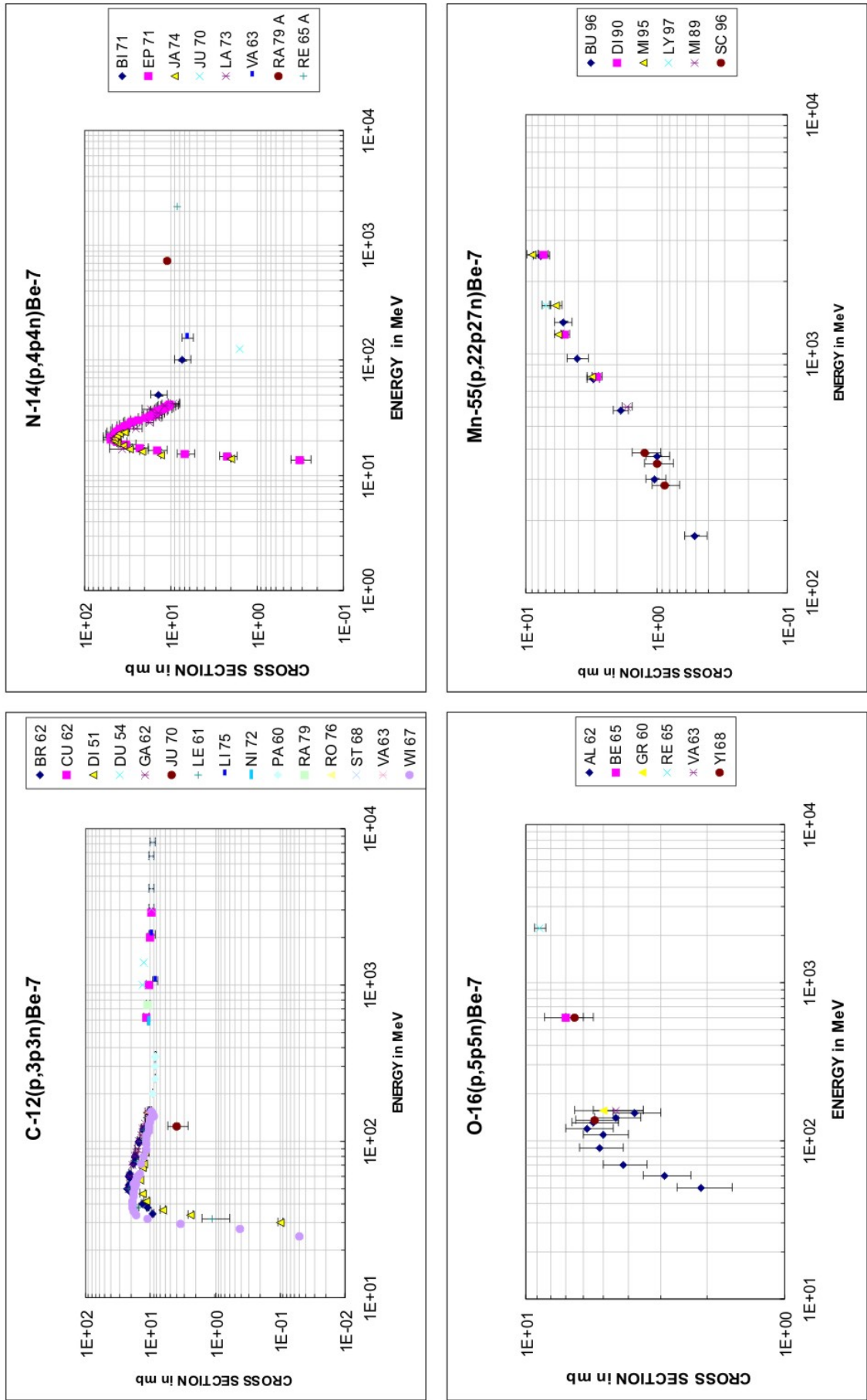


Figure C.6: Experimental data for the production of  ${}^7\text{Be}$  from  ${}^{12}\text{C}$ ,  ${}^{14}\text{N}$ ,  ${}^{16}\text{O}$  and  ${}^{55}\text{Mn}$

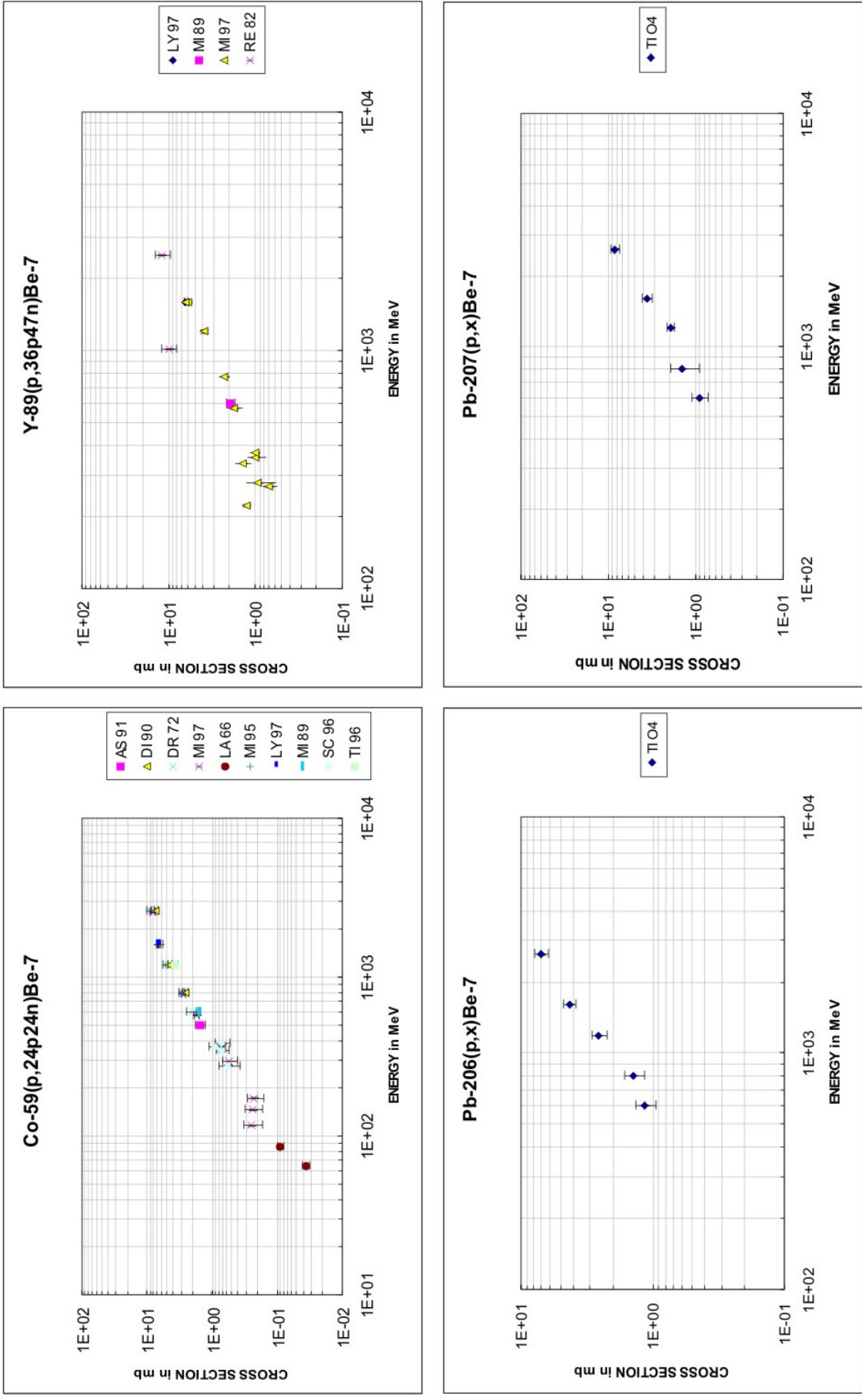


Figure C.7: Experimental data for the production of  ${}^7\text{Be}$  from  ${}^{59}\text{Co}$ ,  ${}^{89}\text{Y}$ ,  ${}^{206}\text{Pb}$  and  ${}^{207}\text{Pb}$

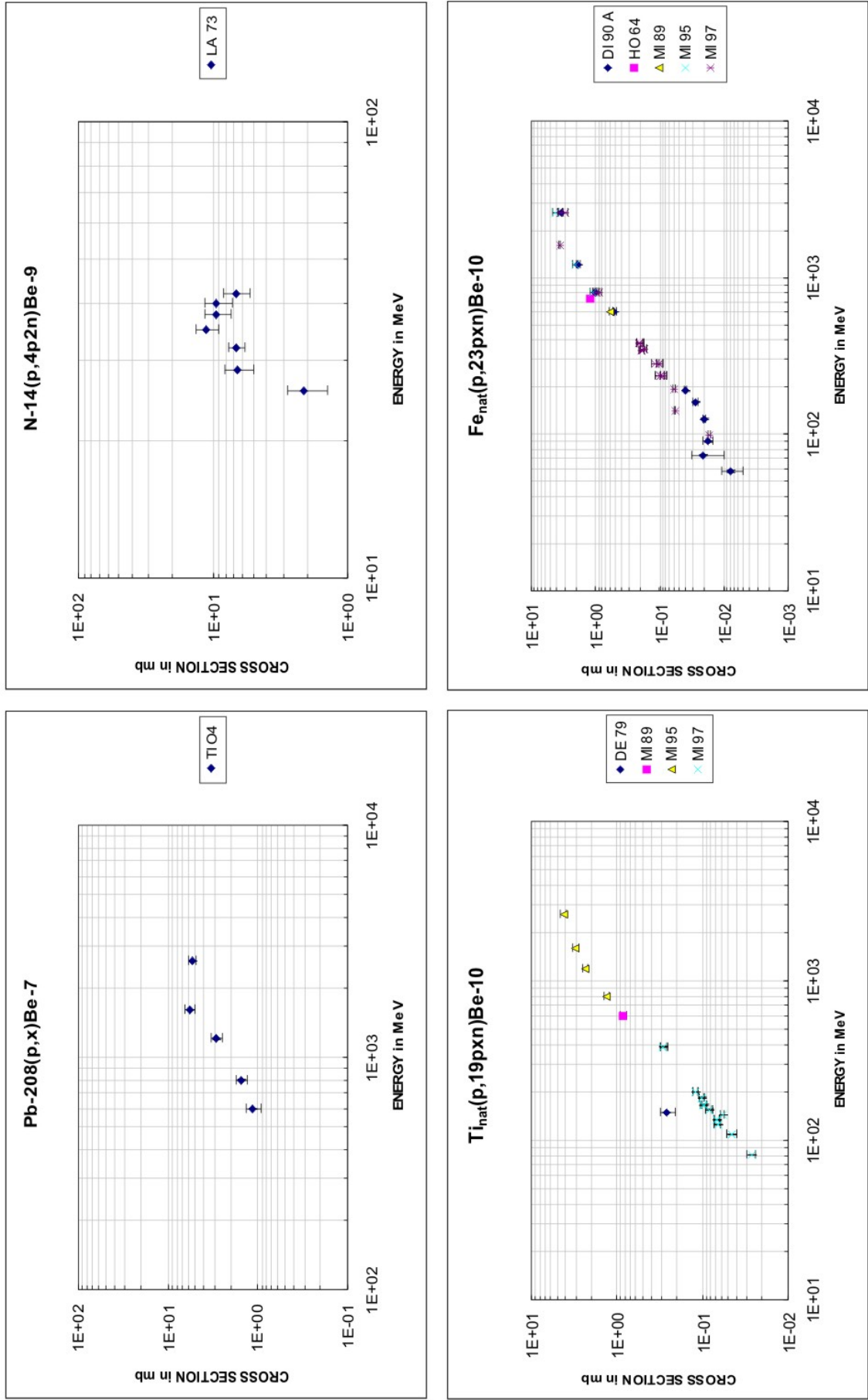


Figure C.8: Experimental data for the production of  $^7\text{Be}$  from  $^{208}\text{Pb}$ , of  $^9\text{Be}$  from  $^{14}\text{N}$  and of  $^{10}\text{Be}$  from natural Ti and Fe

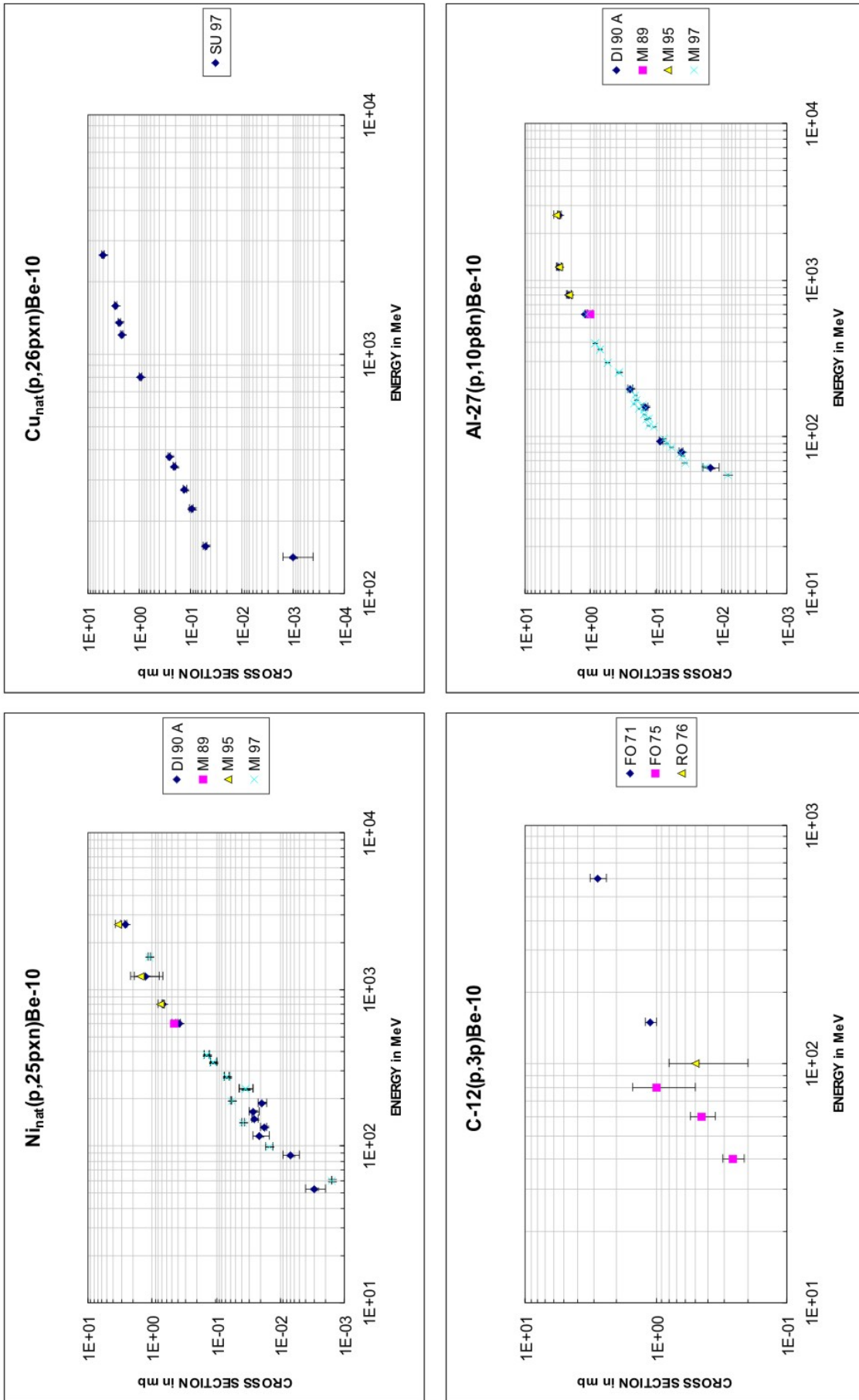


Figure C.9: Experimental data for the production of  $^{10}\text{Be}$  from natural Ni, Cu,  $^{12}\text{Cu}$  and  $^{27}\text{Al}$



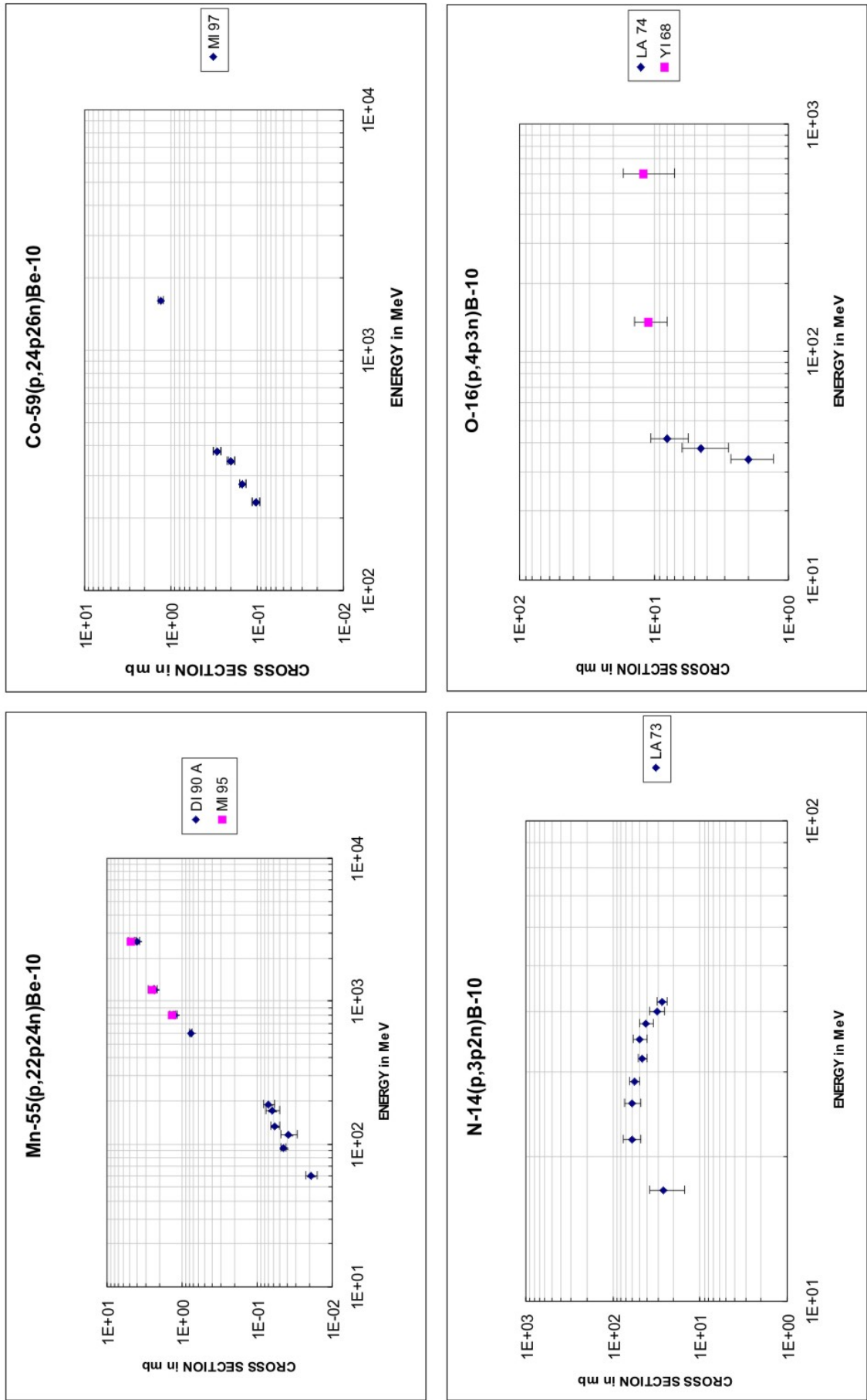


Figure C.10: Experimental data for the production of  $^{10}\text{Be}$  from  $^{55}\text{Mn}$ ,  $^{59}\text{Co}$  and  $^{10}\text{B}$  from  $^{14}\text{N}$  and  $^{16}\text{O}$

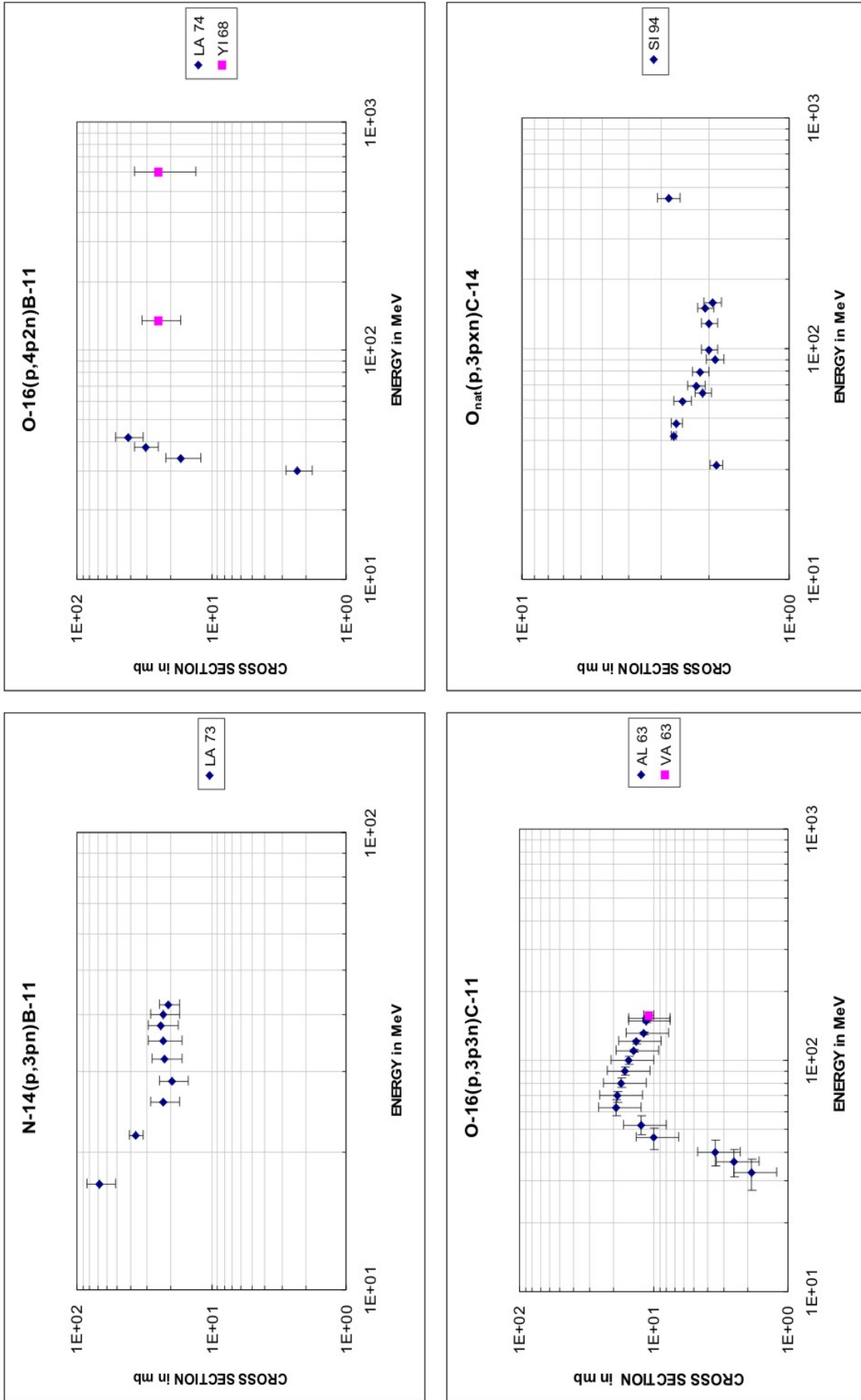


Figure C.11: Experimental data for the production of  $^{11}B$  from  $^{14}N$  and  $^{16}O$ , of  $^{11}C$  from  $^{16}O$  and of  $^{14}C$  from natural  $O$



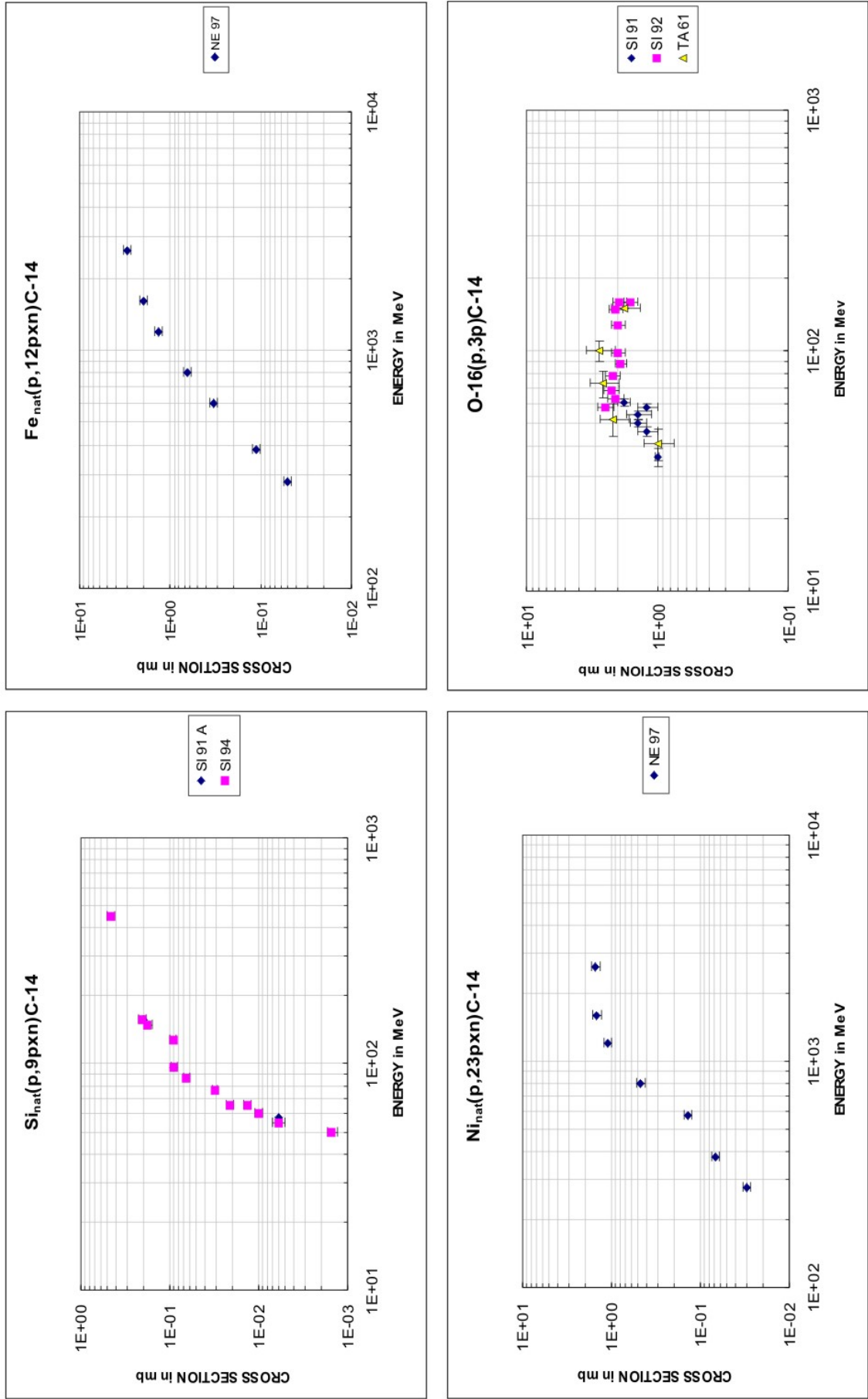


Figure C.12: Experimental data for the production of  $^{14}\text{C}$  from natural Si, Fe, Ni and  $^{16}\text{O}$

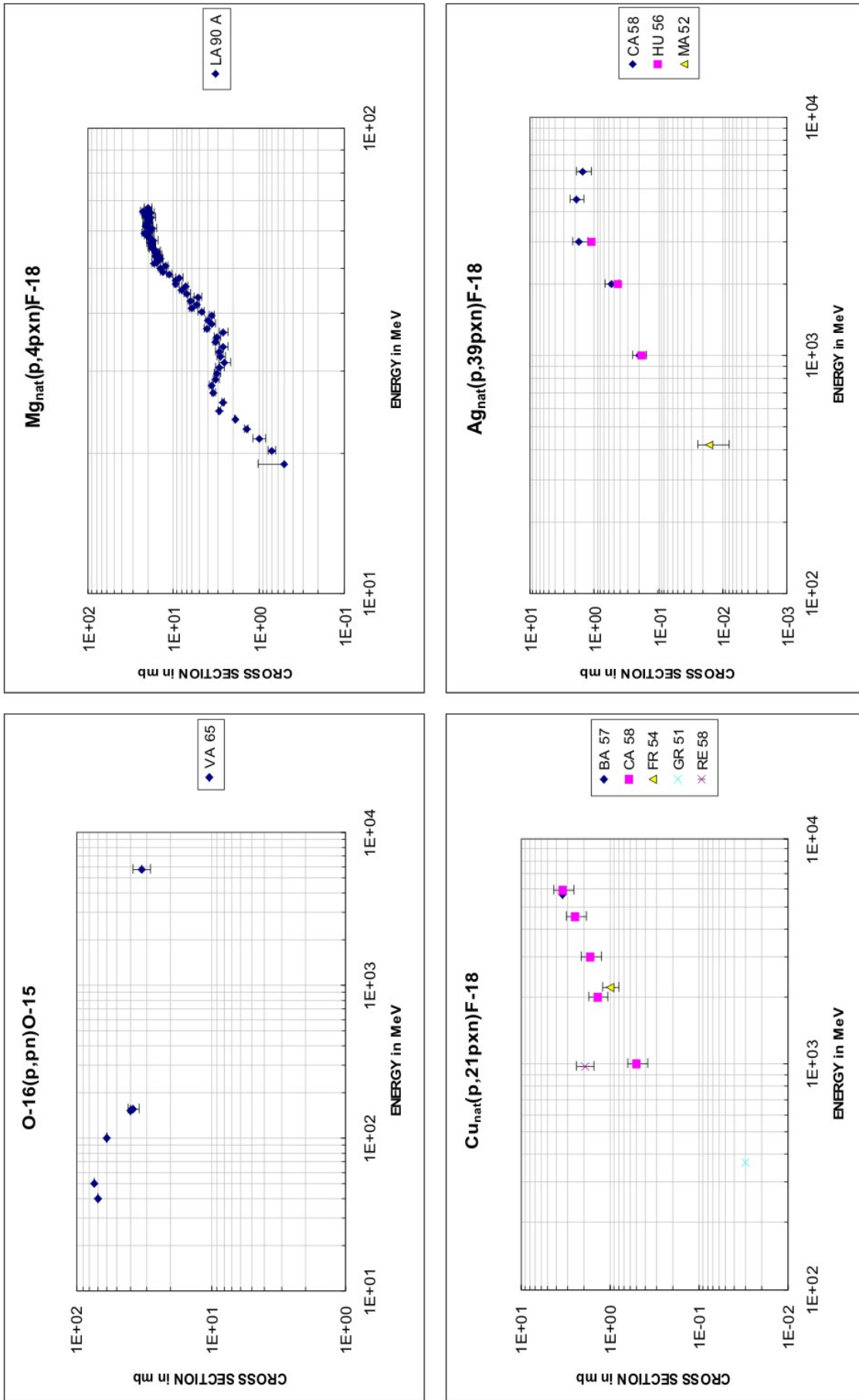


Figure C.13: Experimental data for the production of  $^{15}\text{O}$  from  $^{16}\text{O}$  and of  $^{18}\text{F}$  from natural Mg, Cu and Ag

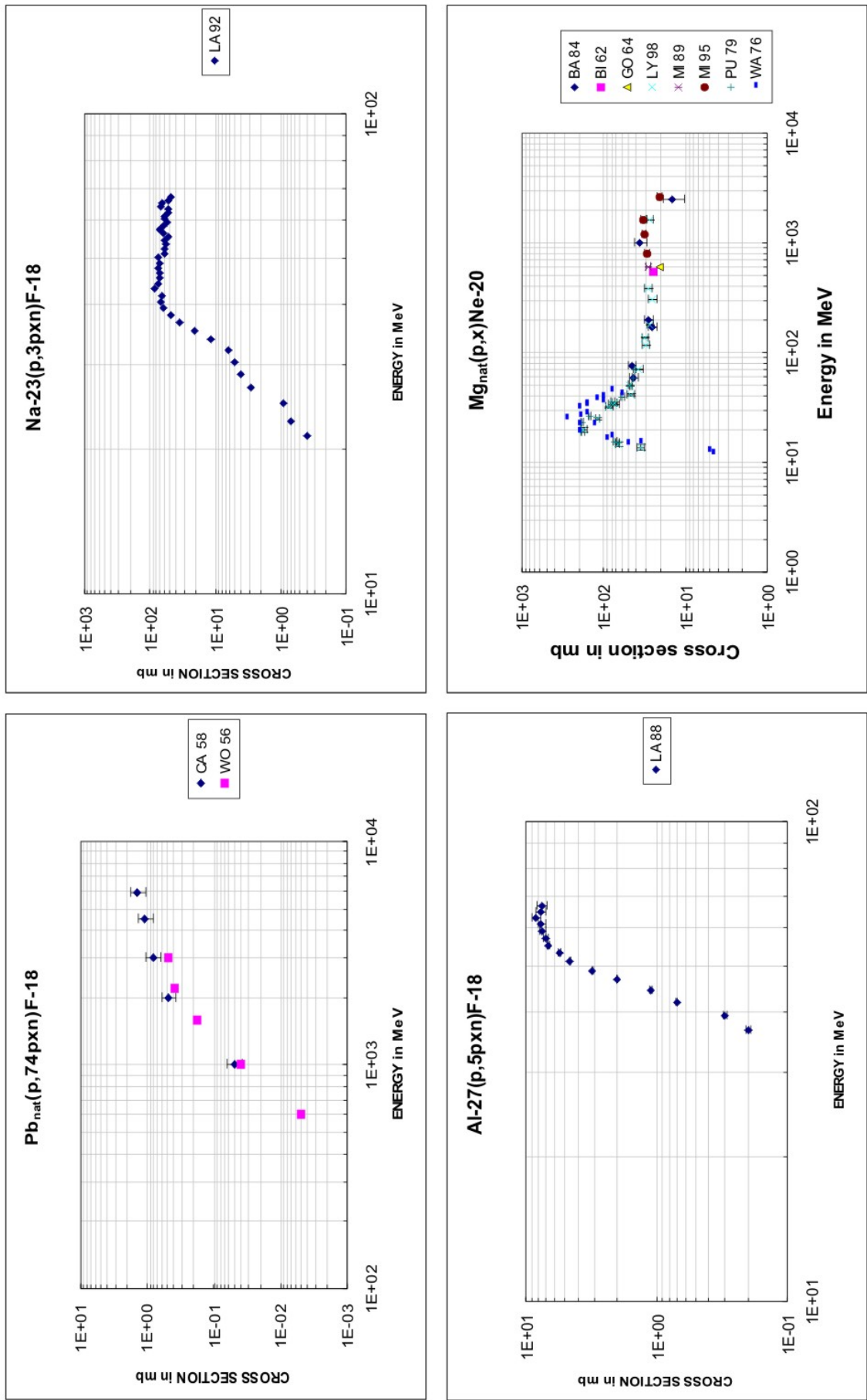


Figure C.14: Experimental data for the production of  $^{18}\text{F}$  from  $\text{Pb}$ ,  $^{23}\text{Na}$  and  $^{27}\text{Al}$  and of  $^{20}\text{Ne}$  from natural  $\text{Mg}$

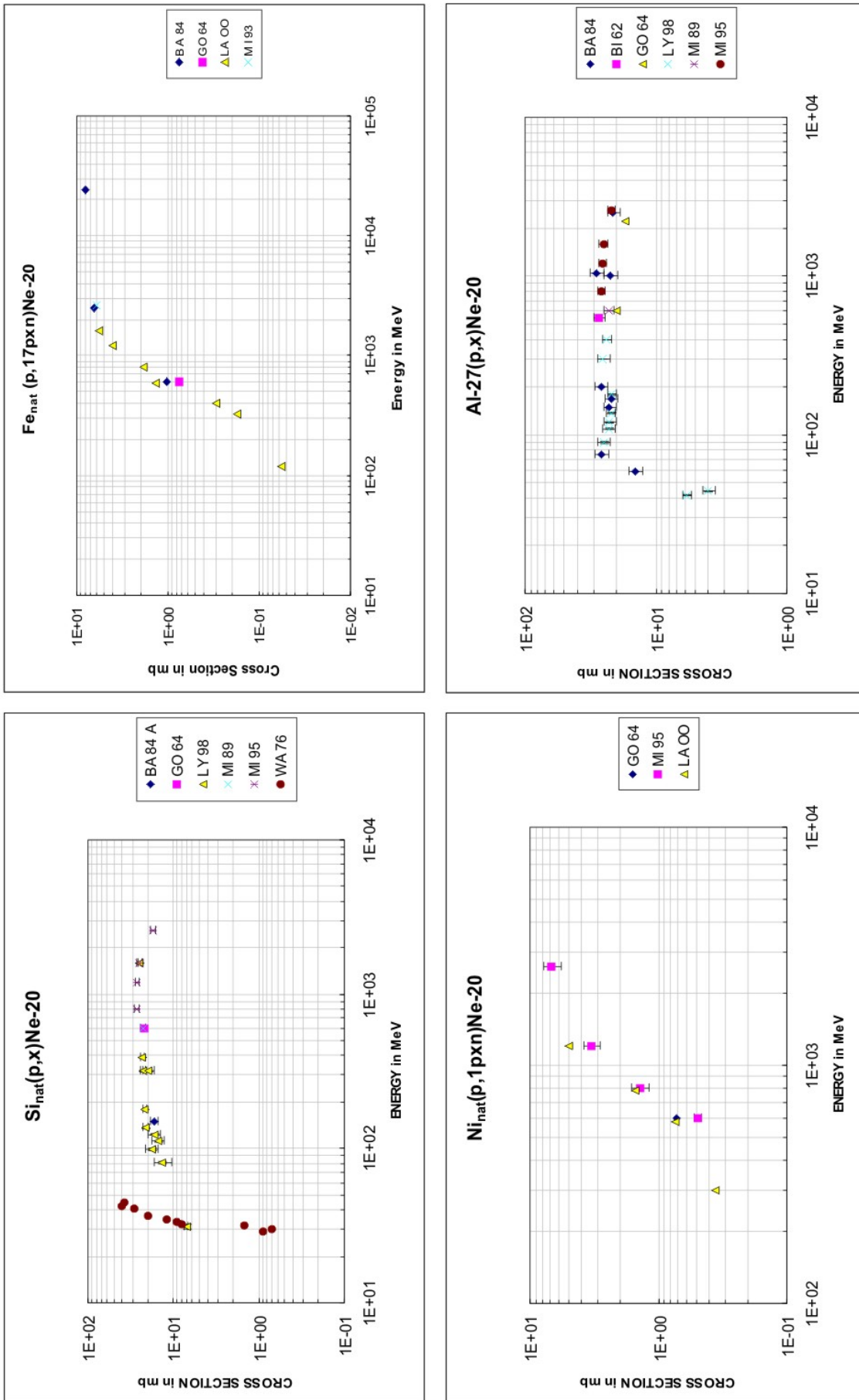


Figure C.15: Experimental data for the production of  $^{20}\text{Ne}$  from natural Si, Fe, Ni and  $^{27}\text{Al}$

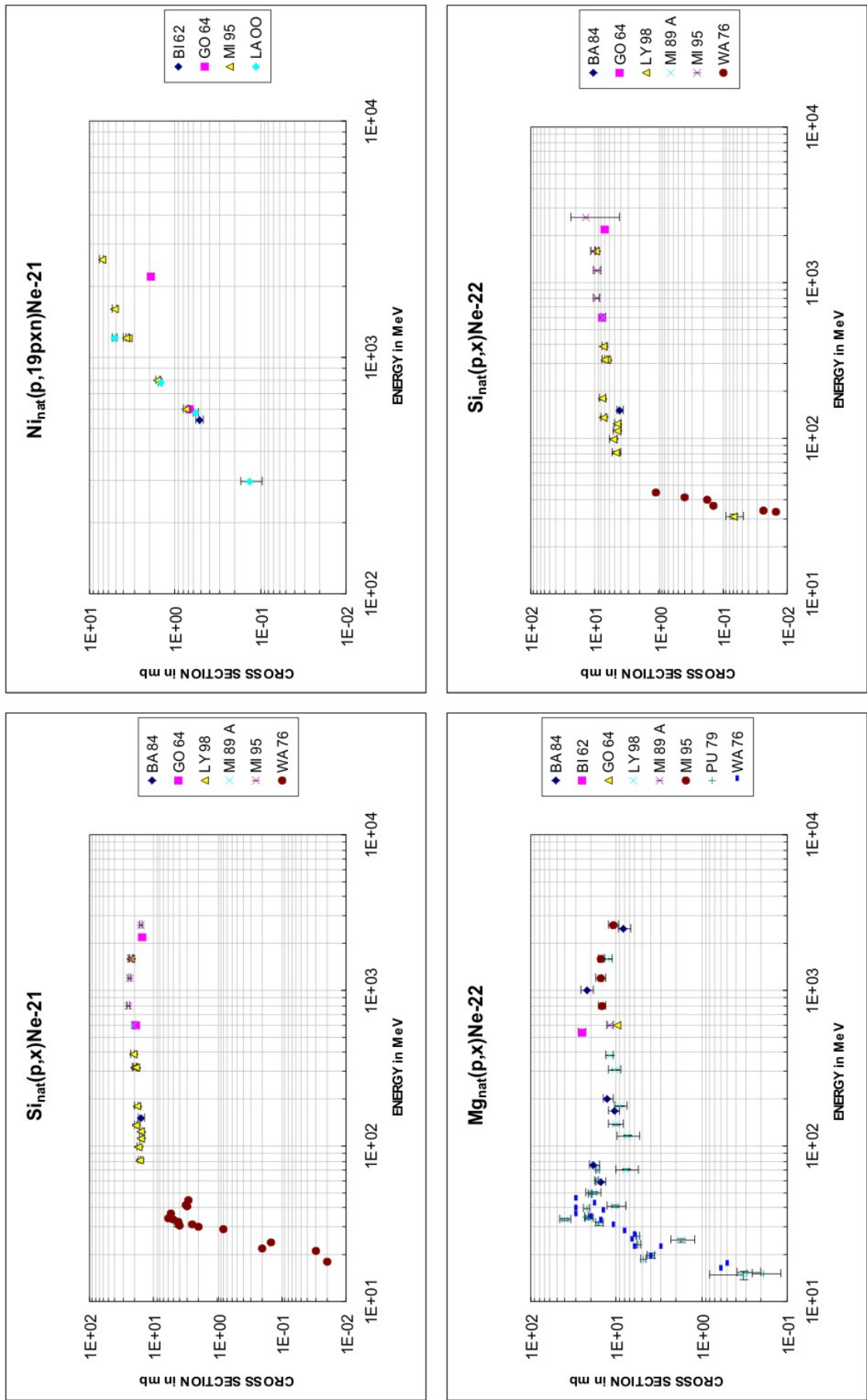


Figure C.16: Experimental data for the production of  $^{21}\text{Ne}$  from natural Si and Ni and of  $^{22}\text{Ne}$  from natural Mg and Si

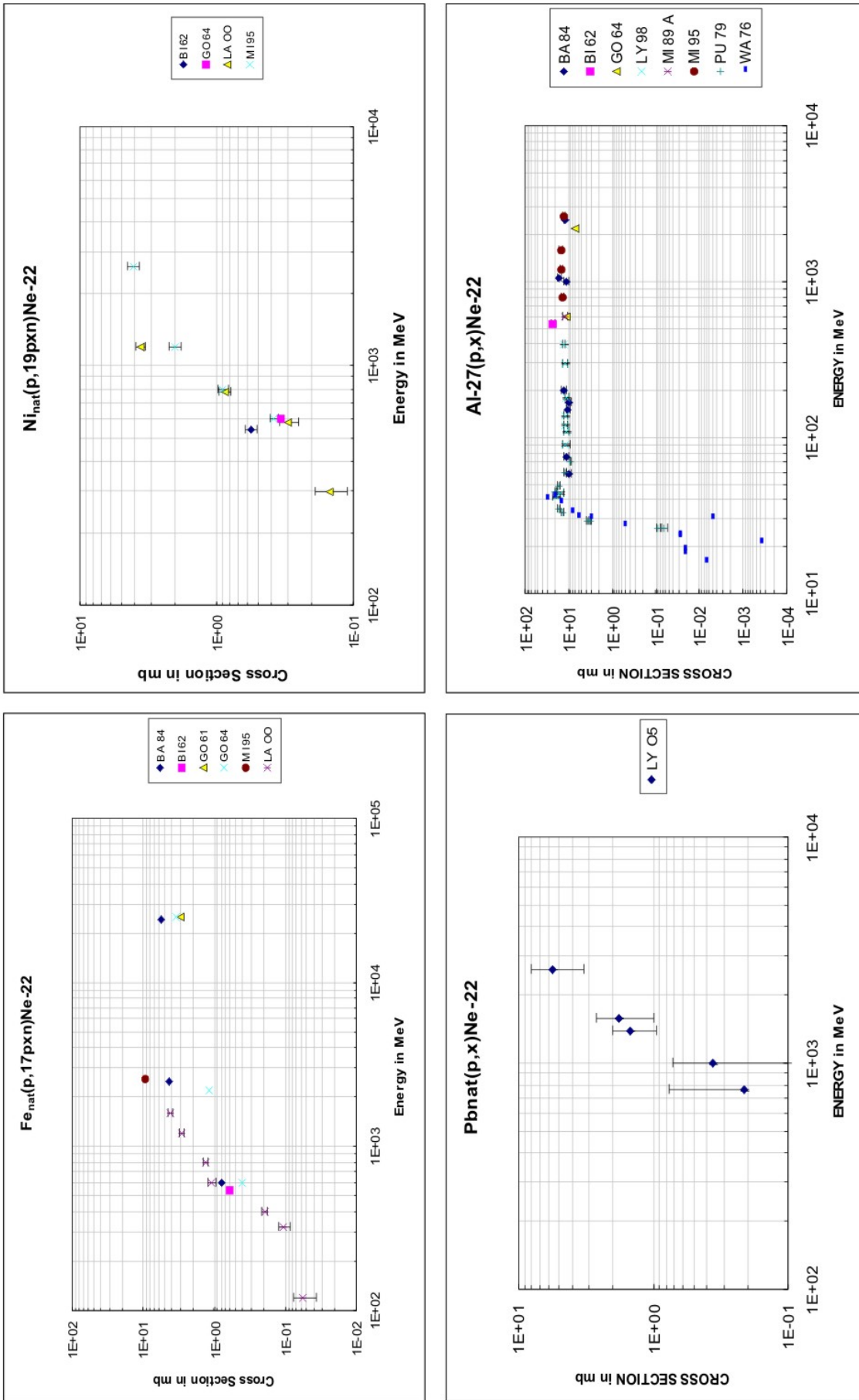


Figure C.17: Experimental data for the production of  $^{22}\text{Ne}$  from natural Fe, Ni, Pb and  $^{27}\text{Al}$



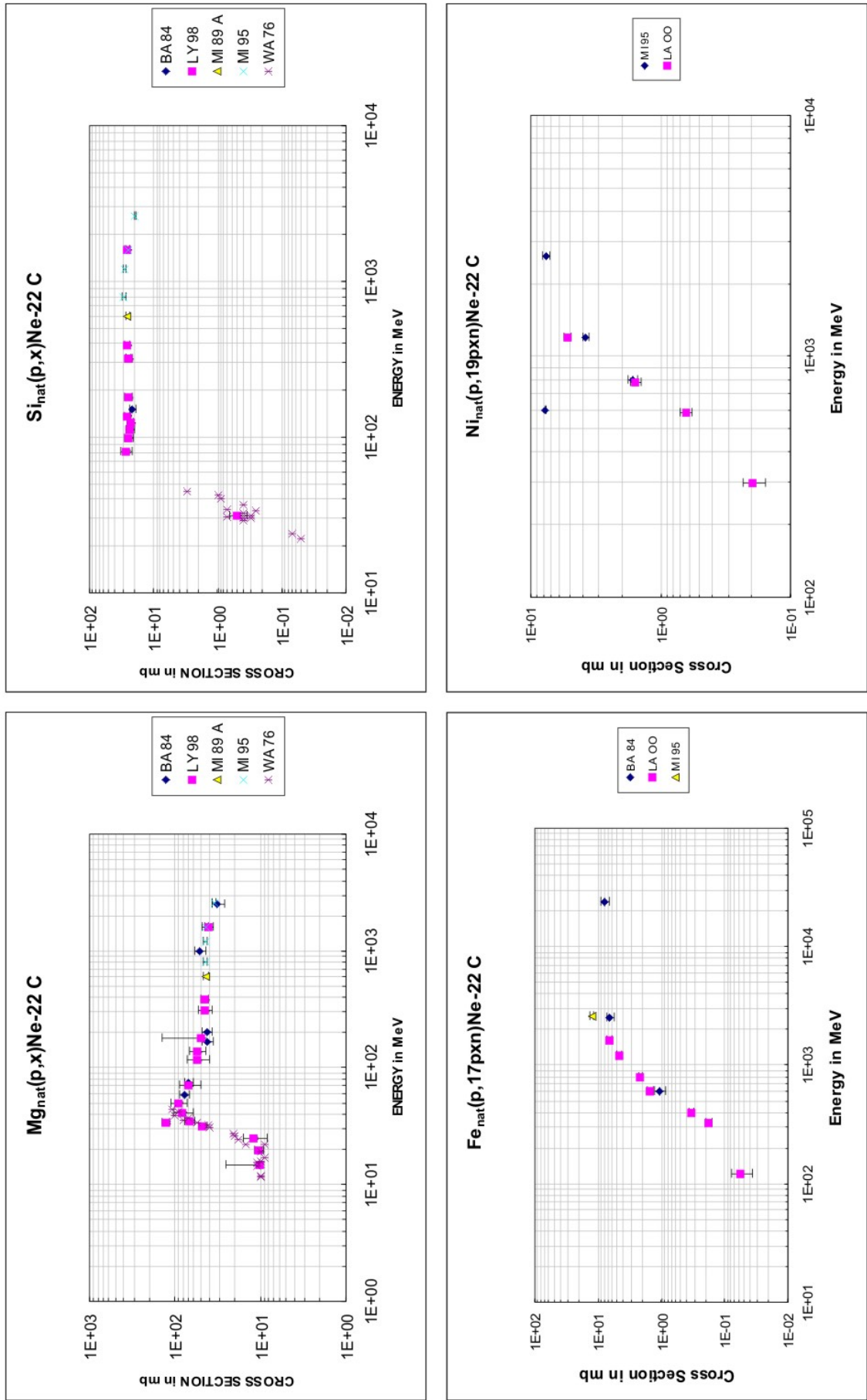


Figure C.18: Experimental data for the production of  $^{22}Ne_c$  from natural Mg, Si, Fe and Ni

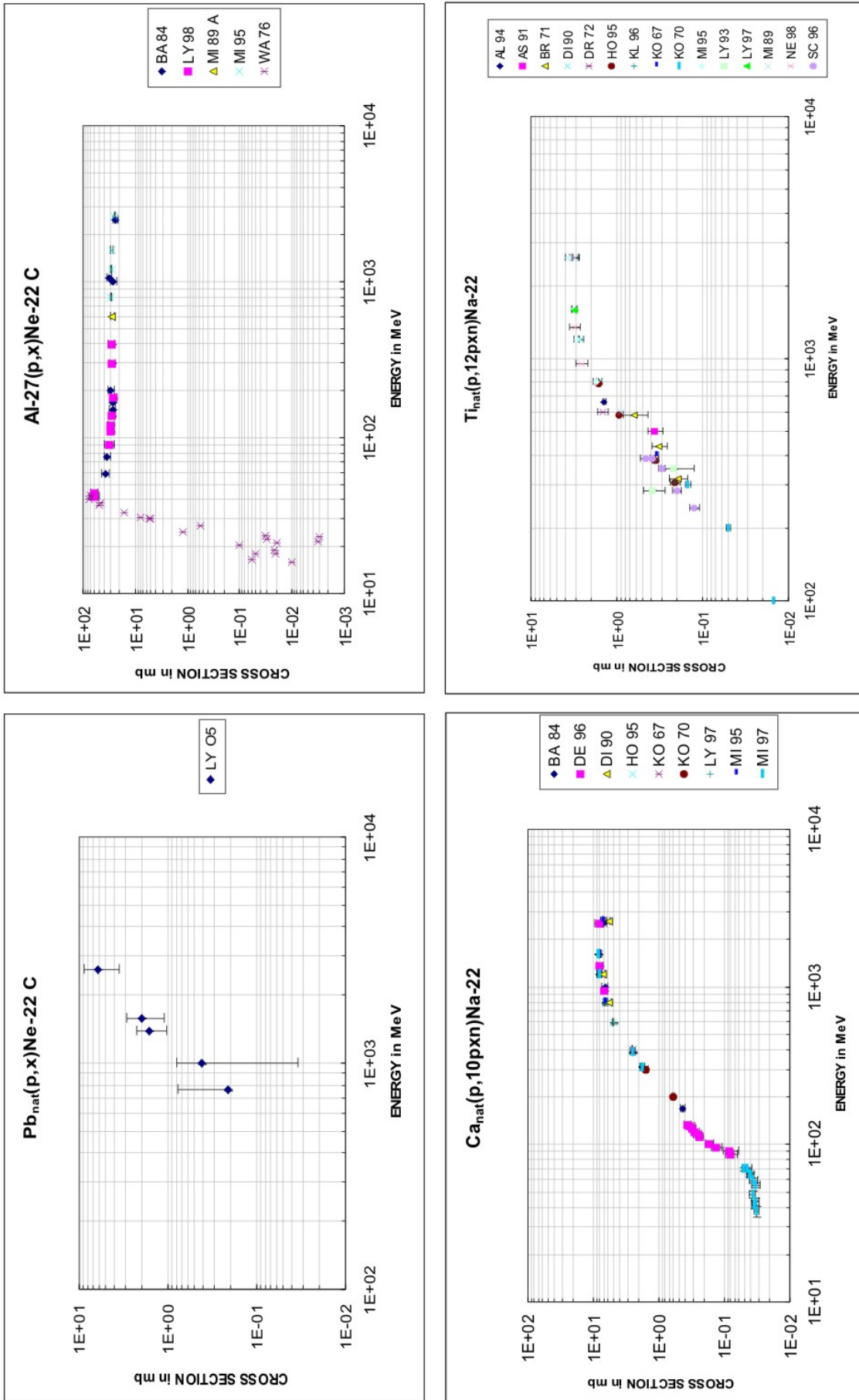


Figure C.19: Experimental data for the production of  $^{22}Ne_c$  from Pb and  $^{27}Al$  and of  $^{22}Na$  from natural Ca and Ti



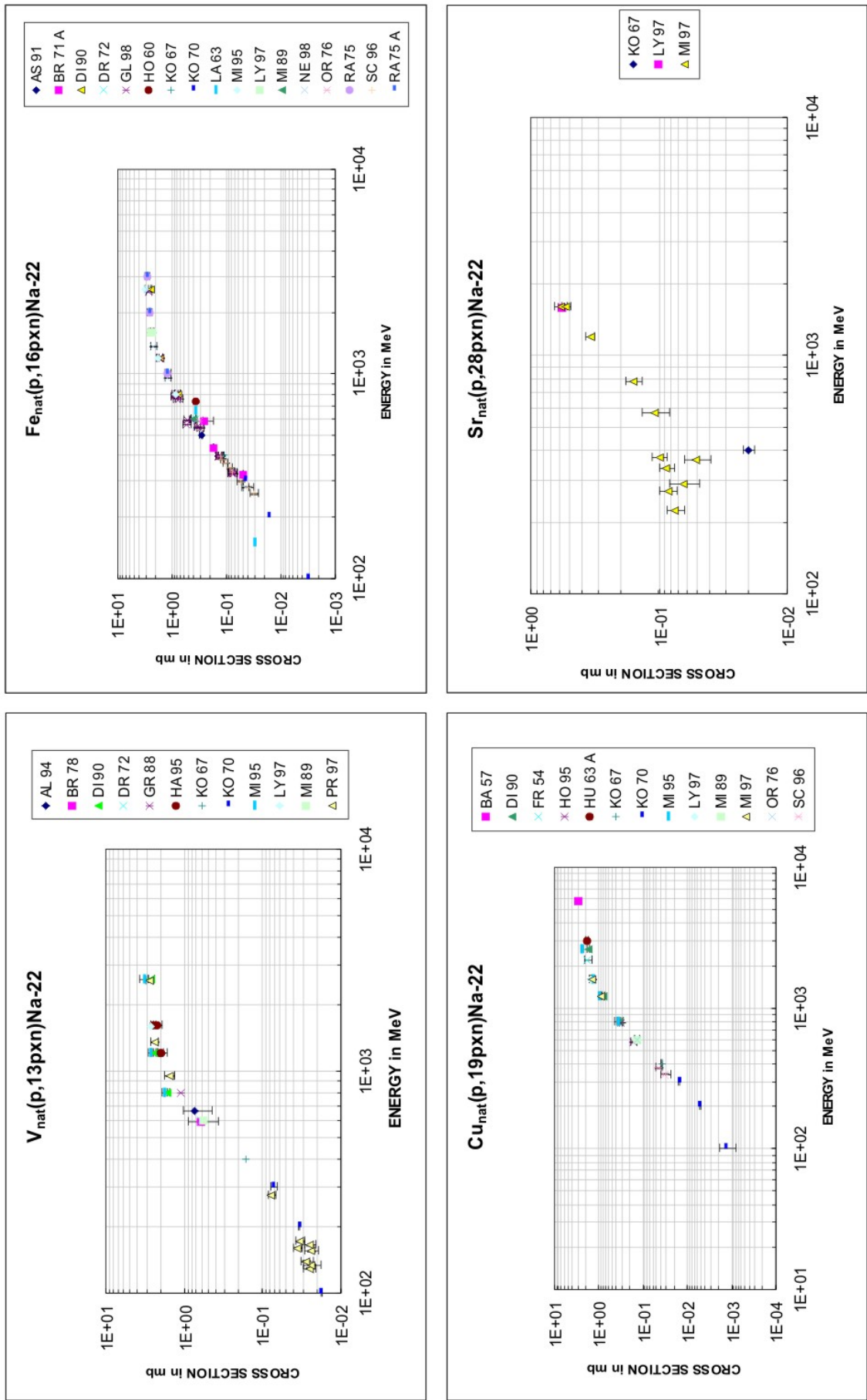


Figure C.20: Experimental data for the production of  $^{22}\text{Na}$  from natural V, Fe, Cu and Sr

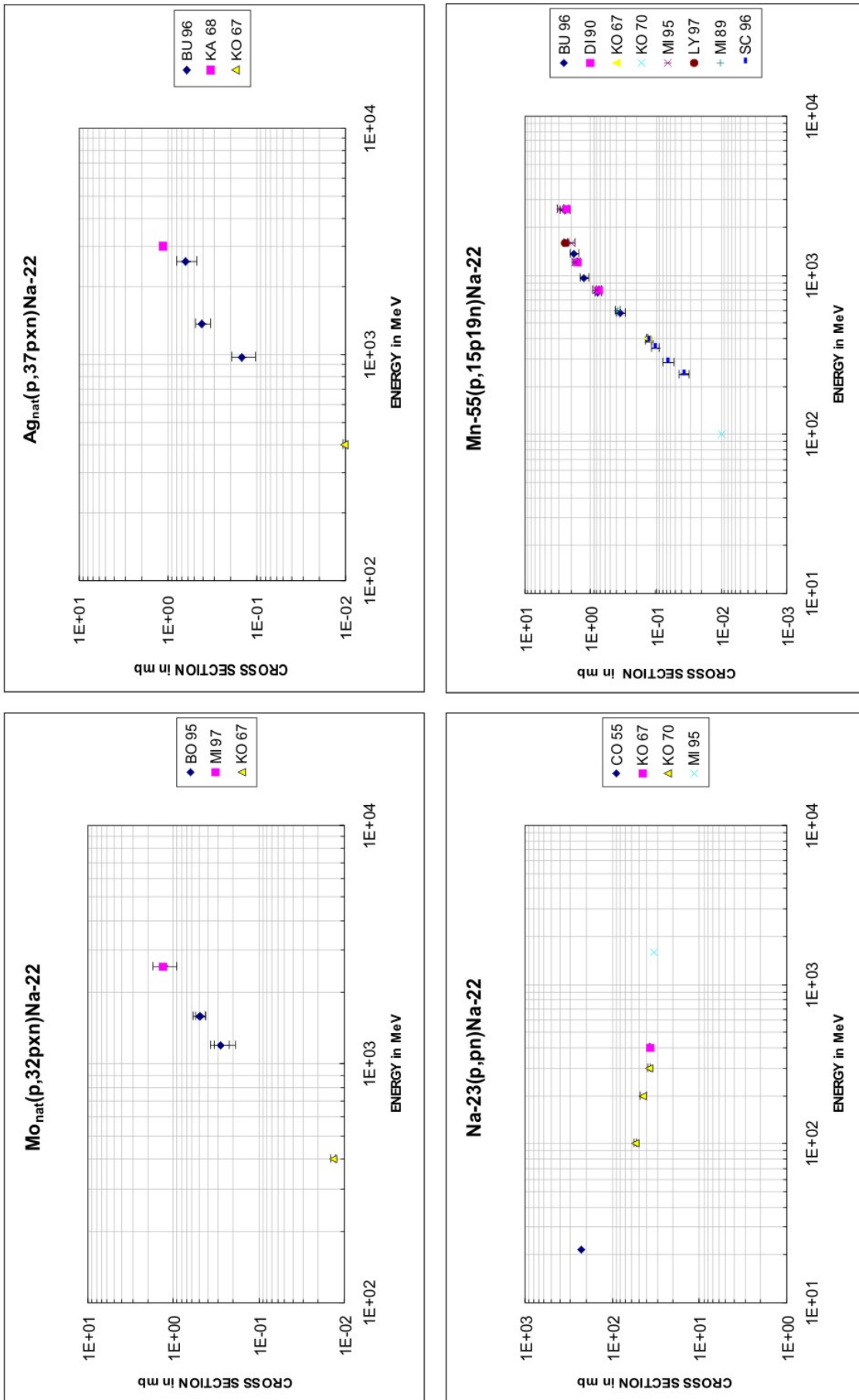


Figure C.21: Experimental data for the production of  $^{22}\text{Na}$  from natural Mo and Ag,  $^{23}\text{Na}$  and  $^{55}\text{Mn}$

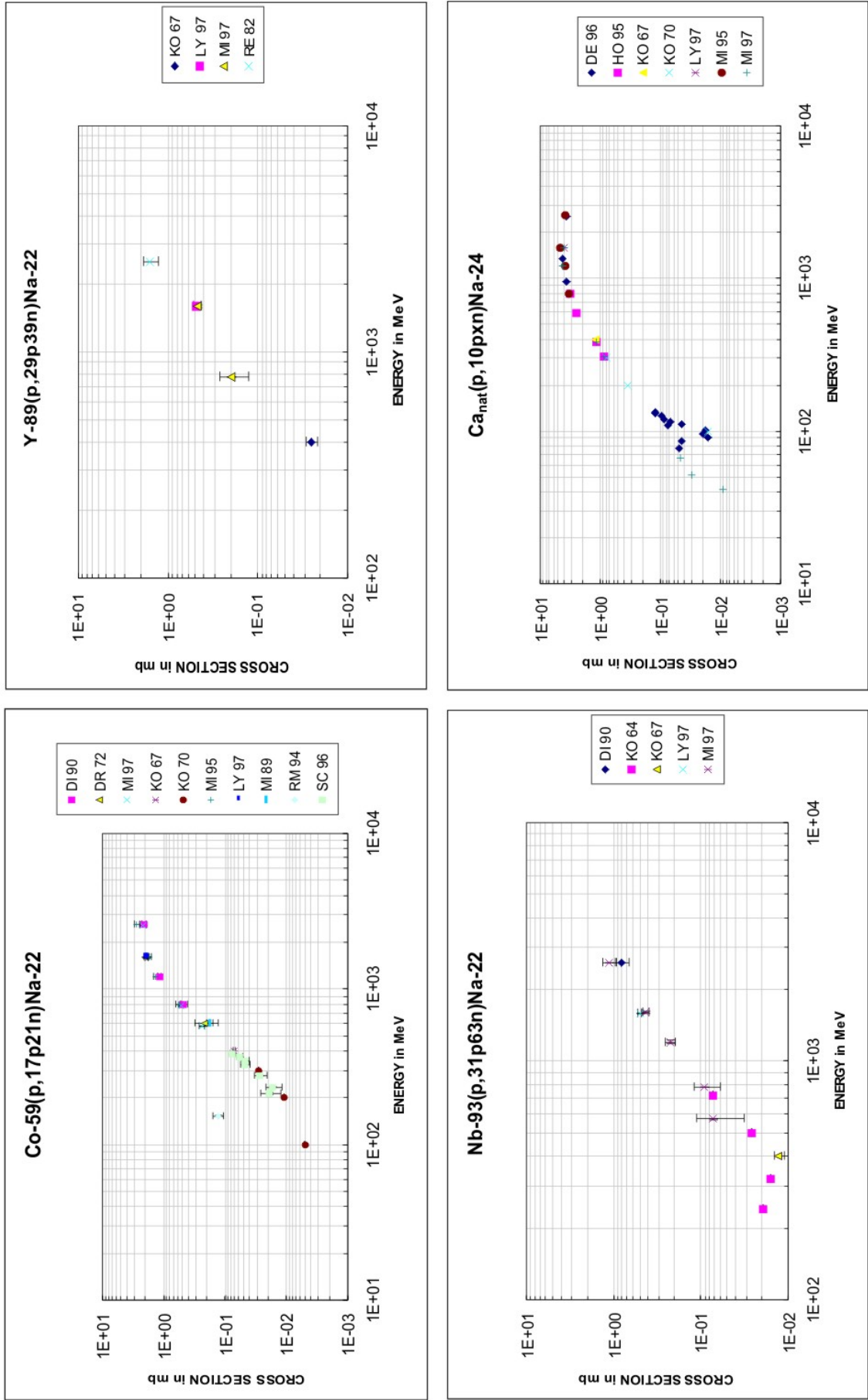


Figure C.22: Experimental data for the production of  $^{22}\text{Na}$  from  $^{59}\text{Co}$ ,  $^{89}\text{Y}$ ,  $^{93}\text{Nb}$  and of  $^{24}\text{Na}$  from natural Ca

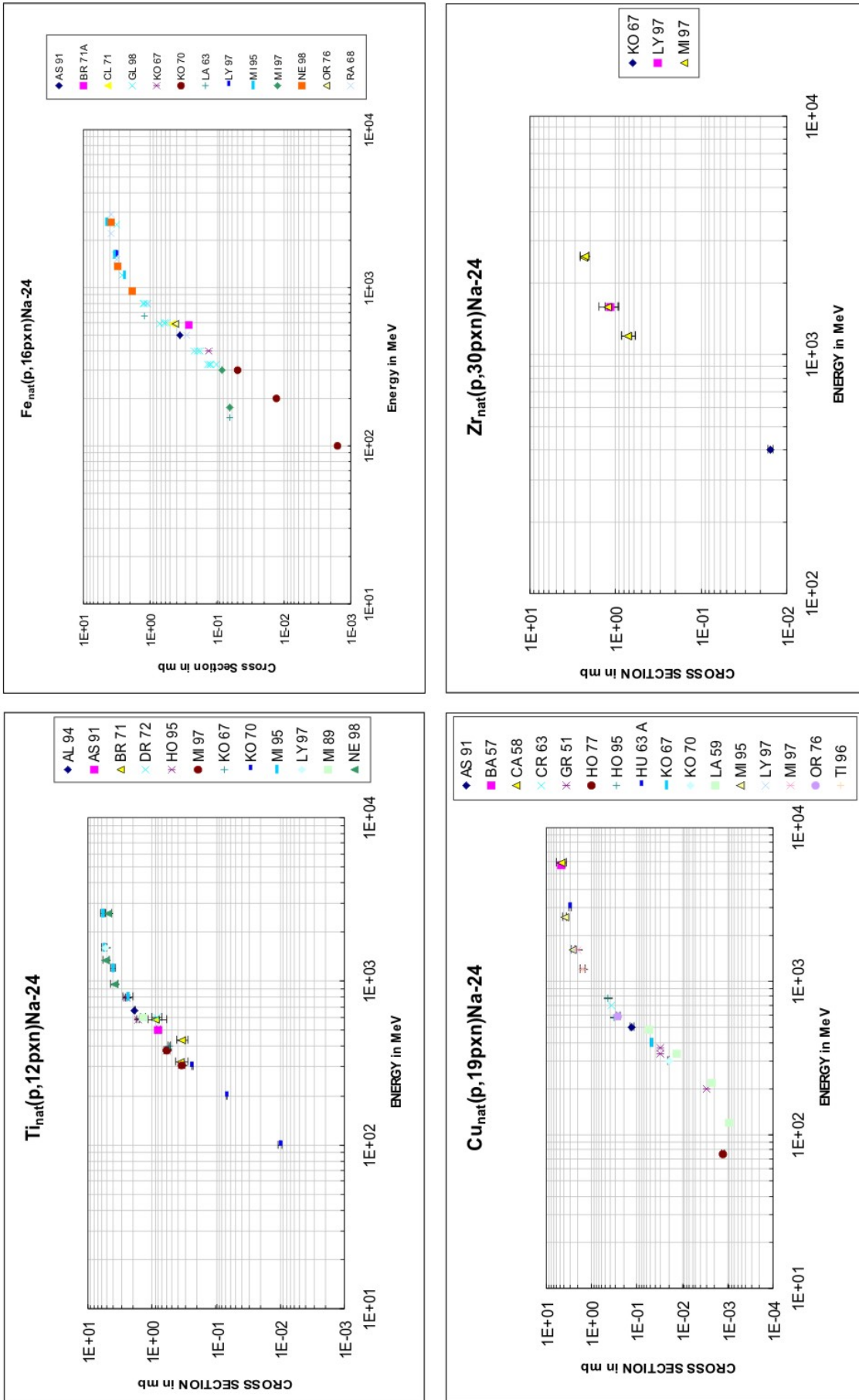


Figure C.23: Experimental data for the production of  $^{24}\text{Na}$  from natural Ti, Fe, Cu and Zr

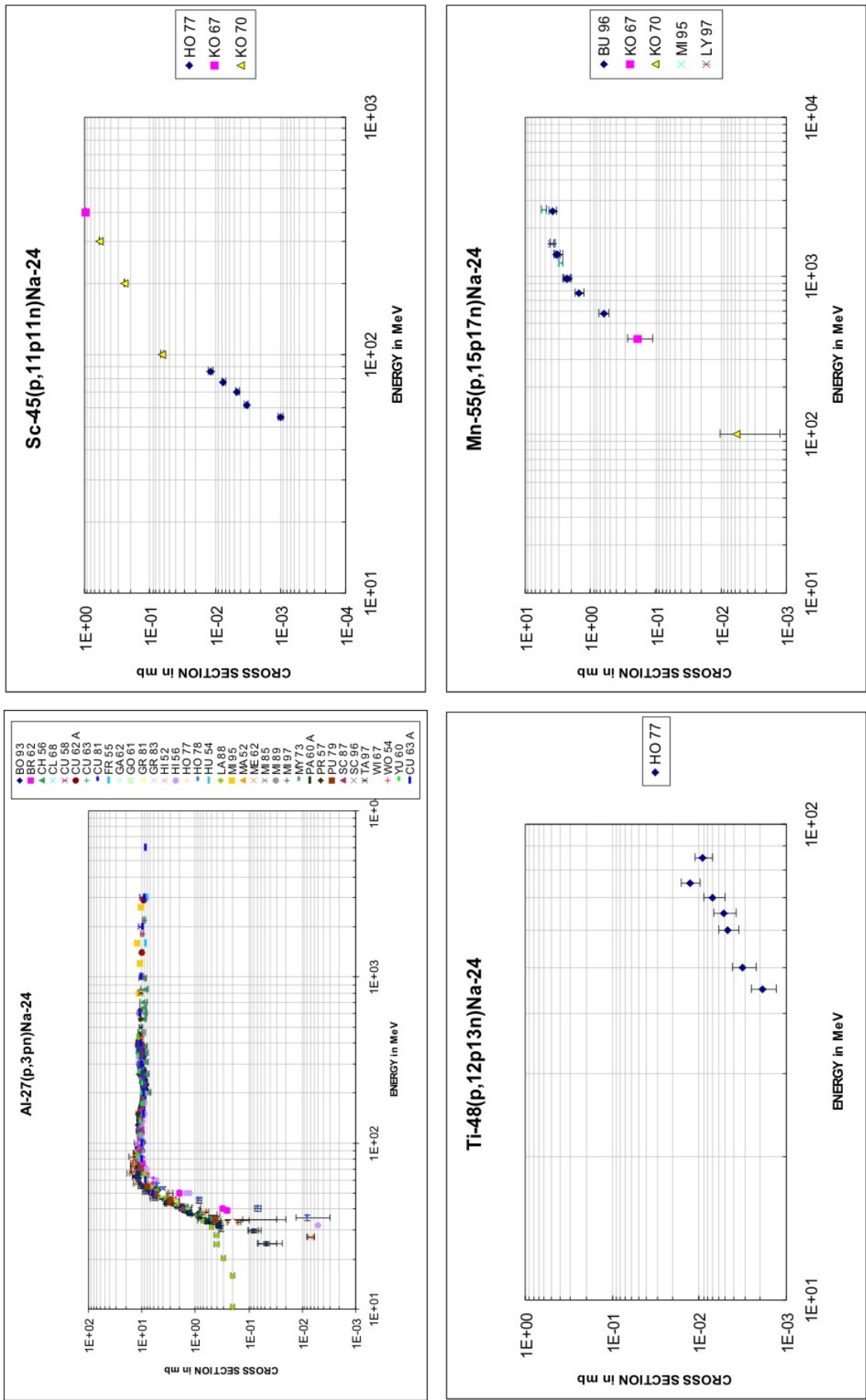


Figure C.24: Experimental data for the production of  $^{24}Na$  from  $^{27}Al$ ,  $^{45}Sc$ ,  $^{48}Ti$  and  $^{55}Mn$

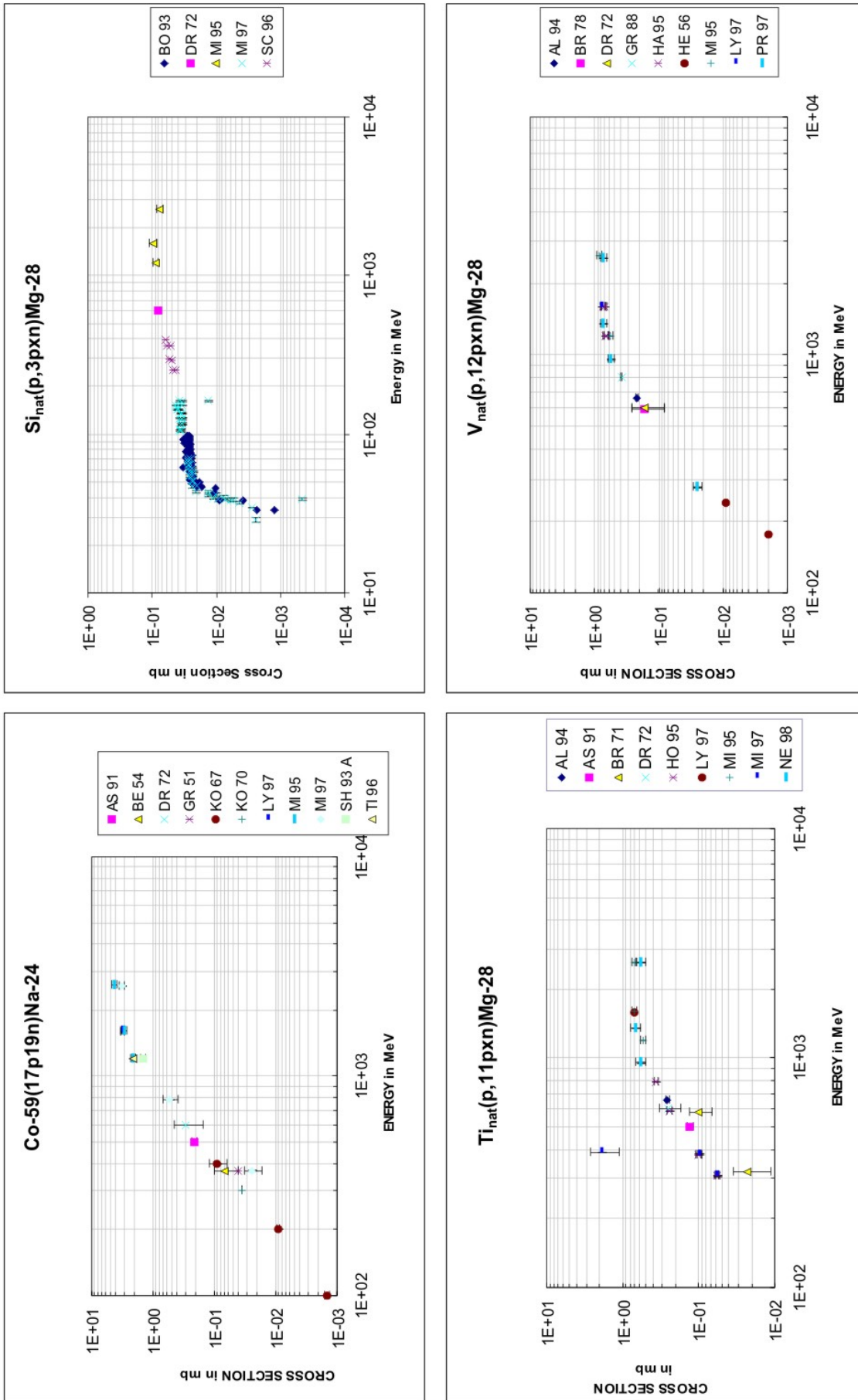


Figure C.25: Experimental data for the production of  $^{24}Na$  from  $^{59}Co$  and of  $^{28}Mg$  from natural Si, Ti and V



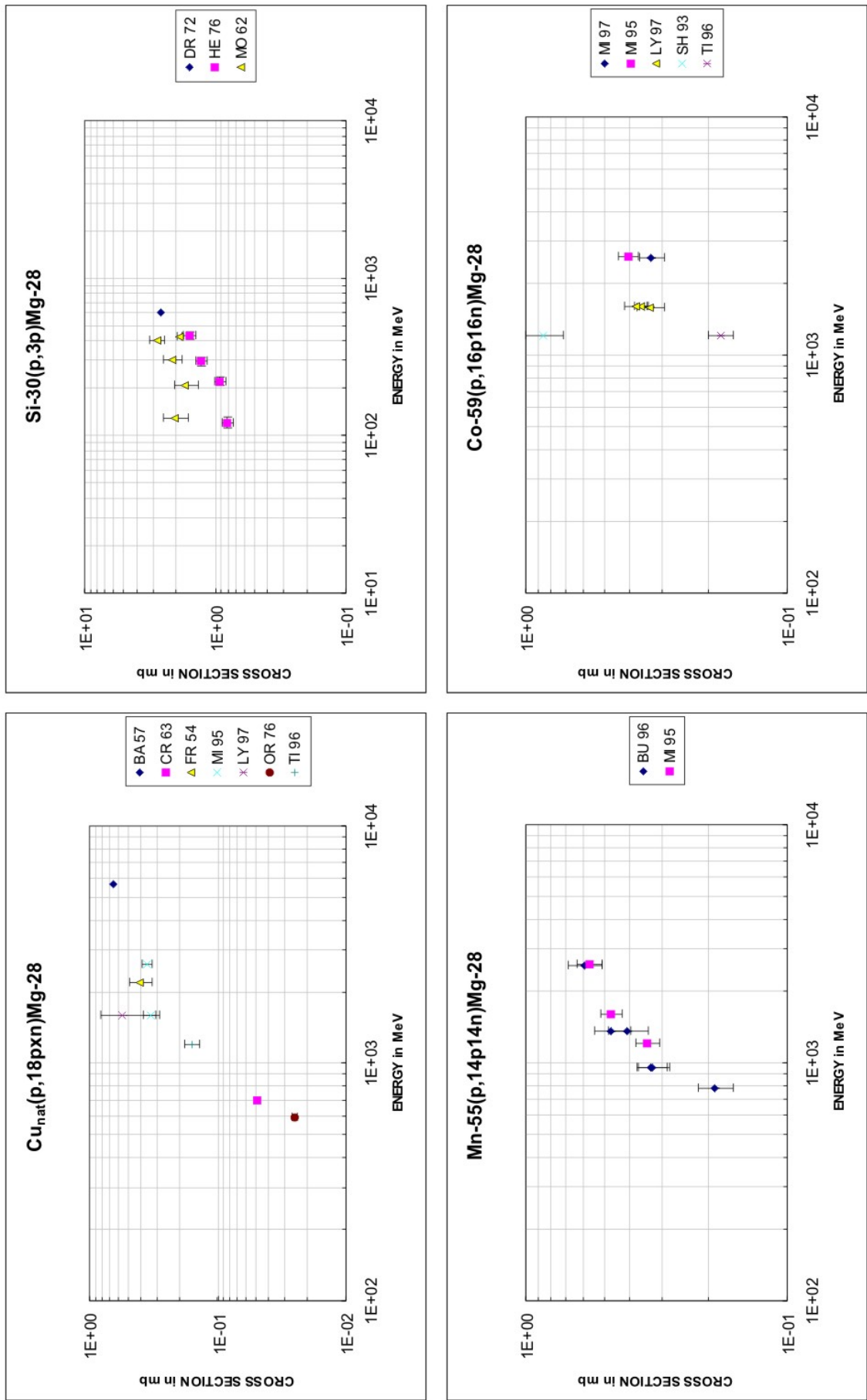


Figure C.26: Experimental data for the production of  $^{28}\text{Mg}$  from natural  $\text{Cu}$ ,  $^{30}\text{Si}$ ,  $^{55}\text{Mn}$  and  $^{59}\text{Co}$

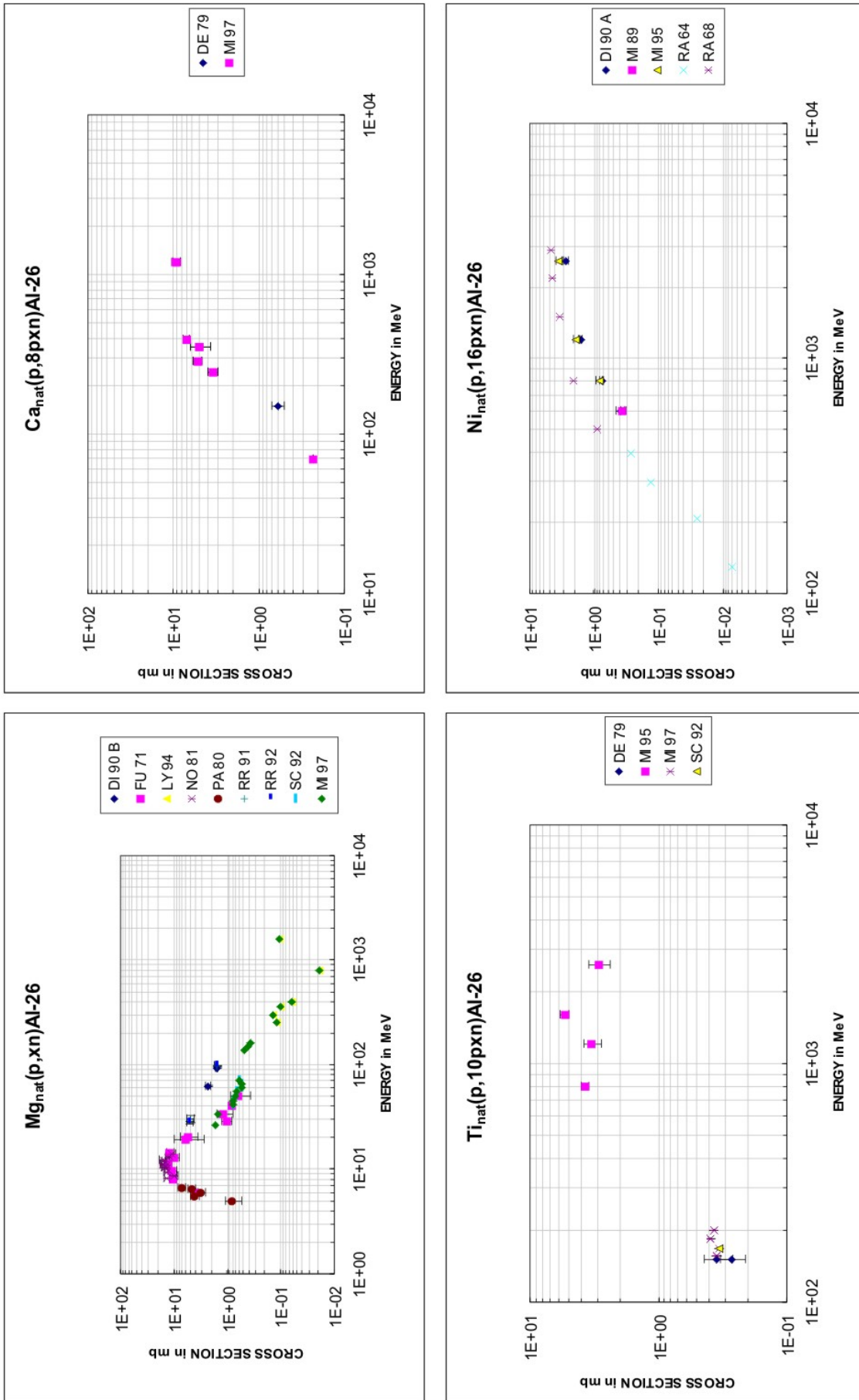


Figure C.27: Experimental data for the production of  $^{26}\text{Al}$  from natural Ca, Mg, Ti and Ni



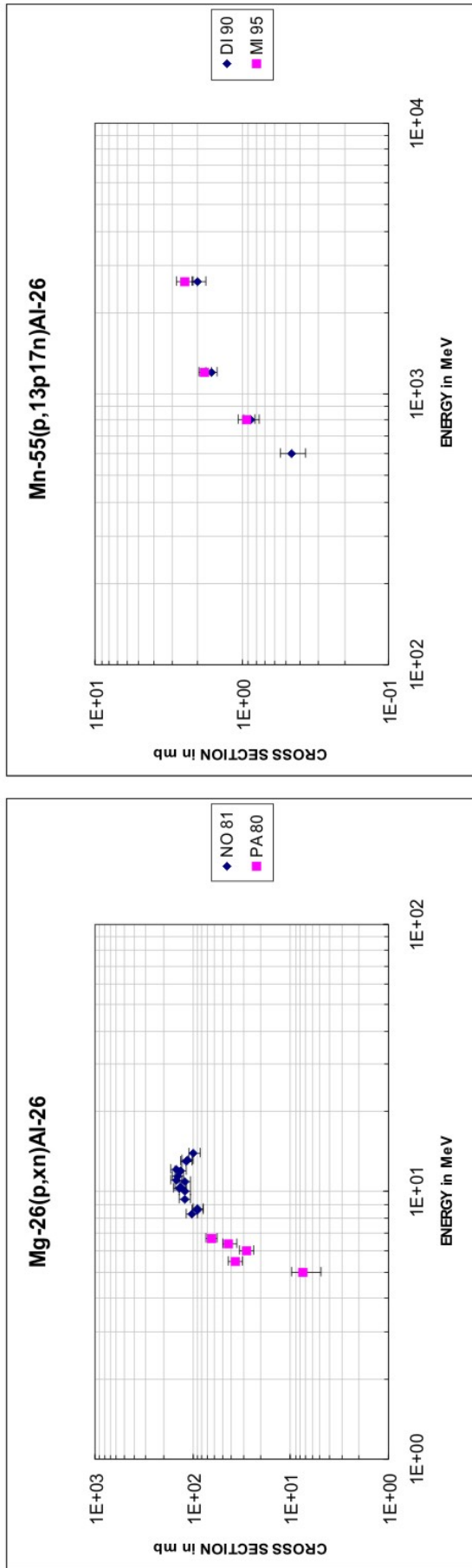


Figure C.28: Experimental data for the production of  $^{26}\text{Al}$  from  $^{26}\text{Mg}$  and  $^{55}\text{Mn}$



## D Product-target combinations covered for Talys calculations

Target	Product	Considered Progenitors
<sup>nat</sup> O	<sup>14</sup> C	<sup>14</sup> B
<sup>nat</sup> Si	<sup>14</sup> C	independent
<sup>16</sup> O	<sup>14</sup> C	independent
<sup>16</sup> O	<sup>15</sup> O	independent
<sup>nat</sup> Mg	<sup>18</sup> F	<sup>18</sup> Ne
<sup>23</sup> Na	<sup>18</sup> F	<sup>18</sup> Ne
<sup>27</sup> Al	<sup>18</sup> F	<sup>18</sup> Ne
<sup>nat</sup> Mg	<sup>20</sup> Ne	<sup>20</sup> F, <sup>20</sup> O, <sup>20</sup> Na, <sup>20</sup> Mg
<sup>nat</sup> Si	<sup>20</sup> Ne	<sup>20</sup> F, <sup>20</sup> O, <sup>20</sup> Na, <sup>20</sup> Mg
<sup>27</sup> Al	<sup>20</sup> Ne	<sup>20</sup> F, <sup>20</sup> O, <sup>20</sup> Na, <sup>20</sup> Mg
<sup>nat</sup> Mg	<sup>21</sup> Ne	<sup>21</sup> F, <sup>21</sup> O, <sup>21</sup> Na, <sup>21</sup> Mg
<sup>nat</sup> Si	<sup>21</sup> Ne	<sup>21</sup> F, <sup>21</sup> O, <sup>21</sup> Na, <sup>21</sup> Mg
<sup>27</sup> Al	<sup>21</sup> Ne	<sup>21</sup> F, <sup>21</sup> O, <sup>21</sup> Na, <sup>21</sup> Mg
<sup>nat</sup> Mg	<sup>22</sup> Ne	<sup>22</sup> Mg, <sup>22</sup> Al, <sup>22</sup> F, <sup>22</sup> O
<sup>nat</sup> Si	<sup>22</sup> Ne	<sup>22</sup> Mg, <sup>22</sup> Al, <sup>22</sup> F
<sup>27</sup> Al	<sup>22</sup> Ne	<sup>22</sup> Mg, <sup>22</sup> Al, <sup>22</sup> F
<sup>nat</sup> Mg	<sup>22</sup> Ne-C	<sup>22</sup> Na, <sup>22</sup> Mg, <sup>22</sup> Al, <sup>22</sup> F, <sup>22</sup> O
<sup>nat</sup> Si	<sup>22</sup> Ne-C	<sup>22</sup> Na, <sup>22</sup> Mg, <sup>22</sup> Al, <sup>22</sup> F
<sup>27</sup> Al	<sup>22</sup> Ne-C	<sup>22</sup> Na, <sup>22</sup> Mg, <sup>22</sup> Al, <sup>22</sup> F
<sup>nat</sup> Mg	<sup>22</sup> Na	<sup>22</sup> Mg, <sup>22</sup> Al
<sup>nat</sup> Si	<sup>22</sup> Na	<sup>22</sup> Mg
<sup>nat</sup> Ca	<sup>22</sup> Na	<sup>22</sup> Mg
<sup>24</sup> Mg	<sup>22</sup> Na	<sup>22</sup> Mg, <sup>22</sup> Al
<sup>25</sup> Mg	<sup>22</sup> Na	<sup>22</sup> Mg, <sup>22</sup> Al
<sup>26</sup> Mg	<sup>22</sup> Na	<sup>22</sup> Mg
<sup>27</sup> Al	<sup>22</sup> Na	<sup>22</sup> Mg, <sup>22</sup> Al
<sup>nat</sup> Mg	<sup>24</sup> Na	<sup>24</sup> Ne
<sup>nat</sup> Si	<sup>24</sup> Na	<sup>24</sup> Ne
<sup>27</sup> Al	<sup>24</sup> Na	<sup>24</sup> Ne
<sup>nat</sup> Si	<sup>28</sup> Mg	independent
<sup>nat</sup> Mg	<sup>26</sup> Al	independent
<sup>nat</sup> Si	<sup>26</sup> Al	<sup>26</sup> Si
<sup>26</sup> Mg	<sup>26</sup> Al	independent
<sup>27</sup> Al	<sup>26</sup> Al	<sup>26</sup> Si



---

## E Comparison with Talys for NUDATRA data

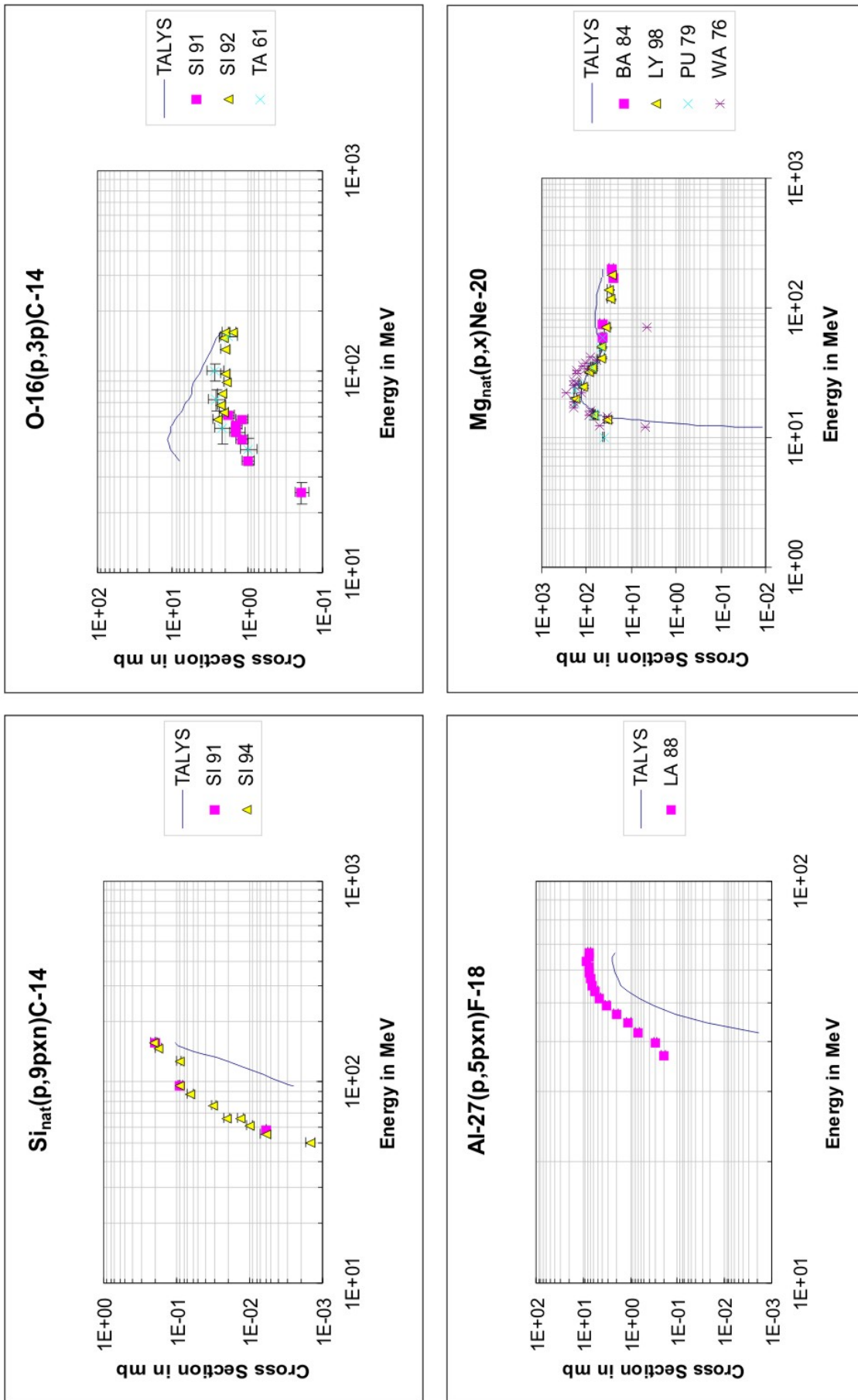


Figure E.1: Data for the production of  $^{14}\text{C}$  from natural Si and  $^{16}\text{O}$ , of  $^{18}\text{F}$  from  $^{27}\text{Al}$  and of  $^{20}\text{Ne}$  from natural Mg

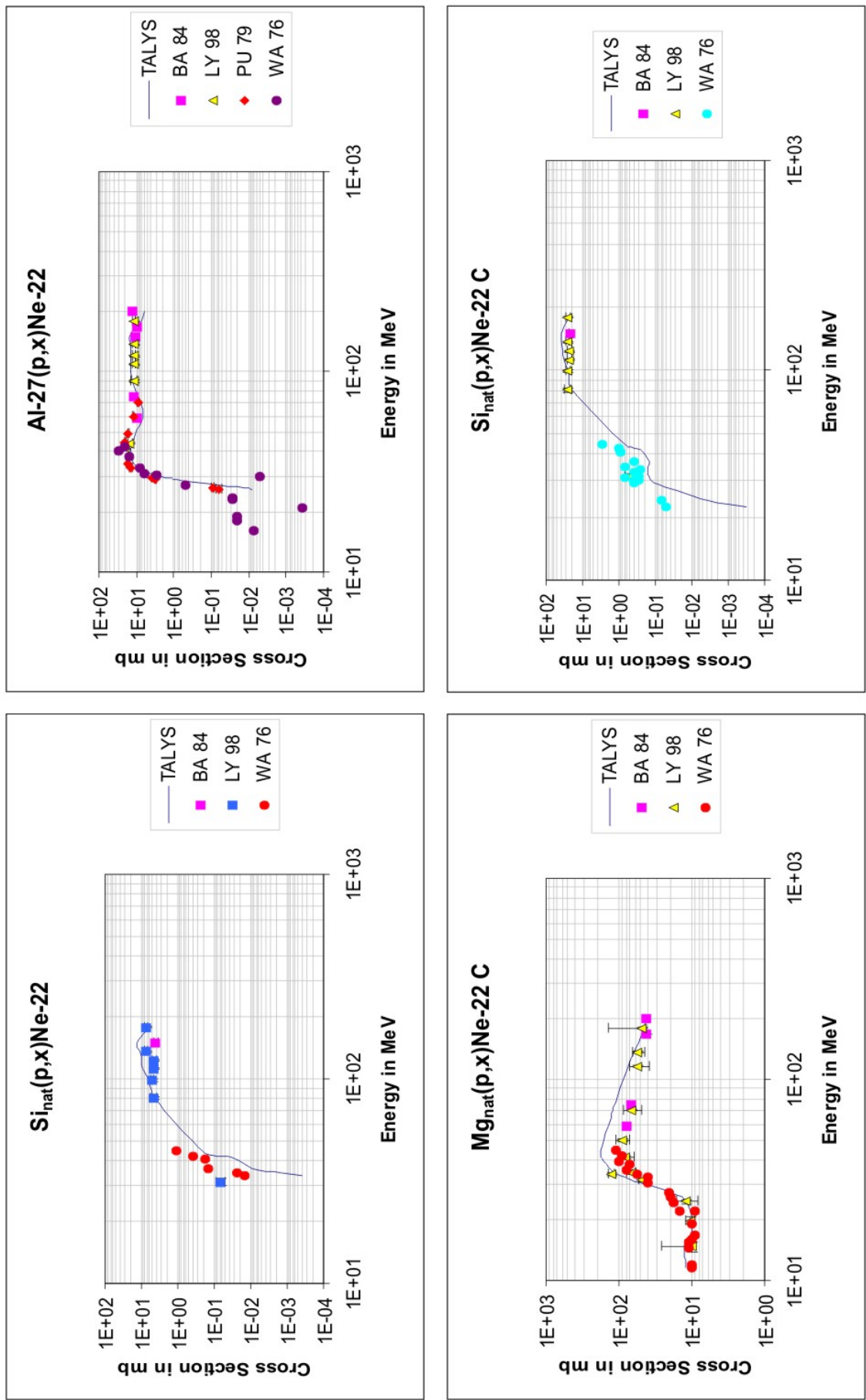


Figure E.3: Data for the production of  $^{22}\text{Ne}$  from natural Si and  $^{27}\text{Al}$ , of  $^{22}\text{Ne}$  from  $^{27}\text{Al}$  and of  $^{22}\text{Ne}_c$  from natural Mg and Si

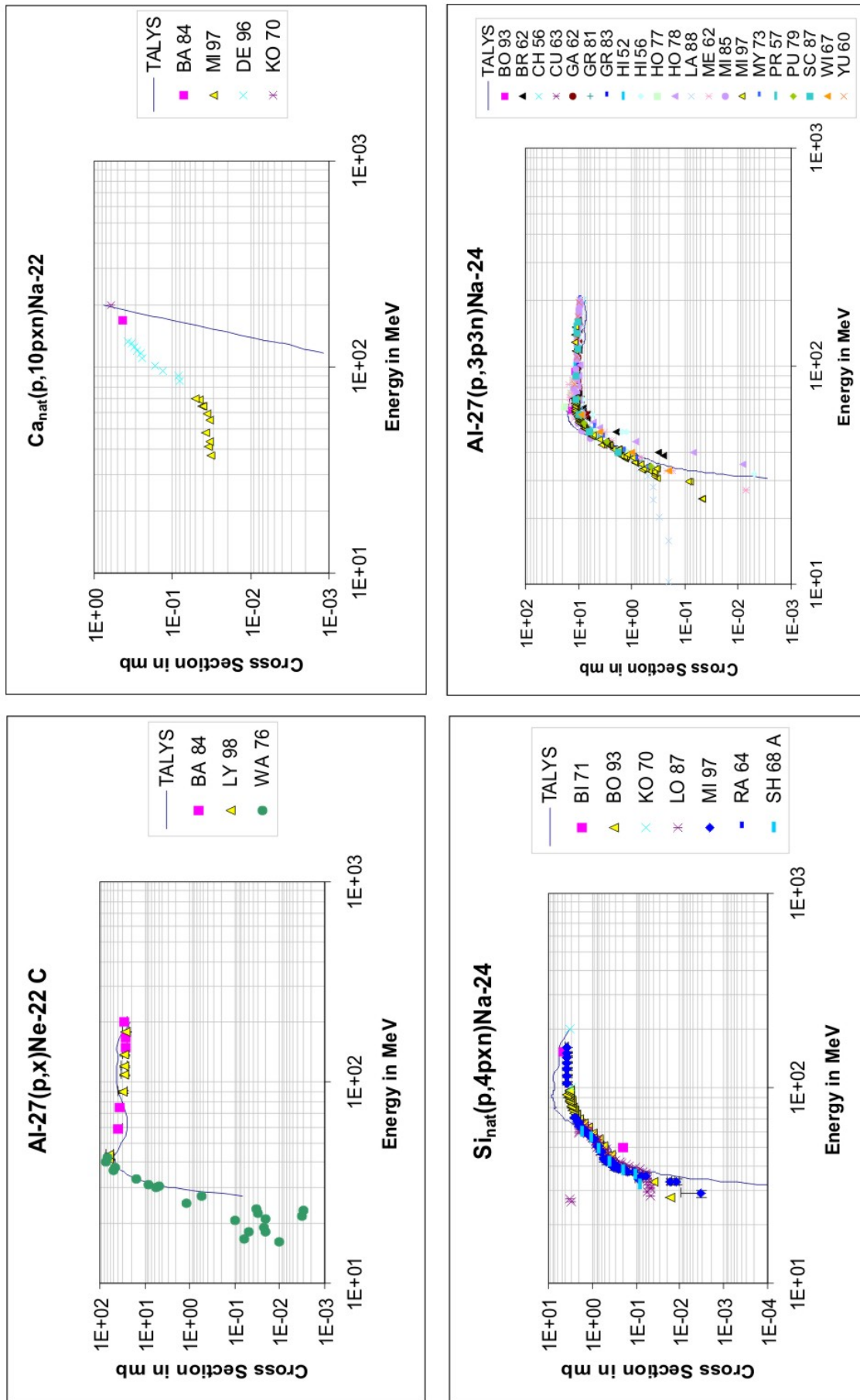


Figure E.4: Data for the production of  $^{22}Ne_c$  from  $^{27}Al$ , of  $^{24}Na$  from natural Ca and Si and of  $^{27}Al$  from natural Si and  $^{27}Al$



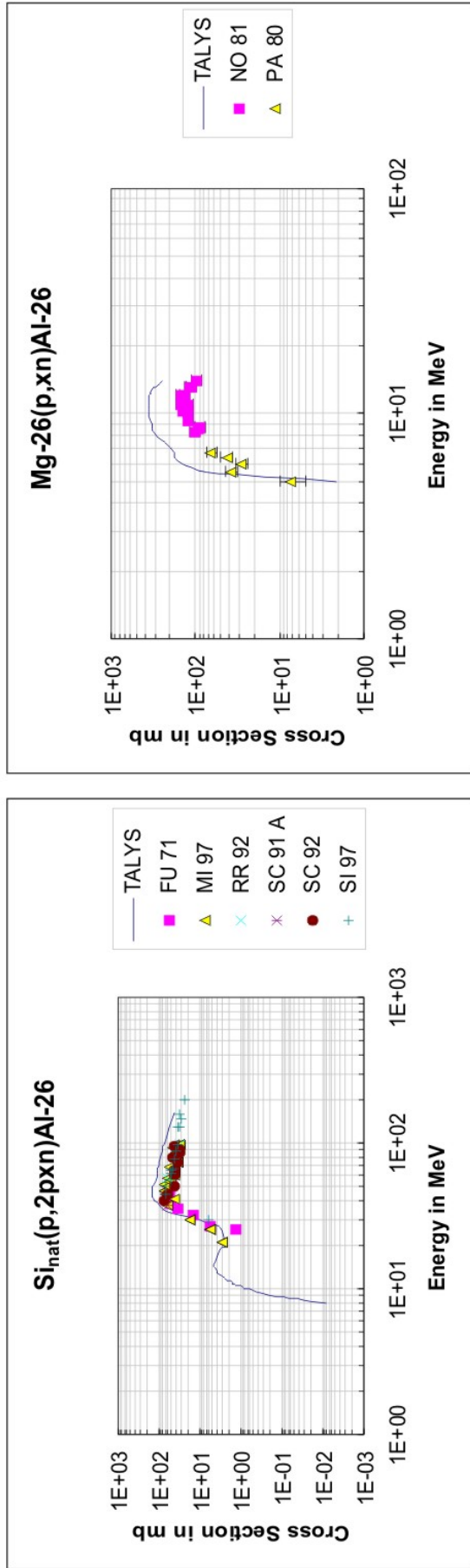


Figure E.5: Data for the production of  $^{26}\text{Al}$  from natural Si and  $^{26}\text{Mg}$



---

**F Experimental data for SACL0L, UPPS0H and UPPS0S**

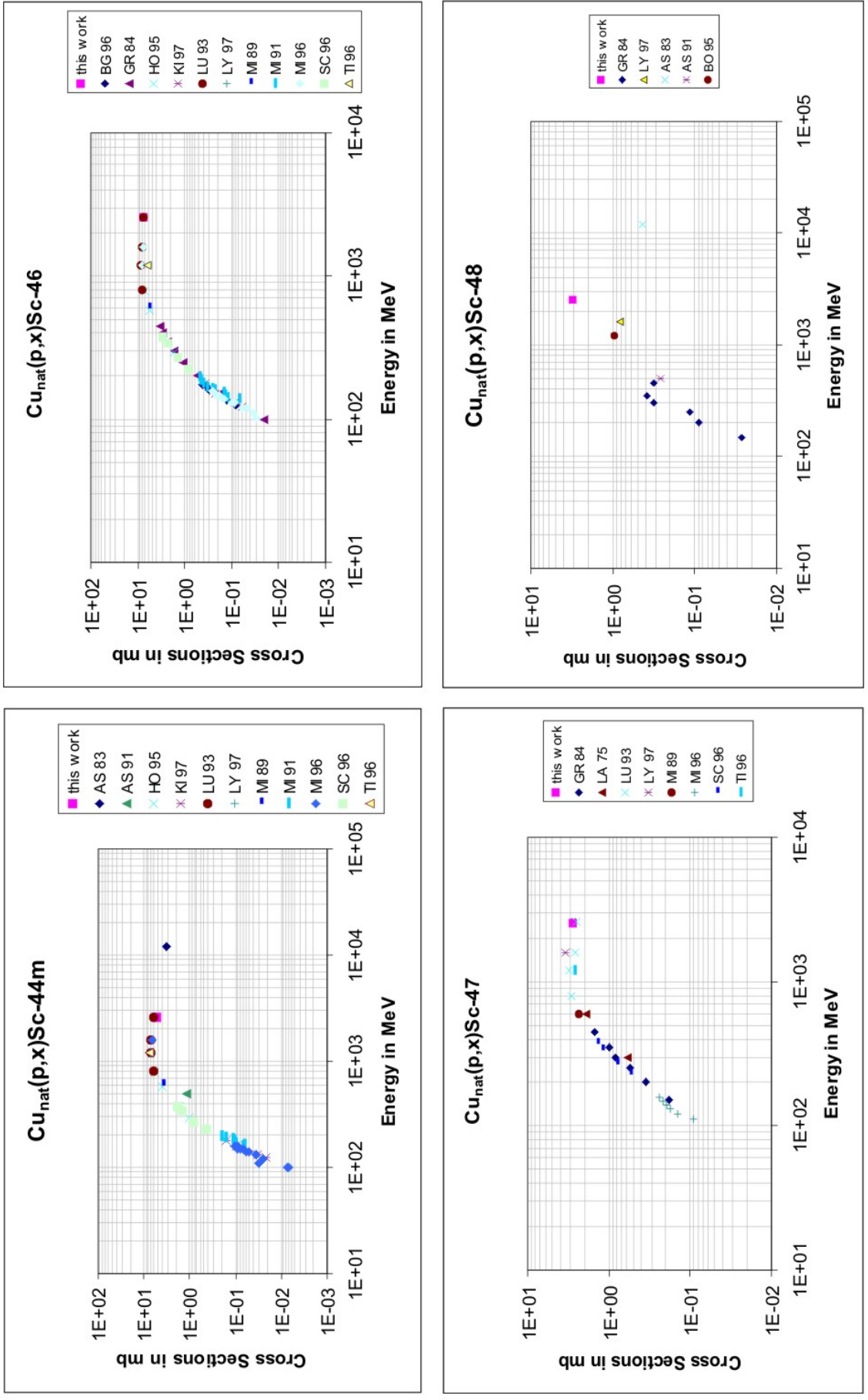


Figure F.1: Experimental data for the production of  $^{44}\text{Sc}_m$ ,  $^{46}\text{Sc}$ ,  $^{47}\text{Sc}$  and  $^{48}\text{Sc}$  from natural Cu

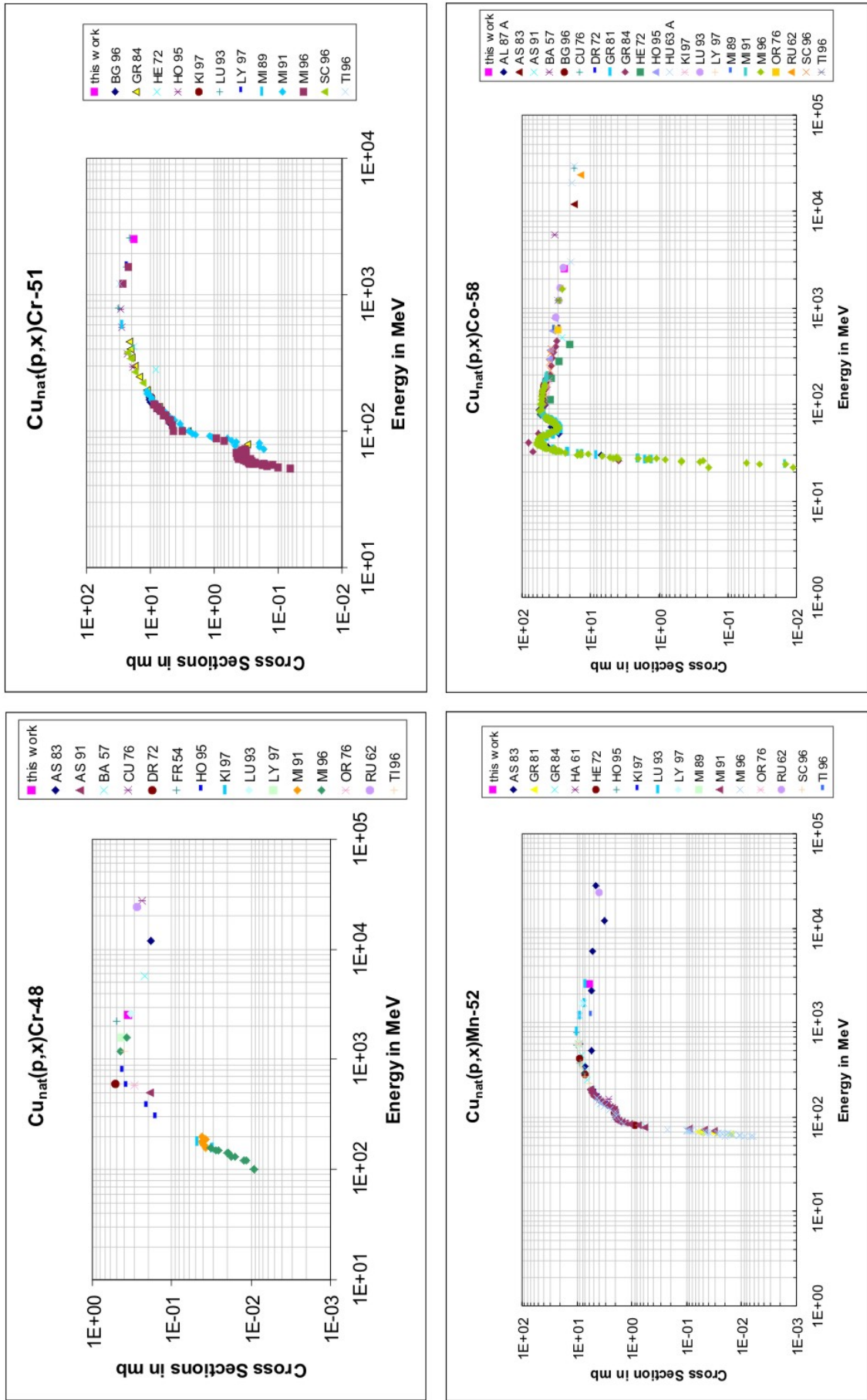


Figure F.2: Experimental data for the production of  $^{48}\text{Cr}$ ,  $^{51}\text{Cr}$ ,  $^{52}\text{Mn}$  and  $^{58}\text{Co}$  from natural Cu

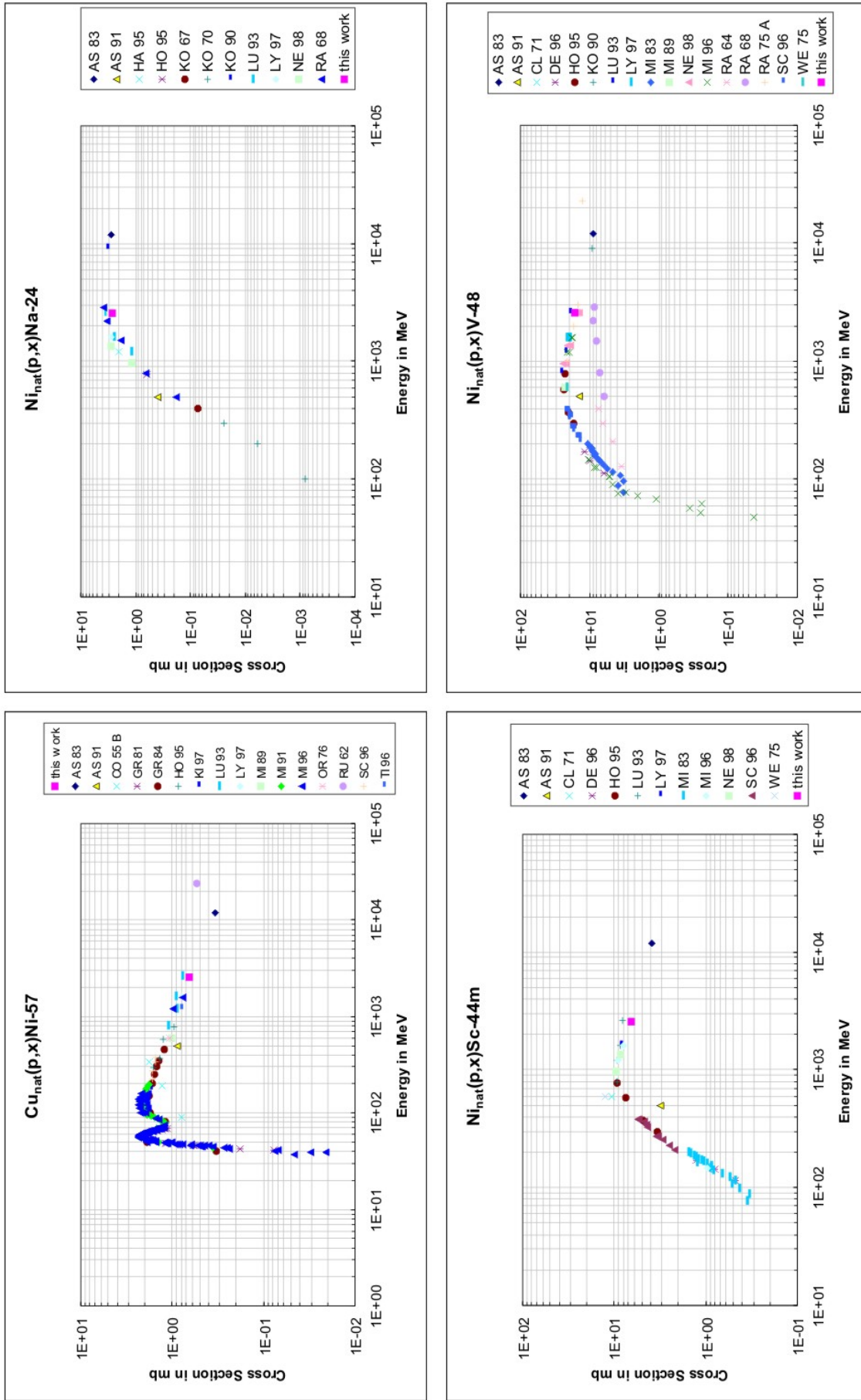


Figure F.3: Experimental data for the production of  $^{57}Ni$  from natural Cu and of  $^{24}Na$ ,  $^{44}Sc_m$  and of  $^{48}V$  from natural Ni

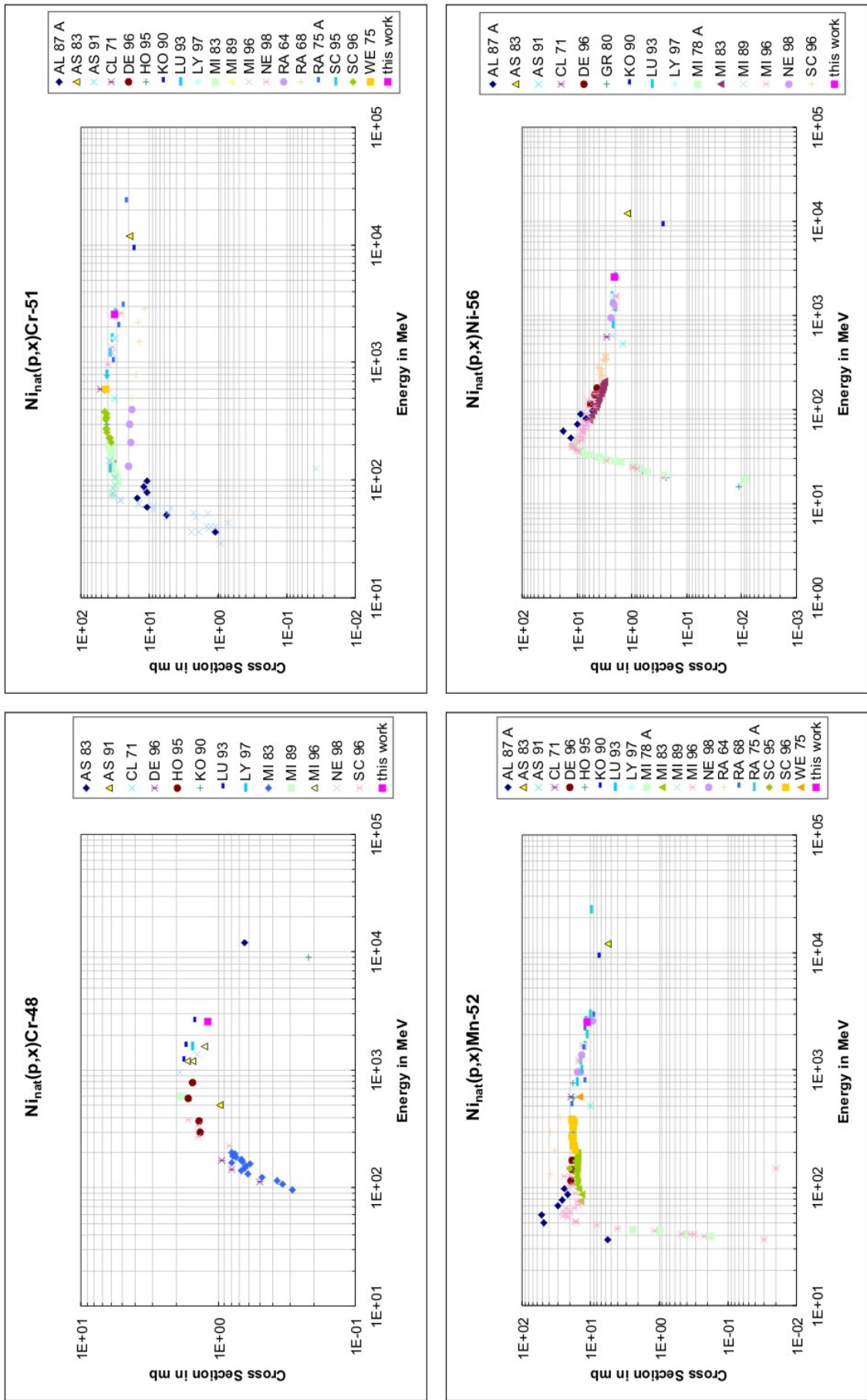


Figure F.4: Experimental data for the production of  $^{48}Cr$ ,  $^{51}Cr$ ,  $^{52}Mn$  and of  $^{56}Ni$  from natural Ni



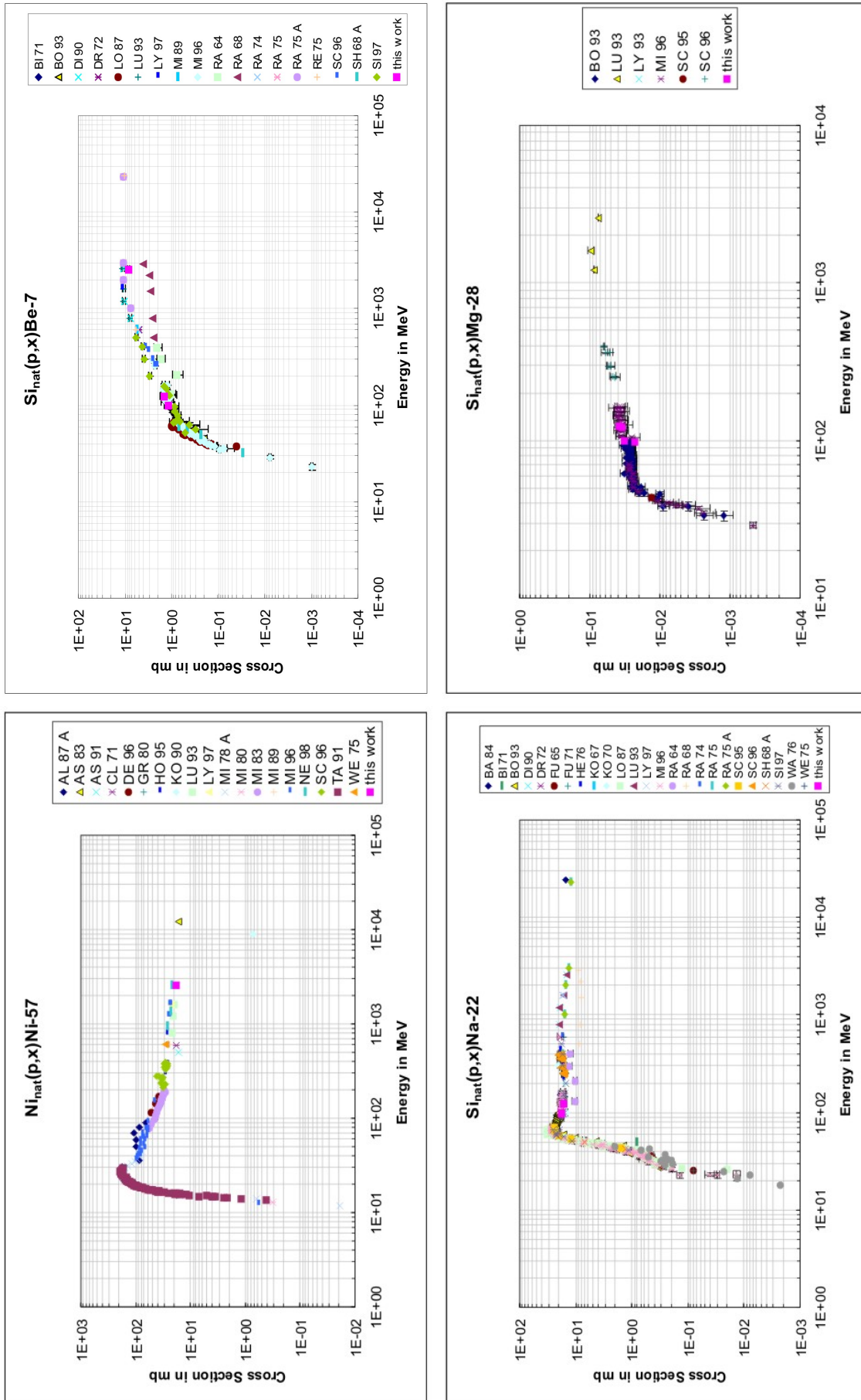


Figure F.5: Experimental data for the production of  $^{57}Ni$  from natural Ni and of  $^7Be$ ,  $^{22}Na$  and  $^{28}Mg$  from natural Si



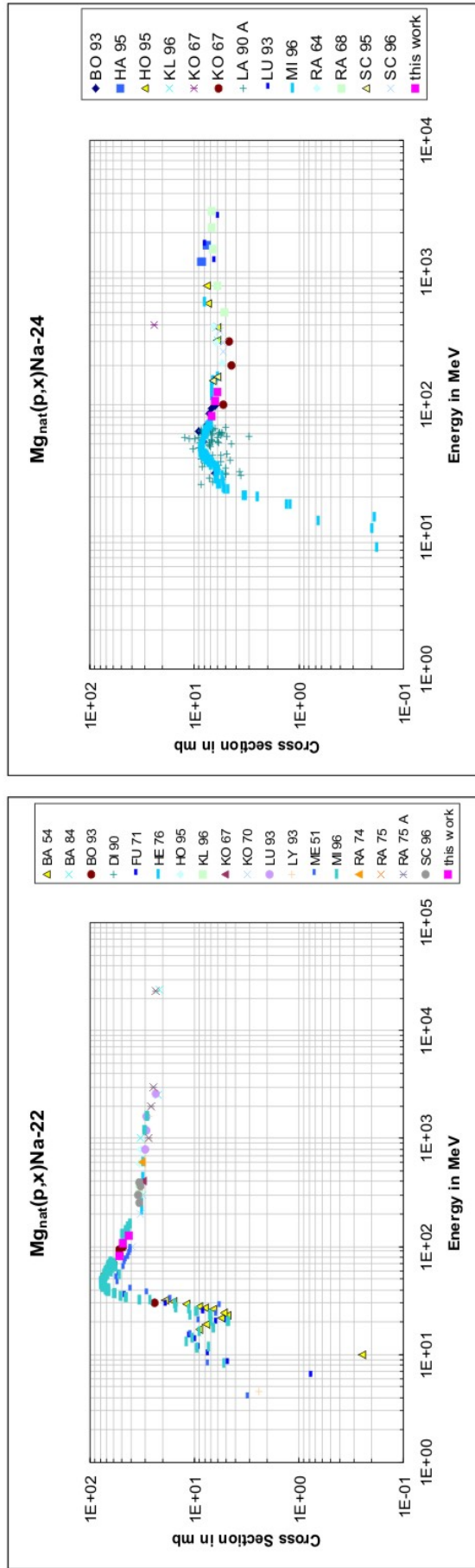


Figure F.6: Experimental data for the production of  $^{22}Na$  and  $^{24}Na$  from Mg



---

**G Comparison with Talys for SACL0L, UPPS0H  
and UPPS0S data**

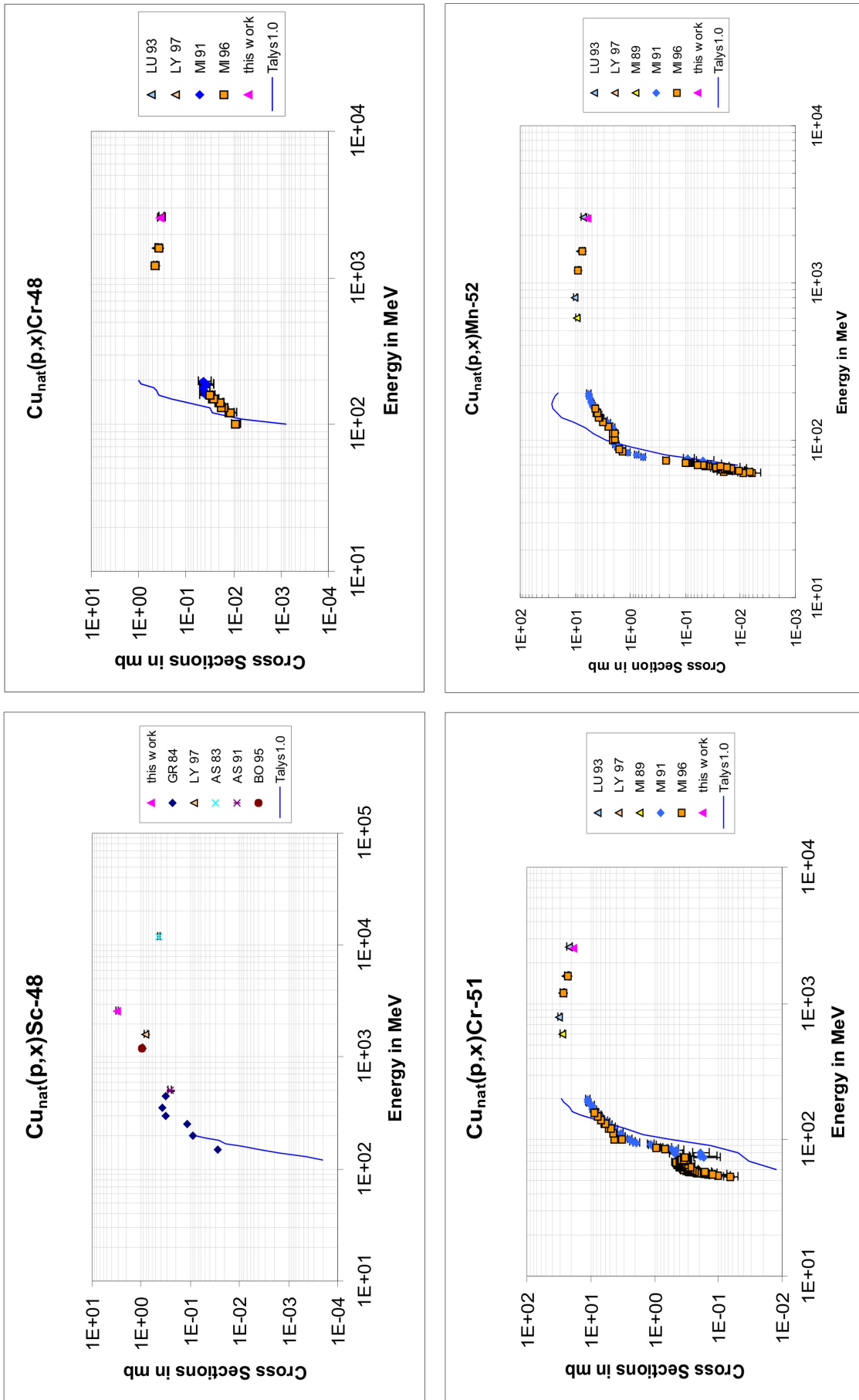


Figure G.1: Experimental data for the production of  $^{48}\text{Sc}$ ,  $^{48}\text{Cr}$ ,  $^{51}\text{Cr}$  and of  $^{52}\text{Mn}$  from natural Cu

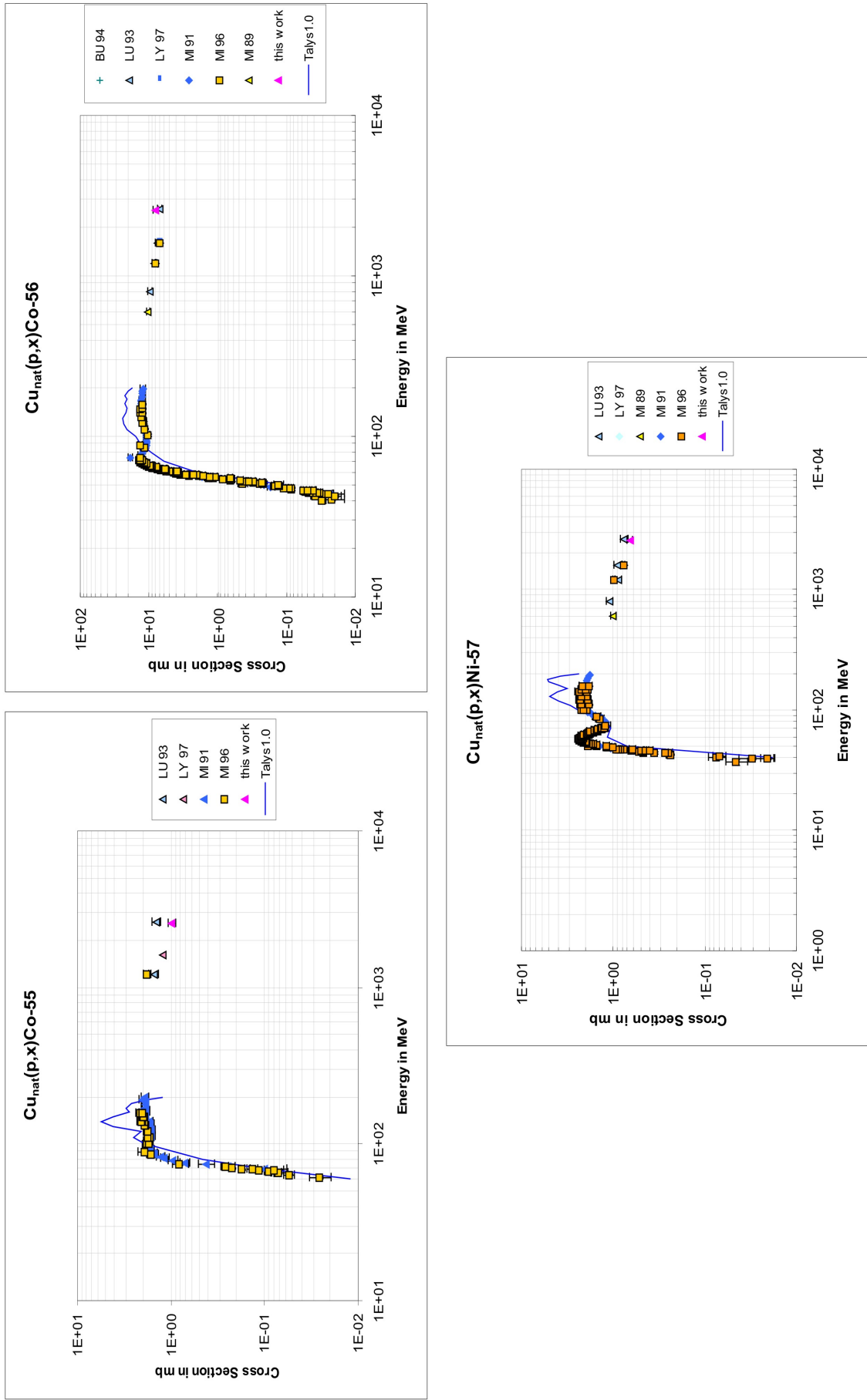


Figure G.2: Experimental data for the production of  $^{55}\text{Co}$ ,  $^{56}\text{Co}$  and of  $^{57}\text{Ni}$  from natural Cu

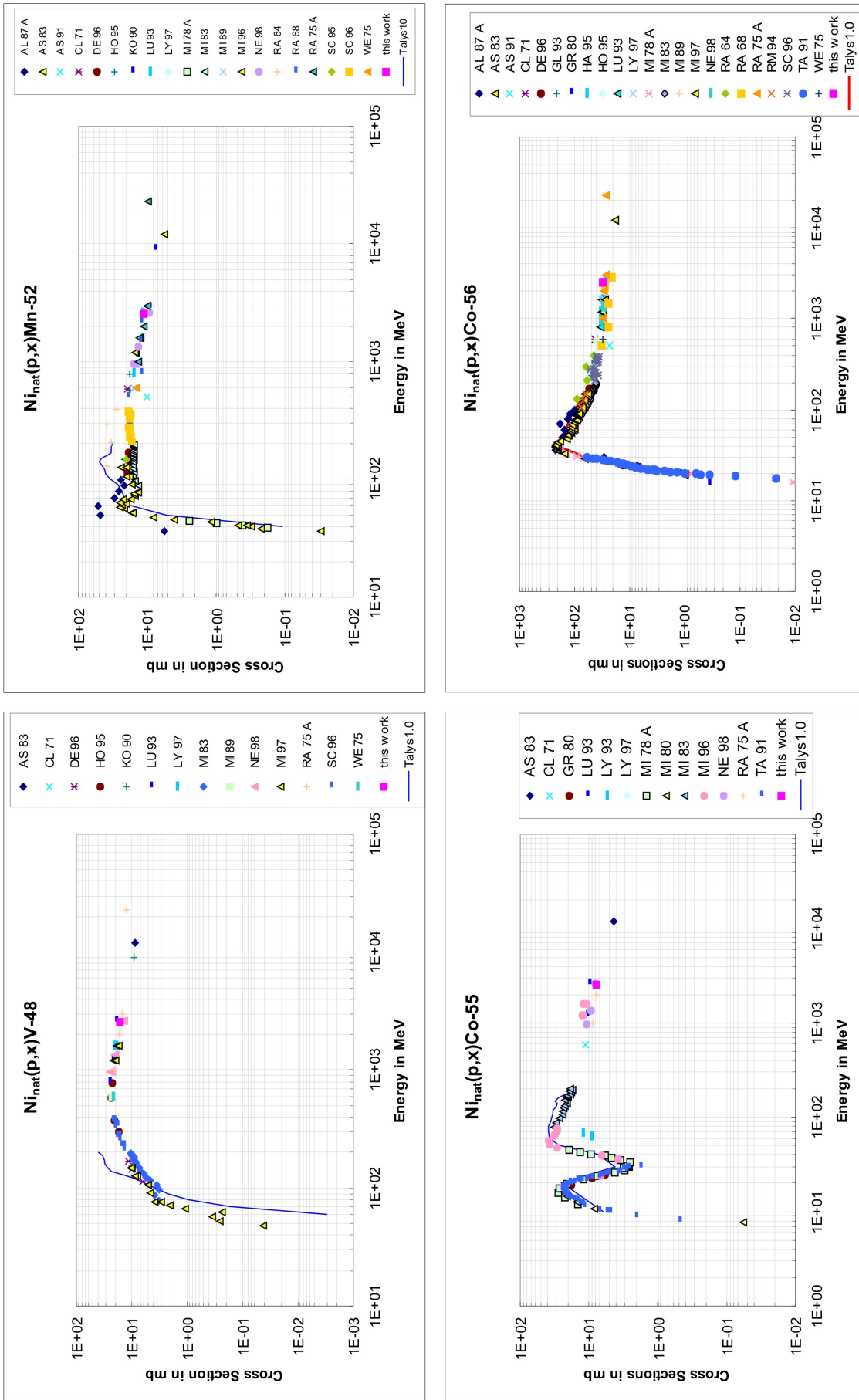


Figure G.3: Experimental data for the production of  $^{48}V$ ,  $^{52}Mn$ ,  $^{55}Co$  and of  $^{56}Co$  from natural Ni

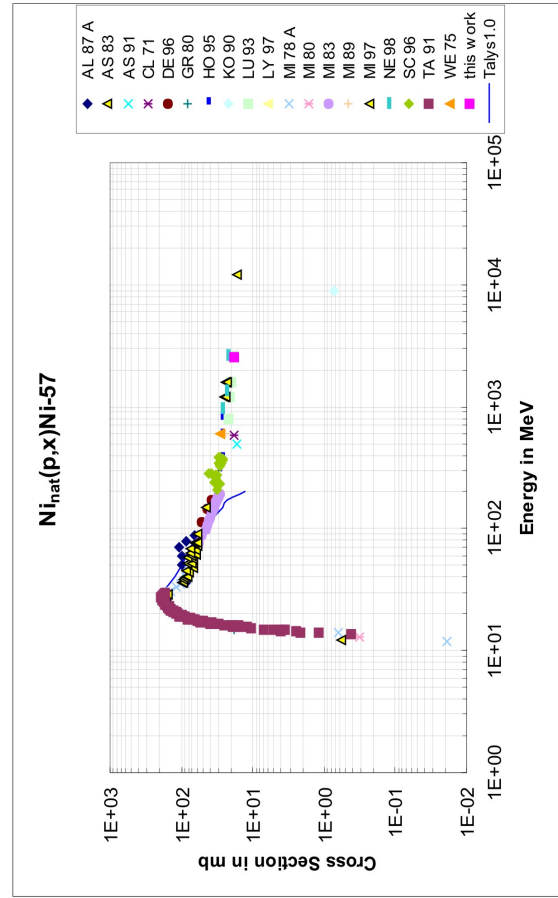
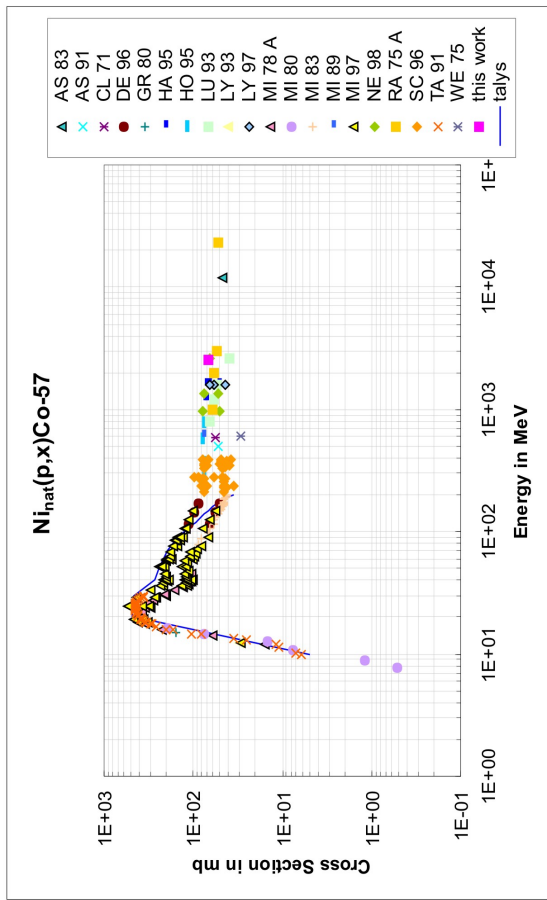
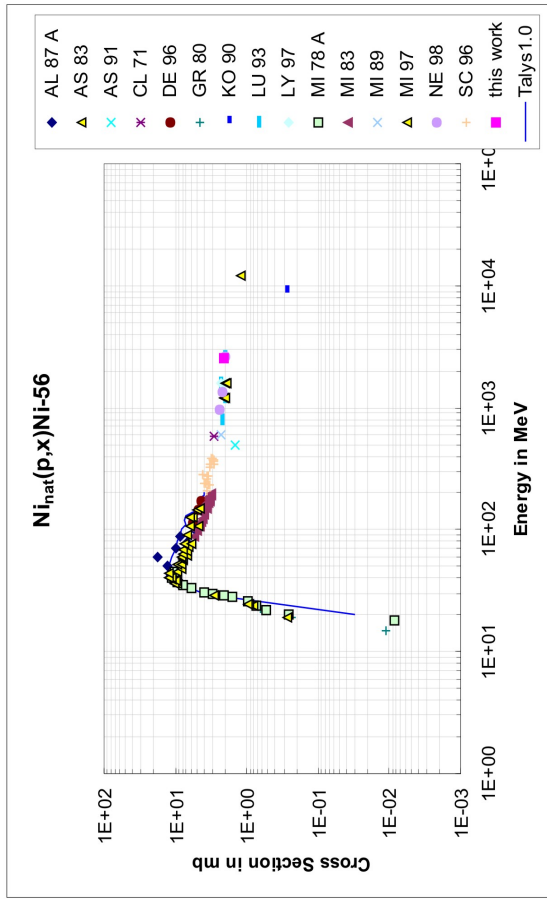


Figure G.4: Experimental data for the production of  $^{57}\text{Co}$ ,  $^{56}\text{Ni}$  and of  $^{57}\text{Ni}$  from natural Ni





---

## H Curriculum Vitae

Last name: Tutuc

Maiden name: Lazar

First name: Mihaela

Birth date and place: 25.05.1981, Bucharest, Romania

Education:

*1996 - 2000* - “Mihai Eminescu” Theoretical High School, Bucharest

*2000 - 2005* - University of Bucharest, Faculty of Physics; diploma thesis - “ $n$ - $\gamma$   $\beta$  Delayed Spectroscopy”

*2005 - 2009* - Doctoral student at Center for Radiation Protection and Radioecology, University of Hannover

Scientific activity:

*Nov. 2003* - GANIL, Caen, France, research stage

*Jun. 2004* - GANIL, Caen, France, research stage, contribution to experiment E377b  
“Search for an isomeric state in  $^{44}\text{S}$ ”

*Nov. 2004* - GANIL, Caen, France, research stage, contribution to experiment E287c  
“Evolution of the  $N=28$  shell gap in the Si isotopes”

*2004 - 2005* - Asistent II at “Horia Hulubei” National Institute of Physics and Nuclear Engineering/IFIN-HH (NIPNE)

*2005 - 2009* - Wissenschaftlichen Mitarbeiterin at Center for Radiation Protection and Radioecology (ZSR), University of Hannover



---

## I Publications

### “Observation of the $0_2^+$ state in $^{44}\text{S}$ ”

S. Grévy, F. Negoita, I. Stefan, N.L. Achouri, J.C. Angélique, B. Bastin, R. Borcea, A. Buta, J.M. Daugas, F. De Oliveira, O. Giarmana, C. Jollet, B. Laurent, M. Lazar, E. Liénard, F. Maréchal, J. Mrázek, D. Pantelica, Y. Penionzhkevich, S. Piétri, O. Sorlin, M. Stanoiu, C. Stodel and M.G. St-Laurent  
European Physical Journal, A 25(2005) 111-113

### “Collapse of the N=28 Shell Closure in $^{42}\text{Si}$ ”

B. Bastin, S. Grévy, D. Sohler, O. Sorlin, Zs. Dombrádi, N.L. Achouri, J.C. Angélique, F. Asaiez, D. Baiborodin, R. Borcea, C. Bourgeois, A. Buta, A. Bürger, R. Chapman, J.C. Dalouzy, Z. Dlouhy, A. Drouard, Z. Elekes, S. Franchoo, S. Iacob, B. Laurent, M. Lazar, X. Liang, E. Liénard, J. Mrázek, L. Nalpas, F. Negoita, N. A. Orr, Y. Penionzhkevich, Zs Podolyák, F. Pougheon, P. Roussel-Chomaz, M.G. Saint-Laurent, M. Stanoiu and I. Stefan  
F. Nowacki and A. Poves  
Physical Review Letters, 99, 022503 (2007)

### “Production of Light and Intermediate Mass Residues”

R. Michel and M.Tutuc  
Report for EUROTRANS/NUDATRA Milestone M5.19